Genetic Risk Mapping and Insights into Esophageal Adenocarcinoma Development (Risk Mapping of Esophageal Adenocarcinoma)

Authors

Wenjie Li

Correspondence

1239424226@qq.com (W. Li)

Graphical Abstract

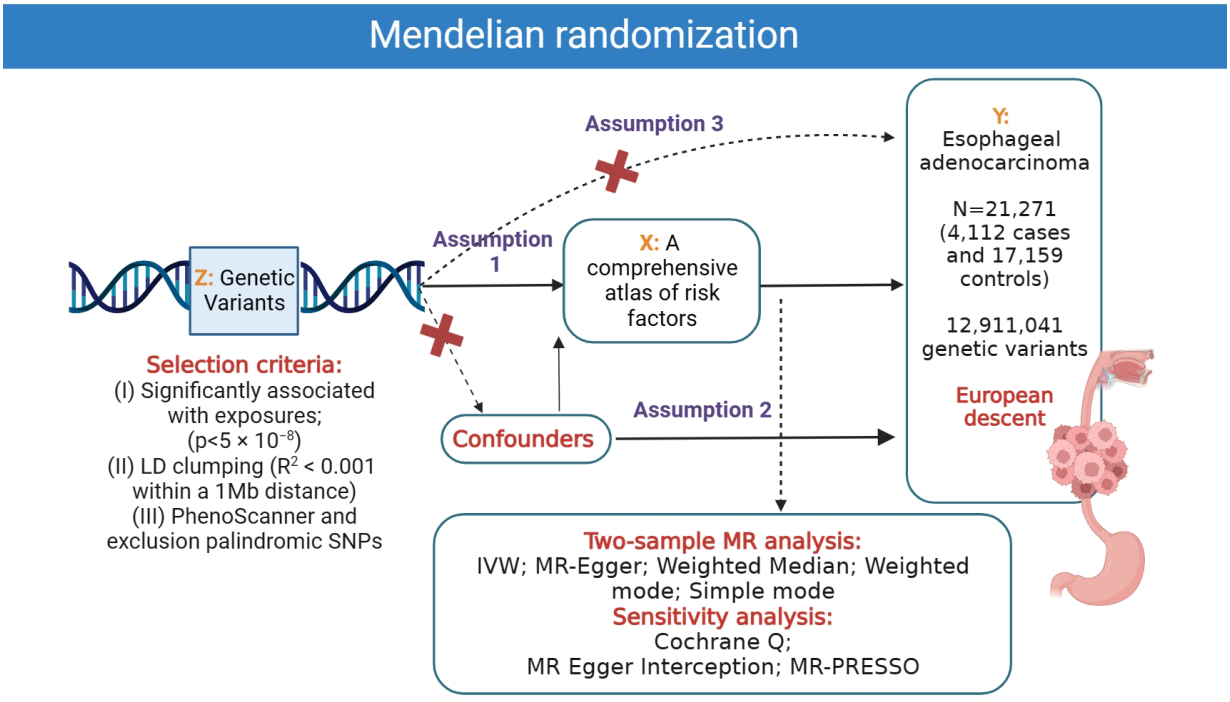

https://doi.org/10.71321/mczdpt96

Short Communication Life Conflux

Genetic Risk Mapping and Insights into Esophageal Adenocarcinoma Development (Risk Mapping of Esophageal Adenocarcinoma)

Wenjie Li[1*]

Received: 2025-01-25 | Accepted: 2025-03-27 | Published online: 2025-03-30

Abstract

Background: Esophageal adenocarcinoma (EAC) is a malignant tumor that has been increasing in incidence over the past few decades. Identifying the risk factors associated with EAC is crucial for prevention and early detection strategies.
Methods: This study aimed to investigate the potential risk factors for EAC using a Mendelian randomization (MR) approach. We attained genetic variants associated with 52 exposure factors s from available large-scale genome-wide association studies.
Results: Genetic predisposition to childhood body mass index, forced expiratory volume in 1-second, glomerular filtration rate, telomere length, alcohol consumption, anxiety or depression, smoking, coffee consumption, time spent watching television, basal metabolic rate, body fat percentage, body mass index, hip circumference, obesity class 1, obesity class 2, trunk fat percentage, waist circumference, waist-to-hip ratio, iron, Barrett's esophagus, and gastroesophageal reflux disease were associated with increased risk of EAC. In addition, we demonstrated that age at first birth, age at first sexual intercourse, age at menarche, years of schooling, type 1 diabetes, and fruit intake could suggestively decrease the odds of EAC.
Conclusion: This study represents the inaugural MR investigation to present a comprehensive atlas of risk factors associated with EAC, which will aid in advancing the formulation of efficacious preventive and early detection approaches.
Keywords: Esophageal adenocarcinoma; Mendelian randomization; single-nucleotide polymorphisms; risk factor; early detection

Introduction

Esophageal carcinoma is globally positioned as the eighth most prevalent form of cancer, and ranks as the sixth leading contributor to cancer-related mortality [5]. While esophageal squamous cell carcinoma maintains a significant presence worldwide, the incidence of esophageal adenocarcinoma (EAC) is progressively assuming a dominant role in developed nations [4]. EAC exhibits a markedly favorable prognosis when identified at an early stage, confined to the mucosal and submucosal layers of the esophagus. However, the majority of cases are detected at advanced stages, where outcomes remain poor [7,20]. The 5-year overall survival rate for patients with esophageal adenocarcinoma is less than 20%, a figure comparable to the dismal survival rates observed in malignancies of the liver, lung, and pancreas [7,20]. These statistics underscore the urgent need for the development and implementation of effective screening strategies to facilitate earlier diagnosis and improve patient outcomes.
In efforts to thwart the progression of EAC, the implementation of effective screening strategies is anticipated to assume a pivotal role, consequently presenting a promising avenue for reducing mortality rates in the future. Currently, smoking, gastroesophageal reflux disease, and Barrett esophagus stand recognized as the principal risk factors accountable for EAC development [4]. However, our current comprehension of additional potential risk factors for EAC remains restricted. Moreover, the execution of randomized controlled trials aimed at investigating these risk factors poses considerable challenges, thereby predominantly relying on observational studies to offer valuable insights. It is crucial to recognize the inherent limitations of observational studies, including limited sample sizes and inadequate adjustment for confounding variables, which can potentially compromise the accurate assessment of cancer development. Hence, there arises a pressing necessity for a groundbreaking approach to effectively estimate the causal risk factors associated with EAC. Mendelian randomization (MR) analysis, employing single nucleotide polymorphisms (SNPs) as instrumental variables (IVs), stands as an innovative methodology for elucidating causal inferences between exposures and outcomes [2,11,19]. Of remarkable significance, this epidemiological approach serves to mitigate the impact of potential confounding factors [2,11,19]. Against this backdrop, we embarked upon an MR analysis utilizing a vast cohort of European individuals, with the aim of constructing a comprehensive compendium of the risk factors intricately associated with EAC.

1 Department of Radiation Oncology, Nanfang Hospital, Southern Medical University, Baiyun District, Guangzhou, Guangdong, 510515, China
* Corresponding Author.

https://doi.org/10.71321/mczdpt96

Methods

The study examined 52 risk factors associated with EAC using MR analysis and summary-level data from large-scale GWASs (Supplementary Table S1, Figure 1). SNPs significantly linked to EAC ($p < 5 \times 10-8$) were selected, with minimal linkage disequilibrium (R2 < 0.001) to ensure independent effects. Pleiotropic effects were addressed using the PhenoScanner database, and palindromic SNPs were excluded. The inverse variance weighted (IVW) method was the primary approach, with additional MR methods employed. Detailed methods are provided in the supplementary materials.

Phenotypes	SNPs	OR (95%CI)	P-value
Individual characters			
Age at first birth	55	0.81 (0.73–0.91)	0.0005#
Age at first sexual intercourse	53	0.68 (0.47–0.99)	0.0484*
Age at menopause	55	0.84 (0.70–0.99)	0.0469*
Birth weight	122	0.93 (0.73–1.19)	0.5825
Childhood body mass index	15	1.33 (1.04–1.70)	0.0217*
Forced expiratory volume in 1–second	75	1.49 (1.06–2.10)	0.0215*
Glomerular filtration rate (creatinine)	38	3.39 (1.01–11.30)	0.0473*
Telomere length	124	1.35 (1.03–1.77)	0.0304*
Socioeconomic variables			
Average total household income	44	0.93 (0.53–1.65)	0.8096
Townsend deprivation index	17	1.06 (0.35–3.20)	0.9143
Years of schooling	262	0.69 (0.51–0.95)	0.0214*
Lifestyle			
Alcohol consumption	90	1.39 (1.07–1.79)	0.0121*
Anxiety or depression	34	6.76 (1.44–31.68)	0.0153*
Beef intake	11	1.00 (0.12–8.67)	0.9999
Cigarettes	73	1.55 (1.18–2.04)	0.0015*
Cereal intake	34	0.55 (0.21–1.42)	0.2148
Coffee consumption	35	2.71 (1.13–6.49)	0.0254*
Fruit intake	35	0.23 (0.10–0.54)	0.0008#
Insomnia	32	1.00 (0.38–2.62)	0.9946
Milk assumption	3	0.0002 (0.00–9E+3)	0.4276
Sleep duration	2	2.26 (0.58–8.84)	0.24296
Time spent watching television	101	2.02 (1.19–3.43)	0.0088*
Vigorous physical activity	7	2.43 (0.21–28.03)	0.4756
Cardiometabolic factors			
Basal metabolic rate	343	1.29 (1.02–1.64)	0.0348*
Body fat percentage	230	2.23 (1.66–2.98)	0#
Body mass index	448	1.60 (1.34–1.91)	0#
C–reactive protein	48	0.88 (0.71–1.10)	0.2784
Estradiol levels	10	0.97 (0.83–1.15)	0.7498
Fasting glucose	9	0.95 (0.55–1.65)	0.8562
Hip circumference	51	1.44 (1.02– 2.03)	0.0363*
HDL–C	85	1.10 (0.95–1.29)	0.2086
IGF–1	282	1.12 (0.96–1.30)	0.1558
LDL–C	76	0.99 (0.86–1.14)	0.9005
Leptin	4	0.97 (0.51–1.87)	0.9316
Obesity class 1	14	1.26 (1.10–1.46)	0.0011*
Obesity class 2	11	1.23 (1.11–1.37)	0.0001#
Testosterone levels	153	0.88 (0.60–1.30)	0.5339
Total Cholesterol	81	0.97 (0.83–1.13)	0.6916
Triglycerides	55	0.95 (0.81–1.13)	0.5809
Type 1 diabetes	36	0.94 (0.88–0.99)	0.038
Type 2 diabetes	52	0.96 (0.85–1.09)	0.5401
Trunk fat percentage	316	1.87 (1.47–2.37)	0#
Waist circumference	37	1.72 (1.20–2.48)	0.0033*
Waist–to–hip ratio	28	1.64 (1.05–2.56)	0.0311*
Weight	325	0.95 (0.85–1.06)	0.3525
Micronutrients			
25–Hydroxyvitamin D	102	1.16 (0.90–1.50)	0.2454
Vitamin D	76	1.17 (0.87–1.57)	0.3139
Calcium	204	0.90 (0.76–1.08)	0.2585
Iron	3	1.22 (1.0001–1.49)	0.0487*
Copper	2	1.03 (0.86–1.24)	0.7398
Esophageal diseases			
Barrett's esophagus	12	2.24 (1.88–2.66)	0#
Gastroesophageal reflux disease	66	1.60 (1.29–2.00)	0#

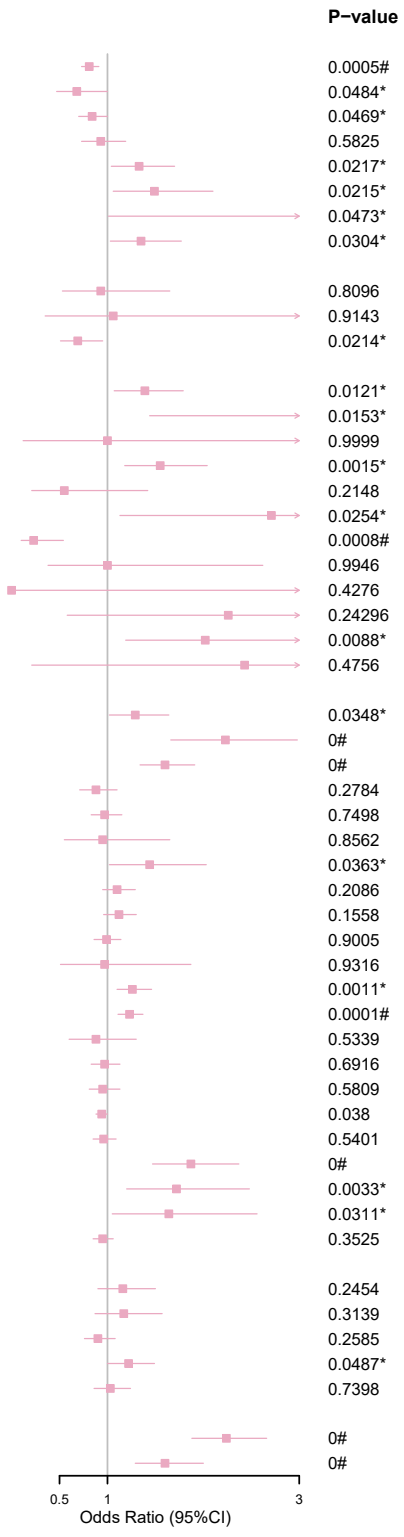

Figure 1. The overview of the present study depicting a comprehensive atlas of risk factor related to esophageal adenocarcinoma. Within this intricate analysis, genetic variants (Z) assume the crucial role of genetic instruments, enabling an assessment of the causal relationship between exposures (X) and outcomes (Y). The numerical labels 1 to 3 archetypally correspond to assumptions 1 to 3.

Results

A comprehensive atlas of risk factors associated with EAC

The MR estimates revealed a suggestive or significant relationship between an elevated risk of EAC and 27 key risk and protective factors. Among these, body mass index (OR IVW: 1.6; 95% CI 1.34–1.91, p<0.001), Barrett's esophagus (OR IVW: 2.24; 95% CI 1.88–2.66, p<0.001), and fruit intake (OR IVW: 0.23; 95% CI 0.1–0.54, p<0.001) stood out as the most critical determinants of risk and protection, respectively. Body mass index, along with obesity traits such as trunk fat percentage (OR IVW: 1.87; 95% CI 1.47–2.37, p<0.001), waist circumference (OR IVW: 1.72; 95% CI 1.20–2.48, p=0.003), and waist-to-hip ratio (OR IVW: 1.64; 95% CI 1.05–2.56, p=0.03), was strongly associated with increased EAC risk, highlighting the role of adiposity in carcinogenesis. In contrast, fruit intake demonstrated significant protective effects, potentially due to its antioxidative and anti-inflammatory properties.

Beyond these major factors, the analysis identified additional modifiable and non-modifiable contributors to EAC risk. Modifiable factors included smoking (OR IVW: 1.55; 95% CI 1.18–2.04, p=0.0015), alcohol consumption (OR IVW: 1.39; 95% CI 1.07–1.79, p=0.01), coffee consumption (OR IVW: 2.71; 95% CI 1.13–6.49, p=0.025), and sedentary behavior as indicated by time spent watching television (OR IVW: 2.02; 95% CI 1.19–3.43, p=0.0088). These factors underscore the importance of lifestyle interventions in mitigating EAC risk. On the other hand, non-modifiable factors such as telomere length (OR IVW: 1.35; 95% CI 1.03–1.77, p=0.03), glomerular filtration rate (OR IVW: 3.39; 95% CI 1.01–11.3, p=0.04), and childhood body mass index (OR IVW: 1.33; 95% CI 1.04–1.7, p=0.02) reflect intrinsic biological and physiological predispositions contributing to EAC risk.

The study also revealed suggestive causal relationships between genetically predicted protective factors and a decreased risk of EAC, including age at first birth (OR IVW: 0.81; 95% CI 0.73–0.91, p=0.0005), age at first sexual intercourse (OR IVW: 0.68; 95% CI 0.47–0.99, p=0.04), age at menarche (OR IVW: 0.84; 95% CI 0.70–0.99, p=0.04), years of schooling (OR IVW: 0.69; 95% CI 0.51–0.95, p=0.02), type 1 diabetes (OR IVW: 0.94; 95% CI 0.88–0.99, p=0.04), and fruit intake (OR IVW: 0.23; 95% CI 0.1–0.54, p=0.0008). Alternative MR methods, including simple mode, weighted mode, weighted median, and MR-Egger regression, yielded consistent results with the IVW findings, supporting the robustness of these conclusions. No evidence of causality was found for other risk factors (all p-values > 0.05) (Figure 1 and Supplementary Table S2).

Sensitivity analyses

To ensure fidelity of our initial MR discoveries, we have conducted sensitivity analyses that strictly adhere to the three first principles of MR (Figure 1). Table 1 displays the results of these sensitivity analyses. We have identified SNPs that are significantly associated with exposures at a noteworthy p-value threshold (p < 5 x 10-8) and excluded SNPs associated with potential confounders, indicating that the first and third assumptions of MR were not violated. Cochrane's Q test and MR-Egger intercept regression analyses primarily yielded non-significant p-values (the majority of p-values were greater than 0.05), suggesting an absence of significant heterogeneity and horizontal pleiotropy, respectively (Table 1). Furthermore, the MR PRESSO global test identified rs543874, rs429358, rs4627713, rs2041376, rs957919, and rs1516725 as potential sources of pleiotropy (Table 1). Previous studies have suggested that multiplicative interactions exist between rs543874[12], rs429358[6], and rs1516725[15] with traits such as obesity or apolipoproteins. These findings highlight the importance of cautious interpretation of results involving these SNPs. While the inclusion of these SNPs marginally affected the causal estimate, exclusion analyses yielded consistent results, reinforcing the robustness of our primary findings, suggesting that the potential pleiotropy associated with these SNPs does not substantially undermine the validity of our conclusions.

Discussion

To the best of our knowledge, this study represents a novel and comprehensive examination of latent and modifiable risk factors associated with EAC. Beyond the established risk factors such as alcohol consumption, smoking, Barrett's esophagus, and gastroesophageal reflux disease, our findings provide insights into previously underexplored dimensions of EAC risk, offering a more nuanced understanding of its etiology. Of note, the progression from Barrett's esophagus to EAC is driven by a series of molecular and cellular changes that result in dysregulated cell growth, altered gene expression, and increased resistance to apoptosis. One of the key events in this process is the accumulation of genetic mutations that facilitate carcinogenesis. Mutations in tumor suppressor genes, such as TP53, and the amplification of oncogenes like c-MYC and cyclin D1, have been frequently observed in the transition from Barrett's esophagus to EAC [17,18]. These genetic alterations contribute to the loss of normal growth control, allowing abnormal cells to proliferate uncontrollably and form a tumor. Moreover, smoking induces chronic inflammation and DNA damage through the generation of reactive oxygen species, while alcohol enhances acetaldehyde production, further promoting mutagenesis.

In the present study, we have identified several factors related to individual characteristics that may either protect or increase the risk of EAC. These factors include age at first birth, age at first sexual intercourse, age at menarche, birth weight, forced expiratory volume in 1-second, glomerular filtration rate, and telomere length. We also confirmed associations previously suggested by other studies, such as the link between reproductive factors [14] and telomere length [23] with cancer. However, our study is the first to establish these associations with EAC specifically. Additionally, our study uniquely identifies lung and kidney function as potential risk factors for EAC, suggesting that systemic physiological health may influence esophageal carcinogenesis. Reduced forced expiratory volume in one second may reflect compromised respiratory function and chronic exposure to oxidative stress or inflammation, which could contribute to cancer risk. Similarly, impaired glomerular filtration rate, indicative of kidney dysfunction, could be linked to an altered metabolic profile, systemic inflammation, or impaired clearance of carcinogenic compounds, all of which may play a role in EAC development [13].

Table 1. Sensitivity analyses.

Phenotypes	SNPs	F-value	Cochrane Q test			MR Egger Interceotion			MR PRESSO	
			Q	Q_df	P-value	Intercept	SE	P-value	Potential outliers	global test_ P-value
Individual characters										
Age at first birth	55.00	NA	50.96	54.00	0.59	0.01	0.02	0.53	NO	0.61
Age at first sexual intercourse	53.00	NA	47.70	52.00	0.64	0.01	0.02	0.56	NO	0.66
Age at menopause	55.00	93.04	45.79	54.00	0.78	0.01	0.02	0.58	NO	0.79
Birth weight	122.00	56.99	138.94	121.00	0.13	0.01	0.01	0.11	NO	0.11
Childhood body mass index	15.00	NA	23.60	14.00	0.05	-0.04	0.04	0.36	rs543874	0.00
Forced expiratory volume in 1-second	75.00	46.72	126.78	74.00	0.00	-0.04	0.02	0.07	NO	0.00
Glomerular filtration rate (creatinine)	38.00	66.38	42.60	37.00	0.24	0.01	0.02	0.61	NO	0.27
Telomere length	124.00	115.33	166.27	123.00	0.01	0.00	0.01	0.93	NO	0.01
Socioeconomic variables										
Average total household income	44.00	40.92	60.30	43.00	0.04	-0.01	0.02	0.61	NO	0.05
Townsend deprivation index	17.00	35.51	21.31	16.00	0.17	0.04	0.07	0.64	NO	0.17
Years of schooling	262.00	49.26	328.01	261.00	0.00	0.01	0.01	0.23	NO	0.00
Lifestyle										
Alcohol assumption	90.00	53.78	99.38	89.00	0.21	0.01	0.01	0.11	NO	0.21
Anxiety or depression	34.00	37.20	40.59	33.00	0.17	0.02	0.04	0.61	NO	0.18
Beef intake	11.00	39.67	19.27	10.00	0.04	-0.07	0.07	0.39	rs429358	0.00
Cigarettes	73.00	42.42	75.62	72.00	0.36	0.01	0.02	0.66	NO	0.39
Cereal intake	34.00	45.50	49.12	33.00	0.04	0.02	0.03	0.47	NO	0.05
Coffee consumed	35.00	77.66	57.96	34.00	0.01	0.00	0.01	0.90	NO	0.01
Fruit intake	35.00	40.36	41.17	34.00	0.19	-0.02	0.03	0.54	NO	0.20
Insomnia	32.00	45.46	42.21	31.00	0.09	0.03	0.02	0.17	NO	0.10
Milk assumption	3.00	38.17	6.09	2.00	0.05	-0.03	0.29	0.93	NO	NA
Sleep duration	2.00	49.45	NA	NA	NA	NA	NA	NA	NO	NA
Time spent watching television	101.00	41.41	114.91	100.00	0.15	-0.01	0.02	0.71	NO	0.15

Vigorous physical activity	7.00	40.81	5.35	6.00	0.50	0.04	0.10	0.71	NO	0.53
Cardiometabolic factors										
Basal metabolic rate	343.00	70.37	407.23	342.00	0.01	0.00	0.00	0.47	rs4627713	0.00
Body fat percentage	230.00	51.95	274.91	229.00	0.02	-0.01	0.01	0.35	rs2041376	0.00
Body mass index	448.00	71.65	493.32	447.00	0.06	-0.01	0.00	0.19	NO	0.07
C-reactive protein	48.00	128.08	67.05	47.00	0.03	0.00	0.01	0.95	NO	0.03
Estradiol levels	10.00	67.65	11.28	9.00	0.26	0.02	0.04	0.60	NO	0.34
Fasting glucose	9.00	NA	10.42	8.00	0.24	0.02	0.03	0.45	NO	0.29
Hip circumference	51.00	55.29	73.86	50.00	0.02	-0.04	0.01	0.02	rs4889606	0.00
HDL-C	85.00	121.06	89.75	84.00	0.31	0.00	0.01	0.60	NO	0.32
IGF-1	282.00	101.83	334.61	281.00	0.02	0.00	0.00	0.44	NO	0.01
LDL-C	76.00	158.18	98.38	75.00	0.04	0.00	0.01	0.86	NO	0.04
Leptin	4.00	39.68	3.70	3.00	0.30	0.00	0.11	0.97	rs4731702	0.01
Obesity class 1	14.00	67.39	16.13	13.00	0.24	-0.04	0.02	0.08	NO	0.25
Obesity class 2	11.00	61.46	16.98	10.00	0.07	-0.08	0.03	0.02	NO	0.11
Testosterone levels	153.00	81.61	173.66	152.00	0.11	0.00	0.01	0.95	NO	0.11
Total Cholesterol	81.00	137.98	110.12	80.00	0.01	0.00	0.01	0.59	NO	0.02
Triglycerides	55.00	169.89	65.97	54.00	0.13	0.01	0.01	0.38	NO	0.15
Type 1 diabetes	36.00	NA	51.72	35.00	0.03	-0.01	0.01	0.24	NO	0.04
Type 2 diabetes	52.00	NA	60.56	51.00	0.17	0.01	0.01	0.47	NO	0.19
Trunk fat percentage	316.00	59.17	388.99	315.00	0.00	-0.01	0.01	0.22	rs957919	0.00
Waist circumference	37.00	50.57	48.35	36.00	0.08	-0.03	0.02	0.14	rs1516725	0.01
Waist-to-hip ratio	28.00	45.42	27.78	27.00	0.42	-0.04	0.03	0.14	NO	0.40
Weight	325.00	79.19	320.78	324.00	0.54	0.00	0.00	0.60	NO	0.55
Micronutrients										
25-Hydroxyvitamin D	102.00	113.03	122.41	101.00	0.07	0.01	0.01	0.03	NO	0.07
Vitamin D	76.00	133.61	97.70	75.00	0.04	0.00	0.01	0.50	NO	0.05
Calcium	204.00	101.29	214.01	203.00	0.28	0.00	0.00	0.29	NO	0.30
Iron	3.00	NA	0.83	2.00	0.66	0.02	0.04	0.68	NO	NA
Copper	2.00	NA	NA	NA	NA	NA	NA	NA	NO	NA
Esophageal diseases										
Barrett's esophagus	12.00	35.88	16.82	11.00	0.11	0.02	0.07	0.79	NO	0.24
Gastroesophageal reflux disease	66.00	38.95	80.79	65.00	0.09	-0.02	0.02	0.33	NO	0.09

Our study has identified several modifiable risk factors that contribute to an increased risk of EAC. These include habits like alcohol consumption, smoking, coffee consumption, and sedentary behavior (measured by television viewing duration). On the other hand, fruit consumption exhibited a potentially protective effect against the development of EAC. Fruit consumption exhibits a protective effect against EAC are consistent with prior studies that have emphasized the role of diet in cancer prevention. Mechanistically, fruits are rich sources of antioxidants, such as vitamins C and E, flavonoids, and carotenoids, which can neutralize reactive oxygen species and reduce oxidative stress—a key driver of carcinogenesis[8,21]. Additionally, fruits contain anti-inflammatory compounds that may mitigate chronic inflammation, a well-recognized precursor to EAC development. For instance, polyphenols in fruits have been shown to downregulate pro-inflammatory pathways, such as NF-κB signaling, which is frequently activated in EAC[3]. Furthermore, dietary fiber found in fruits contributes to gut microbiome health, promoting the production of short-chain fatty acids that exhibit anti-tumorigenic properties[22]. These multifaceted benefits underscore the biological plausibility of the protective role of fruit consumption in EAC prevention.

Moreover, our findings have not only confirmed previous large-scale cohort studies linking obesity to a significant increase in esophageal and gastric cancer incidence[1], but have also expanded upon these findings by establishing links between specific obesity traits (such as obesity class 1 and 2, trunk fat percentage, waist circumference, and waist-to-hip ratio) and an elevated risk of EAC. Obesity has long been recognized as an important factor in the pathogenesis of various cancers, including EAC, colorectal cancer, breast cancer, and endometrial cancer. The relationship between BMI and cancer is multifactorial, involving complex mechanisms such as chronic low-grade inflammation, hormonal dysregulation, and altered metabolic processes. One of the primary mechanisms through which obesity contributes to cancer risk is the pro-inflammatory state induced by excess adipose tissue. Adipocytes secrete a variety of pro-inflammatory cytokines, including interleukins, tumor necrosis factor-alpha, and leptin, which can promote chronic inflammation[1,10]. This chronic inflammatory environment facilitates cellular mutations, tumor initiation, and progression. These observations underscore the critical role of fat distribution and central obesity, beyond generalized body mass index, in influencing cancer susceptibility, likely through mechanisms involving systemic inflammation, hormonal dysregulation, and altered metabolic profiles. Additionally, we have identified a causal relationship between genetically predicted risk of EAC and type 1 diabetes, as well as serum iron levels. Elevated serum iron levels could exacerbate oxidative stress through the Fenton reaction, generating reactive oxygen species that damage DNA, proteins, and lipids[9,16]. Conversely, dysregulated iron homeostasis might impair cellular energy metabolism and immune responses, further promoting tumor initiation and progression[16]. These findings provide a compelling rationale for exploring iron modulation as a potential therapeutic or preventative strategy in high-risk populations.

Our work sheds light on a comprehensive range of risk factors associated with EAC. While these findings significantly contribute to understanding the etiology of EAC, several limitations must be acknowledged. First, in our present study, the participants analyzed were of European ancestry. Our findings for specific cancers might lack validation using multiple datasets. Consequently, caution must be exercised when extrapolating these findings to other populations, as it may introduce bias and limit the generalizability of the results. Additionally, despite employing robust statistical methods, such as MR Egger intercept tests, MR PRESSO global tests, and Cochran's Q tests, to identify and mitigate the effects of pleiotropy, it is not possible to entirely rule out residual pleiotropy in our analysis. Certain SNPs, such as rs429358 and rs543874, were identified as potential sources of pleiotropic effects, given their known associations with multiple phenotypes beyond the primary exposures studied. These findings emphasize the need for cautious interpretation of causal estimates, particularly for associations involving these SNPs. Further functional validation and investigations in diverse populations are necessary to confirm and extend our findings. Nonetheless, these results provide a valuable foundation for preventive measures, early detection, and targeted interventions to reduce the incidence of this disease.

Conclusion

Our work is to shed light on a comprehensive range of risk factors associated with EAC. These findings contribute to our understanding of the etiology of EAC and may have implications for preventive measures, early detection, and targeted interventions to reduce the incidence of this disease.

Acknowledgements

We appreciate the work of the open GWAS project (https://gwas.mrcieu.ac.uk/).

Authors' Contributions

Wenjie Li: Conceptualization, methodology, data curation, software and writing-review & editing, project administration, supervision and validation. The work reported in the paper has been performed by the authors, unless clearly specified in the text.

Conflict of Interest

The authors declare that the study was performed in the absence of the conflict of interest.

Consent for Publication

Not applicable.

Data Availability Statement

The original data are available in the open GWAS project

(https://gwas.mrcieu.ac.uk/).

Ethics Statement

No ethics approval and written consent were needed for the secondary analysis of public data.

Funding Sources

None.

Reference

[1] Avgerinos, K. I., Spyrou, N., Mantzoros, C. S., & Dalamaga, M. (2019, Mar). Obesity and cancer risk: Emerging biological mechanisms and perspectives. Metabolism, 92, 121-135. https://doi.org/10.1016/j.metabol.2018.11.001

[2] Burgess, S., & Labrecque, J. (2018). Mendelian randomization with a binary exposure variable: interpretation and presentation of causal estimates. European journal of epidemiology, 33(10), 947-952. https://doi.org/10.1007/s10654-018-0424-6

[3] Chen, L., Lu, H., Peng, D., Cao, L. L., Ballout, F., Srirmajayam, K., et al. (2023, Mar). Activation of NOTCH signaling via DLL1 is mediated by APE1-redox-dependent NF-κB activation in oesophageal adenocarcinoma. Gut, 72(3), 421-432. https://doi.org/10.1136/gutjnl-2022-327076

[4] Coleman, H. G., Xie, S.-H., & Lagergren, J. (2018, 2018/1//). The Epidemiology of Esophageal Adenocarcinoma. Gastroenterology, 154(2), 390-405. https://doi.org/10.1053/j.gastro.2017.07.046

[5] Global Burden of Disease Cancer, C., Kocarnik, J. M., Compton, K., Dean, F. E., Fu, W., Gaw, B. L., et al. (2022, 2022/3/1/). Cancer Incidence, Mortality, Years of Life Lost, Years Lived With Disability, and Disability-Adjusted Life Years for 29 Cancer Groups From 2010 to 2019: A Systematic Analysis for the Global Burden of Disease Study 2019. JAMA oncology, 8(3), 420-444. https://doi.org/10.1001/jamaoncol.2021.6987

[6] Innes, H., Nischalke, H. D., Guha, I. N., Weiss, K. H., Irving, W., Gotthardt, D., et al. (2022, May). The rs429358 Locus in Apolipoprotein E Is Associated With Hepatocellular Carcinoma in Patients With Cirrhosis. Hepatol Commun, 6(5), 1213-1226. https://doi.org/10.1002/hep4.1886

[7] Joseph, A., Raja, S., Kamath, S., Jang, S., Allende, D., McNamara, M., et al. (2022, May 2). Esophageal adenocarcinoma: A dire need for early detection and treatment. Cleve Clin J Med, 89(5), 269-279. https://doi.org/10.3949/ccjm.89a.21053

[8] Kashif, M., Yao, H., Schmidt, S., Chen, X., Truong, M., Tüksammel, E., et al. (2023, Apr). ROS-lowering doses of vitamins C and A accelerate malignant melanoma metastasis. Redox Biol, 60, 102619. https://doi.org/10.1016/j.redox.2023.102619

[9] Kawabata, T. (2022, Jul 8). Iron-Induced Oxidative Stress in Human Diseases. Cells, 11(14). https://doi.org/10.3390/cells11142152

[10] Lega, I. C., & Lipscombe, L. L. (2020, Feb 1). Review: Diabetes, Obesity, and Cancer-Pathophysiology and Clinical Implications. Endocr Rev, 41(1). https://doi.org/10.1210/endrev/bnz014

[11] Li, W., Wang, R., & Wang, W. (2022). Exploring the causality and pathogenesis of systemic lupus erythematosus in breast cancer based on Mendelian randomization and transcriptome data analyses. Front Immunol, 13, 1029884. https://doi.org/10.3389/fimmu.2022.1029884

[12] Mei, H., Yin, B., Yang, W., Zhang, J., Lu, H., Qi, X., et al. (2022). Associations between Gene-Gene Interaction and Overweight/Obesity of 12-Month-Old Chinese Infants. Biomed Res Int, 2022, 1499454. https://doi.org/10.1155/2022/1499454

[13] Nøst, T. H., Alcala, K., Urbarova, I., Byrne, K. S., Guida, F., Sandanger, T. M., et al. (2021, Aug). Systemic inflammation markers and cancer incidence in the UK Biobank. Eur J Epidemiol, 36(8), 841-848. https://doi.org/10.1007/s10654-021-00752-6

[14] Peng, H., Wu, X., Wen, Y., Du, X., Li, C., Liang, H., et al. (2021, 2021/4//). Age at first birth and lung cancer: a two-sample Mendelian randomization study. Translational lung cancer research, 10(4), 1720-1733. https://doi.org/10.21037/tlcr-20-1216

[15] Pisanu, C., Williams, M. J., Ciuculete, D. M., Olivo, G., Del Zompo, M., Squassina, A., et al. (2019, Nov 21). Evidence that genes involved in hedgehog signaling are associated with both bipolar disorder and high BMI. Transl Psychiatry, 9(1), 315. https://doi.org/10.1038/s41398-019-0652-x

[16] Qin, M., Shao, B., Lin, L., Zhang, Z. Q., Sheng, Z. G., Qin, L., et al. (2023, Jan). Molecular mechanism of the unusual biphasic effects of the natural compound hinokitiol on iron-induced cellular DNA damage. Free Radic Biol Med, 194, 163-171. https://doi.org/10.1016/j.freeradbiomed.2022.11.042

[17] Rajendra, S., Sharma, P., Gautam, S. D., Saxena, M., Kapur, A., Sharma, P., et al. (2020, Feb 5). Association of Biomarkers for Human Papillomavirus With Survival Among Adults With Barrett High-grade Dysplasia and Esophageal Adenocarcinoma. JAMA Netw Open, 3(2), e1921189. https://doi.org/10.1001/jamanetworkopen.2019.21189

[18] Redston, M., Noffsinger, A., Kim, A., Akarca, F. G., Rara, M., Stapleton, D., et al. (2022, Feb). Abnormal TP53 Predicts Risk of Progression in Patients With Barrett's Esophagus Regardless of a Diagnosis of Dysplasia. Gastroenterology, 162(2), 468-481. https://doi.org/10.1053/j.gastro.2021.10.038

[19] Sekula, P., Del Greco M, F., Pattaro, C., & Köttgen, A. (2016, 2016/11//). Mendelian Randomization as an Approach to Assess Causality Using Observational Data. Journal of the American Society of Nephrology, 27(11), 3253-3265. https://doi.org/10.1681/ASN.2016010098

[20] Siegel, R. L., Miller, K. D., & Jemal, A. (2020, Jan). Cancer statistics, 2020. CA Cancer J Clin, 70(1), 7-30. https://doi.org/10.3322/caac.21590

[21] Su, X., Shen, Z., Yang, Q., Sui, F., Pu, J., Ma, J., et al. (2019). Vitamin C kills thyroid cancer cells through ROS-dependent inhibition of MAPK/ERK and PI3K/AKT pathways via distinct mechanisms. Theranostics, 9(15), 4461-4473. https://doi.org/10.7150/thno.35219

[22] Tanes, C., Bittinger, K., Gao, Y., Friedman, E. S., Nessel, L., Paladhi, U. R., et al. (2021, Mar 10). Role of dietary

fiber in the recovery of the human gut microbiome and its metabolome. Cell Host Microbe, 29(3), 394-407.e395. https://doi.org/10.1016/j.chom.2020.12.012

[23] Telomeres Mendelian Randomization, C., Haycock, P. C., Burgess, S., Nounu, A., Zheng, J., Okoli, G. N., et al. (2017, 2017/5/1/). Association Between Telomere Length and Risk of Cancer and Non-Neoplastic Diseases: A Mendelian Randomization Study. JAMA oncology, 3(5), 636-651. https://doi.org/10.1001/jamaoncol.2016.5945

Research Article Life Conflux

Sphingomyelin mediates the association between natural killer cell receptor 2B4 (CD244) and head and neck cancer

Authors

Boxuan Han, Shaokun Liu

Correspondence

lsk8870@163.com (S. Liu)

Graphical Abstract

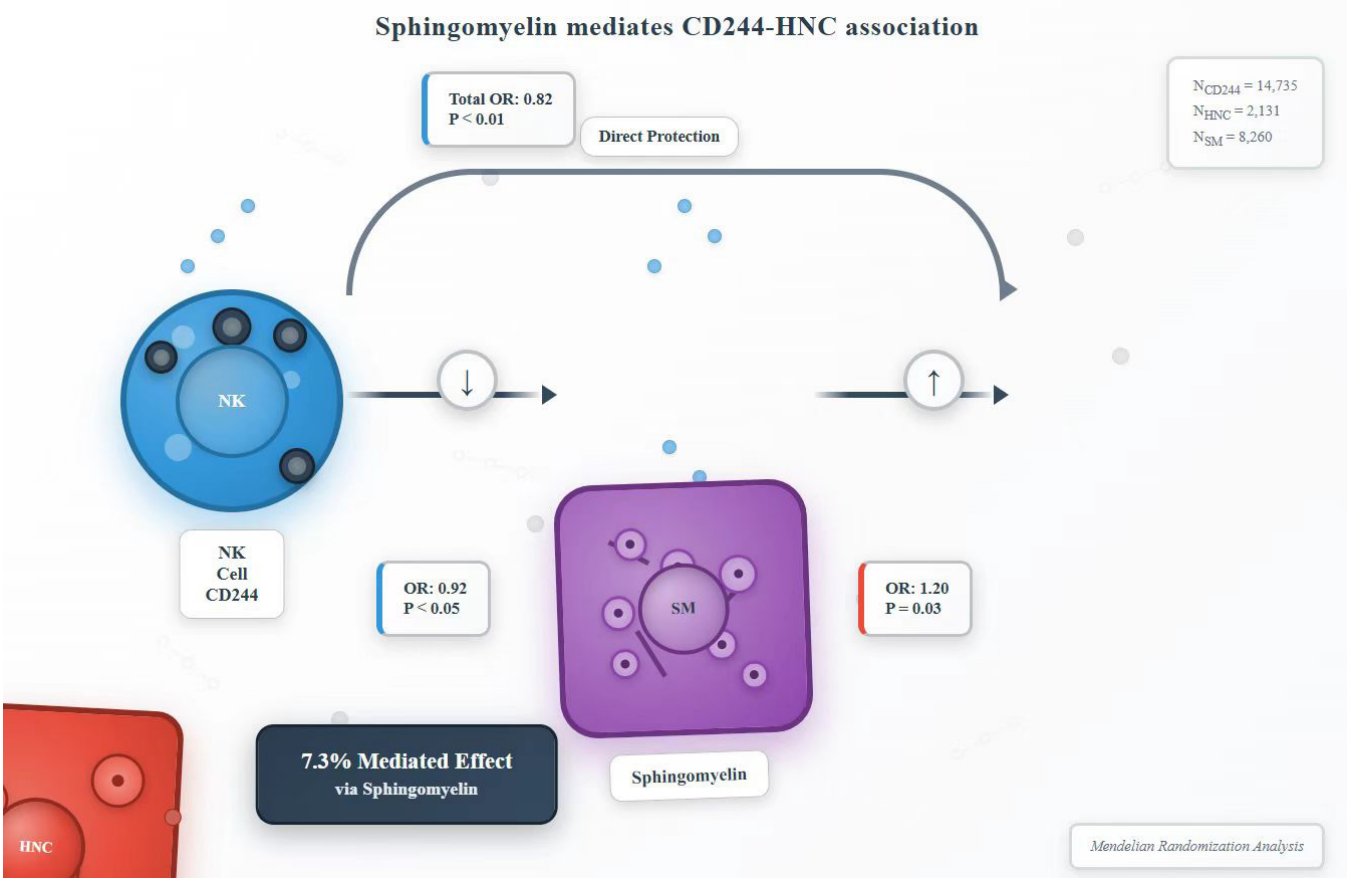

https://doi.org/10.71321/cdx1k098

Research Article Life Conflux

Sphingomyelin mediates the association between natural killer cell receptor 2B4 (CD244) and head and neck cancer

Boxuan Han[1], Shaokun Liu [2*]

Received: 2025-01-30 | Accepted: 2025-02-23 | Published online: 2025-03-30

Abstract

Objective: To investigate the causal link between natural killer (NK) cell receptor CD244 and head and neck cancer (HNC), and to evaluate sphingomyelin (SM) as a potential mediator of this relationship.

Methods: A two-sample Mendelian randomization (MR) analysis was conducted using genome-wide association study (GWAS) summary statistics from European cohorts (NCD244=14,735; NHNC=2,131; NSM=8,260). Instrumental variables (32 SNPs for CD244, 79 SNPs for HNC) were selected at genome-wide significance ($P<5\times10^{-8}$ /5×10^{-6}) after rigorous linkage disequilibrium clumping. Causal estimates were generated using inverse variance weighting (IVW), MR-Egger, and weighted median methods. Mediation analysis quantified SM's contribution to CD244-HNC associations.

Results: Genetically predicted CD244 levels showed a protective effect against HNC (IVW OR=0.82 per SD, 95% CI:0.71-0.94, P<0.01), while elevated CD244 was associated with reduced SM levels (IVW OR=0.92, 95% CI:0.86-0.98, P<0.05). Conversely, SM demonstrated risk-enhancing effects on HNC (IVW OR=1.20, 95% CI:1.01-1.41, P=0.03). Mediation analysis revealed that SM accounted for 7.3% of the total CD244-associated HNC risk.

Conclusion: This study establishes a causal protective role of CD244 in HNC pathogenesis, partially mediated through SM. The findings highlight CD244 and SM metabolism as potential targets for HNC immunomodulatory therapies. Future research should validate these mechanisms in diverse populations and explore additional mediators.

Keywords: NK cell; CD244; Head and Neck Cancer, Sphingomyelin; Mendelian Randomization

Introduction

Natural Killer (NK) cells are a type of cytotoxic lymphocyte that play a significant role in the innate immune system. These cells can recognize and eliminate infected cells as well as cancerous cells without prior sensitization or activation [1].

The receptor 2B4 (also known as CD244) is a protein found on the surface of NK cells. It belongs to the signaling lymphocytic activation molecule (SLAM) family of receptors [2]. It serves as a co-stimulatory molecule, contributing to NK cell activation and cytotoxicity when engaged [3–5]. The interaction of CD244 with its ligands on target cells or other immune cells helps regulate NK cell-mediated cytotoxicity and can influence the immune response against infections and tumors [6,7]. Dysfunction or alterations in CD244 signaling might impact the activity of NK cells and consequently affect immune responses and disease outcomes [8–10].

Head and neck carcinoma (HNC) is a type of cancer that primarily affects the oral cavity, sinonasal cavity, pharynx, and larynx [11]. It ranks about sixth in terms of incidence and mortality rate worldwide, with approximately 800,000 new cases and 44,000 deaths reported annually [12]. Current diagnostic methods for HNC include physical examination, endoscopic examination, imaging examination, biopsy, and tumor biomarker detection [13]. However, these methods have their limitations. For example, the sensitivity of visual examination of the mouth for detecting oral precancerous and cancerous lesions varies, and when the affected area is not easily accessible, the accuracy may be lower [14]. This challenge also applies to tissue biopsy. Therefore, there is a need for alternative diagnostic approaches and Therapeutic target.

Sphingomyelin (SM) is a type of lipid molecule that belongs to the class of phospholipids and is an essential component of cell membranes. It consists of a sphingosine backbone linked to phosphorylcholine, forming a molecule that plays a crucial role in the structure and function of cell membranes. It plays significant roles in cell signaling, maintaining membrane integrity, and is particularly important in the nervous system as a major component of neuronal membranes [15].

Mendelian Randomization (MR) is a causal inference method that utilizes genetic variation as an instrumental variable

1. Department of Otorhinolaryngology Head and Neck Surgery, Beijing Tongren Hospital, Capital Medical University, Beijing 100730, China

2. Department of Radiooncology and Radiotherapy, Charité - Universitätsmedizin Berlin, Corporate Member of Freie Universität Berlin and Humboldt-Universität zu Berlin, Charitéplatz 1, 10117, Berlin, Germany.

* Corresponding Author.

to assess the impact of exposure factors on outcomes in observational data. This ensures a relatively low correlation between the exposure variable and other potential confounding factors, thereby enhancing the credibility of causal inference. Simultaneously, MR helps to avoid reverse causality, as genetic variations typically precede exposure factors, reducing the likelihood of reverse causation [16]. The study aims to ascertain whether there is a causal relationship between CD244 and HNC, and to evaluate the extent to which the effects of CD244 on HNC are mediated by sphingomyelin.

Methods

Study design

The data utilized in our analysis were sourced from publicly available datasets and received approval from the institutional review committee in the respective studies. Consequently, no additional sanctions were required. All outcomes derived from this analysis are comprehensively outlined in the main article and its supplementary materials.

In this research, we explored the bidirectional causal relationship between CD244 and HNC through a two-sample MR approach. In our investigation, single nucleotide polymorphisms (SNPs) were identified as instrumental variables (IVs) [17].

GWAS summary data sources

All the data employed in our research were sourced from publicly accessible datasets, and the individuals included in the Genome-Wide Association Study (GWAS) belonged to European ancestry.

The genetic correlations related to CD244 levels were extracted from a GWAS meta-analysis conducted by Zhao and collaborators, encompassing a total of 14,735 participants (https://www.ebi.ac.uk/gwas/studies/GCST90274771) [18].

We obtained summary statistics for HNC from the FinnGen research project (https://www.finngen.fi/en). The research project conducted a GWAS involving 2,131 individuals of Finnish descent, with a gender distribution of 1,466 males and 665 females [19].

Sphingomyelin level summary statistics were extracted from a study conducted by Chen and collaborators [20], involving 8,260 unrelated individuals of European descent. The original publication detailed the study design, encompassing sample collection, quality control protocols, and imputation techniques. The GWAS data originated from separate consortia or organizations, ensuring the absence of sample overlap.

Instrumental variable selection and data harmonization

We incorporated SNPs that achieved genome-wide significance ($P < 5 \times 10^{-8}$). In cases where no SNPs met the criteria for genome-wide significance as instrumental variables (IVs), SNPs with significance levels below the genome-wide threshold ($P < 5 \times 10^{-6}$) were considered as potential IVs. Subsequently, these SNPs underwent clustering based on linkage disequilibrium (with a window size of 10,000 kb and $r^2 < 0.001$). The estimation of linkage disequilibrium levels was derived from European samples within the 1000 Genomes Project [21]. If a particular SNP associated with the exposure was not present in the outcome dataset, proxy SNPs were employed using LD tagging. Palindromic and ambiguous SNPs were excluded from the instrumental variables utilized in the Mendelian randomization analysis [22].

Statistical analysis

We conducted MR analysis using the R software (version 4.2.0, http://www.r-project.org).

To assess the causal relationship between CD244 levels and HNC, we employed various statistical methods, including inverse variance weighting (IVW) [23], weighted median-based [24] and mode-based methods [25]. These analyses were predominantly conducted using the 'Mendelian-Randomization' package (version 0.4.3) [26].

Cochran's Q statistic and corresponding p values were employed to examine the heterogeneity among the chosen instrumental variables (IVs). In case the null hypothesis is rejected, the random effects Inverse Variance Weighting (IVW) method was employed instead of the fixed-effects IVW [23]. To address the influence of horizontal pleiotropy, a widely used approach known as MR-Egger was employed. The utilization of MR-Egger indicates the potential existence of horizontal multiplicity, particularly if the intercept term is found to be significant [27]. Furthermore, we employed the MR-PRESSO method, a resilient approach, to detect and remove potential horizontal pleiotropic outliers that could have a substantial impact on the estimation results within the MR-PRESSO package [28]. In addition, we utilized scatter plots and funnel plots in our analysis. The scatter plots demonstrated the resilience of outcomes to outliers, while the funnel plots illustrated the robustness of the correlation and the absence of heterogeneity.

Primary analysis

Figure 1 provides a schematic overview of the analysis. A two-sample bidirectional MR was conducted to examine the reciprocal causation between CD244 levels and HNC, as illustrated in Figure 1A. This analysis focused on determining the total effects.

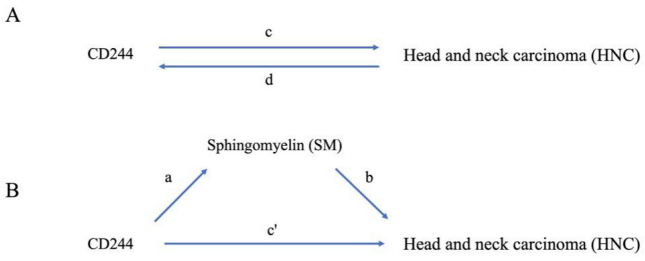

Figure 1 Illustrations in this study depict the associations under investigation. In (**A**), the total effect between CD244 and head and neck carcinoma (HNC) are presented. "c" represents the total effect utilizing genetically predicted CD244 as the exposure and HNC as the outcome, while "d" depicts the total effect using genetically predicted HNC as the exposure and CD244 as the outcome. Moving to (**B**), the total effect is further dissected into two components: (i) the indirect effect employing a two-step approach (where "a" denotes the total effect of CD244 on SM, and "b" signifies the effect of SM on HNC) and the product method (a × b), and (ii) the direct effect (c' = c − a × b). The proportion mediated is calculated by dividing the indirect effect by the total effect.

Inverse variance weighting (IVW) employs meta-analysis to amalgamate the Wald ratios of causal effects associated with each individual SNP [22,29]. Then, MR-Egger [27] and weighted-median [24] methods were employed as supplementary analyses to complement the Inverse Variance Weighting (IVW) method. Various methods, aligned with different validity assumptions, have been employed to derive MR estimates. The utilization of the Inverse Variance Weighting (IVW) method is contingent upon the assumption that all Single Nucleotide Polymorphisms (SNPs) serve as valid instrumental variables. Hence, this approach has the potential to generate precise estimation outcomes. MR-Egger evaluates directional pleiotropy concerning instrumental variables, with the intercept serving as an estimate of the average pleiotropy associated with genetic variation. The weighted median method offers the benefit of retaining greater precision, indicated by a smaller standard deviation, in comparison to MR-Egger analysis. In situations involving horizontal pleiotropy, the weighted median consistently yields estimates, maintaining accuracy even when 50% of the genetic variants are deemed invalid instrumental variables [30].

Mediation analysis

We performed a mediation analysis using a two-step MR design to explore the potential mediation role of sphingomyelin levels in the causal pathway from CD244 levels to the occurrence of HNC (Figure 1B). The total effect can be broken down into an indirect effect, which operates through mediators, and a direct effect, which occurs independently of any mediators [31]. The overall influence of CD244 levels on HNC was dissected into two components: 1) the direct effects of CD244 levels on HNC (represented as c' in Figure 1B) and 2) the indirect effects mediated by CD244 through an intermediary (expressed as a × b in Figure 1B). The proportion mediated by the intermediary effect was determined by dividing the indirect effect by the total effect.

Results

Association of CD244 levels with HNC

After the exclusion of palindromic and ambiguous SNPs, along with SNPs lacking proxies and those exhibiting incorrect causal directions flagged by MR Steiger filtering, a total of 32 SNPs were found to be linked with CD244 levels. Additionally, 79 SNPs associated with HNC were identified and utilized as instrumental variables (refer to Supplementary Tables S1).

We utilized IVW, MR-Egger, and weighted median regression techniques to estimate the causal association between CD244 levels and HNC, as illustrated in Figures 2 and 3. Among the three statistical methods, two of them supported the negative association of CD244 levels with HNC (IVW odds ratio [OR] per SD increase in CD244 levels = 0.82 [95% CI, 0.71-0.94], P < 0.01; MR-Egger OR per SD increase in CD244 levels = 0.72 [95% CI, 0.55-0.95], P < 0.05). Nevertheless, our MR analysis did not uncover any indications of reverse causation concerning genetically predicted CD244 levels and HNC. In other words, there is no evidence suggesting a causal relationship where HNC influences CD244 levels. The odds ratio (OR) calculated through the Inverse Variance Weighting (IVW) method was 0.99 [95% CI, 0.97-1.01; p = 0.37], as illustrated in Figure 3.

Association of CD244 levels with SM

We successfully identified 32 instrumental variables with genome-wide significance. This accomplishment involved the exclusion of palindromic and ambiguous SNPs, along with SNPs lacking proxies and those flagged by MR Steiger filtering for being in the incorrect causal direction. Based on the analyses conducted using the IVW, MR–Egger, and weighted median methods, it was observed that CD244 levels exhibited a negative correlation with the risk of sphingomyelin (IVW method, odds ratio 0.92; [95% CI, 0.86-0.98], P < 0.05). The findings are visually represented in Figure 3.

Association of sphingomyelin with HNC

We have identified and presented all genetic instruments linked to SM at the genome-wide significance level ($P < 5 \times 10^{-8}$). In Figure 3, the genetically predicted levels of sphingomyelin showed a positive correlation with HNC [OR=1.20, 95% CI 1.01-1.41; P=0.03] when utilizing the IVW method.

Proportion of the association between CD244 levels and HNC mediated by SM

We conducted an analysis of SM as a mediator in the pathway connecting CD244 levels to HNC. The results of our study indicate a correlation between elevated CD244 levels and decreased SM, thereby leading to an increased risk of HNC. As depicted in Figure 4, our research illustrates that sphingomyelin accounted for 7.3% of the elevated HNC risk associated with CD244 levels.

Sensitivity analysis

Several sensitivity analyses were implemented to explore and address the potential presence of pleiotropy in the causal estimates. The absence of heterogeneity or asymmetry among these SNPs in their causal relationship was revealed through Cochran's Q-test and funnel plot, as indicated in Supplementary Table S2 and Supplementary Figure S1. Our study utilized the MR-Egger intercept, indicating no signs of pleiotropy at the directional level of the CD244 levels instrument, as presented in Supplementary Table S2. Horizontal pleiotropy was not observed based on the MR-PRESSO global test, as detailed in Supplementary Table S2. The impact of each SNP on the overall causal estimates was validated through leave-one-out analysis, as depicted in Supplementary Figure S2. Following the exclusion of each SNP, a comprehensive reevaluation of the MR analysis for the remaining SNPs was undertaken. The results consistently upheld the significance of the causal relationship, underscoring the pivotal role of all SNPs in establishing its importance.

Discussion

Recent studies [32,33] have explored the correlation between CD244 and HNC. However, existing evidence relies predominantly on observational studies, potentially susceptible to the influence of confounding factors. Our study sought to elucidate the causal relationship between CD244 and HNC. Employing MR analysis, we examined the link between CD244 and HNC using available GWAS data, aiming to determine whether the observed causal relationship involves mediation through SM. Our findings indicate that CD244 is associated

Figure 2 Forest plot to visualize causal effect of each single SNP on total HNC risk.

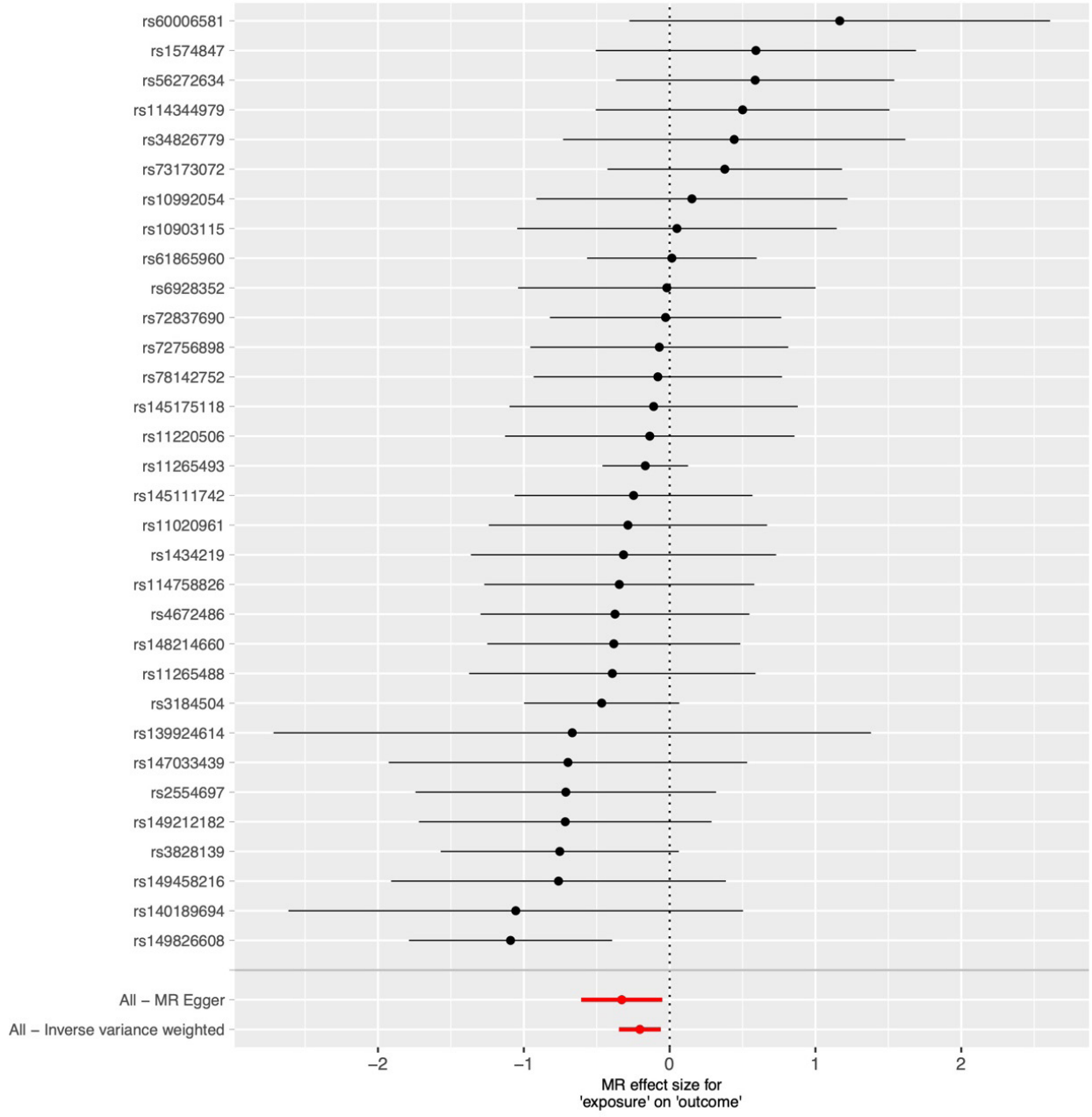

Figure 3 Forest plot to visualize the causal effects of SM with CD244 and HNC.

exposure	MR.method	nsnp	pval	forest	or_lci95	or_uci95	OR(95%CI)
CD244 on HNC	MR Egger	32	0.027710897		0.5450521	0.9509987	0.72(0.55 to 0.95)
CD244 on HNC	Weighted median	32	0.143246216		0.6700240	1.0597505	0.84(0.67 to 1.06)
CD244 on HNC	Inverse variance weighted	32	0.005271927		0.7061043	0.9410087	0.82(0.71 to 0.94)
HNC on CD244	MR Egger	79	0.570123144		0.9786348	1.0401065	1.01(0.98 to 1.04)
HNC on CD244	Weighted median	79	0.643054905		0.9680119	1.0202797	0.99(0.97 to 1.02)
HNC on CD244	Inverse variance weighted	79	0.368217378		0.9749184	1.0094612	0.99(0.97 to 1.01)
CD244 on SM	MR Egger	32	0.213310159		0.8045684	1.0474170	0.92(0.80 to 1.05)
CD244 on SM	Weighted median	32	0.477592180		0.8687693	1.0680626	0.96(0.87 to 1.07)
CD244 on SM	Inverse variance weighted	32	0.011121097		0.8635056	0.9812942	0.92(0.86 to 0.98)
SM on HNC	MR Egger	30	0.499984810		0.7966587	1.6011270	1.13(0.80 to 1.60)
SM on HNC	Weighted median	30	0.054855404		0.9952498	1.5874035	1.26(1.00 to 1.59)
SM on HNC	Inverse variance weighted	30	0.033926843		1.0136717	1.4110363	1.20(1.01 to 1.41)

P<0.05 was considered statistically significant

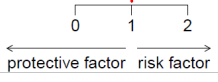

Figure 4 Schematic diagram of the SM mediation effect.

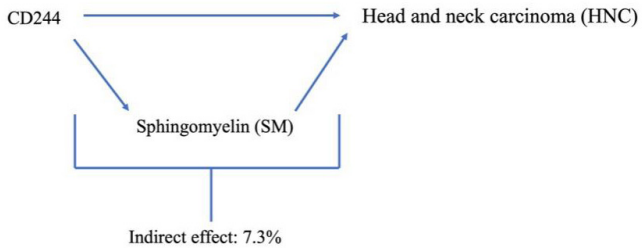

with a reduced risk of HNC (an 18% decrease in HNC risk for every 1 standard deviation increase in CD244). Furthermore, our analysis suggests that 7.3% of this effect is mediated through SM.

We are pioneering the exploration of the causal association between CD244 and the susceptibility to HNC through MR techniques. Additionally, we provide evidence showcasing SM as a mediator in this relationship. Our results align with previous observations derived from conventional observational approaches. As part of the SLAM family, 2B4, when binding with its ligand CD48, exhibits dual functionalities involving both activation and inhibition. Notably, 2B4 plays a crucial regulatory role in conditions such as malignant tumors, chronic viral infections, and autoimmune disorders [34]. Altavater et al. discovered that the 2B4 receptor plays a powerful role as a costimulatory factor in NK cells. By integrating the internal domain of 2B4 into chimeric receptors with T-cell receptor zeta, they observed a substantial improvement in various facets of NK cell activation when encountering leukemia or neuroblastoma cells expressing antigens. This improvement includes heightened lysosome release, enhanced growth inhibition, and the successful overcoming of NK cell resistance in autologous leukemia cells, all while preserving antigen specificity [35]. In contrast, Agresta et al. observed a correlation between elevated CD244 expression and PD-L1 expression, as well as heightened spontaneous expression of immune-suppressive mediators, in a study focused on head and neck squamous cell cancer (HNSCC) [36]. Moreover, their findings indicated that mice lacking CD244 (CD244-/-) exhibited significantly impaired tumor growth in the context of HNSCC. When wild-type (WT) mice were subjected to interventional treatment with an anti-CD244 monoclonal antibody, there was a notable reduction in the growth of established HNC tumors, accompanied by an increase in tumor-infiltrating CD8+ T cells.

The findings from our analysis demonstrate a positive association between SM and HNC. This conclusion is substantiated by a study conducted by Wang et al. [37]. The correlation between disease progression and the concentrations of SM 42:2 and SM 42:3 was identified, suggesting their potential utility as biomarkers for diagnosing laryngeal cancer. In contrast, Zheng et al. observed a distinctive phenotype in intratumoral NK cells characterized by a smooth and rounded appearance, deviating from the typical villi-rich, rough surface of normal NK cells. This unique phenotype was associated with a specific deficiency in membrane sphingomyelin lipids, leading to an impairment in the ability to kill tumor cells [38].

The SLAM-family receptors, including CD244, have a substantial impact on various biological processes, such as cytotoxicity, humoral immune responses, autoimmune diseases, lymphocyte development, cell survival, and cell adhesion. Growing evidence suggests their involvement in cancer progression, positioning them as emerging immune checkpoints on T cells [39]. Additionally, the SM metabolic pathway has gained recognition as a novel therapeutic target. A recent study demonstrated the use of anti-angiogenic drugs to enhance chemotherapy sensitivity in tumors by specifically targeting SM [40].

This study is subject to several limitations. Firstly, the analysis was conducted using data exclusively from the European population, which restricts the generalizability of our findings. Secondly, the limited number of HNC cases in the GWAS dataset presents a constraint; we anticipate that larger GWAS datasets will become available for future validation. Thirdly, despite efforts to identify and eliminate outlier variants, we cannot entirely rule out the potential impact of horizontal pleiotropy on our results. Fourthly, our study relied on summary-level statistics rather than individual-level data, preventing further exploration of causal relationships within subgroups, such as females and males. Additionally, our findings suggest a relatively low genetic prediction of CD244 mediated by SM, standing at only 7.3%. Consequently, further research is imperative to quantify additional mediators.

Conclusion

In summary, our research established a causal link between CD244 and HNC. While a minor portion of the impact is mediated by SM, the predominant influence of CD244 on HNC remains ambiguous. Additional investigations are warranted to delve into other potential risk factors that may act as mediators in this relationship.

Abbreviations

Abbreviation	Full Term
NK	Natural Killer cells
CD244	Cluster of Differentiation 244 (2B4)
SLAM	Signaling lymphocytic activation molecule
HNC	Head and neck cancer
HNSCC	Head and neck squamous cell carcinoma
SM	Sphingomyelin
MR	Mendelian randomization
GWAS	Genome-wide association study
SNP	Single nucleotide polymorphism
IVW	Inverse variance weighting
IVs	Instrumental variables
OR	Odds ratio
CI	Confidence interval
WT	Wild-type

Acknowledgments

I would like to thank Dr. Shaokun Liu for his guidance and support throughout this research.

Author Contributions

BH and SL conceived and designed the study. BH analyzed data and wrote the manuscript. SL reviewed the paper. Both authors read and approved the final manuscript.

Funding

None.

Conflict of Interest

The authors declare that the research was conducted in the absence of any commercial or financial relationships that could be construed as a potential conflict of interest.

Data Availability

The genetic data of circulating inflammatory proteins and plasma metabolites used in this article are derived from two studies published in Nature (doi:10.1038/s41590-023-01588-w and 10.1038/s41588-022-01270-1). The genetic data of HNC (Head and Neck Cancer) patients are sourced from the Finngen database, with detailed descriptions available in the Materials section.

References

[1] Nersesian S, Carter EB, Lee SN, Westhaver LP, Boudreau JE. Killer instincts: natural killer cells as multifactorial cancer immunotherapy. Front Immunol. 2023 Nov 28;14:1269614. https://doi.org/10.3389/fimmu.2023.1269614

[2] Mathew SO, Rao KK, Kim JR, Bambard ND, Mathew PA. Functional role of human NK cell receptor 2B4 (CD244) isoforms. Eur J Immunol. 2009 Jun;39(6):1632-41. https://doi.org/10.1002/eji.200838733

[3] Veillette A, Latour S. The SLAM family of immune-cell receptors. Curr Opin Immunol. 2003 Jun;15(3):277-85. https://doi.org/10.1016/s0952-7915(03)00041-4.

[4] Brown MH, Boles K, van der Merwe PA, Kumar V, Mathew PA, Barclay AN. 2B4, the natural killer and T cell immunoglobulin superfamily surface protein, is a ligand for CD48. J Exp Med. 1998 Dec 7;188(11):2083-90. https://doi.org/10.1084/jem.188.11.2083

[5] Latchman Y, McKay PF, Reiser H. Identification of the 2B4 molecule as a counter-receptor for CD48. J Immunol. 1998 Dec 1;161(11):5809-12. https://doi.org/10.4049/jimmunol.161.11.5809

[6] Chuang SS, Kim MH, Johnson LA, Albertsson P, Kitson RP, Nannmark U, et al. 2B4 stimulation of YT cells induces natural killer cell cytolytic function and invasiveness. Immunology. 2000 Jul;100(3):378-83. https://doi.org/10.1046/j.1365-2567.2000.00031.x

[7] Mathew SO, Kumaresan PR, Lee JK, Huynh VT, Mathew PA. Mutational analysis of the human 2B4 (CD244)/CD48 interaction: Lys68 and Glu70 in the V domain of 2B4 are critical for CD48 binding and functional activation of NK cells. J Immunol. 2005 Jul 15;175(2):1005-13. https://doi.org/10.4049/jimmunol.175.2.1005

[8] Wu Y, Kuang DM, Pan WD, Wan YL, Lao XM, Wang D, et al. Monocyte/macrophage-elicited natural killer cell dysfunction in hepatocellular carcinoma is mediated by CD48/2B4 interactions. Hepatology. 2013 Mar;57(3):1107-16. https://doi.org/10.1002/hep.26192

[9] Pende D, Meazza R, Marcenaro S, Aricò M, Bottino C. 2B4 dysfunction in XLP1 NK cells: More than inability to control EBV infection. Clin Immunol. 2019 Jul;204:31-36. https://doi.org/10.1016/j.clim.2018.10.022

[10] Schlaphoff V, Lunemann S, Suneetha PV, Jaroszewicz J, Grabowski J, Dietz J, et al. Dual function of the NK cell receptor 2B4 (CD244) in the regulation of HCV-specific CD8+ T cells. PLoS Pathog. 2011 May;7(5):e1002045. https://doi.org/10.1371/journal.ppat.1002045

[11] Chow LQM. Head and Neck Cancer. N Engl J Med. 2020 Jan 2;382(1):60-72. https://doi.org/10.1056/NEJMra1715715

[12] Sung H, Ferlay J, Siegel RL, Laversanne M, Soerjomataram I, Jemal A, et al. Global Cancer Statistics 2020: GLOBOCAN Estimates of Incidence and Mortality Worldwide for 36 Cancers in 185 Countries. CA Cancer J Clin. 2021 May;71(3):209-249. https://doi.org/10.3322/caac.21660

[13] Rasheduzzaman M, Kulasinghe A, Dolcetti R, Kenny L, Johnson NW, Kolarich D, et al. Protein glycosylation in head and neck cancers: From diagnosis to treatment. Biochim Biophys Acta Rev Cancer. 2020 Dec;1874(2):188422. https://doi.org/10.1016/j.bbcan.2020.188422

[14] Mehanna H, Paleri V, West CM, Nutting C. Head and neck cancer--Part 1: Epidemiology, presentation, and prevention. BMJ. 2010 Sep 20;341:c4684. https://doi.org/10.1136/bmj.c4684

[15] Slotte JP. Biological functions of sphingomyelins. Prog Lipid Res. 2013 Oct;52(4):424-37. https://doi.org/10.1016/j.plipres.2013.05.001

[16] Emdin CA, Khera AV, Kathiresan S. Mendelian Randomization. JAMA. 2017 Nov 21;318(19):1925-1926. https://doi.org/10.1001/jama.2017.17219

[17] Davey Smith G, Hemani G. Mendelian randomization: genetic anchors for causal inference in epidemiological studies. Hum Mol Genet. 2014 Sep 15;23(R1):R89-98. https://doi.org/10.1093/hmg/ddu328

[18] Zhao JH, Stacey D, Eriksson N, Macdonald-Dunlop E, Hedman ÅK, Kalnapenkis A, et al. Genetics of circulating inflammatory proteins identifies drivers of immune-mediated disease risk and therapeutic targets. Nat Immunol. 2023 Sep;24(9):1540-1551. https://doi.org/10.1038/s41590-023-01588-w

[19] Kurki MI, Karjalainen J, Palta P, Sipilä TP, Kristiansson K, Donner KM, et al. FinnGen provides genetic insights

from a well-phenotyped isolated population. Nature. 2023 Jan;613(7944):508-518. https://doi.org/10.1038/s41586-022-05473-8
[20] Chen Y, Lu T, Pettersson-Kymmer U, Stewart ID, Butler-Laporte G, Nakanishi T, et al. Genomic atlas of the plasma metabolome prioritizes metabolites implicated in human diseases. Nat Genet. 2023 Jan;55(1):44-53. https://doi.org/10.1038/s41588-022-01270-1
[21] 1000 Genomes Project Consortium, Abecasis GR, Altshuler D, Auton A, Brooks LD, Durbin RM, et al. A map of human genome variation from population-scale sequencing. Nature. 2010 Oct 28;467(7319):1061-73. https://doi.org/10.1038/nature09534
[22] Hemani G, Zheng J, Elsworth B, Wade KH, Haberland V, Baird D, et al. The MR-Base platform supports systematic causal inference across the human phenome. Elife. 2018 May 30;7:e34408. https://doi.org/10.7554/eLife.34408
[23] Burgess S, Small DS, Thompson SG. A review of instrumental variable estimators for Mendelian randomization. Stat Methods Med Res. 2017 Oct;26(5):2333-2355. https://doi.org/10.1177/0962280215597579
[24] Bowden J, Davey Smith G, Haycock PC, Burgess S. Consistent Estimation in Mendelian Randomization with Some Invalid Instruments Using a Weighted Median Estimator. Genet Epidemiol. 2016 May;40(4):304-14. https://doi.org/10.1002/gepi.21965
[25] Hartwig FP, Davey Smith G, Bowden J. Robust inference in summary data Mendelian randomization via the zero modal pleiotropy assumption. Int J Epidemiol. 2017 Dec 1;46(6):1985-1998. https://doi.org/10.1093/ije/dyx102
[26] Yavorska OO, Burgess S. MendelianRandomization: an R package for performing Mendelian randomization analyses using summarized data. Int J Epidemiol. 2017 Dec 1;46(6):1734-1739. https://doi.org/10.1093/ije/dyx034
[27] Burgess S, Thompson SG. Interpreting findings from Mendelian randomization using the MR-Egger method. Eur J Epidemiol. 2017 May;32(5):377-389. https://doi.org/10.1007/s10654-017-0255-x
[28] Verbanck M, Chen CY, Neale B, Do R. Detection of widespread horizontal pleiotropy in causal relationships inferred from Mendelian randomization between complex traits and diseases. Nat Genet. 2018 May;50(5):693-698. https://doi.org/10.1038/s41588-018-0099-7
[29] Burgess S, Butterworth A, Thompson SG. Mendelian randomization analysis with multiple genetic variants using summarized data. Genet Epidemiol. 2013 Nov;37(7):658-65. https://doi.org/10.1002/gepi.21758
[30] Zhang Y, Liu Z, Choudhury T, Cornelis MC, Liu W. Habitual coffee intake and risk for nonalcoholic fatty liver disease: a two-sample Mendelian randomization study. Eur J Nutr. 2021 Jun;60(4):1761-1767. https://doi.org/10.1007/s00394-020-02369-z
[31] Carter AR, Sanderson E, Hammerton G, Richmond RC, Davey Smith G, Heron J, et al. Mendelian randomisation for mediation analysis: current methods and challenges for implementation. Eur J Epidemiol. 2021 May;36(5):465-478. https://doi.org/10.1007/s10654-021-00757-1
[32] Gao P, Lu W, Hu S, Zhao K. Differentially Infiltrated Identification of Novel Diagnostic Biomarkers Associated with Immune Infiltration in Nasopharyngeal Carcinoma. Dis Markers. 2022 Nov 17;2022:3934704. https://doi.org/10.1155/2022/3934704
[33] Tan L, Cheng D, Wen J, Huang K, Zhang Q. Identification of prognostic hypoxia-related genes signature on the tumor microenvironment in esophageal cancer. Math Biosci Eng. 2021 Sep 7;18(6):7743-7758. https://doi.org/10.3934/mbe.2021384
[34] Chiha J, Mitchell P, Gopinath B, Burlutsky G, Plant A, Kovoor P, et al. Prediction of Coronary Artery Disease Extent and Severity Using Pulse Wave Velocity. PLoS One. 2016 Dec 22;11(12):e0168598. https://doi.org/10.1371/journal.pone.0168598
[35] Altvater B, Landmeier S, Pscherer S, Temme J, Schweer K, Kailayangiri S, et al. 2B4 (CD244) signaling by recombinant antigen-specific chimeric receptors costimulates natural killer cell activation to leukemia and neuroblastoma cells. Clin Cancer Res. 2009 Aug 1;15(15):4857-66. https://doi.org/10.1158/1078-0432.CCR-08-2810
[36] Agresta L, Lehn M, Lampe K, Cantrell R, Hennies C, Szabo S, et al. CD244 represents a new therapeutic target in head and neck squamous cell carcinoma. J Immunother Cancer. 2020 Mar;8(1):e000245. https://doi.org/10.1136/jitc-2019-000245
[37] Wang H, Luo Y, Chen H, Hou H, Hu Q, Ji M. Non-Targeted Serum Lipidomics Analysis and Potential Biomarkers of Laryngeal Cancer Based on UHPLC-QTOF-MS. Metabolites. 2022 Nov 9;12(11):1087. https://doi.org/10.3390/metabo12111087
[38] Zheng X, Hou Z, Qian Y, Zhang Y, Cui Q, Wang X, et al. Tumors evade immune cytotoxicity by altering the surface topology of NK cells. Nat Immunol. 2023 May;24(5):802-813. https://doi.org/10.1038/s41590-023-01462-9
[39] Farhangnia P, Ghomi SM, Mollazadehghomi S, Nickho H, Akbarpour M, Delbandi AA. SLAM-family receptors come of age as a potential molecular target in cancer immunotherapy. Front Immunol. 2023 May 11;14:1174138. https://doi.org/10.3389/fimmu.2023.1174138
[40] Jacobi J, García-Barros M, Rao S, Rotolo JA, Thompson C, Mizrachi A, et al. Targeting acid sphingomyelinase with anti-angiogenic chemotherapy. Cell Signal. 2017 Jan;29:52-61. https://doi.org/10.1016/j.cellsig.2016.09.010

Research Article Life Conflux

Development and Validation of Nomogram for Predicting the Risk of Community-acquired Pneumonia after Kidney Transplantation of Deceased Donors

Authors

Dongsheng Li, Mo Yang, Ji Zhang, Jinbiao Zhong, Handong Ding, Wei Chen, Jiashan Pan, Guiyi Liao

Correspondence

pjs0510@126.com (J. Pan), liaoguiyi@ahmu.edu.cn (G. Liao)

Graphical Abstract

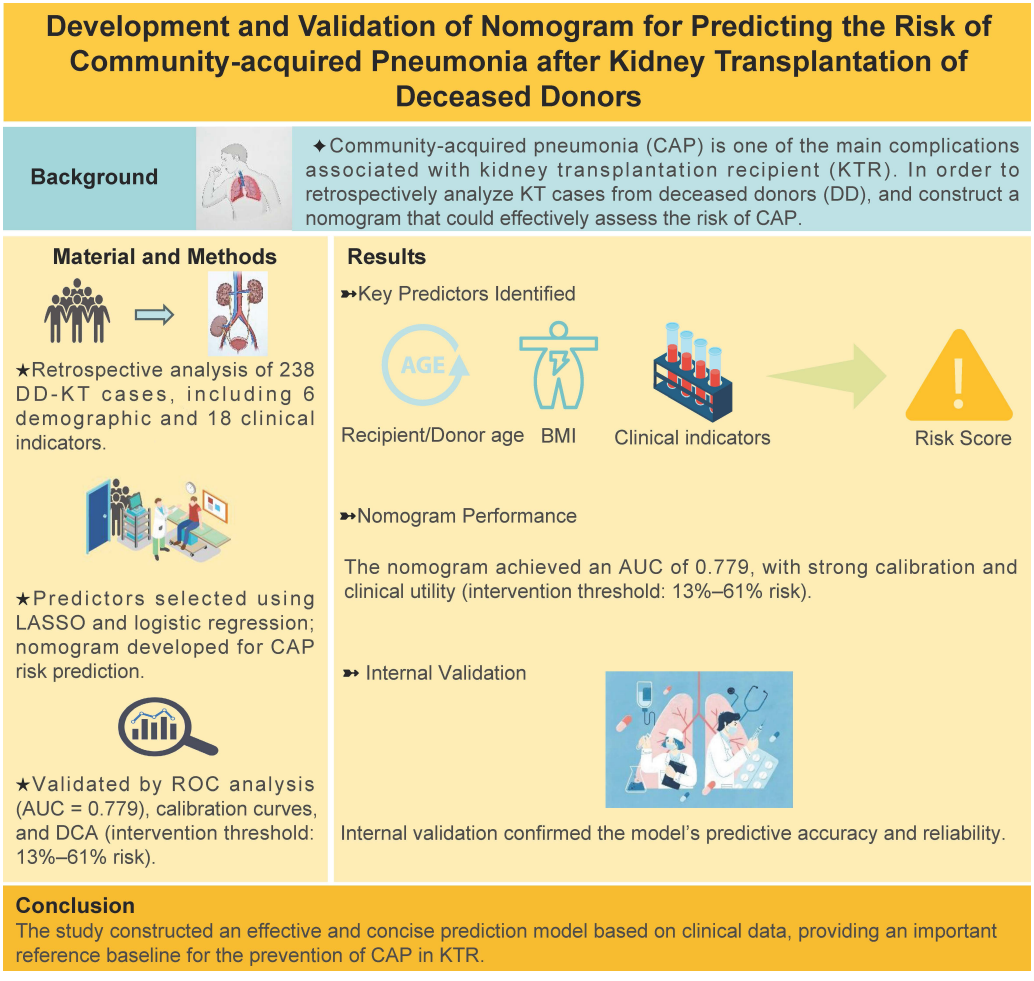

https://doi.org/10.71321/kbfm1398

Research Article

Life Conflux

Development and Validation of Nomogram for Predicting the Risk of Community-acquired Pneumonia after Kidney Transplantation of Deceased Donors

Dongsheng Li [1,2,3†], Mo Yang [1,2,3†], Ji Zhang [1,2,3†], Jinbiao Zhong [1,2,3], Handong Ding [1,2,3], Wei Chen [1,2,3], Jiashan Pan [1,2,3*], Guiyi Liao [1,2,3*]

Received: 2025-01-05 | Accepted: 2025-03-15 | Published online: 2025-03-30

Abstract

Background: Community-acquired pneumonia (CAP) is one of the main complications associated with kidney transplantation recipient (KTR). In order to retrospectively analyze KT cases from deceased donors (DD), and construct a nomogram that could effectively assess the risk of CAP.

Material and Methods: We employed logistic regression and the least absolute shrinkage and selection operator (LASSO) to identify predictors from 238 cases collected at Department of Urology, The First Affiliated Hospital of Anhui Medical University, between January 1, 2018, and May 31, 2023. The dataset comprised 6 demographic and 18 clinical indicators, which were used for training and validation. A nomogram was constructed using these predictors, and its effectiveness was evaluated through receiver operating characteristic (ROC) analysis, calibration curves, and clinical decision analysis. Internal validation further confirmed the model's predictive accuracy.

Results: The predictive factors screened in terms of demographic data included recipient/donor age and body mass index. The clinical data screened eight predictors to obtain 'RiskScore'. The Area under Curve value for the nomogram constructed using the aforementioned predictors was recorded to be 0.779. The calibration curve showed that the model exhibited better predictive performance. In particular, DCA showed that in cases where the probability for the prediction of CAP was 0.13–0.61, the clinical intervention was recommended. The internally verified data established a better predictive ability of the model.

Conclusion: The study constructed an effective and concise prediction model based on clinical data, providing an important reference baseline for the prevention of CAP in KTR.

Keywords: deceased donor; kidney transplantation; community-acquired pneumonia; nomogram; risk predictor

Introduction

For end-stage renal disease (ESRD), kidney transplantation (KT) is the preferred choice of treatment[1], primarily owing to its ability to improve survival and quality of life as compared to dialysis therapy[2, 3]. In recent years, there has been a steady increase in the number of transplants in China. However, results for clinical studies showed that the postoperative effect of DD was worse as compared to live KT[4], thereby presenting several challenges to postoperative clinical management. Among these, community-acquired pneumonia (CAP) is one the most common postoperative complication. Since the recipients are treated with immunosuppressive drugs following transplantation, for the entire life, the body's immune mechanism gets damaged. In fact, it is one of the main causes of death related to KT[5]. A large number of clinical studies previously reported several independent risk factors for postoperative CAP. In particular, to overcome the scarcity of kidney donor resources, several countries have successively expanded the criteria of donor age, however, this has also resulted in a significant increase in the probability of CAP[6]. Similarly, in a previous study conducted by Chen et al.[7], the advanced age of the recipient was identified as an important risk factor for CAP. In addition to this, Flavouris et al. reported that recipients with a body mass index (BMI) > 25kg/m^2 exhibited a significantly increased probability of postoperative infection and a shortened life span[8]. However, these risk factors were usually acquired after transplantation. In order to improve the quality of life for kidney transplant recipients and reduce the impact of diseases unrelated to the transplanted organ, such as CAP, it is imperative to develop a clinical model that can effectively predict CAP. By actively conducting research and collaborating with healthcare experts, our ultimate goal is to establish a robust clinical model that aids in forecasting CAP and effectively managing this vulnerability in the kidney transplant population. However,

1 Department of Urology, The First Affiliated Hospital of Anhui Medical University, Hefei, China

2 Institute of Urology, Anhui Medical University, Hefei, China

3 Anhui Province Key Laboratory of Urological and Andrological Diseases Research and Medical Transformation, Anhui Medical University, Hefei, China

† These authors have contributed equally to this work.

* Corresponding Author.

only a few studies have previously assessed the influence of preoperative clinical blood indexes of donors and recipients on the risk of CAP after surgery. The present study aimed to develop a nomogram that could effectively predict CAP based on preoperative demographic and clinical data (including both donors and recipients). Altogether, the findings of the study would assist the clinicians in the assessment of CAP risk in the recipients, and providing timely treatment.

Material and methods

Data collection and diagnostic criteria

The data on the recipients and their matched donors were collected from the Urology Kidney Transplant Ward of the First Affiliated Hospital of Anhui Medical University.. The recipient request was the first kidney transplant for organ donation after the death of a citizen. The operation time range is from January 1, 2018 to May 31, 2023. The data was collected through the inpatient system of the hospital and the Chinese Scientific Registry of Kidney Transplantation (CSRKT). The current study was approved by the Ethics Committee of the First Affiliated Hospital of Anhui Medical University. The database was divided into demographic data and clinical indicators of donors and recipients. Among them, donor-age (D-age), D-gender, D-BMI, recipient-age (R-age), R-gender, and R-BMI were included for 6 demographic variables. On the other hand, the clinical indicators included R-creatinine (R-Cr), R-alanine transaminase (R-ALT), R-aspartate transaminase (R-AST), R-recipient total bilirubin (R-TB), R-alkaline phosphatase (R-ALP), R-total protein (R-TP), R-Kalium (R-K^+), R-Natrium (R-Na^+), R-Chloride (R-Cl^-), dialysis time (DT), length of hospital stay (LHS), warm ischemia time (WIT), cold ischemia time (CIT), D-Na^+, D-K^+, D-TB, D-urea, and D-albumin (D-ALB), totaling 18 clinical indicators.

CAP diagnostic criteria: We referred to the CAP diagnostic criteria established by China's Infection Group, Respiratory Diseases Branch of Chinese Medical Association, and The 2007 CAP Guidelines of the American Society of Infectious Diseases/American Thoracic Society[9, 10]: 1 The clinical symptoms included cough, sputum expectoration, and fever (fever was generally persistent or intermittent low- or high-fever and the renal function test was normal); clinical signs: signs of pulmonary consolidation or (and) damp rales in the lungs. 2 Blood monitoring: Neutrophils, C-reactive protein, and pre-procalcitonin in the blood after transplantation served as the sensitive indicators to distinguish between bacterial and non-bacterial infections. 3 Imaging examination: Lung CT was mainly performed in our department. CAP showed new characteristic changes such as multifocal patchy infiltrating shadow, consolidation shadow of leaf or segment, ground-glass shadow, and irregular nodular shadow, with or without pleural effusion[11]. Pathogen detection: Oral, throat, sputum, and other sources specimens were regularly collected for cultivation for differential diagnosis. Plain CT scans formed the primary basis for the diagnosis of CAP. The appearance of 2 or 3 symptoms, together with the characteristic changes of 1 formed the basis for diagnosing CAP.

The follow-up endpoints were as follows: 1. The follow-up time was until June 30, 2023; 2. During the follow-up period, the endpoint of the observation was the loss of the graft or the death of the recipient.

Immunosuppressive regime

All patients received anti-thymocyte globulin as induction therapy and standard maintenance therapy. The postoperative immunosuppressive regimen involved prednisone acetate + mycophenolate mofetil (MMF) + tacrolimus. During KT and on the first and second days of surgery, 500 mg of methylprednisolone (BMI ≥50 kg) or 250 mg (BMI <50 kg) was used for pulse therapy, and, on the 3rd to 5th day of operation, 120, 80, and 40 mg were applied, respectively. Moreover, on the 6th day, the patient was changed to oral prednisone acetate (10 mg/day). Antithymocyte globulin (ATG) or basiliximab was not routinely used for immune induction. Oral MMF (1.0 g/day) was started on the first postoperative day, and tacrolimus (0.1 mg/kg/d) was routinely used on the second postoperative day. The usage was adjusted according to the blood concentration of MMF and controlling the area under the blood concentration-time curve of mycophenolic acid to 30-60 mg/h/L. The dosage was adjusted according to the trough value of the blood concentrations of tacrolimus; after 1, 2-3, 4-6, and after 6 months, the trough values of blood drug concentration were maintained at 10-15, 9-12, 7-10, and 4-8 ng/mL, respectively.

Statistical analyses

Statistical data analysis and visualization were performed using the R software (Version 4.0.3; https://www.R-project.org). The only exception was the Kaplan–Meier (K-M) curves (for mapping the survival of recipients after KT), which were created using the GraphPad Prism 8.0. In our analysis, the tables were prepared with Microsoft® Word 2019.

First, all collected data were continuous variables. The four variables donor age, BMI value, recipient age, and BMI value in the demographics were screened out for predictors with $P < 0.05$ through logistic regression analysis. Best-separation and logistic regression helped screen 18 clinical data points to determine the best cut-off value, P-value, odds ratio (OR), and area under the curve (AUC) under the receiver operating characteristic (ROC) curve; $P < 0.05$ were selected to convert these predictors into binary variables. Then, the variables selected from the clinical data were added to the least absolute shrinkage and selection operator (LASSO) algorithm to select the final predictor[12-14]. Then, the selected predictors in the clinical data were combined into the RiskScore (RiskScore was obtained by adding the coefficients of each predictor selected by the LASSO algorithm). Finally, the RiskScore and the selected demographic predictors were used to jointly construct a nomogram for predicting CAP. In terms of model verification, the AUC value under the ROC was used to verify the sensitivity and specificity of the nomogram. Although the model wasn't fully calibrated per the significance test, its clinical usefulness was considered through decision curve analysis (DCA) [15, 16]. In addition, the CAP nomogram underwent bootstrapping verification (1,000 bootstrap resampling) to calculate the relative corrected AUC value. Each group was divided into a training group and a verification group at the ratio of 5:5. The 5:5 ratio for dividing the training and validation sets was intentionally chosen to ensure an equal distribution of data for both model development and evaluation. This approach allows for a more balanced assessment of the model's performance,

particularly in smaller datasets, by providing sufficient data for both training and validation phases. Each group provides the AUC value, false-positive rate, and true positive rate, among others. The entire workflow is illustrated in Figure 1.

Figure 1. Flow chart of the prediction model of community-acquired pneumonia after KT from the deceased donors.

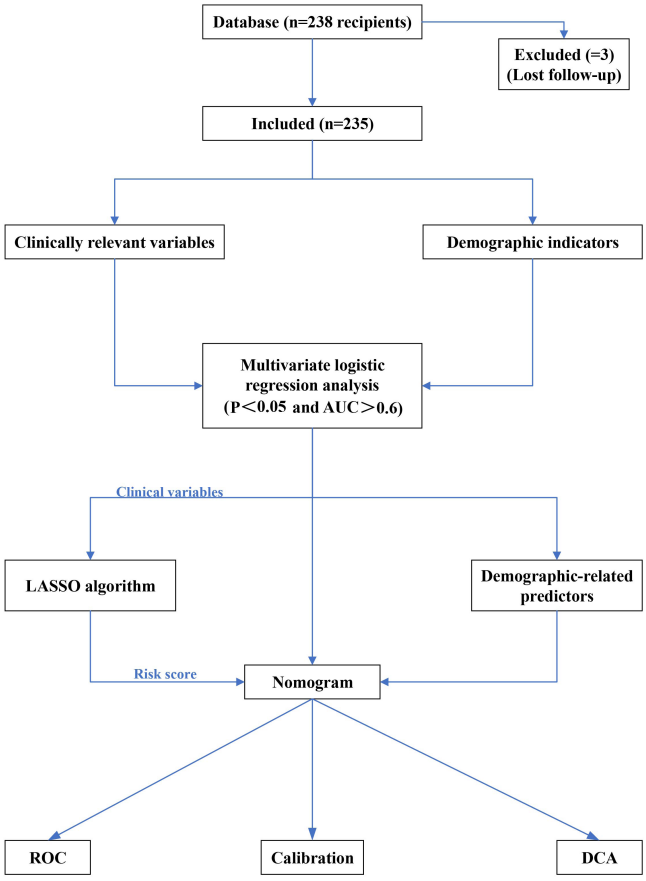

Results

The present study involved data collection from 238 recipients. However, three patients were excluded from the study owing to incomplete patient data and other reasons (e.g. loss to follow-up). Finally, 235 recipients and 141 matching donors were included in the study. Recipient male-to-female ratio was 165:70. Importantly, the average age of the recipients was recorded to be 41.5 ± 9.5 years. Among these, 88 patients were aged > 50 years (~37.4%), and 20 patients were aged > 55 years (~8.5%). In comparison to this, the ratio of male to female donors was 126:15, while the average age was 43.0 ± 16.7 years. Among these, 80 donors were aged > 50 years (~ 56.7%), and 23 donors were aged > 60 years (~ 16.3%). The number of patients with postoperative CAP was recorded to be 55 (CAP incidence was recorded as the first occurrence only), which accounted for ~23.4% of the total number of recipients. The data collected for the community-acquired pneumonia group and non-community-acquired pneumonia group is shown in Table 1.

This database identified the best cut-off value for clinical indicators through best-separation and transformed it into a dichotomous variable. For P < 0.05, the study included R-Cr, R-TB, R-Cl^-, DT, LHS, WIT, D-K^+, D-urea, and R-Na^+ as variables. The aforementioned variables were further obtained using the LASSO algorithm. This included R-Cr, R-TB, R-Cl^-, DT, LHS, WIT, D-K^+, and D-urea. A total of eight variables fulfilled the conditions (excluding R-Na+) (Figure 3A and 3B), and the nonzero coefficient, OR value, and 95% confidence interval of the predictor were obtained. The values for the same are shown in Table 2. These 8 predictor variables were further combined into a RiskScore. Finally, to the RiskScore, we added four demographic predictors (D-age, R-age, D-BMI, and R-BMI, which exhibited P < 0.05 in the logistic regression) to form a nomogram constructed to visually predict the CAP model (Figure 3C). In terms of internal verification, the ROC curve showed that the nomogram exhibited excellent predictive ability for CAP.

As shown in Figure 3A, the AUC value under ROC was 0.779 and 95% CI was 0.687–0.872. The calibration curve verification model is shown in Figure 3B (P=0.12 indicates good calibration). DCA showed that when the probability for prediction of CAP was in the range of 0.13–0.61, Within this range, the model yields a net benefit greater than both full intervention and no intervention strategies, the clinical intervention was recommended for the ESRD patients (Figure 3C). This further proved the excellent clinical effect of the model. To evaluate the universality of model performance, 10-fold cross-validation was performed on the models in the training queue, and good CAP prediction capabilities were achieved (Table 3). For 235 recipients included in the study, the average follow-up time was 35.0 ± 14.0 months, wherein recipient death or kidney transplant failure acted as a follow-up endpoint. The maximum follow-up time was recorded to be 53 months. During the follow-up period, 18 patients died, of which 11 experienced CAP. According to the statistical analysis, P-value was calculated to be <0.001. In addition to this, 16 patients lost their transplanted kidneys, which included 10 patients from the CAP group (P = 0.0002). The risk of death in the CAP group was HR=2.5, 95% CI: 1.8–3.4. Overall, the life span or transplant kidney function of the recipients belonging to the CAP group was observed to be worse as compared to the non-community-acquired pneumonia group. The Kaplan–Meier (K–M) curve for survival status and function of the transplanted kidney after KT is shown in Figure 3A and 3B.

Discussion

Following the completion of KT in ESRD patients, the clinicians primarily focus on the reduction of postoperative complications and extension of life expectancy. In the case of extremely limited kidney donor pools, it is important to construct a model that could effectively predict postoperative CAP.

KT is often the first choice of treatment for patients with ESRD[17, 18]. With China's organ transplantation field advancement and newer immunosuppressive drugs, KT success rate and patient lifespan have improved significantly. However, post-KT CAP presents a substantial challenge. This study used deceased donor KT data to create a nomogram predicting post-KT surgery CAP risk. The findings of the

Table 1. Basic demographic characteristics and the clinical data characteristics

Characteristics	Non-CAP group (%)	CAP group (%)	Total	P -value	AUC
	n=180	n=55	n=235		
Clinical data of recipient					
R-Cr(umol/L)				0.004	0.640
>889.1	142(60.4)	34(14.5)	176(74.9)		
≤889.1	38(16.2)	21(8.9)	59(25.1)		
R-ALT(U/L)				0.169	0.543
>28	59(25.1)	24(10.2)	83(35.3)		
≤28	121(51.5)	31(13.2)	152(64.7)		
R-AST(U/L)				0.209	0.527
>17	92(39.1)	32(13.6)	124(52.8)		
≤17	88(37.4)	23(9.8)	111(47.2)		
R-TB(umol/L)				0.004	0.609
>16.8	80(34.0)	11(4.7)	29(12.3)		
≤16.8	100(42.6)	44(18.7)	144(61.3)		
R-TP(g/L)				0.100	0.546
>80.1	37(15.7)	12(5.1)	49(20.9)		
≤80.1	143(60.9)	43(18.3)	186(79.1)		
R-K(mmol/L)				0.111	0.546
>4.86	85(36.2)	29(12.3)	63(26.8)		
≤4.86	95(40.4)	26(11.1)	78(33.2)		
R-Na(mmol/L)				0.041	0.568
>141.9	60(25.5)	9(3.8)	69(29.4)		
≤141.9	120(51.1)	46(19.6)	166(70.6)		
R-Cl(mmol/L)				0.010	0.547
>95.2	165(70.2)	34(14.5)	199(84.7)		
≤95.2	15(6.4)	21(8.9)	36(15.3)		
LHS (day)				0.005	0.670
>24	78(33.2)	36(15.3)	104(44.3)		
≤24	102(43.4)	19(8.1)	121(51.5)		
DT (month)				0.019	0.605
>38	88(37.4)	33(14.0)	121(51.5)		
≤38	92(39.1)	22(9.4)	114(48.5)		
R-ALP (umol/L)				0.142	0.540
>76	129(54.9)	32(13.6)	161(68.5)		
≤76	51(21.7)	23(9.8)	74(31.5)		
Clinical data of donor					

D-Na(mmol/L)				0.288	0.531
>145.1	64(27.2)	12(5.1)	76(32.3)		
≤145.1	116(49.4)	43(18.3)	159(67.7)		
D-K(mmol/L)				0.004	0.545
>3.13	170(72.3)	38(16.2)	208(88.5)		
≤3.13	10(4.3)	17(7.2)	27(11.5)		
D-TB (umol/L)				0.056	0.563
>9.9	79(33.6)	10(4.3)	89(37.9)		
≤9.9	101(43.0)	45(19.1)	146(6.8)		
D-urea (umol/L)				0.024	0.593
>6.64	87(37.0)	11(4.7)	98(41.7)		
≤6.64	93(39.6)	44(18.7)	137(58.3)		
D-ALB (umol/L)				0.099	0.569
>35.5	112(47.7)	39(16.6)	151(64.3)		
≤35.5	68(28.9)	16(6.8)	84(35.7)		
WIT (min)				0.006	0.558
>19	10(4.3)	9(3.8)	19(8.1)		
≤19	170(72.3)	46(19.6)	216(91.9)		
CIT(h)				0.420	0.526
>9	80(34.0)	20(8.5)	100(42.6)		
≤9	100(42.6)	35(14.9)	135(57.4)		
demographic data					
D-age(y)				0.001	0.618
>47	87(37.0)	41(17.4)	128(54.5)		
≤47	93(39.6)	14(6.0)	107(45.5)		
D-BMI (kg/m2)				0.031	0.521
>17.9	165(70.2)	43(18.3)	208(88.5)		
≤17.9	15(6.4)	12(5.1)	27(11.5)		
R-age(y)				0.002	0.625
>46	72(30.6)	33(14.0)	105(44.7)		
≤46	108(46.0)	22(9.4)	130(55.3)		
R-BMI (kg/m2)				0.013	0.604
>22.1	87(37.0)	31(13.2)	118(50.2)		
≤22.1	93(39.6)	24(10.2)	117(49.8)		

R-: recipient; D-: donor; Cr: creatinine; ALT: alanine aminotransferase; AST: aspartate transaminase; TB: total bilirubin; WIT: warm ischemia time; CIT: cold ischemia time; TP: total protein; K+: Kalium; Na+: sodium; Cl-: chloridion; LHS: length of hospital stay; DT; dialysis time; ALP: alkaline phosphatase; ALB: albumin.

Figure 2. Feature selection of the clinical indicators using the LASSO binary regression model. (**A**) In the LASSO model, the best lambda parameter was selected using 5-fold cross-validation and minimal criteria. The curve of the partial likelihood deviance (binomial deviance) was plotted versus the logarithm of the lambda parameter. Dotted vertical lines were drawn at the optimal values using the minimum criteria and the I SE of the minimum criteria (I-SE criteria). (**B**) For 8 characteristics, the LASSO coefficient profiles were created. Each coefficient profile was displayed against the lambda parameter's logarithm. The vertical line was generated using 5-fold cross-validation at the selected value, where the best lambda value was generated in 8 features with nonzero coefficients. Abbreviation: SE: Standard Error. (**C**) The nomogram for predicting the occurrence of community-acquired pneumonia after KT from the deceased donors. The nomogram of community-acquired pneumonia after KT developed by cohort included Riskcore, D-age, R-age, D-BMI, and R-BMI. The RiskScore includes 8 clinical predictors of R-Cr, R-TB, R-Cl-, DT, LHS, WIT, D-K+, and D-urea.

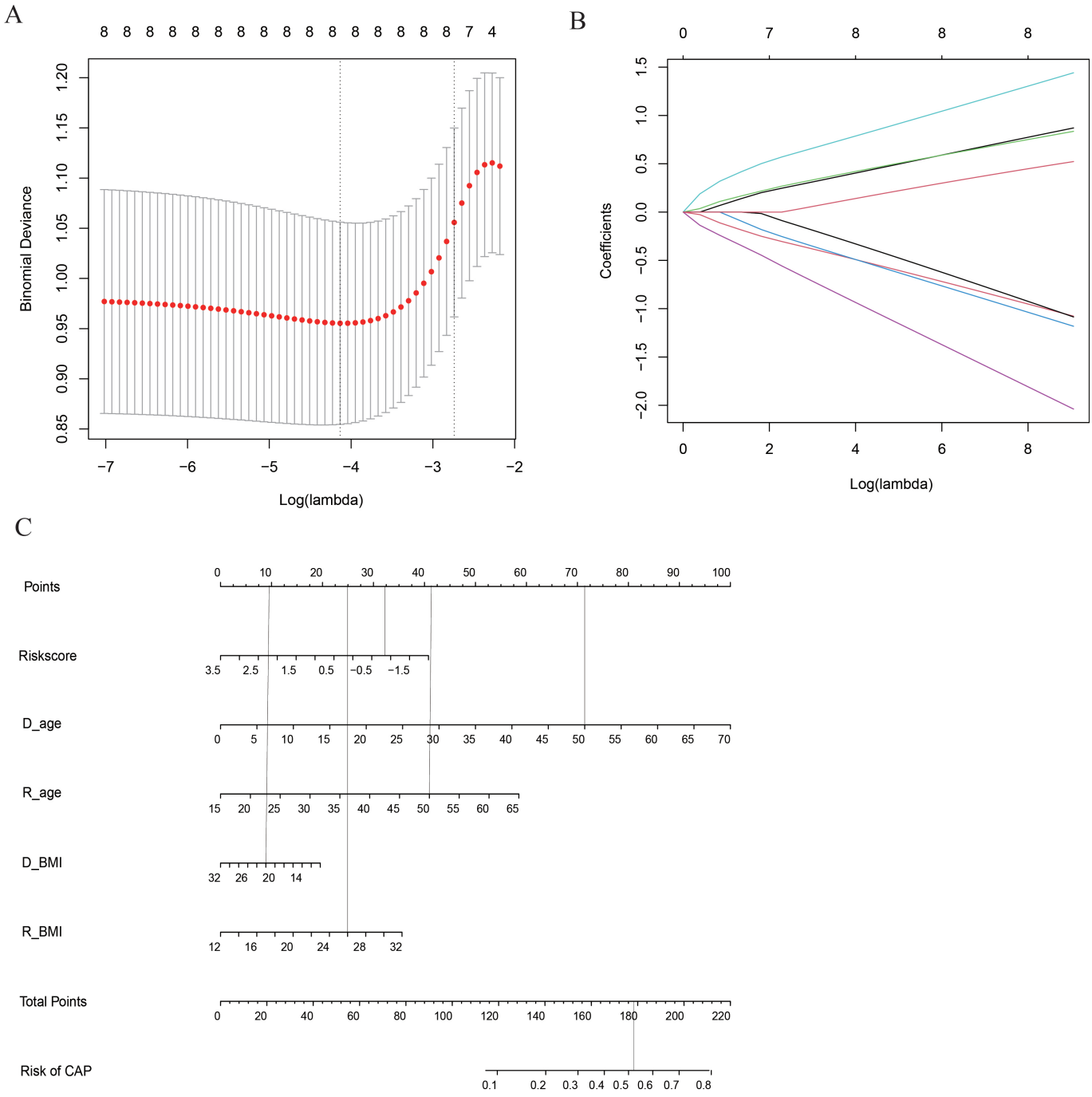

https://doi.org/10.71321/kbfm1398

Figure 3. Effectiveness evaluation of the nomogram model. (**A**) The receiver operating characteristic (ROC) curve of the nomogram of the risk prediction after transplantation. The X-axis and Y-axis reflect the false positive rate and true positive rate of post-transplant morbidity prediction. The AUC value was 0.779. (**B**) The calibration curve of the CAP-risk prediction nomogram after transplantation. After transplantation, the CAP prediction is represented on the X-axis, while the actual CAP is represented on the Y-axis. The perfect prediction result of the ideal model matches the diagonal dashed line. The nomogram performance is represented by a solid line, and a match closer to the diagonal dashed line indicates a better prediction. (**C**) For CAP after transplantation, decision curve analysis (DCA) was performed. The Y-axis represents the net income. The CAP risk nomogram after transplantation is indicated by a red line. The thin solid line represents the hypothesis that all recipients could survive after transplantation, while the thick solid line represents the hypothesis that all kidney recipients will suffer CAP after transplantation. The decision curve indicates that the threshold probabilities for patients and doctors are >0.13 and <0.61, respectively. The current study results indicate that the morbidity risk nomogram could be used for post-KT morbidity risk prediction as it is more helpful than intervention-for-all-recipients or no-intervention schemes.

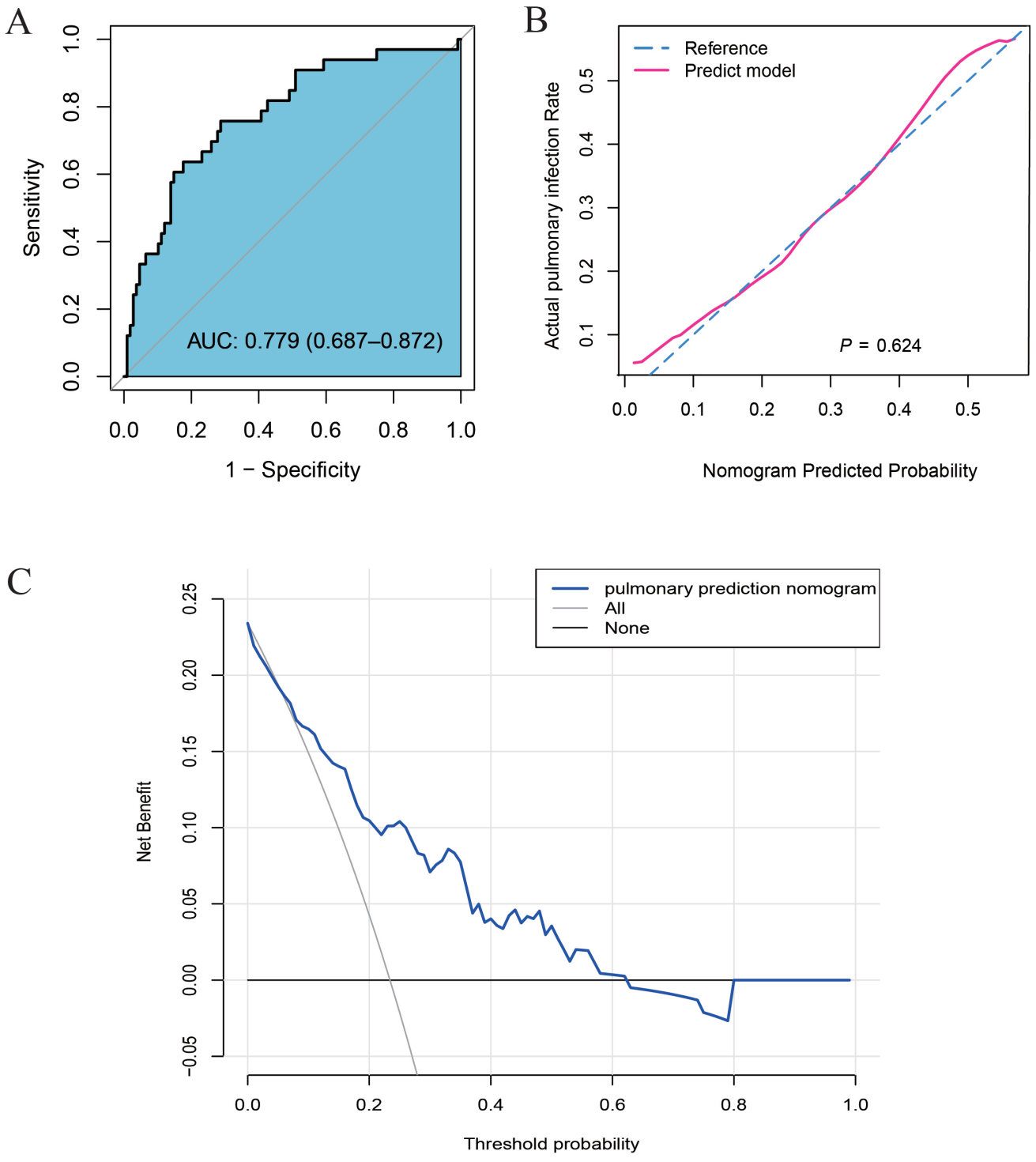

Table 2. Morbidity of community-acquired pneumonia prediction factors after kidney transplantation from the deceased donors

Predictors	*β*	*P*-value	OR (95%CI)
Length of hospital stay	0.840012333	0.005	3.268 (1.437-7.432)
R-creatinine	0.681181964	0.004	0.294 (0.129-0.669)
R-TB	-0.832945333	0.004	4.261 (1.588-11.435)
R-Cl-	0.66932031	0.01	0.298 (0.119-0.744)
WIT	-0.898453394	0.006	7.778 (1.826-33.124)
D-K+	1.171816463	0.004	0.184 (0.058-0.578)
D-urea	-1.58720191	0.024	0.375 (0.160-0.881)
Dialysis-time	-0.770738912	0.019	2.767 (1.178-6.500)

β, the regression coefficient; CI, confidence interval

Table 3. Evaluation results of the model in 10 randomly selected independent subgroups

Groups	Training group			Validation group		
	AUC	False positive rate	True positive rate	AUC	False positive rate	True positive rate
1	0.820	0.554	1.000	0.765	0.846	0.706
2	0.881	0.877	0.867	0.784	0.549	0.944
3	0.797	0.800	0.765	0.796	0.755	0.750
4	0.799	0.852	0.667	0.777	0.852	0.667
5	0.783	0.765	0.714	0.766	0.877	0.583
6	0.922	0.831	0.923	0.690	0.531	0.850
7	0.821	0.714	0.812	0.769	0.692	0.824
8	0.723	0.620	0.818	0.920	0.724	1.000
9	0.744	0.741	0.714	0.815	0.840	0.684
10	0.762	0.755	0.737	0.884	0.655	1.000
AVG (M + 95%CI)	0.805 (0.744-0.881)	0.751 (0.620-0.852)	0.802 (0.714-0.923)	0.797 (0.765-0.884)	0.732 (0.549-0.852)	0.801 (0.667-1.000)

A total of 235 patients were randomly assigned to the training group and the verification group at a ratio of 5:5.

Figure 4. (A) The K-M curve of recipient survival after kidney transplantation. (**B**) The K-M curve of transplanted kidney functions after kidney transplantation. ***P < 0.001

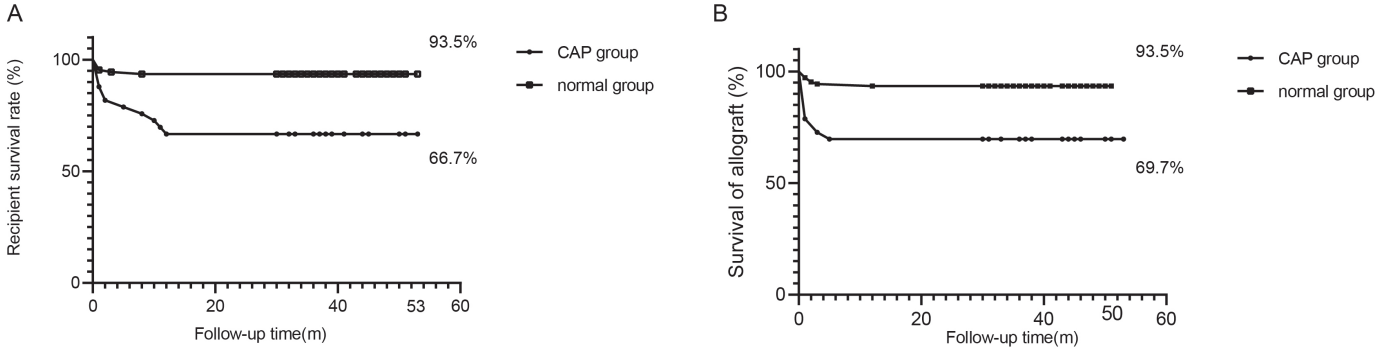

study would assist in the matching of donors' kidneys to ideal recipients. Additionally, it would assist surgeons in making clinical decisions. The study leveraged extensive clinical and demographic data to characterize CAP, after KT, from several different dimensions. Therefore, based on the logistics regression model, the LASSO algorithm was introduced to optimize the selection of features for the risk model, such that relatively unimportant variable coefficients became zero and were excluded from the model. This further ensured that optimal variables screened out from logistics regression were included in the nomogram.

The model used two aspects to construct model predictors. In particular, demographic variables screened out four predictors of D-age, R-age, D-BMI, and R-BMI. In comparison to this, eight predictors were screened out of clinical indicators, namely R-Cr, R-TB, R-Cl^-, DT, LHS, WIT, D-K^+, and D-urea, and these were used to obtain RiskScore. Finally, the two types of predictors were used to construct a nomogram, and the AUC value of this model was recorded to be 0.779, which showed good predictive ability. Importantly, as mentioned previously in the introduction, demographic data has been widely utilized to identify strong risk factors for the occurrence and development of CAP. Therefore, demographic predictors with $P < 0.05$ were listed independently in the nomogram, and there was no need to enter the LASSO algorithm. In the past, very few studies assessed the impact of clinical data on CAP, resulting in absence of any consensus.

In this study, we included clinical data not previously proven to strongly impact CAP development into a RiskScore using logistic regression and the LASSO algorithm. In a previous study, Mao et al.[19] combined five radioactive risk factors into the 'Radiomics Signature'. It was then incorporated into a nomogram along with other indicators to predict axillary lymph node metastasis in breast cancer. The prediction model was intuitive, concise, and accurate. In addition to this, the sex ratio of donors was found to be extremely unbalanced in the original database included in the present study. This was related to the country's social ideology, family income, and insufficient hospital publicity efforts. Consequently, this imbalance would lead to bias errors in the model and affect the overall model effect. Therefore, to increase the universality of the model, the present study did not incorporate gender factors into the model for consideration.

Our RiskScore contained six easily obtainable pre-surgery blood indicators, including D-urea and R-Cr levels, reflecting the donor's pre-death and recipient's pre-surgery renal function. Additionally, R-Cl^- and D-K^+ levels were also included, which reflected electrolyte balance in the donor and recipient body environment. Therefore, blood indicators played an active role in the assessment of CAP risk after surgery.

While the cold ischemia time (CIT) is often considered crucial for kidney transplant surgery quality, it was excluded from our model, which contradicts previous studies. This contradicted previous reports[20, 21]. With advancements in the field of KT and in-depth assessment of the mechanism of CIT, it has been observed that the impact of CIT on the prognosis of KT surgery has gradually weakened. In a previous study, Adani L et al.[22] found that the use of low-temperature mechanical perfusion technology and improvement in the technique used for the preservation of kidney sources, during transportation, significantly reduced the incidence of postoperative infections caused by CIT in DD. The analysis of large-scale clinical data by Chapal et al.[23] revealed that the use of immunosuppressive agents after KT could ignore the impact of CIT on postoperative CAP, suggesting CIT's declining role in predicting postoperative CAP.

Demographic factors greatly influence the nomogram model. Figure 3 shows that donor and recipient age significantly affect post-KT CAP risk, especially the donor age. Our study had generally older donors and recipients, with ~56.7% donors aged >50 years, whose average creatinine value was 120.9 ± 56.7 μmol/L. About 30.0% of donor deaths were due to cerebrovascular accidents. These data suggest older donors and recipients have increased CAP risk post-KT. Given the aging global population, it's vital to adjust donor risk factor evaluation, recipient complication strategies, and optimize organ allocation and immunosuppression methods[24].

Obesity in ESRD patients has been seen as a relative contraindication to kidney transplantation (KT) due to increased risks of rejection, kidney loss, or death[25, 26]. Our data showed a higher recipient's BMI correlated with an increased post-KT CAP risk.

From clinical statistics, it was observed that the human/kidney survival rate in the CAP group was indeed lower than the non-CAP group, which was similar to the results obtained for transplantation statistics of other countries[27]. The recent global spread of SARS-COV-2 increased the physical and mental burden on KT patients, the "sensitive population". Elias et al. reported that transplant patients suffering from COVID-19 exhibited a higher risk of kidney transplant loss and death as compared to the general population[28]. Given the increased life expectancy of transplant patients, it's crucial to focus on individualized treatment and CAP risk factors control, thus reducing post-KT CAP risk. This was our motivation for developing this clinical model.

In our previous research, we successfully explored a predictive model for the occurrence of delayed graft function (DGF) in kidney transplant recipients[29]. As another severe complication following kidney transplantation, early diagnosis and treatment of community-acquired pneumonia (CAP) are also crucial. Therefore, the findings from our study on the CAP predictive model can assist in predicting CAP and help elucidate the unique susceptibility mechanisms associated with it. Looking ahead, integrating microbiological studies to examine the relationship between pulmonary microbiota and infection risk could help explore strategies for reducing the risk of CAP in kidney transplant patients, including those with DGF.

This study has limitations. To improve the model's fit and reduce error regression, more data samples are needed. It's crucial to validate the model with multi-center data. Our database was primarily provincial, so to enhance the model's generalizability and practicality, verification in other provinces or countries is required. Notably, our prediction model only applies to first-time deceased donor kidney transplant recipients.

Conclusions

In summary, the prediction model established using this database integrated two aspects of donors and recipients,

screened out 12 risk predictors including demographic and clinical blood indicators, which could effectively predict CAP. The findings of the study would further assist the clinicians in timely diagnosis, and providing timely treatment.

Acknowledgments

The authors are grateful for the invaluable support and useful discussions with other members of the urological department.

Author Contributions

All authors made substantial contributions to conception and design, acquisition of data, or analysis and interpretation of data; took part in drafting the article or revising it critically for important intellectual content; gave final approval of the version to be published; and agree to be accountable for all aspects of the work.

Ethics Approval and Consent to Participate

This study was conducted with approval from the Ethics Committee of the First Affiliated Hospital of Anhui Medical University (approval number: Quick-PJ 2022-01-33). This study was conducted in accordance with the declaration of Helsinki. Written informed consent was obtained from all participants. Moreover, all kidneys were donated voluntarily with written informed consent, and this was conducted with the Declaration of Istanbul.

Funding Information

This research was supported by grants to GY Liao from the National Natural Science Foundation of China (No. 82470783), to J Zhang from the Anhui Hongde-Shanyi Foundation Clinical Research Development Special Fund, and to J Zhang from the National Natural Science Foundation of China (No. 82400890).

Competing Interests

The authors declare that they have no existing or potential commercial or financial relationships that could create a conflict of interest at the time of conducting this study.

Data Availability

All data needed to evaluate the conclusions in the paper are present in the paper or the Supplementary Materials. Additional data related to this paper may be requested from the authors.

References

[1] Wolfe RA, Ashby VB, Milford EL, Ojo AO, Ettenger RE, Agodoa LY, et al. (1999). Comparison of mortality in all patients on dialysis, patients on dialysis awaiting transplantation, and recipients of a first cadaveric transplant. N Engl J Med, 341(23), 1725-1730. https://doi.org/10.1056/nejm199912023412303

[2] Merion RM, Ashby VB, Wolfe RA, Distant DA, Hulbert-Shearon TE, Metzger RA, et al. (2005). Deceased-donor characteristics and the survival benefit of kidney transplantation. Jama, 294(21), 2726-2733. https://doi.org/10.1001/jama.294.21.2726

[3] Hernandez-Fuentes MP, & Lechler RI. (2005). Chronic graft loss. Immunological and non-immunological factors. Contrib Nephrol, 146, 54-64. https://doi.org/10.1159/000082065

[4] Zhang X, Lyu J, Yu X, Wang L, Peng W, Chen J, et al. (2020). Comparison of Graft Outcome Between Donation After Circulatory Death and Living-Donor Kidney Transplantation. Transplant Proc, 52(1), 111-118. https://doi.org/10.1016/j.transproceed.2019.10.001

[5] Kinnunen S, Karhapää P, Juutilainen A, Finne P, & Helanterä I. (2018). Secular Trends in Infection-Related Mortality after Kidney Transplantation. Clin J Am Soc Nephrol, 13(5), 755-762. https://doi.org/10.2215/cjn.11511017

[6] Stratta RJ, Rohr MS, Sundberg AK, Farney AC, Hartmann EL, Moore PS, et al. (2006). Intermediate-term outcomes with expanded criteria deceased donors in kidney transplantation: a spectrum or specter of quality? Ann Surg, 243(5), 594-601; discussion 601-593. https://doi.org/10.1097/01.sla.0000216302.43776.1a

[7] Chen G, Zhang Z, Gu J, Qiu J, Wang C, Kung R, et al. (2010). Incidence and risk factors for pulmonary mycosis in kidney transplantation. Transplant Proc, 42(10), 4094-4098. https://doi.org/10.1016/j.transproceed.2010.10.010

[8] Flabouris K, Chadban S, Ladhani M, Cervelli M, & Clayton P. (2019). Body mass index, weight-adjusted immunosuppression and the risk of acute rejection and infection after kidney transplantation: a cohort study. Nephrol Dial Transplant, 34(12), 2132-2143. https://doi.org/10.1093/ndt/gfz095

[9] Qu JM, & Cao B. (2016). [Guidelines for the diagnosis and treatment of adult community acquired pneumonia in China (2016 Edition)]. Zhonghua Jie He He Hu Xi Za Zhi, 39(4), 241-242. https://doi.org/10.3760/cma.j.issn.1001-0939.2016.04.001

[10] Mandell LA, Wunderink RG, Anzueto A, Bartlett JG, Campbell GD, Dean NC, et al. (2007). Infectious Diseases Society of America/American Thoracic Society consensus guidelines on the management of community-acquired pneumonia in adults. Clin Infect Dis, 44 Suppl 2(Suppl 2), S27-72. https://doi.org/10.1086/511159

[11] Saran R, Robinson B, Abbott KC, Agodoa LY, Albertus P, Ayanian J, et al. (2017). US Renal Data System 2016 Annual Data Report: Epidemiology of Kidney Disease in the United States. Am J Kidney Dis, 69(3 Suppl 1), A7-a8. https://doi.org/10.1053/j.ajkd.2016.12.004

[12] Friedman J, Hastie T, & Tibshirani R. (2010). Regularization Paths for Generalized Linear Models via Coordinate

Descent. J Stat Softw, 33(1), 1-22.
[13] Sauerbrei W, Royston P, & Binder H. (2007). Selection of important variables and determination of functional form for continuous predictors in multivariable model building. Stat Med, 26(30), 5512-5528. https://doi.org/10.1002/sim.3148
[14] Kidd AC, McGettrick M, Tsim S, Halligan DL, Bylesjo M, & Blyth KG. (2018). Survival prediction in mesothelioma using a scalable Lasso regression model: instructions for use and initial performance using clinical predictors. BMJ Open Respir Res, 5(1), e000240. https://doi.org/10.1136/bmjresp-2017-000240
[15] Kramer AA, & Zimmerman JE. (2007). Assessing the calibration of mortality benchmarks in critical care: The Hosmer-Lemeshow test revisited. Crit Care Med, 35(9), 2052-2056. https://doi.org/10.1097/01.Ccm.0000275267.64078.B0
[16] Vickers AJ, Cronin AM, Elkin EB, & Gonen M. (2008). Extensions to decision curve analysis, a novel method for evaluating diagnostic tests, prediction models and molecular markers. BMC Med Inform Decis Mak, 8, 53. https://doi.org/10.1186/1472-6947-8-53
[17] Purnell TS, Auguste P, Crews DC, Lamprea-Montealegre J, Olufade T, Greer R, et al. (2013). Comparison of life participation activities among adults treated by hemodialysis, peritoneal dialysis, and kidney transplantation: a systematic review. Am J Kidney Dis, 62(5), 953-973. https://doi.org/10.1053/j.ajkd.2013.03.022
[18] Silva SB, Caulliraux HM, Araújo CA, & Rocha E. (2016). Cost comparison of kidney transplant versus dialysis in Brazil. Cad Saude Publica, 32(6). https://doi.org/10.1590/0102-311x00013515
[19] Mao N, Yin P, Li Q, Wang Q, Liu M, Ma H, et al. (2020). Radiomics nomogram of contrast-enhanced spectral mammography for prediction of axillary lymph node metastasis in breast cancer: a multicenter study. Eur Radiol, 30(12), 6732-6739. https://doi.org/10.1007/s00330-020-07016-z
[20] Schlott F, Steubl D, Hoffmann D, Matevossian E, Lutz J, Heemann U, et al. (2017). Primary Cytomegalovirus Infection in Seronegative Kidney Transplant Patients Is Associated with Protracted Cold Ischemic Time of Seropositive Donor Organs. PLoS One, 12(1), e0171035. https://doi.org/10.1371/journal.pone.0171035
[21] Sucher R, Wagner T, Köhler H, Sucher E, Quice H, Recknagel S, et al. (2022). Hyperspectral Imaging (HSI) of Human Kidney Allografts. Ann Surg, 276(1), e48-e55. https://doi.org/10.1097/sla.0000000000004429
[22] Adani GL, Pravisani R, Tulissi P, Isola M, Calini G, Terrosu G, et al. (2021). Hypothermic machine perfusion can safely prolong cold ischemia time in deceased donor kidney transplantation. A retrospective analysis on postoperative morbidity and graft function. Artif Organs, 45(5), 516-523. https://doi.org/10.1111/aor.13858
[23] Chapal M, Le Borgne F, Legendre C, Kreis H, Mourad G, Garrigue V, et al. (2014). A useful scoring system for the prediction and management of delayed graft function following kidney transplantation from cadaveric donors. Kidney Int, 86(6), 1130-1139. https://doi.org/10.1038/ki.2014.188
[24] Sutherland AI, JN IJ, Forsythe JL, & Dor FJ. (2016). Kidney and liver transplantation in the elderly. Br J Surg, 103(2), e62-72. https://doi.org/10.1002/bjs.10064
[25] Meier-Kriesche HU, Arndorfer JA, & Kaplan B. (2002). The impact of body mass index on renal transplant outcomes: a significant independent risk factor for graft failure and patient death. Transplantation, 73(1), 70-74. https://doi.org/10.1097/00007890-200201150-00013
[26] Ladhani M, Lade S, Alexander SI, Baur LA, Clayton PA, McDonald S, et al. (2017). Obesity in pediatric kidney transplant recipients and the risks of acute rejection, graft loss and death. Pediatr Nephrol, 32(8), 1443-1450. https://doi.org/10.1007/s00467-017-3636-1
[27] Sarnak MJ, & Jaber BL. (2001). Pulmonary infectious mortality among patients with end-stage renal disease. Chest, 120(6), 1883-1887. https://doi.org/10.1378/chest.120.6.1883
[28] Elias M, Pievani D, Randoux C, Louis K, Denis B, Delion A, et al. (2020). COVID-19 Infection in Kidney Transplant Recipients: Disease Incidence and Clinical Outcomes. J Am Soc Nephrol, 31(10), 2413-2423. https://doi.org/10.1681/asn.2020050639
[29] Pan J, & Liao G. (2021). Development and Validation of Nomogram for Predicting Delayed Graft Function After Kidney Transplantation of Deceased Donor. Int J Gen Med, 14, 9103-9115. https://doi.org/10.2147/ijgm.S331854

Research Progress of Epigenetic Regulation in Stroke Treatment

Authors

Tian-cai Yang, Lei Feng

Correspondence

flneuro@163.com (L. Feng)

Graphical Abstract

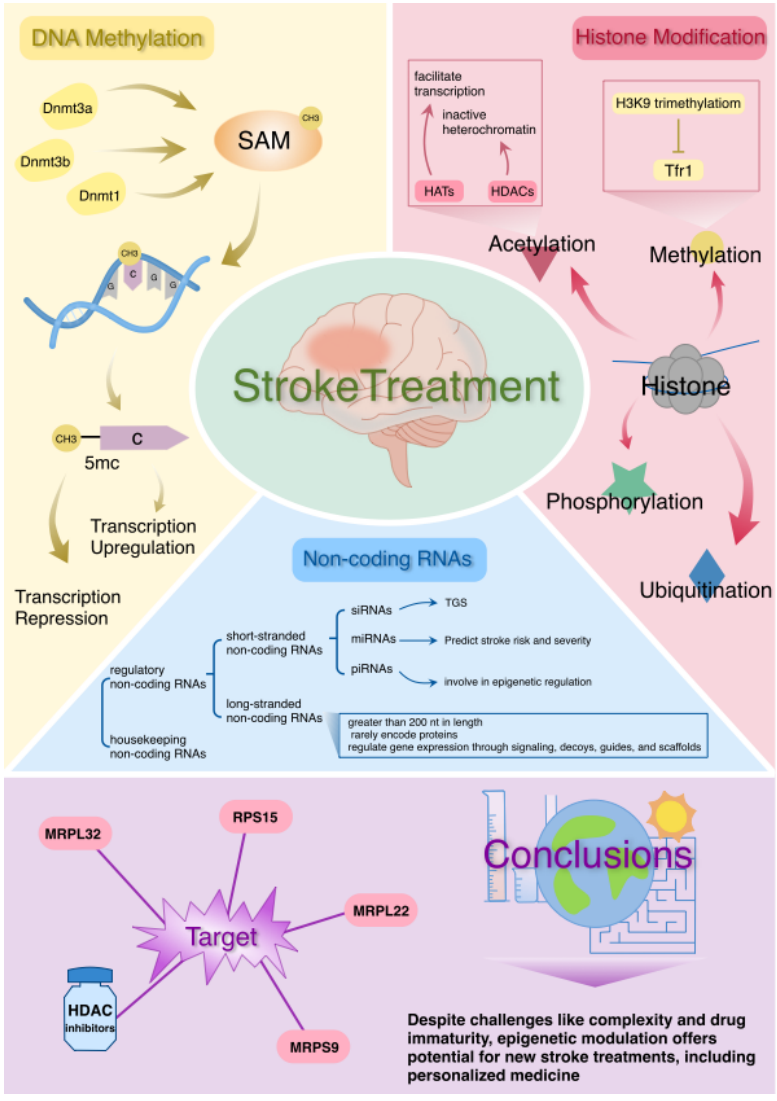

https://doi.org/10.71321/y2sx8j49

Review Article

Life Conflux

Research Progress of Epigenetic Regulation in Stroke Treatment

Tian-cai Yang [1] **,** Lei Feng [2*]

Received: 2025-01-05 | Accepted: 2025-03-20 | Published online: 2025-03-30

Abstract

Cerebrovascular diseases are a serious threat to human health, among which stroke is extremely harmful. In recent years, more and more studies have shown that epigenetic regulation is crucial in the development of cerebrovascular diseases. In this review, we focus on the research progress of epigenetic regulation in stroke treatment, detailing the regulatory mechanisms of DNA methylation, histone modification and non-coding RNAs, and analyzing their roles in the pathophysiology of stroke. It was found that ischemic stroke causes dynamic changes in DNA methylation, which affects gene expression and alters the process of injury and recovery; histone modification levels are also altered after stroke, which affects chromatin status and gene transcription; and noncoding RNAs, such as miRNAs, siRNAs, piRNAs, and lncRNAs, which play a key role in gene expression regulation, are associated with the risk of stroke, severity and symptom onset. In addition, therapeutic strategies targeting epigenetic regulation are also discussed. Although facing challenges such as complex mechanisms, susceptibility to environmental influences, and the early stage of drug development, epigenetic regulation is still very promising in the treatment of stroke, and it is expected to provide a new theoretical basis and research direction for the prevention and treatment of stroke in the future.

Keywords: Epigenetic regulation; Stroke; DNA methylation; Histone modification; Non-coding RNA; Therapeutic targets

Introduction

In 2021, stroke maintained its status as the second most prevalent cause of death globally, surpassed only by ischaemic heart dise ase, and occupied the third spot in terms of Disability-Adjusted Life Years lost due to noncommunicable diseases , trailing behind ischaemic heart disease and neonatal disorders[11].

Cerebrovascular diseases are lesions of blood vessels in the brain, including cerebral infarction, cerebral hemorrhage, and subarachnoid hemorrhage, which will lead to stroke[72]. In recent years, epigenetic regulation has played an important role in stroke pathogenesis and stroke repair as a higher-order regulatory mechanism for tissue repair. Epigenetic regulation refers to mechanisms that regulate gene expression through non-DNA sequence changes (DNA methylation, histone modifications, and non-coding RNAs)[44] .These changes can affect multiple aspects of gene transcription, splicing, RNA stability and translation without altering the DNA sequence[29]. Epigenetic regulation is a key post-transcriptional regulation of gene expression and plays an important regulatory role in organogenesis, homeostasis and pathology[67].

In cerebrovascular diseases, alterations in epigenetic regulation may lead to neuronal damage and abnormal responses of vascular endothelial cells. Therefore, investigating the role of epigenetic regulation in cerebrovascular diseases can help us better understand the pathogenesis of these diseases and find new therapeutic strategies.

Epigenetic regulation

DNA methylation

DNA methylation is the process by which methyl groups are added to the DNA molecule. This modification can occur at different locations in the genome and plays an important role in gene regulation. Several enzymes are involved in DNA methylation, including DNA methyltransferases (dnmt) such as Dnmt3a, Dnmt3b, and Dnmt1. DNMTs catalyze the transfer of methyl groups from S-adenosylmethionine (SAM) to cytosine residues in DNA to form 5-methylcytosine (5mC). However, post-mitotic neurons in the mature mammalian brain still express a large number of Dnmts, raising the possibility

1 Jining Medical University, Jining First People's Hospital, Jining, Shandong, China.

2 Neurosurgery Department, Jining First People's Hospital, Institute of Central Nervous Vascular Injury and Repair, Jining Academy of Medical Sciences, Jining Key Laboratory of Stroke and Neural Repair, Jining, Shandong, China.

* Corresponding Author.

that Dnmts and DNA methylation may play new roles in the brain[18, 24].

DNA methylation can influence the pathogenesis of stroke by modulating genetic or environmental risk factors. DNA methylation regulation is shaped by two opposing processes, the addition and removal of the fifth methyl group of cytosine in DNA[31, 33, 36, 37]. It causes transcriptional repression or transcriptional upregulation by preventing RNA polymerase from recognizing specific DNA regions or by eliminating "DNA methylation breaks", respectively. The effect of DNA methylation on the expression of transcripts depends on their location in the gene region (promoter and or gene body), and transcriptional changes are usually dependent on methylation at multiple locations in a given gene[36, 37].DNA methylation can be a biomarker for stroke[40].

Zhan, L. et al. demonstrated that the Piwil2/piRNAs pathway plays a role in the epigenetic regulation of CREB2 expression and neuroprotection of tGCI by HPC in rats. Specifically, HPC-induced downregulation of Piwil2 in rat CA1 inhibited CREB2 hypermethylation and promoted CREB2 transcription by retraining DNMT3A to induce promoter site CpG methylation, leading to an increase in CREB2 after tGCI[75].

Histone modifications

Histone modifications include several types, each with a specific function. Histone methylation can occur on the Lys and Arg residues of histones and has the effect of reducing the positive charge carried by histones and directly or indirectly affecting the transcriptional activity of genes. Histone methylation is usually associated with gene activation or gene silencing[5]. Histone acetylation occurs predominantly and diversely on core histones. The degree of acetylation is higher in the structural domains of DNA containing active genes. Acetylation/deacetylation modifications can regulate the level of gene transcription, participate in DNA repair, splicing and replication, chromosome assembly, and cellular signaling[61]. Histone phosphorylation is involved in gene transcription, DNA repair, apoptosis and chromosome condensation[27]. Histone ubiquitination is involved in X chromosome inactivation and affects histone methylation and gene transcription[70].

Histone acetyltransferases (HATs) acetylate lysine residues in histone tails. This promotes DNA unfolding and chromatin deconcentration, which facilitates transcription and protein synthesis. Histone deacetylases remove acetyl groups from histones. This leads to the formation of transcriptionally inactive heterochromatin in which gene expression is blocked. To maintain the transcriptionally active state of chromatin, HATs and hdac need to work in concert[30, 58, 69].

H3K9 trimethylation is a specific methylation modification of the 9th amino acid lysine of histone 3 that inhibits the key transferrin receptor (Tfr1), which determines whether or not a neuron will experience iron death. By decreasing H3K9 trimethylation protects neurons from iron death, whereas increasing it leads to neuronal iron death[42].

non-coding RNA

Non-coding RNAs that are not translated into proteins can be categorized into housekeeping non-coding RNAs and regulatory non-coding RNAs. RNAs with regulatory roles are divided into two main categories according to their size: short-stranded non-coding RNAs (including siRNAs, miRNAs and piRNAs) and long-stranded non-coding RNAs (LncRNAs)[63, 74].In recent years, a large number of studies have shown that non-coding RNAs play an important role in epigenetic modifications, which can regulate expression at the gene level and chromosome level and control cell differentiation[2, 12, 23, 73].

siRNA is derived from long double-stranded RNA molecules (including RNA produced by viral replication, transposon activity, or gene transcription) that can be cleaved by Dicer's enzyme into 19-24 nt (nt: nucleotide) RNA fragments, which are then loaded onto the Argonaute (AGO) protein to perform their function[34, 52].

miRNAs are single-stranded RNAs of approximately 19-24 nt, 50% of which are located in chromosomal regions prone to structural changes[57].Initially, it was thought that there were two main differences between siRNAs and miRNAs as a class of regulatory RNAs. One is that miRNAs are endogenous, being the products of biological gene expression, whereas siRNAs are exogenous, originating from viral infections, gene transfer points, or gene targets. The other difference is that miRNAs consist of incomplete hairpin-shaped double-stranded RNAs processed by Drosha and Dicer, whereas siRNAs are products of fully complementary long double-stranded RNAs processed by Dicer[9].Despite these differences, it has been hypothesized that miRNAs and siRNAs have similar mechanisms of action in mediating transcriptional gene silencing because miRNAs and siRNAs are closely related, e.g., the two fragments are similar in size. Recently, nearly 1,800 putative miRNAs have been identified in the human genome, and the number of miRNAs continues to increase rapidly due to the development of high-throughput sequencing technologies[26, 41, 47].

piRNAs are a class of RNA molecules approximately 26-31 nt in length. Its name piRNA (Piwi-interacting RNA) reflects the fact that piRNA binds to Piwi proteins under physiological conditions.The role of Piwi proteins as epigenetic regulators is reflected by their silencing of the homeobox gene by binding to PcGs (polycistronic ribosomal histones) to genomic PcG response elements. Thus, it has been hypothesized that piRNAs associated with Piwi proteins should also play an important role in epigenetic regulation[45].

LncRNAs are another class of non-coding regulatory RNAs. lncRNAs are generally greater than 200 nt in length, are located in the nucleus or cytoplasm, and rarely encode proteins.[8, 51].

LncRNAs are another class of non-coding regulatory RNAs. lncRNAs are generally greater than 200 nt in length, are located in the nucleus or cytoplasm, and rarely encode proteins[55]. However, these five major categories mainly involve only four typical mechanisms by which lncRNAs regulate gene expression: signaling, decoys, guides, and scaffolds[65].

Non-coding rna (ncRNAs) are key regulators of gene expression, and the most studied ncRNAs are long-stranded non-coding rna (lncRNAs), micro rna (miRNAs), and circular rna (circRNAs)[66].For ischemic stroke, the search for biomarkers is crucial for early diagnosis and guiding treatment. Changes in ncRNA expression profiles during ischemic stroke have gradually attracted attention[10, 22]. The relative stability, specificity, and reproducibility of ncRNAs make them promising biomarkers for early disease recognition[46].

Table 1. Comparison of Epigenetic Regulation Types and Mechanisms

Regulation Type	Specific Modification	Mechanism	Impact on Gene Expression
DNA Methylation	Methyl group addition	By DNMTs	Promoter: often represses; Gene body: varies
Histone Modification	Methylation	Alters chromatin	Activation or silencing
	Acetylation	HATs add, HDACs remove	HATs promote, HDACs inhibit
Non - coding RNA	siRNA	With AGO, TGS	Silences genes
	miRNA	Bind mRNA	Negatively regulates
	lncRNA	4 mechanisms	Multi - level regulation

Epigenetic regulation and stroke

Association of Epigenetic Modulation with Stroke

Ischemic Stroke Leads to Dynamic Changes in DNA Methylation and Regulates Widespread Differential Gene Expression, Altering Injury and Recovery Processes[3, 13, 60].

Whole blood whole genome methylation levels were higher in adults with ischemic smog disease than in healthy individuals. A total of 759 methylation probes were significantly different between cases and controls. The hypermethylated regions were mainly concentrated in gene spacer regions. Among the genes with the highest degree of differential expression, KCNMA1 and GALNT2 were upregulated and SOX6 and RBM33 were downregulated[28].

Hypomethylation of TNF Receptor-Related Factor 3 (TRAF3), Hypermethylation of thrombospondin-1 (THBS1), and Increased DNMT3A Activity Also Predict Stroke Outcome and the Extent of Ischemic Injury[13, 20].To date, it has been reported that within the BBB, hypermethylation of the TIMP2 promoter or hypomethylation of the VCAM-1 promoter controls BBB permeability and leukocyte recruitment[54, 60].

Ischemic stroke typically reduces overall gene expression levels by inhibiting acetylation of histones H3 and H4[32, 43]. Ischemic stroke overall reduced histone acetylation levels in the ischemic core, penumbral regions, and hemispheres of the affected brain. Acetylation of histone H3 lysine 9 (H3K9Ac) in the ischemic penumbral region of rat cerebral cortex decreased 2-fold at 1 hour and more than 4-fold at 4 and 24 hours after photothrombotic stroke[16]. In addition, Demyanenko's study showed that acetylation levels of histone H4 in the ipsilateral cortical penumbra were either increased or unaffected 7 days after ischemic stroke. Interestingly, the increased acetylation levels returned to control levels 14 days after ischemic stroke[14, 15]. Histone H3 and H4 acetylation levels were reduced in oligodendrocytes of cerebral white matter 7 days after ischemic stroke. The acetylation level of histone H4 in the ipsilateral cortex was not altered at 7 or 14 days after ischemic stroke[68].

It has been shown that ICH significantly reduced the acetylation level of histone H4 in the ipsilateral cortex, and that sodium butyrate (NaB), an HDAC inhibitor, increased the acetylation level and eliminated the decrease in acetylation level caused by ICH. In addition, HDAC inhibitors slightly ameliorated dyskinesia after ICH, and exercise increased the acetylation levels of histones (H3 and H4) in bilateral cortex; interestingly, no synergistic effect of exercise and NaB administration on histone acetylation was observed[48].

RNA modifications are an important part of epigenetic modifications. Currently, more than 160 chemical modifications have been identified in RNA, which are involved in regulating the structural properties of RNA or altering the affinity of mRNA for ribosomes[76].miRNAs can predict the risk and severity of stroke and the onset of cerebral infarction symptoms, and up- or down-regulation of multiple miRNAs, rather than a single miRNA, occurs during stroke[1, 62].

Clinical studies and experimental results

Recent studies have shown that siRNAs can lead to cellular transcriptional gene silencing (TGS) through DNA methylation and histone modification[7, 39, 53]. Zhou et al. demonstrated

Table 2. Epigenetic Changes Related to Stroke and Their Associations

Stroke Type	Epigenetic Changes	Key Genes/Molecules	Main Impact
Ischemic Stroke	DNA meth. change; histone acetylation↓; ncRNA expression change	KCNMA1, SOX6; H3K9Ac; miRNAs	Affects gene expression, recovery, BBB
ICH	Histone H4 acetylation↓ in ipsilateral cortex	Histone H4	Affects neuronal survival

that siRNA silencing of EZH2 reversed cisplatin resistance in human non-small cell lung cancer and gastric cancer cells[77]. EZH2 acts as a histone methyltransferase that causes methylation of H3K27, which then serves as an anchor for CpG methylation, leading to the formation of silent chromatin and ultimately TGS[64].Chromatin immunoprecipitation experiments showed that the binding of EZH2-inhibited DNMTs to specific genes depends on the presence of EZH2. Bisulfite sequencing results also demonstrated that EZH2 is required for methylation of target promoters repressed by EZH2, suggesting that EZH2 is involved in DNA methylation by recruiting DNA methyltransferases[71].

Dysregulation of histone methylation has been linked to a variety of diseases, including cancer, neurodegenerative diseases and genetic disorders. Histone methylation marks are also thought to be inherited through mitosis and meiosis, which provides a potential mechanism for transgenerational transmission of epigenetic information[6].

Many histone methyltransferases and demethyltransferases have been identified that catalyze the addition and removal of methyl groups from histone tails. These enzymes are key regulators of histone methylation dynamics, which in turn control the transcription of specific genes and gene networks[17].Histone methyltransferases commonly act as oncogenes in cancer, promoting cell proliferation and survival[50],and Histone Demethylases Are Associated with Neurodegenerative Diseases and Age-Related Cognitive Decline[49].

The exploration of epigenetic mechanisms in Parkinson's disease (PD) has witnessed significant advancements, with a particular focus on the role of DNA methylation in the context of PD. A study on a Sudanese cohort has provided valuable insights into this complex relationship.In this clinical investigation, researchers gathered a cohort of 172 Sudanese individuals, with 90 diagnosed with PD and 82 serving as healthy controls. An interesting aspect was the relatively young age of onset in the PD patients, averaging 40.6 ± 22.4 years, and a notable 64 patients had a family history of the disease.The study's findings regarding the methylation of the SNCA gene were quite revealing. Among the analyzed CpG sites, CpGs 16 - 23 exhibited significant hypomethylation in PD patients when compared to the control group. The P - values, ranging from 0.023 to 0.003, indicated a strong association. When sporadic cases were excluded from the analysis, the significance of these results was further enhanced. This suggests that the hypomethylation of these specific CpG sites might be a crucial epigenetic factor contributing to the development of PD, especially in familial cases[4].

Aberrant histone methylation has been reported in a variety of cancers, with global loss and gain of specific histone methylation marks observed. These changes are thought to promote dysregulation of gene expression programs for cancer development by driving cellular transformation and metastasis. Histone methylation is also involved in DNA repair, where histone H3K36 methylation is a key signal for mismatch repair. Defects associated with histone methylation and DNA repair have been linked to hereditary diseases such as hereditary nonpolyposis colorectal cancer and xeroderma pigmentosum[35, 56].

Epigenetic regulation as a therapeutic target

Histone methylation is a dynamic epigenetic mark in health, disease, and heredity, and understanding its regulation and function is critical to understanding normal biology and disease etiology[25]. A number of small molecule inhibitors of histone methyltransferases and demethyltransferases have been developed, and these inhibitors are currently being evaluated in preclinical trials for the treatment of cancer and other diseases[50]. Histone acetylation is also a target for epigenetic therapies, and drugs such as histone deacetylase inhibitors show promise in the treatment of neurodegenerative diseases and other disorders caused by aberrant histone acetylation[21].

Fujii et al. showed that daily consumption of large amounts of vegetables reduced ABCA1 gene methylation and lowered cholesterol and atherosclerosis. But interestingly, only women validated this study[19].

Exercise and HDAC inhibitors can alter epigenetic modifications in the motor cortex. These changes include increased DNA methylation, decreased histone deacetylase activity, and increased histone acetylation levels. These modifications can affect gene expression and promote neuronal plasticity and anti-inflammatory responses[48].It has been shown that in an ischemic stroke model, administration of a histone deacetylase inhibitor (HDACi) improves motor and cognitive function after stroke, with concomitant neuroplasticity, neurogenesis, and attenuated inflammation[32, 38, 60].

A researcher conducted a PPI network analysis of differential miRNAs, differential genes, and differentially methylated sites, and the results of the study showed that MRPS9, MRPL22, MRPL32, and RPS15 were identified as potential diagnostic and therapeutic targets for ischemic stroke progression. This implies that these genes may be involved in the process of ischemic stroke onset and progression, and therefore could be potential therapeutic targets[78].

Table 3. Epigenetic Regulation as Therapeutic Targets for Stroke and Related Drug Development

Regulation Type	Therapeutic Target	Interventions	Research Stage
DNA Methylation	Gene methylation sites	Diet - based	Clinical obs.
Histone Modification	Methyl/demethyl - transferases; HDACs	Small - molecule inhibitors; HDAC inhibitors	Pre - clinical; some clinical (HDACi)
Non - coding RNA	Differential miRNA/lncRNA pathways	Antisense oligonucleotides, mimics	Pre - clinical

Hypomethylation and altered expression of the miR-223 gene may lead to its inactivation or reduced degradation at the post-transcriptional level, which increases its inhibitory effect on target genes, and consequently contributes to the development and progression of stroke risk factors such as atherosclerosis[59].

Conclusions

Epigenetic modulation as a therapeutic strategy for stroke also faces several challenges. First, epigenetic mechanisms are complex and involve the interaction of multiple factors. This makes therapeutic strategies targeting specific epigenetic modifications difficult. Second, epigenetic modifications may be influenced by a variety of factors such as environment and lifestyle, which increases the difficulty of implementing effective interventions in stroke patients. In addition, most of the current epigenetic drugs are in their early stages and require further research and clinical trials to validate their safety and efficacy.

Despite the challenges, epigenetic modulation holds great promise in stroke treatment. First, by studying epigenetic mechanisms, we can gain a deeper understanding of stroke onset and progression. This can help discover new therapeutic targets and predictive biomarkers. Second, epigenetic drugs have the potential to improve stroke symptoms and prognosis by regulating specific gene expression. For example, neuronal damage after stroke can be reduced by upregulating the expression of genes with protective effects. Finally, epigenetic therapies can target individual differences for precision medicine and provide more personalized treatment plans for stroke patients.

Acknowledgements

Not applicable.

Author Contributions

All authors were involved in the conceptualization and design of the study. Data collection, first draft of the manuscript, and translation were done by Tiancai Yang. All authors commented on a previous version of the manuscript. All authors read and approved the final manuscript.

Consent for Publication

Not applicable.

Funding Information

This study was supported by the Jining City Key R&D Program Project (2022YXNS137).

Competing Interests

The authors declare that they have no existing or potential commercial or financial relationships that could create a conflict of interest at the time of conducting this study.

Data Availability

The data that support the findings of this study are available on request from the corresponding author.

References

[1] Abe A, Tanaka M, Yasuoka A, Saito Y, Okada S, Mishina M, et al. (2020) Changes in Whole-Blood microRNA Profiles during the Onset and Treatment Process of Cerebral Infarction: A Human Study. Int J Mol Sci, 21(9). https://doi.org/10.3390/ijms21093107

[2] Amaral PP, Dinger ME, Mercer TR, Mattick JS. (2008) The eukaryotic genome as an RNA machine. Science, 319(5871)1787-9. https://doi.org/10.1126/science.1155472

[3] Baccarelli A, Tarantini L, Wright RO, Bollati V, Litonjua AA, Zanobetti A, et al. (2010) Repetitive element DNA methylation and circulating endothelial and inflammation markers in the VA normative aging study. Epigenetics, 5(3)222-8. https://doi.org/10.4161/epi.5.3.11377

[4] Bakhit Y, Schmitt I, Hamed A, Ibrahim EAA, Mohamed IN, El-Sadig SM, et al. (2022) Methylation of alpha-synuclein in a Sudanese cohort. Parkinsonism Relat Disord, 1016-8. https://doi.org/10.1016/j.parkreldis.2022.05.009

[5] Barski A, Cuddapah S, Cui K, Roh TY, Schones DE, Wang Z, et al. (2007) High-resolution profiling of histone methylations in the human genome. Cell, 129(4)823-37. https://doi.org/10.1016/j.cell.2007.05.009

[6] Basavarajappa BS, Subbanna S. (2021) Histone Methylation Regulation in Neurodegenerative Disorders. Int J Mol Sci, 22(9). https://doi.org/10.3390/ijms22094654

[7] Bayne EH, Allshire RC. (2005) RNA-directed transcriptional gene silencing in mammals. Trends Genet, 21(7)370-3. https://doi.org/10.1016/j.tig.2005.05.007

[8] Cao X, Yeo G, Muotri AR, Kuwabara T, Gage FH. (2006) Noncoding RNAs in the mammalian central nervous system. Annu Rev Neurosci, 2977-103. https://doi.org/10.1146/annurev.neuro.29.051605.112839

[9] Carthew RW, Sontheimer EJ. (2009) Origins and Mechanisms of miRNAs and siRNAs. Cell, 136(4)642-55. https://doi.org/10.1016/j.cell.2009.01.035

[10] Chen J, Liu P, Dong X, Jin J, Xu Y. (2021) The role of lncRNAs in ischemic stroke. Neurochem Int, 147105019. https://doi.org/10.1016/j.neuint.2021.105019

[11] Collaborators GBDSRF. (2024) Global, regional, and national burden of stroke and its risk factors, 1990-2021: a systematic analysis for the Global Burden of Disease Study 2021. Lancet Neurol, 23(10)973-1003. https://doi.org/10.1016/S1474-4422(24)00369-7

[12] Costa FF. (2008) Non-coding RNAs, epigenetics and

complexity. Gene, 410(1)9-17. https://doi.org/10.1016/j.gene.2007.12.008
[13] Cullell N, Soriano-Tarraga C, Gallego-Fabrega C, Carcel-Marquez J, Torres-Aguila NP, Muino E, et al. (2022) DNA Methylation and Ischemic Stroke Risk: An Epigenome-Wide Association Study. Thromb Haemost, 122(10)1767-78. https://doi.org/10.1055/s-0042-1749328
[14] Demyanenko S, Berezhnaya E, Neginskaya M, Rodkin S, Dzreyan V, Pitinova M. (2019) capital ES, Cyrilliclass II histone deacetylases in the post-stroke recovery period-expression, cellular, and subcellular localization-promising targets for neuroprotection. J Cell Biochem, 120(12)19590-609. https://doi.org/10.1002/jcb.29266
[15] Demyanenko S, Neginskaya M, Berezhnaya E. (2018) Expression of Class I Histone Deacetylases in Ipsilateral and Contralateral Hemispheres after the Focal Photothrombotic Infarction in the Mouse Brain. Transl Stroke Res, 9(5)471-83. https://doi.org/10.1007/s12975-017-0595-6
[16] Demyanenko S, Uzdensky A. (2019) Epigenetic Alterations Induced by Photothrombotic Stroke in the Rat Cerebral Cortex: Deacetylation of Histone h3, Upregulation of Histone Deacetylases and Histone Acetyltransferases. Int J Mol Sci, 20(12). https://doi.org/10.3390/ijms20122882
[17] Deng P, Chen QM, Hong C, Wang CY. (2015) Histone methyltransferases and demethylases: regulators in balancing osteogenic and adipogenic differentiation of mesenchymal stem cells. Int J Oral Sci, 7(4)197-204. https://doi.org/10.1038/ijos.2015.41
[18] Feng J, Chang H, Li E, Fan G. (2005) Dynamic expression of de novo DNA methyltransferases Dnmt3a and Dnmt3b in the central nervous system. J Neurosci Res, 79(6)734-46. https://doi.org/10.1002/jnr.20404
[19] Fujii R, Yamada H, Munetsuna E, Yamazaki M, Mizuno G, Tsuboi Y, et al. (2019) Dietary vegetable intake is inversely associated with ATP-binding cassette protein A1 (ABCA1) DNA methylation levels among Japanese women. Nutrition, 651-5. https://doi.org/10.1016/j.nut.2019.02.010
[20] Gallego-Fabrega C, Carrera C, Reny JL, Fontana P, Slowik A, Pera J, et al. (2016) TRAF3 Epigenetic Regulation Is Associated With Vascular Recurrence in Patients With Ischemic Stroke. Stroke, 47(5)1180-6. https://doi.org/10.1161/STROKEAHA.115.012237
[21] Gediya P, Parikh PK, Vyas VK, Ghate MD. (2021) Histone deacetylase 2: A potential therapeutic target for cancer and neurodegenerative disorders. Eur J Med Chem, 216113332. https://doi.org/10.1016/j.ejmech.2021.113332
[22] Ghafouri-Fard S, Shoorei H, Taheri M. (2020) Non-coding RNAs participate in the ischemia-reperfusion injury. Biomed Pharmacother, 129110419. https://doi.org/10.1016/j.biopha.2020.110419
[23] Ghildiyal M, Zamore PD. (2009) Small silencing RNAs: an expanding universe. Nat Rev Genet, 10(2)94-108. https://doi.org/10.1038/nrg2504
[24] Goto K, Numata M, Komura JI, Ono T, Bestor TH, Kondo H. (1994) Expression of DNA methyltransferase gene in mature and immature neurons as well as proliferating cells in mice. Differentiation, 56(1-2)39-44. https://doi.org/10.1046/j.1432-0436.1994.56120039.x
[25] Greer EL, Shi Y. (2012) Histone methylation: a dynamic mark in health, disease and inheritance. Nat Rev Genet, 13(5)343-57. https://doi.org/10.1038/nrg3173
[26] Griffiths-Jones S, Grocock RJ, van Dongen S, Bateman A, Enright AJ. (2006) miRBase: microRNA sequences, targets and gene nomenclature. Nucleic Acids Res, 34(Database issue)D140-4. https://doi.org/10.1093/nar/gkj112
[27] Gurley LR, Walters RA, Tobey RA. (1973) Histone phosphorylation in late interphase and mitosis. Biochem Biophys Res Commun, 50(3)744-50. https://doi.org/10.1016/0006-291x(73)91307-7
[28] He S, Ye X, Duan R, Zhao Y, Wei Y, Wang Y, et al. (2022) Epigenome-Wide Association Study Reveals Differential Methylation Sites and Association of Gene Expression Regulation with Ischemic Moyamoya Disease in Adults. Oxid Med Cell Longev, 20227192060. https://doi.org/10.1155/2022/7192060
[29] Holliday R. (2006) Epigenetics: a historical overview. Epigenetics, 1(2)76-80. https://doi.org/10.4161/epi.1.2.2762
[30] Hu Z, Zhong B, Tan J, Chen C, Lei Q, Zeng L. (2017) The Emerging Role of Epigenetics in Cerebral Ischemia. Mol Neurobiol, 54(3)1887-905. https://doi.org/10.1007/s12035-016-9788-3
[31] Ito S, D'Alessio AC, Taranova OV, Hong K, Sowers LC, Zhang Y. (2010) Role of Tet proteins in 5mC to 5hmC conversion, ES-cell self-renewal and inner cell mass specification. Nature, 466(7310)1129-33. https://doi.org/10.1038/nature09303
[32] Jhelum P, Karisetty BC, Kumar A, Chakravarty S. (2017) Implications of Epigenetic Mechanisms and their Targets in Cerebral Ischemia Models. Curr Neuropharmacol, 15(6)815-30. https://doi.org/10.2174/1570159X14666161213143907
[33] Jiang D, Wang Y, Shen Y, Xu Y, Zhu H, Wang J, et al. (2016) Estrogen and promoter methylation in the regulation of PLA2G7 transcription. Gene, 591(1)262-7. https://doi.org/10.1016/j.gene.2016.07.048
[34] Jinek M, Doudna JA. (2009) A three-dimensional view of the molecular machinery of RNA interference. Nature, 457(7228)405-12. https://doi.org/10.1038/nature07755
[35] Joensuu EI, Nieminen TT, Lotsari JE, Pavicic W, Abdel-Rahman WM, Peltomaki P. (2015) Methyltransferase expression and tumor suppressor gene methylation in sporadic and familial colorectal cancer. Genes Chromosomes Cancer, 54(12)776-87. https://doi.org/10.1002/gcc.22289
[36] Jones PA. (2012) Functions of DNA methylation: islands, start sites, gene bodies and beyond. Nat Rev Genet, 13(7)484-92. https://doi.org/10.1038/nrg3230
[37] Jones PA, Baylin SB. (2007) The epigenomics of cancer. Cell, 128(4)683-92. https://doi.org/10.1016/j.cell.2007.01.029
[38] Kassis H, Shehadah A, Chopp M, Zhang ZG. (2017) Epigenetics in Stroke Recovery. Genes (Basel), 8(3). https://doi.org/10.3390/genes8030089
[39] Kawasaki H, Taira K. (2004) Induction of DNA methylation and gene silencing by short interfering RNAs in human cells. Nature, 431(7005)211-7. https://doi.org/10.1038/nature02889
[40] Kim M, Long TI, Arakawa K, Wang R, Yu MC, Laird PW.

(2010) DNA methylation as a biomarker for cardiovascular disease risk. PLoS One, 5(3)e9692. https://doi.org/10.1371/journal.pone.0009692
[41] Kozomara A, Griffiths-Jones S. (2014) miRBase: annotating high confidence microRNAs using deep sequencing data. Nucleic Acids Res, 42(Database issue) D68-73. https://doi.org/10.1093/nar/gkt1181
[42] Lan T, Hu L, Sun T, Wang X, Xiao Z, Shen D, et al. (2023) H3K9 trimethylation dictates neuronal ferroptosis through repressing Tfr1. J Cereb Blood Flow Metab, 43(8)1365-81. https://doi.org/10.1177/0271678X231165653
[43] Lanzillotta A, Pignataro G, Branca C, Cuomo O, Sarnico I, Benarese M, et al. (2013) Targeted acetylation of NF-kappaB/RelA and histones by epigenetic drugs reduces post-ischemic brain injury in mice with an extended therapeutic window. Neurobiol Dis, 49177-89. https://doi.org/10.1016/j.nbd.2012.08.018
[44] Li Y. (2021) Modern epigenetics methods in biological research. Methods, 187104-13. https://doi.org/10.1016/j.ymeth.2020.06.022
[45] Lin H. (2007) piRNAs in the germ line. Science, 316(5823)397. https://doi.org/10.1126/science.1137543
[46] Lu M, Dong X, Zhang Z, Li W, Khoshnam SE. (2020) Non-coding RNAs in Ischemic Stroke: Roles in the Neuroinflammation and Cell Death. Neurotox Res, 38(3)564-78. https://doi.org/10.1007/s12640-020-00236-7
[47] Luo M, Hao L, Hu F, Dong Y, Gou L, Zhang W, et al. (2015) MicroRNA profiles and potential regulatory pattern during the early stage of spermatogenesis in mice. Sci China Life Sci, 58(5)442-50. https://doi.org/10.1007/s11427-014-4737-8
[48] Maejima H, Okamura M, Inoue T, Takamatsu Y, Nishio T, Liu Y. (2023) Epigenetic modifications in the motor cortex caused by exercise or pharmacological inhibition of histone deacetylases (HDACs) after intracerebral hemorrhage (ICH). Brain Res, 1806148286. https://doi.org/10.1016/j.brainres.2023.148286
[49] Maes T, Mascaro C, Ortega A, Lunardi S, Ciceri F, Somervaille TC, et al. (2015) KDM1 histone lysine demethylases as targets for treatments of oncological and neurodegenerative disease. Epigenomics, 7(4)609-26. https://doi.org/10.2217/epi.15.9
[50] Mandumpala JJ, Baby S, Tom AA, Godugu C, Shankaraiah N. (2022) Role of histone demethylases and histone methyltransferases in triple-negative breast cancer: Epigenetic mnemonics. Life Sci, 292120321. https://doi.org/10.1016/j.lfs.2022.120321
[51] Mercer TR, Dinger ME, Mattick JS. (2009) Long non-coding RNAs: insights into functions. Nat Rev Genet, 10(3)155-9. https://doi.org/10.1038/nrg2521
[52] Moazed D. (2009) Small RNAs in transcriptional gene silencing and genome defence. Nature, 457(7228)413-20. https://doi.org/10.1038/nature07756
[53] Morris KV, Chan SW, Jacobsen SE, Looney DJ. (2004) Small interfering RNA-induced transcriptional gene silencing in human cells. Science, 305(5688)1289-92. https://doi.org/10.1126/science.1101372
[54] Ng GY, Lim YA, Sobey CG, Dheen T, Fann DY, Arumugam TV. (2018) Epigenetic regulation of inflammation in stroke. Ther Adv Neurol Disord, 111756286418771815. https://doi.org/10.1177/1756286418771815
[55] Ponting CP, Oliver PL, Reik W. (2009) Evolution and functions of long noncoding RNAs. Cell, 136(4)629-41. https://doi.org/10.1016/j.cell.2009.02.006
[56] Rechtsteiner A, Ercan S, Takasaki T, Phippen TM, Egelhofer TA, Wang W, et al. (2010) The histone H3K36 methyltransferase MES-4 acts epigenetically to transmit the memory of germline gene expression to progeny. PLoS Genet, 6(9)e1001091. https://doi.org/10.1371/journal.pgen.1001091
[57] Ruvkun G. (2001) Molecular biology. Glimpses of a tiny RNA world. Science, 294(5543)797-9. https://doi.org/10.1126/science.1066315
[58] Schweizer S, Meisel A, Marschenz S. (2013) Epigenetic mechanisms in cerebral ischemia. J Cereb Blood Flow Metab, 33(9)1335-46. https://doi.org/10.1038/jcbfm.2013.93
[59] Sharma AR, Shashikiran U, Uk AR, Shetty R, Satyamoorthy K, Rai PS. (2020) Aberrant DNA methylation and miRNAs in coronary artery diseases and stroke: a systematic review. Brief Funct Genomics, 19(4)259-85. https://doi.org/10.1093/bfgp/elz043
[60] Stanzione R, Cotugno M, Bianchi F, Marchitti S, Forte M, Volpe M, et al. (2020) Pathogenesis of Ischemic Stroke: Role of Epigenetic Mechanisms. Genes (Basel), 11(1). https://doi.org/10.3390/genes11010089
[61] Struhl K. (1998) Histone acetylation and transcriptional regulatory mechanisms. Genes Dev, 12(5)599-606. https://doi.org/10.1101/gad.12.5.599
[62] Tan KS, Armugam A, Sepramaniam S, Lim KY, Setyowati KD, Wang CW, et al. (2009) Expression profile of MicroRNAs in young stroke patients. PLoS One, 4(11) e7689. https://doi.org/10.1371/journal.pone.0007689
[63] Tchurikov NA. (2005) Molecular mechanisms of epigenetics. Biochemistry (Mosc), 70(4)406-23. https://doi.org/10.1007/s10541-005-0131-2
[64] Vire E, Brenner C, Deplus R, Blanchon L, Fraga M, Didelot C, et al. (2006) The Polycomb group protein EZH2 directly controls DNA methylation. Nature, 439(7078)871-4. https://doi.org/10.1038/nature04431
[65] Wang KC, Chang HY. (2011) Molecular mechanisms of long noncoding RNAs. Mol Cell, 43(6)904-14. https://doi.org/10.1016/j.molcel.2011.08.018
[66] Wang SW, Liu Z, Shi ZS. (2018) Non-Coding RNA in Acute Ischemic Stroke: Mechanisms, Biomarkers and Therapeutic Targets. Cell Transplant, 27(12)1763-77. https://doi.org/10.1177/0963689718806818
[67] Wang Y, Zhang X, Liu H, Zhou X. (2021) Chemical methods and advanced sequencing technologies for deciphering mRNA modifications. Chem Soc Rev, 50(24)13481-97. https://doi.org/10.1039/d1cs00920f
[68] Wang Z, Tsai LK, Munasinghe J, Leng Y, Fessler EB, Chibane F, et al. (2012) Chronic valproate treatment enhances postischemic angiogenesis and promotes functional recovery in a rat model of ischemic stroke. Stroke, 43(9)2430-6. https://doi.org/10.1161/STROKEAHA.112.652545
[69] Wang Z, Zang C, Cui K, Schones DE, Barski A, Peng W, et al. (2009) Genome-wide mapping of HATs and HDACs reveals distinct functions in active and inactive genes. Cell, 138(5)1019-31. https://doi.org/10.1016/j.cell.2009.06.049

[70] Weake VM, Workman JL. (2008) Histone ubiquitination: triggering gene activity. Mol Cell, 29(6)653-63. https://doi.org/10.1016/j.molcel.2008.02.014
[71] Wei JW, Huang K, Yang C, Kang CS. (2017) Non-coding RNAs as regulators in epigenetics (Review). Oncol Rep, 37(1)3-9. https://doi.org/10.3892/or.2016.5236
[72] Wolf PA, Grotta JC. (2000) Cerebrovascular disease. Circulation, 102(20 Suppl 4)IV75-80. https://doi.org/10.1161/01.cir.102.suppl_4.iv-75
[73] Yu H. (2009) [Epigenetics: advances of non-coding RNAs regulation in mammalian cells]. Yi Chuan, 31(11)1077-86. https://doi.org/10.3724/sp.j.1005.2009.01077
[74] Zaratiegui M, Irvine DV, Martienssen RA. (2007) Noncoding RNAs and gene silencing. Cell, 128(4)763-76. https://doi.org/10.1016/j.cell.2007.02.016
[75] Zhan L, Chen M, Pang T, Li X, Long L, Liang D, et al. (2023) Attenuation of Piwil2 induced by hypoxic postconditioning prevents cerebral ischemic injury by inhibiting CREB2 promoter methylation. Brain Pathol, 33(1)e13109. https://doi.org/10.1111/bpa.13109
[76] Zhao LY, Song J, Liu Y, Song CX, Yi C. (2020) Mapping the epigenetic modifications of DNA and RNA. Protein Cell, 11(11)792-808. https://doi.org/10.1007/s13238-020-00733-7
[77] Zhou W, Wang J, Man WY, Zhang QW, Xu WG. (2015) siRNA silencing EZH2 reverses cisplatin-resistance of human non-small cell lung and gastric cancer cells. Asian Pac J Cancer Prev, 16(6)2425-30. https://doi.org/10.7314/apjcp.2015.16.6.2425
[78] Zhu MX, Zhao TY, Li Y. (2023) Insight into the mechanism of DNA methylation and miRNA-mRNA regulatory network in ischemic stroke. Math Biosci Eng, 20(6)10264-83. https://doi.org/10.3934/mbe.2023450

Impact of heavy metals on allostatic load in adults: a NHANES study

Authors

Yiyin Rong, Shenglin Luo, Cong Wu, Haozhe Huang, Ming Chen, Xingyu Liu, Shaobo Wu

Correspondence

wushaobo@stu.xjtu.edu.cn (S. Wu)

Graphical Abstract

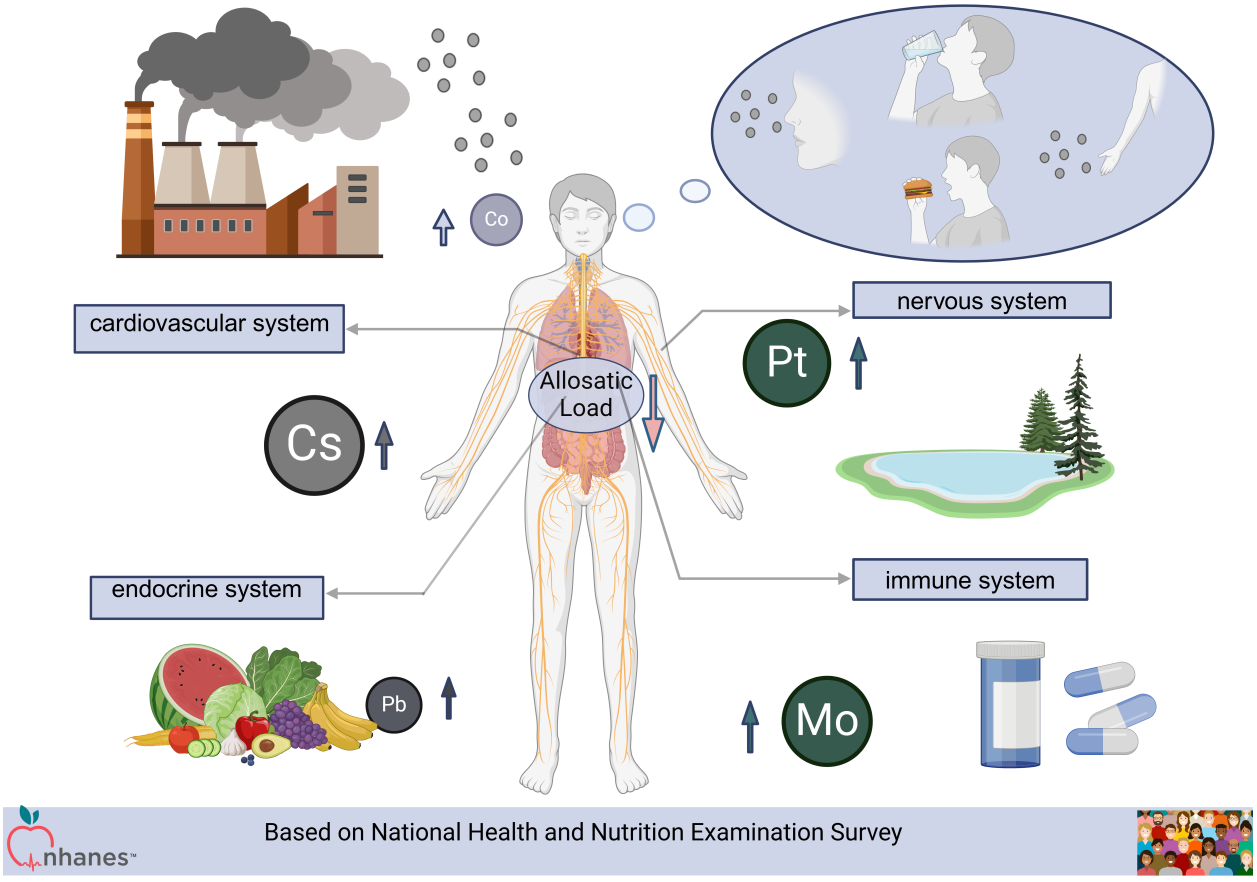

https://doi.org/10.71321/3b9xjm29

Research Article Life Conflux

Impact of heavy metals on allostatic load in adults: a NHANES study

Yiyin Rong [1] , Shenglin Luo [1] , Cong Wu [1] , Haozhe Huang [1] , Ming Chen [1] , Xingyu Liu [1] , Shaobo Wu [1*]

Received: 2025-01-25 | Accepted: 2025-03-26 | Published online: 2025-03-30

Abstract

Background: Allostatic load, defined as the cumulative strain resulting from the chronic stress response, is associated with adverse health outcomes. Heavy metals, prevalent in various environmental pollutants, exert cumulative effects on the human body through exposure via water or food sources. However, the relationship between heavy metals and allostatic load remains poorly understood. The aim of this study is to examine the association between urinary metal concentrations and allostatic load.

Methods: This study analyzed data from 4,231 adult participants in the National Health and Nutrition Examination Survey (NHANES) conducted between 2005 and 2010. We employed linear regression analysis, Bayesian kernel machine regression (BKMR), weighted quantile sum (WQS), and quantile g-computation (qgcomp) to investigate the associations between twelve urinary metals and allostatic load. Additionally, we developed K-nearest neighbors (KNN), random forest (RF), and XGBoost models to predict allostatic load scores (ALS).

Results: Linear regression analysis indicated that the combined effects of the twelve urinary metals were negatively correlated with allostatic load. WQS, qgcomp, and BKMR analyses identified cesium (Cs), molybdenum (Mo), lead (Pb), platinum (Pt), and cobalt (Co) as the primary influencing factors (all p-values < 0.05). Furthermore, when predicting ALS based on heavy metal exposure, the random forest model outperformed the other machine learning algorithms, with a root mean square error (RMSE) of 2.377428, compared to 2.501523 for KNN and 2.377733 for XGBoost.

Conclusion: Our findings indicate that urinary metal concentrations are negatively associated with allostatic load, with Cs, Mo, Pt, Pb, and Co showing the most significant negative correlations. Further research is necessary to explore the causal relationships and underlying mechanisms. Additionally, our analysis demonstrated that the random forest model was the most effective for ALS prediction.

Keywords: Urinary metals; Allostatic load score; National health and nutrition examination survey; Machine Learning.

Introduction

The concept of allostatic load which McEwen and Stellar[1] proposed in an effort to elucidate the process in which various body systems adapt and fluctuate to meet the demands of stress reflects the biological burden of chronic exposure to the downstream effects of various stress-response pathways arising from repeated environmental and physiological challenges[2]. Previous studies have shown that individuals with high AL compared with those with low AL had an increased mortality risk of 22% for all-cause and 31% for CVD mortality[3]. Prior reports also suggested that increased AL disrupt the nervous system and the stress response axis resulting in the disturbance of immune, cardiovascular, metabolic, and neuroendocrine systems, and further increasing cancer risk [4] [2, 5],even death [6]. In addition to some known potential risk factors such as health-damaging behaviors, there may be some risk factors. Identifying potential risk factors for allostatic load is important for understanding how these factors are associated with physiology as well as health and aging outcomes. Allostatic load can be quantified by the allostatic load score, an established measure of the cardiovascular, metabolic, and immune ramifications of stress, which was found to be a good predictor of mortality and decline in physical functioning [7] [8] [9].

Heavy metals are commonly defined as metallic elements with a density of ≥ 5 g/cm³. Lead (Pb), cadmium (Cd), mercury (Hg), selenium (Se), and manganese (Mn) are widely distributed environmental pollutants. Humans are commonly exposed to heavy metals through various sources such as air pollution, domestic effluents, cosmetic products, and food consumption[10]. Growing evidence indicates that heavy metals exert toxicity to individuals by interfering with immune homeostasis and promoting inflammation [4].We have known that physical stressors such as traumatic, infectious, and inflammatory exposures, as well as psychosocial stressors may each lead to frequent activation of allostatic systems, which may lead to high allostatic load [11].We surmise that exposure to mixture of heavy metals can be associated to high allostatic load.

1 Xi'an Jiaotong University

* Corresponding Author.

The study of heavy metal exposure and allostatic load will help us to think about the multilevel physiological regulation and pathological response. At the level of antioxidant and detoxification systems, heavy metals (such as Hg and Cd) can alleviate oxidative damage by inducing the expression of metallothionein, glutathione (GSH) and antioxidant enzymes (catalase, superoxide dismutase) [12]. For example, the lungs of rats exposed to mercury vapor locally adapt by upregulating metallothionein and glutathione, while the kidneys and brain are more vulnerable due to metabolic differences[12]. Cadmium exposure alleviates kidney injury by activating autophagy related genes (Beclin1, LC3), but inhibits the expression of bone formation genes (Osterix, RUNX2), which may lead to osteoporosis risk[13]. However, there are significant differences in detoxification thresholds among different organs, suggesting the need to establish organ-specific exposure limits.

At the same time, long-term low-dose exposure can trigger immune regulatory imbalance, which is manifested by the activation of pro-inflammatory factors (TNF-α, IL-2) pathways and the coexistence of immunosuppressive mechanisms, and this dual effect may increase susceptibility to infection or the risk of autoimmune diseases[13].

Meanwhile, the study of the relationship between heavy metals and adaptive load has far-reaching significance for the multidimensional strategy of public health intervention, such as the establishment of a biomarker early warning system integrating antioxidant indicators (catalase activity), detoxifying proteins (metallothiosin) and genetic damage markers, [12, 14] and further combining regional pollution characteristics to develop differentiated management policies. In this study, we employed data from the National Health and Nutrition Health and Nutrition Examination Survey (NHANES) in the United States to assess the relationship between allostatic load and the levels of 12 metals—barium (Ba), Beryllium(Be),cadmium (Cd), cobalt (Co), cesium (Cs), molybdenum (Mo), lead (Pb), antimony (Sb), thallium (Tl),platinum(Pt), tungsten (W), and uranium (U)—and their mixture in urine. We employed several statistical models, including multiple logistic regression, weighted quantile sum regression (WQS), Bayesian kernel machine regression (BKMR), to conduct our evaluation. Our findings yield epidemiological evidence for future research on the relationship between combined heavy metals exposure and allostatic load. And we found three ML models that could be used to identify ALS by heavy metals' exposure and then compared the performance characteristics of our models.

Methods

Study population

This cross-sectional study used data from 3 cycles in the NHANES website (https://www.cdc.gov/nchs/nhanes/index.htm), which was is a nationally representative study conducted by the National Center of Health Statistics comprising interviews as well as physical and medical examinations. Participants of the NHANES during the 2005 to 2010 cycles were included. Within these cycles, Measurement of urinary metals levels and all serum measurements included within our ALS calculations were completed. Measurements of C-reactive protein levels were not available in NHANES cycles after 2010. After excluding participants under 20 years old, with missing measurements included within our ALS calculations, those with missing urinary heavy metals level variables and those with missing other covariates data, 4231 participants were incorporated into the study, as illustrated in Figure 1.

Figure 1. Flow chart of the study population.

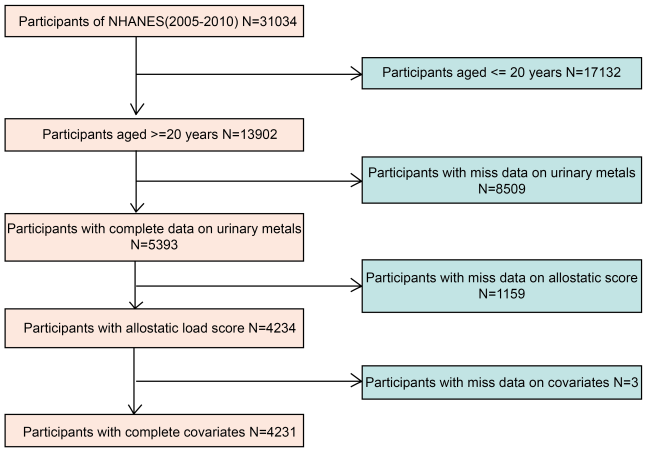

Metal measurements

The NHANES cycles between 2005 and 2010 measured the concentrations of 12 metals in urine, including Ba, Be, Cd, Co, Cs, Pt, Mo, Pb, Sb, Tl, W, and U. Methods for determining these metal concentrations are documented on the NHANES laboratory methods webpage. Natural logarithm (ln) transformations were performed for 12 metal variables to maintain a normal distribution for subsequent analyses. Values below the limit of detection (LOD) are not discarded in order to maintain data integrity.Meanwhile, to account for urine dilution, all metal concentrations were adjusted for creatinine concentration, with the corrected unit measured in μg/g creatinine.

Allostatic Load Score

The biomarkers were the most commonly used in prior studies evaluating ALS and represent certain functional organ systems [7]. For the cardiovascular system, systolic and diastolic blood pressure and total serum cholesterol and high-density lipoprotein (HDL) cholesterol levels were included. For the metabolic system, levels of glycohemoglobin (hemoglobin A1c) and albumin and body mass index (calculated as weight in kilograms divided by height in meters squared) were included. Lastly, for the immune system, levels of C-reactive protein were included. As a primary analysis, based on guidance from Duong [7], ALS was calculated by turning each biomarker into a dichotomous variable based on the statistical distribution of the sample (quartiles). One point was given if the biomarker was in the high-risk range (highest quartile) and if not (lowest 3 quartiles) with the exception of albumin and HDL cholesterol levels. For these 2 variables, a lower score indicated higher risk; thus, 1 point was given for being in the lowest quartile. In the sensitivity analysis, we also categorized each biomarker based on clinical cut points, with 1 point given if the biomarker was in the high-risk range. [15]

[16] [6] Individual biomarker thresholds for clinical cut point ALS determination are listed in Table 1. Overall, possible ALS ranged between 0 and 8, and the higher the ALS, the greater the association of stress with physiologic dysregulation.

Covariates

From within the NHANES interview assessments, we included several covariates, including age (continuous in years), sex (male and female), race and ethnicity (non-Hispanic Black, non-Hispanic White, other Hispanic, and other race [including multiracial]), education (less than high school, high school graduate or equivalent, some college education, or college graduate and greater), marital status (married or living with a partner or other, including widowed, divorced, separated, or never married). Smoking status was defined based on 2 self-reported questions: (1) "smoked at least 100 cigarettes in life" and (2) "Do you now smoke cigarettes?" Participants were categorized as non-smoker (answer of "no" to question 1), former smoker (answer of "yes" to question 1 but "not at all" to question 2), or current smoker (answer of "yes" to question 1 and "every day" or "some days" question 2).

Statistical analyses

The statistical software R (version 4.3.3) was utilized for the aforementioned analysis, with all significance levels set at $P < 0.05$ (two-tailed). Continuous or categorical variables were presented as medians and standard deviation (SD), or numerical and frequency distribution. Prior to any analysis, a logarithmic transformation of metals content in urine was performed.

We conducted weighted linear regression model to evaluate the relationship between urinary metals and allostatic load score. In this model, age, gender, education level, race, marital status, and smoking was adjusted. The results of p values were expressed.

Weighted quantile sum (WQS) and Quantile g-computation (qgcomp)

To examine the combined impacts using parametric inference, the qgcomp and WQS approach can be employed. WQS is a statistical technique used for analyzing high-dimensional data sets through multiple regression. [17] we conducted WQS analysis to assess the combined and individual impacts of heavy metals mixtures on allostatic load score by calculating a weighted linear index and assigning corresponding weights. In this study, we used bootstrapping with 1,000 iterations to construct WQS indexes in both positive and negative directions. When the WQS index was significant, corresponding weights were examined to identify the relative contribution of each heavy metal within the index to the prevalence of sarcopenia. The dataset was randomly divided, with 40% of the data allocated to the training set and the remaining 60% served as the validation set.

Qgcomp integrates the inferential framework of WQS regression with the flexibility of g-computation, addressing issues related to directional homogeneity and allowing for nonlinearity and no additivity in BKMR, thereby yielding more robust results [18]. In this study, we utilized the qgcomp model to evaluate the joint effect of exposure to a mixture of urinary metals on ALS and present both positive and negative weights for each metal in the urinary metals mixture.

Bayesian kernel machine regression (BKMR)

BKMR possesses the capacity to assess the impact of a combination of pollutants on health, as well as to estimate total exposure, individual exposure effects, and chemical interactions [19] [20]. In this study, we conducted a comparison of metals levels in urine samples collected at various percentiles and at the median in order to evaluate their overall influence on Allostatic Load Score. Additionally, we examined the specific effect of individual metals content in urine when other metals content is held constant at different percentiles. Furthermore, we explored the relationship between metals exposure and Allostatic Load Score, including any nonlinear associations. Lastly, Spearman correlation coefficients were computed to assess correlations between metals.

Machine learning component and performance evaluation

we compared the eight different machine learning algorithms including Extreme Gradient Boosting (XGBoost), Random Forest (RF), and K-Nearest Neighbors (KNN). In the comparison of the three algorithms, RF was the best choice.

RF which Breiman proposed [21] is one of the most widely used machine learning techniques. The essence of the RF algorithm is an improvement of the decision tree algorithm, and it can handle a large number of input variables. It has relatively high accuracy, robustness, and user-friendly nature. Two simple approaches for selecting features include mean decrease impurity and mean decrease accuracy [22] [23]. In addition, RF can be used to predict continuous variables and obtain predictions without obvious deviations. [24] [25]

With the test dataset, model performance was evaluated by the root-mean-square error (RMSE) expressed as

$$\mathrm{RMSE} = \sqrt{\frac{1}{n}\sum_{i=1}^{n}(y_i - \hat{y}_i)^2}$$

RMSE is the variance of the difference data to measure the "average error."

Result

Participant characteristics

A total of 4231 participants from the NHANES study conducted between 2005 and 2010 were included. Medians and interquartile ranges (IQR) were calculated for the level of allostatic load score. Table 1 presents their baseline characteristics. Significant differences($P<0.05$) were observed between the groups with different allostatic load score in terms of age, gender, race/ethnicity, education level, marital status, and smoking status. Furthermore, substantial differences were found in the urinary concentrations (μg/g creatinine) of heavy metals such as Be, Cd, Co, Cs, Mo, Pt, and Tl.

Heavy metals exposure and allostatic load score in the multivariate linear regression

To assess the potential link between log10-transformed heavy metals concentrations and the allostatic load score, we employed multivariate linear regression model which was showed in Table 2. It is worth noting that exp(Beta) means when X goes up by 1, the expected value of Y changes by

https://doi.org/10.71321/3b9xjm29

Table1. Baseline characteristics of participants

Characteristic	Overall, N = 4231(100%) [1]	**ALSscorequartiles** Q1, N = 1429(39%) [1]	Q2, N = 900(21%) [1]	Q3, N = 1404(30%) [1]	Q4, N = 498(9.5%) [1]	p-value [2]
Age	46.00±16.37	39.00±15.55	46.00±16.03	51.00±16.08	53.00±14.09	**<0.001**
Gender						0.7
1	2,122(49%)	707(48%)	454(50%)	713(51%)	248(49%)	
2	2,109(51%)	722(52%)	446(50%)	691(49%)	250(51%)	
Race						**<0.001**
1	794(8.6%)	262(8.2%)	177(9.1%)	260(8.6%)	95(9.3%)	
2	381(4.5%)	124(4.1%)	85(5.4%)	118(3.9%)	54(6.1%)	
3	2,113(72%)	787(75%)	434(70%)	690(72%)	202(64%)	
4	774(10%)	184(6.9%)	162(9.9%)	292(12%)	136(18%)	
5	169(5.0%)	72(6.2%)	42(5.5%)	44(3.8%)	11(3.3%)	
Education level						**<0.001**
1	542(6.8%)	127(4.6%)	125(7.5%)	203(8.0%)	87(11%)	
2	709(13%)	209(11%)	144(13%)	244(13%)	112(19%)	
3	979(24%)	320(22%)	210(24%)	342(27%)	107(23%)	
4	1,175(30%)	392(29%)	245(29%)	398(32%)	140(33%)	
5	826(26%)	381(34%)	176(27%)	217(20%)	52(14%)	
DMDMARTL						**<0.001**
1	2,302(58%)	753(54%)	498(60%)	799(62%)	252(56%)	
2	345(5.5%)	54(2.8%)	81(5.7%)	148(7.9%)	62(8.7%)	
3	425(10%)	132(9.6%)	71(8.7%)	153(11%)	69(15%)	
4	147(2.5%)	47(2.7%)	35(2.9%)	47(2.1%)	18(1.8%)	
5	656(16%)	305(21%)	125(13%)	167(11%)	59(13%)	
6	356(8.7%)	138(10%)	90(10%)	90(6.6%)	38(6.0%)	
Smoking status						**0.014**
1	922(23%)	348(25%)	186(23%)	257(18%)	131(27%)	
2	1,102(26%)	322(23%)	229(26%)	417(30%)	134(28%)	
3	2,207(51%)	759(52%)	485(52%)	730(52%)	233(45%)	
Ba	-1.83±0.39	-1.82±0.38	-1.83±0.37	-1.86±0.40	-1.84±0.42	0.3
Be	-3.32±0.33	-3.30±0.34	-3.31±0.34	-3.35±0.31	-3.37±0.27	**<0.001**
Cd	-2.63±0.37	-2.69±0.37	-2.60±0.37	-2.60±0.36	-2.56±0.36	**<0.001**
Co	-2.47±0.29	-2.47±0.28	-2.45±0.29	-2.49±0.30	-2.50±0.27	**0.034**
Cs	-1.35±0.21	-1.35±0.21	-1.34±0.22	-1.36±0.21	-1.38±0.19	**0.006**
Mo	-0.38±0.28	-0.36±0.26	-0.38±0.29	-0.41±0.29	-0.38±0.27	**<0.001**
Pb	-2.28±0.29	-2.31±0.28	-2.26±0.31	-2.27±0.30	-2.27±0.28	0.10

Pt	-4.22±0.39	-4.19±0.39	-4.19±0.38	-4.25±0.40	-4.27±0.43	**<0.001**
Sb	-3.24±0.29	-3.23±0.30	-3.23±0.30	-3.24±0.28	-3.24±0.29	0.4
Tl	-2.83±0.22	-2.81±0.22	-2.82±0.23	-2.85±0.22	-2.88±0.19	**<0.001**
W	-3.12±0.36	-3.11±0.36	-3.09±0.38	-3.13±0.35	-3.12±0.36	0.4
U	-4.22±0.38	-4.23±0.38	-4.22±0.39	-4.23±0.39	-4.18±0.38	0.13

1 median (SD) for continuous; n(%) for categorical.
2 Wilcoxon rank-sum test for complex survey samples; chi-squared test with Rao & Scott's second-order correction

about e exp(Beta). From the positive and negative values of exp(Beta) we can see the relationship between X and Y very well. Comparing with model I, there was a higher correlation between metals and allostatic load score after adjusting other heavy metals. It indicates that there may be interaction or a possible co-exposure pattern between mixed heavy metals. Meanwhile, After controlling for all confounders, the association between Be, Cd, Co, Cs, Mo, Pb, Pt, Sb and Tl and allostatic load score showed significance in multivariate linear regression(P<0.05), and were positively correlated with ALS. In the adjusted model, the risk of high allostatic load score decreased by 33.28% (exp (Beta): -1.1; 95% CI: -1.4, -0.77) for one-unit decrease in Cs concentration.

Heavy metals exposure and allostatic load score in WQS and qgcomp model

Both the WQS and qgcomp models were employed to estimate the weights of each metal in the mixture's overall effect. The interpretation of the results of the WQS model is based on the weighted quantile and (WQS) regression coefficients, reflecting the overall effect of the mixed exposure. The weights represent the relative contributions of each component in the mixed exposure and are used to identify the most important component in the mixed exposure (through the weight magnitude).We applied the WQS model to examine the association between the combined effects of the twelve heavy metals and the allostatic load score. The WQS index of the urinary metals was negatively associated with ALS in total.(Estimate: -0.386; P< 0.001) Figure 2A and Table 3 presented that Pb received the highest weight 0.181 for allostatic load score, followed by weight 0.177 for Cs, weight 0.145 for Mo, weight 0.125 for Pt, weight 0.7180 for Co, and in the negative direction after adjusting for all covariates. The WQS regression in the positive direction did not show any significant association of the heavy metals mixtures with allostatic load score. It is important to note that the WQS model cannot account for the effect of the direction of action of each component in the mixed exposure on the population.

Table 2. Multivariate linear regression analysis of Log10-transformed heavy metals for allostatic load score.The crude model did not adjust for any covariates. Adjusted model I was adjusted for all covariates. Adjusted model II was adjusted for all covariates and other heavy metals.

	Crude model			Adjusted model I			Adjusted model II		
	exp(Beta)	95%CI	p-value	exp(Beta)	95%CI	p-value	exp(Beta)	95%CI	p-value
Ba	1.07	0.88,1.29	0.478	1.22	1.02,1.46	0.026	-0.11	-0.27, 0.04	0.148
Be	0.76	0.58,0.99	0.038	0.77	0.59,1.02	0.058	-0.66	-0.83,-0.49	<0.001
Cd	1.92	1.50,2.46	<0.001	0.92	0.72,1.18	0.498	-0.31	-0.57, -0.06	0.013
Co	0.84	0.66,1.06	0.127	0.8	0.62,1.04	0.082	-0.51	-0.71, -0.31	<0.001
Cs	0.8	0.53,1.22	0.292	0.58	0.39,0.86	0.005	-1.1	-1.4, -0.77	<0.001
Mo	0.78	0.62,1.00	0.041	0.69	0.55,0.88	0.002	-0.56	-0.76, -0.35	<0.001
Pb	1.23	0.98,1.53	0.059	0.71	0.57,0.88	0.001	-0.63	-0.85, -0.42	<0.001
Pt	0.93	0.70,1.24	0.607	0.85	0.64,1.14	0.264	-0.51	-0.71, -0.31	<0.001
Sb	0.89	0.71,1.13	0.326	1	0.78,1.27	0.964	-0.31	-0.53, -0.09	0.005
Tl	0.54	0.37,0.79	<0.001	0.87	0.61,1.23	0.408	-0.84	-1.1, -0.56	<0.001
W	0.97	0.77,1.21	0.761	1.04	0.86,1.26	0.678	-0.16	-0.33, 0.02	0.065
U	1.02	0.85,1.22	0.833	1.01	0.86,1.18	0.886	-0.12	-0.28, 0.03	0.11

https://doi.org/10.71321/3b9xjm29

So we then use the qgomp model, whose results are interpreted based on the overall effect of the mixed exposure, allowing different components to have different effects in different directions, and can be used to assess the net effect of the mixed exposure (taking into account both positive and negative effects). The qgcomp model results further substantiated this finding, determining that the influence of these four heavy metals on the overall effect was negative. (Figure 2B)

Figure 2. WQS and qgcomp models. (A)WQS weights in the WQS regression model between ALS and WQS index of heavy metal mixtures. (B) Qgcomp model regression index weights for urinary heavy metals and ALS. The model adjusted for all covariates. Ba, Barium; Be, Beryllium; Cd, Cadmium; Co, Cobalt; Cs, Cesium; Mo, Molybdenum; Pb, lead; Pt, Platinum; Sb, Antimony; Tl, Thallium; W, Tungsten; U, Uranium.

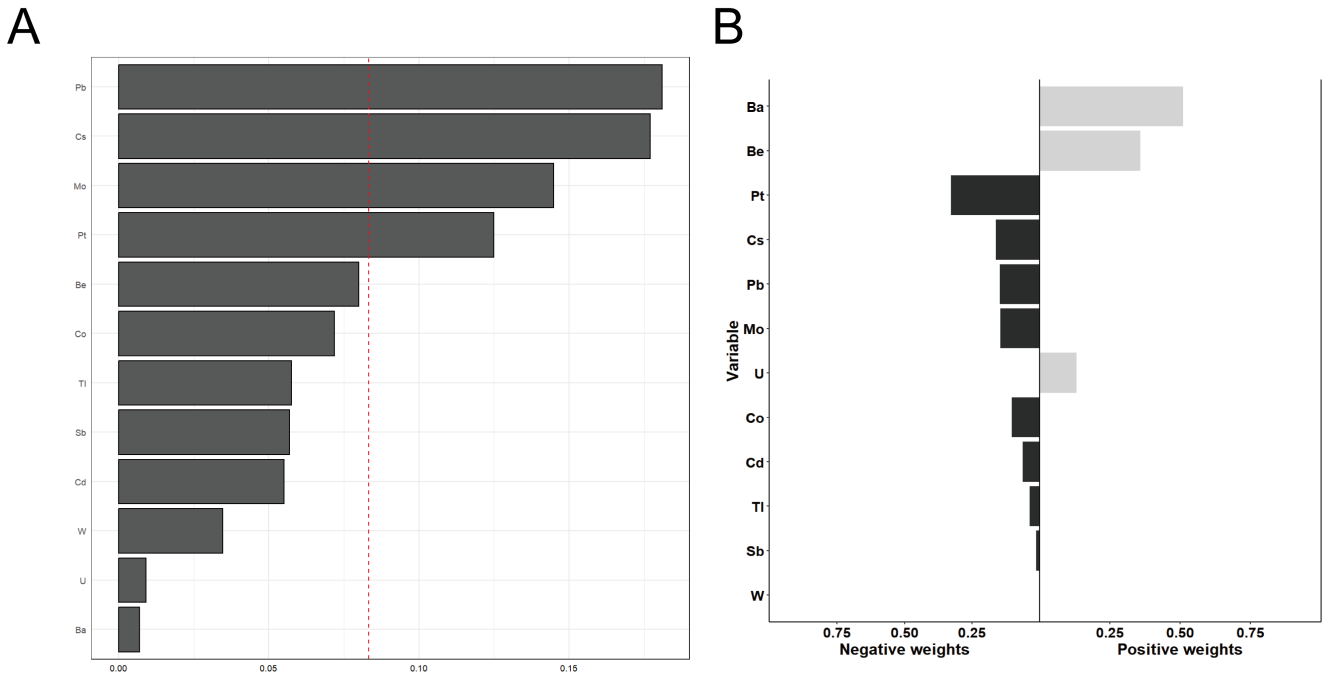

Table. 3. WQS weights in the WQS regression model between ALS and WQS index of heavy metal mixtures. The model adjusted for all covariates. Ba, Barium; Be, Beryllium; Cd, Cadmium; Co, Cobalt; Cs, Cesium; Mo, Molybdenum; Pb, lead; Pt, Platinum; Sb, Antimony; Tl, Thallium; Tu, Tungsten; Ur, Uranium.

Mix name	mean weight
Pb	0.18100
Cs	0.17700
Mo	0.14500
Pt	0.12500
Be	0.07990
Co	0.07180
Tl	0.05760
Sb	0.05690
Cd	0.05520
W	0.03460
U	0.00922
Ba	0.00703

Heavy Metal Correlations in the Spearman correlation matrix

Figure 3 is a heatmap showing the correlations among the 12 heavy metals using a Spearman correlation matrix. A complex exposure profile was observed among metal concentrations, with pairwise Spearman correlations ranging from slightly positive (P= 0.02) to strong positive correlations (P = 0.92). Of the all unique pairwise correlations, the strongest correlation is between urinary platinum and beryllium (P = 0.92), which presents high relation. Besides, urinary **cesium** and thallium present significantly (P = 0.57).

Heavy metals exposure and allostatic load score in BKMR model

In the BKMR model, allostatic load score was decreased for co-exposure to heavy metals mixtures above the 50th percentile compared to the medians. Figure 4A shows the **overall** exposure-response function trend of 12 heavy metals. When the other 11 metals were fixed at the median level, the univariate exposure-response relationship showed Cs, Pt, Pb, Co and Mo have a downward trend with ALS, with non-linear relationship. Notably, the univariate exposure–response curve for Cs and Pt is steeper than that for other three metals. The other seven metals do not show obvious ALS relationship. (Figure.4B).

Table 4 shows higher estimated PIPs for Cs (PIP = 1.0000), Pt (PIP = 1.0000), Mo (PIP = 0.9384), Co (PIP = 0.9272) Pb (PIP=0.9088), consistent with the previous two models. We further explored heavy metal interactions (Figure 4C). We fixed the other heavy metals at the median level and determined the exposure-response function of one heavy metal to a second heavy metal at its 10th, 50th, and 90th percentiles, respectively. No evidence of chemical interaction was found among each two of these heavy metals.

Figure 3. Spearman correlations among the mixed exposure of twelve metals in the participants.

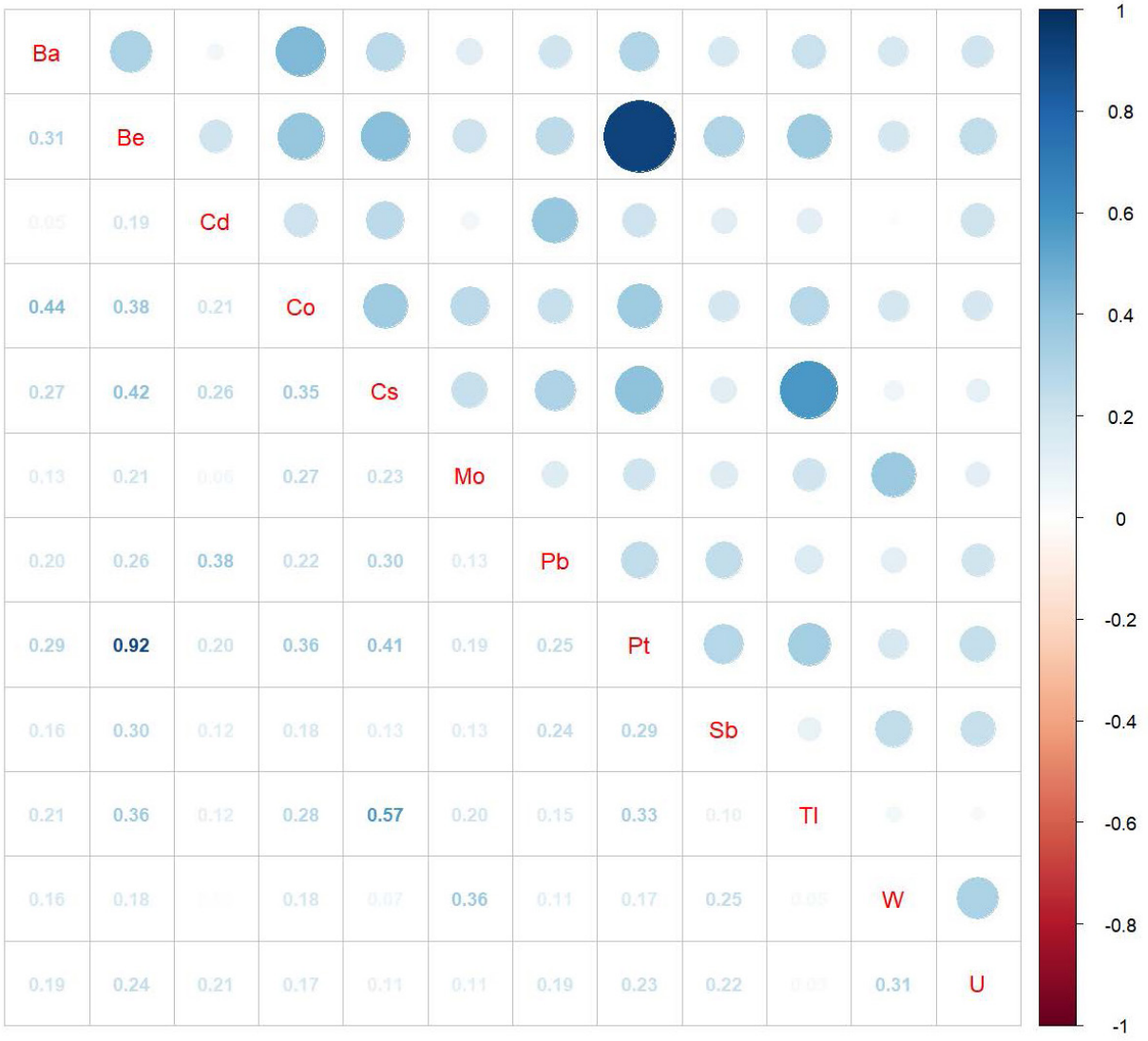

Figure 4. BKMR model. (**A**) Overall effect of metals in urine and ALS based on BKMR. (**B**)Univariate exposure–response function between each heavy metals and ALS when the other heavy metals were fixed at 50th percentiles. (**C**) Bivariate exposure-response relationship between twelve urinary heavy metals and ALS (a visualization for evaluating interactions).The model adjusted for all covariates. Ba, Barium; Be, Beryllium; Cd, Cadmium; Co, Cobalt; Cs, Cesium; Mo, Molybdenum; Pb, lead; Pt, Platinum; Sb, Antimony; Tl, Thallium; W, Tungsten; U, Uranium.

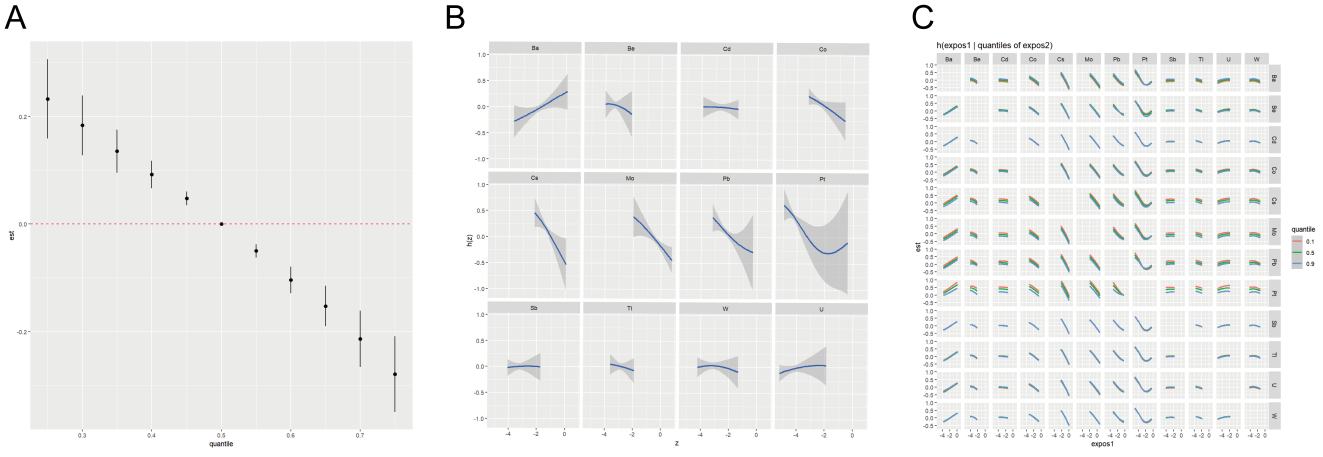

Table 4. The posteriori inclusion probability of single urinary metals

Heavy metals	PIP value
Ba	0.7372
Be	0.8704
Cd	0.8924
Co	0.9272
Cs	1.0000
Mo	0.9384
Pb	0.9088
Pt	1.0000
Sb	0.8736
Tl	0.8780
W	0.8708
U	0.7960

Evaluation and comparison of the ML model

Figure. 5 depicts three ML models. The study used 10-fold cross-validation to divide the entire sample into 10 equally sized subsamples. Among the 10 subsamples, one was retained as the verification data set of the test model, and the remaining nine were used as the training data set. After the cross-validation process was repeated 10 times, 10 results were generated, and the average value was taken as the performance metric. In this paper, the Root Mean Absolute Error (RMAE) was selected as the evaluation index.

Comparing the prediction performance of the RF, KNN and XGBoost prediction model, in terms of the Root Mean Absolute Error (RMAE), the RMAE of the RF prediction model was 2.377428, the RMAE of the KNN model was 2.501523 and the RMAE of the XGBoost model was 2.377733. Respectively. The prediction accuracy of the RF prediction model was best in three model (Table 1). The results were also shown in Figure 5.

Figure 5. Three ML model benchmark test results.

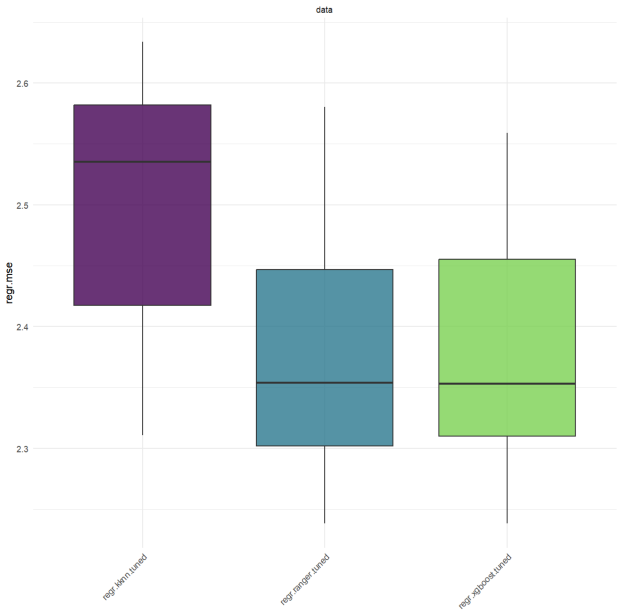

Discussion

Allostatic load which indicates the cumulative strain associated with the chronic stress response due to repeated environmental challenges is quantified by the allostatic load score, an established measure of the cardiovascular, metabolic, and immune ramifications of stress. [7] [8]Some studies was observed that heavy metals had significant and positively associations with CVD. [26] [27] [28]And long-term exposure to heavy metals (either low-dose or high-dose) uniformly causes immunosuppression and directly interferes with the sensitization of the immune system to antigens [29]. However, A study based on the data of NHANES from 2005 to 2018, through WQS and BKMR models, found that the mixed metals content in urine was negatively correlated with Mets. And in the study of single metal, the contents of Cs and Pb in urine are verified to be negatively correlated with Mets through logistic regression and the BKMR model [20].

Based on the data of NHANES from 2005 to 2010, this study analyzed twelve kinds of metals in urine and found that the mixed metals content in urine was negatively correlated with ALS through WQS and BKMR models. In the study of single metal, linear regression and the BKMR model verify that the contents of Cs, Pb, Mo and Pt in urine are negatively correlated with ALS. With the increase in metals content, allostatic load is monotonically decreasing. The result is contrary to our previous speculation. We surmise that there may be one reasons that the effect on metabolism may be the main factor between twelve urinary heavy metals and allostatic load.

According to previous research, Cs is closely related to the diagnostic factors of ALS. A study suggests that Cs are significantly related to HDL by studying chronic exposure of adult, postnatal and in utero rat models to low-dose 137 Cesium [30]. A repeated-measures study of older adults in Beijing showed that Cs were positively correlated with HDL [31], consistent with previous research results [32]. In addition, it is found that Cs have no significant relationship with SBP but have a negative correlation with DBP [31]. A study has found a significant negative correlation between Cs and BMI by utilizing the NHANES 99-02 data [33].

As for the mechanism behind the conclusion that the combined effect of 12 urinary metals is negatively correlated with allostatic load, we speculated that it may be related to the disruption of cell homeostasis by heavy metals such as lead, which can replace bivalent cations such as calcium and zinc, but also activate the Keap1-Nrf2 pathway. After Nrf2 enters the nucleus, it initiates the expression of genes regulated by antioxidant reaction elements (ARE), promotes the production of antioxidant enzymes such as glutathione synthetase and superoxide dismutase (SOD), and enhances the resistance of cells to oxidative stress, thus reducing the contribution of oxidative damage to adaptive load. At the same time, lead exposure induces the upregulation of endoplasmic reticulum (ER) stress proteins, such as glucose-regulating protein GRP78, and activates the unfolded protein response (UPR). Moderate UPR can repair cell function by enhancing protein folding capacity and clearing misfolded proteins, which may relieve stress load in the short term [34].

Regarding the correlation between beryllium and platinum, it has been shown that beryllium ($BeSO_4$) and the platinum

compound (PT-5-sulfomercaptoquinoline salt) both inhibit CA-ATPase activity in the sarcoplasmic reticulum (SR), but their inhibition is weaker than that of other compounds such as aminophenthiazine. This suggests that the two may indirectly affect each other's metabolic or excretory pathways by interfering with the activity of membrane-binding enzymes, such as those associated with calcium ion transport, which may be the reason for the correlation of composition in the urine of the two [35].

Since machine learning algorithms were widely used in diagnosing and prediction, we tried to make a prediction of ALS. We used a machine learning algorithm suitable for large-scale data, including 4231 samples. The RF model with RMSE was 2.377428. The model could be used to predict ALS for individuals, and provided a theoretical basis for further allostatic load targeted interventions.

This study still has some limitations. First, NHANES adopts a cross-sectional design, so it cannot further judge the causal relationship between metals content in urine and ALS. Second, the participants in this study are all Americans, and the results obtained may not apply to other people. Third, NHANES uses random urine samples to detect the metal concentrations in urine, and there may be some deviations in the metals content in urine. Because ALS is a continuous variable, we just use three ML models to predict ALS and the evaluation index of the ML model is single, lacking credibility.

Conclusion

The analysis of NHANES data showed that the mixed effect of twelve metals in urine is negatively correlated with ALS among American adults. The contents of cesium (Cs), Molybdenum (Mo), lead (Pb), Platinum (Pt) in urine were most negatively correlated with ALS. It is hoped that there will be a cohort study in the future to expose the influence of metals on ALS, which can provide higher-level evidence. In addition, it is hoped that relevant basic research can reveal the mechanism of the occurrence and development of metals and allostatic load. Finally, we employed three ML models to establish a predictive model for ALS utilizing heavy metals exposure data from the NHANES. Among these models, the RF approach exhibited superior performance.

Acknowledgements

The data was derived from published National Health and Nutrition Examination Survey (NHANES). The authors thank all investigators for sharing these data.

Author Contributions

Yiyin Rong: Conceptualization, Writing- Original draft preparation. Shenglin Luo: Data curation, Writing- Original draft preparation. Cong Wu: Methodology, Visualization. Haozhe Huang: Visualization. Validation. Ming Chen: Visualization. Xingyu Liu: Investigation. Shaobo Wu: Writing- Reviewing and Editing, Supervision.

Ethics Approval and Consent to Participate

The studies involving human participants were reviewed and approved by the National Center for Health Statistics Research Ethics Review Board. The patients/participants provided their written informed consent to participate in this study. Written informed consent was obtained from the individual(s)for the publication of any potentially identifiable images or data included in this article.

Funding Information

Not applicable.

Competing Interests

The authors declare that they have no existing or potential commercial or financial relationships that could create a conflict of interest at the time of conducting this study.

Data Availability

All data needed to evaluate the conclusions in the paper are present in the paper or the Supplementary Materials. Additional data related to this paper may be requested from the authors.

References

[1] Sterling, P., & Eyer, J. (1988). Allostasis: A New Paradigm to Explain Arousal Pathology. handbook of life stress cognition & health.

[2] Barrett, M., Wilcox, N. S., Huang, A., Levy, R., Demissei, B., Narayan, V., et al. (2022). Bearing allostatic load: insights into a more equitable future within cardio-oncology. Trends Mol Med, 28(12), 1040-1049. https://doi.org/10.1016/j.molmed.2022.09.006

[3] Parker, H. W., Abreu, A. M., Sullivan, M. C., & Vadiveloo, M. K. (2022). Allostatic Load and Mortality: A Systematic Review and Meta-Analysis. American journal of preventive medicine, 63(1), 131-140.

[4] Renu, K., Chakraborty, R., Haritha, M., Rajeshwari, K., & Abilash, V. G. (2021). Molecular mechanism of heavy metals (Lead, Chromium, Arsenic, Mercury, Nickel and Cadmium) induced hepatotoxicity – A review. Chemosphere, 129735.

[5] Mcewen, B. S. (2010). Stress, adaptation, and disease. Allostasis and allostatic load. Annals of the New York Academy of Sciences, 840(NEUROIMMUNOMODULATION: MOLECULAR ASPECTS), 33-44.

[6] Borrell, L. N., Dallo, F. J., & Nguyen, N. (2010). Racial/ethnic disparities in all-cause mortality in U.S. adults: the effect of allostatic load. Public Health Rep, 125(6), 810-816. https://doi.org/10.1177/003335491012500608

[7] Duong, M. T., Bingham, B. A., Aldana, P. C., Chung, S. T., & Sumner, A. E. (2016). Variation in the Calculation

of Allostatic Load Score: 21 Examples from NHANES. Journal of Racial & Ethnic Health Disparities, 4(3), 1-7.
[8] Beckie, & T., M. (2012). A systematic review of allostatic load, health, and health disparities. Biological Research for Nursing, 14(4), 311-346.
[9] Juster, R. P., McEwen, B. S., & Lupien, S. J. (2010). Allostatic load biomarkers of chronic stress and impact on health and cognition. Neurosci Biobehav Rev, 35(1), 2-16. https://doi.org/10.1016/j.neubiorev.2009.10.002
[10] Huang, Q., Wan, J., Nan, W., Li, S., He, B., & Peng, Z. (2024). Association between manganese exposure in heavy metals mixtures and the prevalence of sarcopenia in US adults from NHANES 2011–2018. Journal of Hazardous Materials, (Feb.15), 464.
[11] Guidi, J., Lucente, M., Sonino, N., & Fava, G. A. (2021). Allostatic Load and Its Impact on Health: A Systematic Review. Psychother Psychosom, 90(1), 11-27. https://doi.org/10.1159/000510696
[12] Mieiro, C. L., Duarte, A. C., Pereira, M. E., & Pacheco, M. (2011). Mercury accumulation patterns and biochemical endpoints in wild fish (Liza aurata): a multi-organ approach. Ecotoxicol Environ Saf, 74(8), 2225-2232. https://doi.org/10.1016/j.ecoenv.2011.08.011
[13] Lv, Y. J., Wei, Q. Z., Zhang, Y. C., Huang, R., Li, B. S., Tan, J. B., et al. (2019). Low-dose cadmium exposure acts on rat mesenchymal stem cells via RANKL/OPG and downregulate osteogenic differentiation genes. Environ Pollut, 249, 620-628. https://doi.org/10.1016/j.envpol.2019.03.027
[14] Javed, M., Ahmad, M. I., Usmani, N., & Ahmad, M. (2017). Multiple biomarker responses (serum biochemistry, oxidative stress, genotoxicity and histopathology) in Channa punctatus exposed to heavy metal loaded waste water. Sci Rep, 7(1), 1675. https://doi.org/10.1038/s41598-017-01749-6
[15] Slade, G. D., Sanders, A. E., & By, K. (2012). Role of Allostatic Load in Sociodemographic Patterns of Pain Prevalence in the U.S. Population. Journal of Pain Official Journal of the American Pain Society, 13(7).
[16] Frei, R., Haile, S. R., Mutsch, M., & Rohrmann, S. (2015). Relationship of Serum Vitamin D Concentrations and Allostatic Load as a Measure of Cumulative Biological Risk among the US Population: A Cross-Sectional Study. PLoS One, 10(10), e0139217. https://doi.org/10.1371/journal.pone.0139217
[17] Wheeler, D. C., Rustom, S., Carli, M., Whitehead, T. P., & Metayer, C. (2021). Assessment of Grouped Weighted Quantile Sum Regression for Modeling Chemical Mixtures and Cancer Risk. International Journal of Environmental Research and Public Health, 18(2), 504.
[18] Keil, A. P., Buckley, J. P., O'Brien, K. M., Ferguson, K. K., Zhao, S., & White, A. J. (2020). A Quantile-Based G-Computation Approach to Addressing the Effects of Exposure Mixtures. Environmental Health Perspectives, 128.
[19] Bobb, J. F., Valeri, L., Henn, B. C., Christiani, D. C., & Coull, B. A. (2014). Bayesian kernel machine regression for estimating the health effects of multi-pollutant mixtures. Biostatistics, 16(3), 493.
[20] Zha, B., Liu, Y., & Xu, H. (2023). Associations of mixed urinary metals exposure with metabolic syndrome in the US adult population. Chemosphere, 344, 140330. https://doi.org/10.1016/j.chemosphere.2023.140330
[21] Breiman, L. (2001). Random Forests. Machine Learning, 45(1), 5-32. https://doi.org/10.1023/A:1010933404324
[22] Archer, K. J., & Kimes, R. V. (2008). Empirical characterization of random forest variable importance measures. Computational Statistics & Data Analysis, 52(4), 2249-2260. https://doi.org/10.1016/j.csda.2007.08.015
[23] Tan, K., Ma, W., Wu, F., & Du, Q. (2019). Random forest-based estimation of heavy metal concentration in agricultural soils with hyperspectral sensor data. Environ Monit Assess, 191(7), 446. https://doi.org/10.1007/s10661-019-7510-4
[24] Dai, P., Chang, W., Xin, Z., Cheng, H., Ouyang, W., & Luo, A. (2021). Retrospective Study on the Influencing Factors and Prediction of Hospitalization Expenses for Chronic Renal Failure in China Based on Random Forest and LASSO Regression. Front Public Health, 9, 678276. https://doi.org/10.3389/fpubh.2021.678276https://doi.org/10.3389/fpubh.2021.678276
[25] Ellis, K., Kerr, J., Godbole, S., Lanckriet, G., Wing, D., & Marshall, S. (2014). A random forest classifier for the prediction of energy expenditure and type of physical activity from wrist and hip accelerometers. Physiol Meas, 35(11), 2191-2203. https://doi.org/10.1088/0967-3334/35/11/2191
[26] Guo, J., Su, L., Zhao, X., Xu, Z., & Chen, G. (2016). Relationships between urinary antimony levels and both mortalities and prevalence of cancers and heart diseases in general US population, NHANES 1999–2010. Science of The Total Environment, 571, 452-460. https://doi.org/10.1016/j.scitotenv.2016.07.011
[27] Yang, A. M., Lo, K., Zheng, T. Z., Yang, J. L., & Liu, S. M. (2020). Environmental heavy metals and cardiovascular diseases: Status and future direction. Chronic Diseases and Translational Medicine.
[28] Nguyen, H. D., Oh, H., Hoang, N. H. M., & Kim, M. S. (2021). Association between heavy metals, high-sensitivity C-reaction protein and 10-year risk of cardiovascular diseases among adult Korean population. Nature Publishing Group, (1).
[29] Hoffmann, B., Moebus, S., Dragano, N., Stang, A., Mohlenkamp, S., Schmermund, A., et al. (2009). Chronic residential exposure to particulate matter air pollution and systemic inflammatory markers. Environ Health Perspect, 117(8), 1302-1308. https://doi.org/10.1289/ehp.0800362
[30] Manens, L., Grison, S., Bertho, J. M., Lestaevel, P., Gueguen, Y., Benderitter, M., et al. (2016). Chronic exposure of adult, postnatal and in utero rat models to low-dose 137Cesium: impact on circulating biomarkers. J Radiat Res, 57(6), 607-619. https://doi.org/10.1093/jrr/rrw067
[31] Li, A., Li, Y., Mei, Y., Zhao, J., Zhou, Q., Li, K., et al. (2023). Associations of metals and metals mixture with lipid profiles: A repeated-measures study of older adults in Beijing. Chemosphere, 319, 137833. https://doi.org/10.1016/j.chemosphere.2023.137833
[32] Xu, C., Weng, Z., Zhang, L., Xu, J., Dahal, M., Basnet, T. B., et al. (2021). HDL cholesterol: A potential mediator of the association between urinary cadmium concentration and cardiovascular disease risk. Ecotoxicol Environ Saf, 208, 111433. https://doi.org/10.1016/j.ecoenv.2020.111433

[33] Padilla, M. A., Elobeid, M., Ruden, D. M., & Allison, D. B. (2010). An examination of the association of selected toxic metals with total and central obesity indices: NHANES 99-02. Int J Environ Res Public Health, 7(9), 3332-3347. https://doi.org/10.3390/ijerph7093332

[34] Giedroc, D. P., & Arunkumar, A. I. (2007). Metal sensor proteins: nature's metalloregulated allosteric switches. Dalton Trans, 10.1039/b706769k(29), 3107-3120. https://doi.org/10.1039/b706769k

[35] Tat'ianenko, L. V., Gromova, L. A., & Moshkovskiĭ, I. (1984). [The effect of biologically active compounds on the enzymatic activity of sarcoplasmic reticulum (Ca2+,Mg2+)-dependent ATPase transformed by synthetic phospholipids]. Mol Biol (Mosk), 18(2), 504-511. (Vliianie biologicheski aktivnykh soedineniĭ na fermentativnuiu aktivnost' rekonstruirovannoĭ sinteticheskimi fosfolipidami (Ca2+,Mg2+)-zavisomoĭ ATP-azy sarkoplazmaticheskogo retikuluma.)

Correlation Analysis between Spontaneous Nystagmus Characteristics and Semicircular Canal Dysfunction in Patients with Vestibular Neuritis: A Quantitative Study Using Electronystagmography and Video Head Impulse Test

Authors

Jun Cao, Jingye Wang

Correspondence

jyewang@163.com (J. Wang)

Graphical Abstract

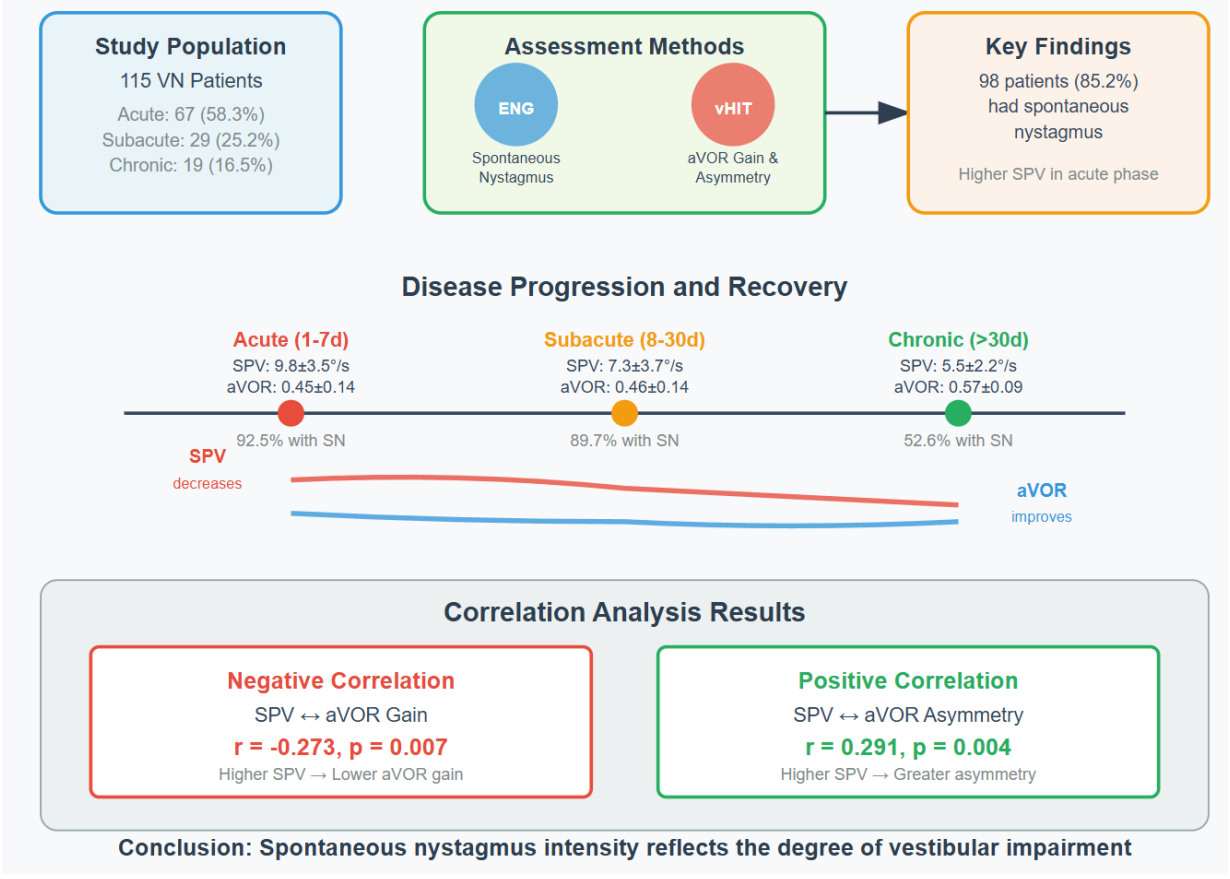

https://doi.org/10.71321/ceerva81

Research Article Life Conflux

Correlation Analysis between Spontaneous Nystagmus Characteristics and Semicircular Canal Dysfunction in Patients with Vestibular Neuritis: A Quantitative Study Using Electronystagmography and Video Head Impulse Test

Jun Cao [1] , Jingye Wang [1*]

Received: 2025-01-30 | Accepted: 2025-03-22 | Published online: 2025-03-30

Abstract

Objective: To compare the characteristics of spontaneous nystagmus (SN) in patients with vestibular neuritis (VN) at different disease stages and to investigate its correlation with semicircular canal dysfunction.

Methods: A total of 115 VN patients were enrolled, who were divided into acute phase (1 – 7 days), subacute phase (8 – 30 days) and chronic phase (>30 days) according to the course of disease. Quantitative assessment of SN was performed using electronystagmography (ENG), with particular focus on the slow phase velocity (SPV) in the horizontal plane. Simultaneously, vestibular-ocular reflex function was systematically evaluated through video head impulse test (vHIT), with quantitative measurements of angular vestibulo-ocular reflex (aVOR) gain and asymmetry of the affected semicircular canals.

Results: Among 115 patients, 67 (58.3%) were in acute phase, 29 (25.2%) in subacute phase and 19 (16.5%) in chronic phase. The mean age of patients in the acute phase was significantly lower than that in the chronic phase ($p = 0.028$), while there was no significant difference between the subacute phase and the other two groups. 98 patients (85.2%) had SN, 62 patients (92.5%) in acute phase, 26 patients (89.7%) in subacute phase and 10 patients (52.6%) in chronic phase. SPV in acute phase was significantly higher than that in subacute phase ($p = 0.003$) and chronic phase ($p < 0.001$), but there was no significant difference between chronic phase and subacute phase. In 112 patients with VN, the horizontal semicircular canals were affected, and the mean aVOR gain and asymmetry of the damaged side were 0.47 ± 0.14 and 0.35 ± 0.14, respectively. The aVOR gain of injured side in chronic phase was significantly higher than that in acute phase ($p < 0.001$) and subacute phase ($p = 0.007$), but there was no significant difference between acute phase and subacute phase ($p = 0.950$). The asymmetry in chronic phase was significantly lower than that in acute phase ($p = 0.001$) and subacute phase ($p = 0.018$), and there was no significant difference between acute phase and subacute phase ($p = 0.312$). SPV in horizontal component was negatively correlated with the aVOR gain of damaged horizontal semicircular canals ($r = -0.273$, $p = 0.007$), and positively correlated with aVOR asymmetry ($r = 0.291$, $p = 0.004$).

Conclusion: The existence of SN is helpful for diagnosis of VN, and its intensity can reflect the degree of vestibular impairment.

Key words: vestibular neuritis; spontaneous nystagmus; video head impulse test

Introduction

Vestibular neuritis (VN) is an acute peripheral vestibular syndrome and the third most common cause of peripheral vestibular disorders. It is characterized by acute or, less frequently, subacute onset of rotational or non-rotational vertigo, accompanied by imbalance, nausea/vomiting, and/or oscillopsia [1]. The video head impulse test (vHIT) is a widely used tool for assessing semicircular canal function, capable of accurately localizing the affected canal and measuring the angular vestibulo-ocular reflex (aVOR) gain of all six semicircular canals [2]. In this study, we compared the extent of vestibular dysfunction and the slow phase velocity (SPV) in VN patients across different disease stages (acute, subacute, and chronic).

Methods

This is a single-center, retrospective study involving patients diagnosed with vestibular neuritis at the Headache and Vertigo Clinic of the Department of Neurology, The First Affiliated Hospital of Anhui Medical University, from June 2022 to May 2024.

Inclusion and Exclusion Criteria

Inclusion Criteria: All patients underwent comprehensive neurological and otological examinations, as well as video infrared goggles testing. All patients also underwent both vHIT and electronystagmography (ENG). Patients with focal

1 Department of Neurology, The First Affiliated Hospital of Anhui Medical University, Hefei 230022, China

* Corresponding Author.

neurological signs underwent brain MRI. Patients with acute vestibular syndrome during vertigo attacks and vHIT results showing unilateral gain <0.7 were included in the subsequent analyses.

Exclusion Criteria: 1) Patients with central nervous system lesions confirmed by MRI. 2) Patients who had taken any vestibular suppressants within 48 hours before vestibular testing. 3) Patients who had undergone vestibular rehabilitation before ENG testing.

Study design

The vHIT device was used to examine the patients. Patients were seated with their heads flexed forward by 30° to align the horizontal semicircular canals parallel to the horizontal plane. They were instructed to fixate on a stationary target 1 m ahead. The examiner then abruptly and randomly rotated the patient's head to the left and right (head rotation angle of 20° – 30°, lasting 150 – 200 ms, with a peak head velocity >150°/s). Subsequently, the patient's head was turned 45° to the left and right, and the examiner performed abrupt, small-amplitude, random up-and-down head rotations in the sagittal plane. Each direction was tested with 20 effective head impulses. The goggles recorded the eye and head movement trajectories and saccades during head rotation. The aVOR gain for each head impulse was calculated as the ratio of peak eye velocity to peak head velocity, and the average value was taken as the gain for each semicircular canal.

During the ENG examination, the presence of SN in the neutral head position and while looking straight ahead was assessed. Instruct the patient to sit upright, wear the goggles, eliminate visual fixation, and record nystagmus for at least 30 seconds. For patients with SN, the horizontal component of the SPV was recorded. Patients were categorized into three groups based on the time interval from symptom onset to examination: acute phase (1 – 7 days), subacute phase (8 – 30 days), and chronic phase (>30 days). We compared the differences in age, gender, aVOR gain and asymmetry among the three groups. The aVOR asymmetry was calculated using the relative asymmetry formula: (higher mean high-speed aVOR gain - lower mean high-speed aVOR gain)/ (higher mean high-speed aVOR gain + lower mean high-speed aVOR gain).

Statistic Analysis

Data were analyzed using SPSS version 26, and figures were created using GraphPad Prism version 9.5. Normally distributed data are presented as mean ± standard deviation, while non-normally distributed data are presented as median and interquartile range. For comparisons of continuous variables between groups, normally distributed data were analyzed using independent samples t-tests, while non-normally distributed data were analyzed using the Mann-Whitney U test (a type of rank-sum test). Categorical data were analyzed using Pearson's chi-square test or Fisher's exact test, as appropriate. All results were considered statistically significant with a two-sided p-value < 0.05.

Result

A total of 115 patients were included in this study, of whom 74 were male (64.3%), with a mean age of 50.2 ± 14.4 years. Vestibular dysfunction was observed on the left side in 75 patients (65.2%) and on the right side in 40 patients (34.8%). The superior vestibular nerve was affected in 108 cases (93.9%), the inferior vestibular nerve in 2 cases (1.7%), and both nerves in 5 cases (4.3%). The horizontal semicircular canal was affected in 112 patients (97.4%), the anterior semicircular canal in 17 patients (14.8%), and the posterior semicircular canal in 7 patients (6.1%). The acute phase was observed in 67 patients (58.3%), the subacute phase in 29 patients (25.2%), and the chronic phase in 19 patients (16.5%). The mean age of patients in the acute phase was 48.3 ± 15.2 years, which was significantly lower than that of the chronic phase (56.6 ± 13.3 years, p = 0.028), while the subacute phase (50.3 ± 12.5 years) showed no significant difference compared with the other two groups. There was no significant difference in the male-to-female ratio among the three groups (p = 0.112).

Spontaneous nystagmus

SN was observed in 98 patients (85.2%). Among them, 62 patients (92.5%) were in the acute phase, 26 (89.7%) in the subacute phase, and 10 (52.6%) in the chronic phase. Of these patients with SN, 95 (96.9%) exhibited a fast phase directed toward the healthy side, while 3 (3.1%) had a fast phase directed toward the affected side. The mean SPV of horizontal nystagmus was 8.7 ± 3.8°/s. The SPV in the acute phase (9.8 ± 3.5°/s) was significantly higher than that in the subacute phase (7.3 ± 3.7°/s, p = 0.003) and the chronic phase (5.5 ± 2.2°/s, p < 0.001), while no significant difference was observed between the subacute and chronic phases (p = 0.173) (Figure.1).

Figure. 1 Comparison of SN and lateral semicircular canal aVOR gain in VN patients with different disease courses (acute, subacute and chronic), **p ≤ 0.01, **p ≤ 0.001.

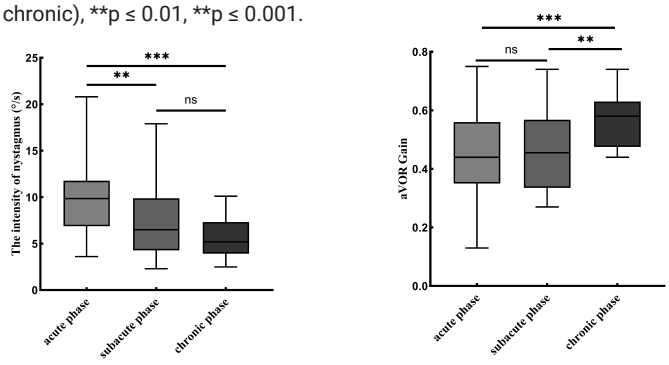

vHIT Results

Among the 112 patients with VN involving the horizontal semicircular canal, the mean gain value of the affected side was 0.47 ± 0.14, and the mean asymmetry ratio was 0.35 ± 0.14. These patients were distributed across three phases: acute phase (67 cases), subacute phase (28 cases), and chronic phase (17 cases). The aVOR gain of the affected side in the chronic phase (0.57 ± 0.09) was significantly higher than that in the acute phase (0.45 ± 0.14, p < 0.001) and subacute phase (0.46 ± 0.14, p = 0.007), while no significant difference

was observed between the acute and subacute phases (p = 0.950). The aVOR asymmetry in the chronic phase (0.25 ± 0.09) was significantly lower than that in the acute phase (0.38 ± 0.14, p = 0.001) and subacute phase (0.35 ± 0.14, p = 0.018), with no significant difference between the acute and subacute phases (p = 0.312) (Figure. 1). In the study, 17 patients had involvement of the anterior semicircular canal, with 10 cases in the acute phase, 5 in the subacute phase, and 2 in the chronic phase. The mean aVOR gain of the affected side was 0.55 ± 0.09, and the mean aVOR asymmetry was 0.25 ± 0.11. Additionally, 7 patients had involvement of the posterior semicircular canal, with 2 cases in the acute phase, 3 in the subacute phase, and 2 in the chronic phase. The mean aVOR gain of the affected side was 0.57 ± 0.10, and the mean aVOR asymmetry was 0.24 ± 0.09.

Among the 98 patients with SN, all exhibited involvement of the horizontal semicircular canal. The SPV of the horizontal component of nystagmus was significantly negatively correlated with the aVOR gain of the affected horizontal semicircular canal (r = -0.273, p = 0.007) and significantly positively correlated with the aVOR asymmetry (r = 0.291, p = 0.004) (Figure. 2).

Figure. 2 Correlation analysis of SN on horizontal component with gain value and asymmetry ratio of damaged side in VN patients.

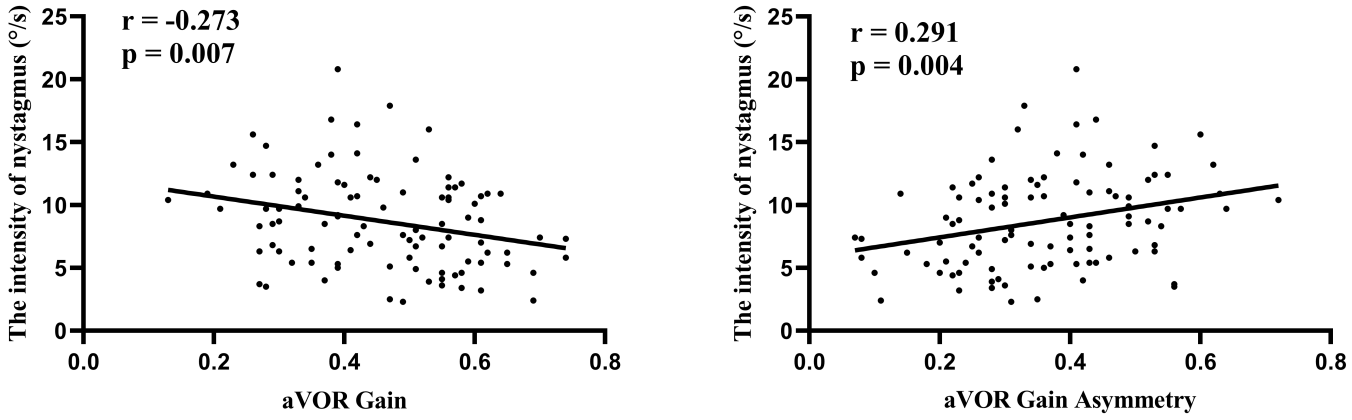

Discussion

The results of this study indicate that involvement of the superior vestibular nerve is the most common (93.9%) among patients with VN, followed by involvement of both the superior and inferior vestibular nerves (4.3%), while isolated involvement of the inferior vestibular nerve is the rarest (1.7%). These findings are consistent with those reported in previous literature [1]. These findings are related to the anatomical characteristics of the vestibular system. First, the osseous canal through which the superior vestibular nerve travels is relatively long and narrow, making it more susceptible to compression when the nerve becomes swollen. Second, latent infections of herpes simplex virus type 1 (HSV-1) in the vestibular ganglion are predominantly located in the superior vestibular ganglion, rendering the superior vestibular nerve more vulnerable to HSV-1 infection [3].

In this study, we found that patients with chronic VN had significantly higher ages compared to the other two groups, suggesting that older patients are more likely to experience chronicity of symptoms. Previous studies have reported that in the follow-up of VN patients, the degree of symptom improvement in the elderly group was significantly lower than that in the younger group [4, 5]. This phenomenon may be attributed to the multisystem degeneration in elderly patients, including the degeneration of the vestibular and visual systems. Therefore, for elderly patients, it is particularly important to develop an early and tailored vestibular rehabilitation therapy (VRT) plan. In addition to vestibular exercises, vision plays a crucial role in compensating for vestibular deficits in older adults. For elderly patients with blurred vision, such as those with cataracts, vision correction should be implemented to prevent imbalance and falls.

After vestibular dysfunction, clinical symptoms can be categorized into static symptoms, which occur in a resting state, and dynamic symptoms, which emerge during body movement. Static symptoms include SN, contrapositional deviation, ocular torsion, head and body tilt, vertigo, and autonomic nervous system responses such as nausea and vomiting. Dynamic symptoms involve changes in aVOR gain, among others. Following vestibular dysfunction, the body gradually alleviates symptoms through vestibular compensation, which is divided into static and dynamic compensation. Static compensation is a transient, spontaneous, neurophysiological change based on the vestibular nuclear complex, while dynamic compensation is a long-term, learned process that involves multiple central nervous system mechanisms. It has been reported in the literature that rodents can complete static vestibular compensation within one week [6]. It has been reported in the literature that rodents can complete static vestibular compensation within one week [7], while cats can complete this process within six weeks [8, 9]. Early studies by Matsuzaki et al. have shown that SN typically disappears completely within 1 month after the onset of vestibular neuritis [10]. In this study, we found that after removing fixation suppression in the dark condition, more than 50% of patients with chronic vestibular neuritis still exhibited SN, which can serve as an important clinical indicator for the diagnosis of the chronic phase of vestibular neuritis. In our study, the SPV in the acute phase was significantly higher than that in the subacute and chronic phases, with no significant difference between the

subacute and chronic phases. Additionally, the aVOR gain on the affected side in the chronic phase was significantly higher than that in the acute and subacute phases, while the aVOR asymmetry was significantly lower than that in the acute and subacute phases; there were no significant differences between the acute and subacute phases. These results suggest that static compensation occurs early in the disease course, while dynamic compensation requires a longer period of time.

After vestibular nerve damage, the generation of SN is due to the reduced resting activity on the affected side, resulting in a neurophysiological imbalance between the bilateral vestibular nuclei [11]. Studies have shown that in the early stages of the disease, the slow phase of SN is directed toward the affected side. As vestibular function recovers on the affected side and static compensation occurs, the SPV gradually diminishes and eventually disappears. In long-term follow-up studies of patients with unilateral vestibular dysfunction, the duration of SN shows significant individual variability, ranging from several days to months or even years. This variability is primarily determined by the rate of vestibular compensation and differences in individual recovery capabilities [12, 13]. In the patients included in this study, vestibular function remained impaired, with over 50% of patients in the chronic phase still exhibiting SN. This suggests that static compensation in these patients is insufficient to overcome the imbalance between the bilateral vestibular systems. Our study found that the SPV is negatively correlated with the aVOR gain on the affected side and positively correlated with the aVOR asymmetry of bilateral gain values. These findings are consistent with previous studies [14]. These findings indicate that the presence of SN not only suggests an imbalance in bilateral vestibular function but also reflects the degree of vestibular dysfunction based on its intensity.

Conclusion

In summary, among patients with VN, older patients tend to experience longer-lasting symptoms and would benefit from early implementation of tailored rehabilitation programs. The persistence of SN in the chronic phase serves as an important diagnostic indicator and reflects the severity of vestibular dysfunction based on its intensity. As a cross-sectional study, our research has the following limitations: First, the study design does not allow for the assessment of the dynamic evolution of vestibular dysfunction over time. Future research should involve longitudinal cohort studies with long-term follow-up of at least 6–12 months to elucidate the temporal characteristics of vestibular compensation. Second, the current evaluation primarily relies on objective measures of vestibular function. We recommend incorporating subjective assessment tools, such as the Vestibular Symptom Scale and the Dizziness Handicap Inventory, to comprehensively evaluate the extent of vestibular dysfunction and its impact on quality of life.

Acknowledgments

The authors would like to thank all the patients.

Author Contribution

JYW and JC conceived and designed the study, and completed the first draft. JC acquired the data. JYW analyzed the data. All authors critically review the content of the manuscript. All authors approved the final version.

Conflicting Interests

The authors declare no competing interests.

Ethics Approval and Consent to Participate

The study protocols were approved by the Institutional Review Board of the First Affiliated Hospital of Anhui Medical University (no. PJ2024-10-65).

Data availability

The datasets used and/or analyzed during the current study are available from the corresponding author on reasonable request.

References

[1] Strupp M, Bisdorff A, Furman J, Hornibrook J, Jahn K, Maire R, Newman-Toker D, Magnusson M (2022) Acute unilateral vestibulopathy/vestibular neuritis: Diagnostic criteria. Journal of vestibular research : equilibrium & orientation 32(5):389-406. https://doi.org/10.3233/ves-220201

[2] Jasinska-Nowacka A, Niemczyk K (2024) Application of a Video Head Impulse Test in the Diagnosis of Vestibular Neuritis. Life (Basel) 14(6). https://doi.org/10.3390/life14060757

[3] Gianoli G, Goebel J, Mowry S, Poomipannit P (2005) Anatomic differences in the lateral vestibular nerve channels and their implications in vestibular neuritis. Otol Neurotol 26(3):489-494. https://doi.org/10.1097/01.mao.0000169787.99835.9f

[4] Jacobson G, McCaslin D (2020) Vestibular Neuritis in Patients Among Different Age Groups: Clinical Features and Outcomes. J Am Acad Audiol 31(9):627-628. https://doi.org/10.1055/s-0041-1723789

[5] Scheltinga A, Honegger F, Timmermans DP, Allum JH (2016) The Effect of Age on Improvements in Vestibulo-Ocular Reflexes and Balance Control after Acute Unilateral Peripheral Vestibular Loss. Front Neurol 7:18. https://doi.org/10.3389/fneur.2016.00018

[6] Lacour M, Helmchen C, Vidal PP (2016) Vestibular compensation: the neuro-otologist's best friend. J Neurol 263 Suppl 1:S54-64. https://doi.org/10.1007/s00415-015-7903-4

[7] Darlington CL, Smith PF (2000) Molecular mechanisms of recovery from vestibular damage in mammals: recent advances. Prog Neurobiol 62(3):313-325. https://doi.

org/10.1016/s0301-0082(00)00002-2
[8] Lacour M, Tighilet B (2010) Plastic events in the vestibular nuclei during vestibular compensation: the brain orchestration of a "deafferentation" code. Restor Neurol Neurosci 28(1):19-35. https://doi.org/10.3233/rnn-2010-0509
[9] Borel L, Lopez C, Péruch P, Lacour M (2008) Vestibular syndrome: a change in internal spatial representation. Neurophysiol Clin 38(6):375-389. https://doi.org/10.1016/j.neucli.2008.09.002
[10] Matsuzaki M, Kamei T (1995) Stage-assessment of the progress of continuous vertigo of peripheral origin by means of spontaneous and head-shaking nystagmus findings. Acta Otolaryngol Suppl 519:188-190. https://doi.org/10.3109/00016489509121900
[11] Robinson DA, Zee DS, Hain TC, Holmes A, Rosenberg LF (1984) Alexander's law: its behavior and origin in the human vestibulo-ocular reflex. Ann Neurol 16(6):714-722. https://doi.org/10.1002/ana.410160614
[12] Choi KD, Oh SY, Kim HJ, Koo JW, Cho BM, Kim JS (2007) Recovery of vestibular imbalances after vestibular neuritis. The Laryngoscope 117(7):1307-1312. https://doi.org/10.1097/MLG.0b013e31805c08ac
[13] Bergenius J, Perols O (1999) Vestibular neuritis: a follow-up study. Acta Otolaryngol 119(8):895-899. https://doi.org/10.1080/00016489950180243
[14] Zhang X, Deng Q, Liu Y, Li S, Wen C, Liu Q, Huang X, Wang W, Chen T (2023) Characteristics of spontaneous nystagmus and its correlation to video head impulse test findings in vestibular neuritis. Front Neurosci 17:1243720. https://doi.org/10.3389/fnins.2023.1243720

Review Article

Life Conflux

Exploring Long Noncoding RNAs and Ferroptosis in Cancer

Authors

Qiulian Mo, Yunshan Qiu, Yuni Liang, Qiaoying Wei, Xuefei Fan, Wenpeng Pang

Correspondence

pang861234617@163.com (W. Pang)

Graphical Abstract

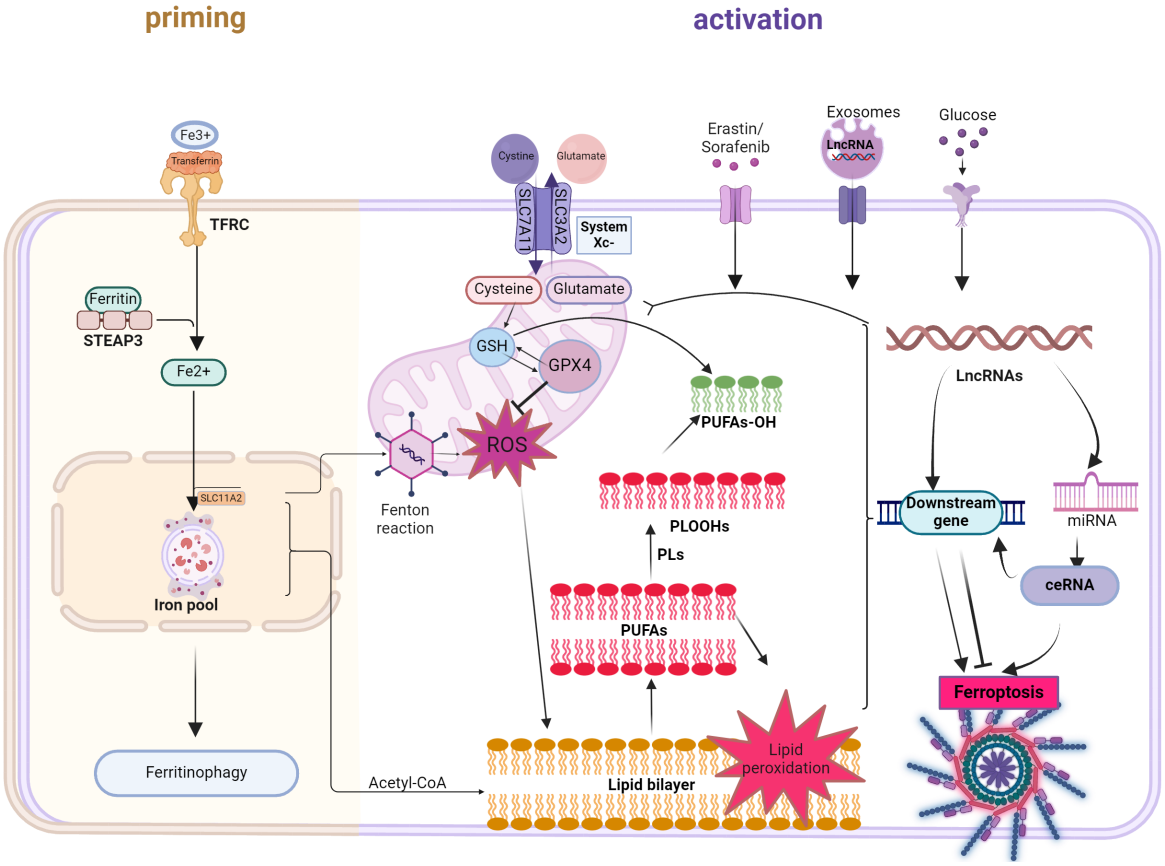

https://doi.org/10.71321/jjrzya36

Research Article Life Conflux

Exploring Long Noncoding RNAs and Ferroptosis in Cancer

Qiulian Mo [2], Yunshan Qiu [2], Yuni Liang [2], Qiaoying Wei [3], Xuefei Fan [4], Wenpeng Pang [1*]

Received: 2025-01-15 | Accepted: 2025-03-21 | Published online: 2025-03-30

Abstract: Ferroptosis is a new type of regulated cell death produced by iron-dependent accumulation of reactive oxygen species in lipids, which is different from apoptosis, pyroptosis and autophagy, and plays the role of a "double-edged sword" in tumor therapy. Ferroptosis-related lncRNA are involved in tumor cell death by regulating lipid metabolism and ferroptosis-associated genes, thus becoming one of the hotspots in the field of tumor-targeted therapy. In this paper, we review the role of ferroptosis and its related lncRNA in inhibiting the development of tumor cells and improving the therapeutic effect of drugs, which is expected to provide a new strategy for the treatment of tumors.
Key words: Ferroptosis; Long non-coding RNAs; Oncotherapy

Introduction

The concept of "ferroptosis" was first introduced by Dixon et al. in 2012[1]. It represents a novel form of regulated cell death (RCD) that differs from apoptosis[2] and pyroptosis[3]. Ferroptosis is an iron-dependent mode of cell death characterized by the accumulation of reactive oxygen species (ROS) leading to lipid peroxidation (LPO)[4-6]. Consequently, similar to other forms of programmed cell death, ferroptosis is gradually emerging as a new therapeutic strategy in oncology. The application of ferroptosis in conjunction with small molecule drug therapies is expected to significantly improve cancer treatment methods.

Long non-coding RNAs (lncRNAs) are a class of RNA molecules longer than 200 nucleotides that do not encode proteins[7, 8]. LncRNAs play crucial regulatory roles in various biological processes, influencing tumor cell proliferation, differentiation, metastasis, and apoptosis at multiple levels[9, 10]. In tumor diagnosis and treatment, lncRNAs also represent promising biomarkers or therapeutic targets.[11, 12]. Recent studies have confirmed that lncRNAs can regulate the occurrence of ferroptosis in tumor cells by mediating lipid metabolism and the expression of ferroptosis-related genes[13]. Thus, lncRNAs constitute an important area of research with broad application prospects, making them potential therapeutic agents for various tumors.

Current therapeutic options remain inadequate, with cancer mortality rates are rising each year. For instance, targeted drug therapy often leads to the development of drug resistance in tumor cells, significantly diminishing treatment efficacy and ultimately threatening patient safety[14]. Therefore, there is a pressing need to develop more effective targeted treatment strategies. Given the importance of lncRNAs and ferroptosis in cancer therapy, this paper reviews the molecular mechanisms of lncRNA-mediated ferroptosis in common clinical tumors and explores the therapeutic potential of ferroptosis-related lncRNAs, aiming to identify novel cancer treatment strategies.

The Main Mechanisms of lncRNA-mediated Ferroptosis in Cancer Cells

Iron metabolism pathway mediating ferroptosis

The molecular mechanisms underlying ferroptosis-induced tumor cell death are complex, involving multiple steps, genes, and proteins[15]. Iron ions participate in the execution of cellular ferroptosis through complex mechanisms[16]. Extracellular trivalent iron ions (Fe^{3+}) bind to transferrin and are subsequently internalized into the cell through transferrin receptor1(TFR1). Subsequently, metalloreductase STEAP3 reduces $Fe^{3+}$to Fe^{2+}, which is released into the cytoplasmic labile iron pool (LIP) via divalent metal-ion transporter 1 (DMT1)[6],[17]. The hydroxyl and lipid radicals in the iron pool can be catalyzed by iron ions, leading to the synthesis of polyunsaturated fatty acids (PUFAs) through the Fenton reaction[18, 19]. When intracellular iron ions increase suddenly, Fenton reactions are likely to be significantly intensified, leading to excessive accumulation of lipid peroxides and

1 Department of Microbiology, Basic Medical College, Guangxi Medical University, Nanning, Guangxi, China,530021.
2 Laboratory Department, First Affiliated Hospital, Guangxi University of Traditional Chinese Medicine, Nanning, Guangxi,China, 530012.
3 People's Hospital of Guangxi Zhuang Autonomous Region and Guangxi Academy of Medical Sciences, Nanning, Guangxi, China,530021.
4 Tuberculosis and AIDS Prevention Division, Wuming District Center for Disease Control and Prevention, Nanning, Guangxi, China,530100.
* Corresponding Author.

resulting in cellular ferroptosis. Recent studies highlight the critical role of post-transcriptional regulation in iron metabolism for ferroptosis sensitivity. For example, hepcidin promotes intracellular Fe^{2+} accumulation by degrading FPN1, thereby enhancing lipid peroxidation[20].

However, the homeostasis of the iron pool is also tightly regulated by iron export proteins ferroportin(FPN1) and iron regulatory proteins (IRPs), thereby controlling intracellular free iron levels[21, 22]. These findings underscore that iron ions act not merely as executors of ferroptosis but also as dynamically balanced elements through multi-layered protein networks that precisely determine cellular fate.

Lipid peroxidation pathway mediating ferroptosis

Lipid peroxidation is one of the most crucial causes of ferroptosis. The occurrence of lipid peroxidation in cells can lead to the destruction of the lipid bilayer and damage to organelles, ultimately resulting in cell rupture and death[23, 24]. Abnormal lipid metabolism can provide the necessary material and energy for rapidly proliferating tumor cells, thus exacerbating their condition[9]. Studies have shown that metabolic stress can promote the binding of PUFAs to membrane phospholipids, making tumor cells more sensitive to ferroptosis[25]. PUFAs are typically enriched in cell membranes and organelle membranes and are prone to react with RO generated by Fe^{2+} and Fe^{2+}-dependent enzymes, leading to ferroptosis[19, 26]. The reaction between iron ions and lipid peroxidation can induce ferroptosis through the generation of ROS. On one hand, ROS can accumulate extensively through the Fenton reaction and inactivation of glutathione peroxidase 4 (GPX4). on the other hand, the continuously accumulating ROS can react with PUFAs, inducing the formation of LPO. Stockwell's research has found that iron chelators can inhibit the transfer of electrons from iron ions to oxygen, thereby reducing the production of ROS in tumor cells, further elucidating the relationship between iron ions and ferroptosis[27].

The system Xc^- -GSH-GPX4 pathway mediating ferroptosis

The cystine-glutamate antiporter system (system Xc^-) is a critical hub in regulating ferroptosis and serves as a key factor for cellular antioxidant defense[28, 29] In the process of regulating ferroptosis, system Xc^- can export intracellular glutamate to the extracellular environment in a 1:1 ratio while simultaneously importing extracellular cystine into the cell[30]. SLC7A11 is a multi-channel transmembrane protein that plays an essential role in the dimerization of system Xc^-, mediating the reverse transport of cystine and glutamate[31]. This allows extracellular cystine to enter the membrane via the SLC7A11 protein, where it is oxidized to cysteine and subsequently catalyzed to produce glutathione (GSH), which participates in inhibiting tumor ferroptosis and the antioxidant process[32]. GSH is crucial for cellular antioxidant defense, and its depletion can lead to an accumulation of lipid ROS and damage to the cell membrane. Long-term deficiency of GSH may result in ferroptosis of the cell[33].

GPX4 is an antioxidant enzyme that relies on glutathione as a co-reductant, catalyzing the conversion of harmful lipid peroxides into relatively harmless water or alcohol, thus promoting the stability of the cell membrane[34, 35]. When GPX4 activity is impaired, its detoxifying effect on lipid peroxides is significantly reduced, leading to the occurrence of ferroptosis[36]. Saturated membrane lipids are insensitive to oxidative stress, while highly saturated membrane lipids help tumor cells avoid damage from ROS. When tumor cells express high levels of GPX4, they can reduce ROS production and maintain redox homeostasis, enabling them to escape ferroptosis.

Overall, the system Xc^--GSH-GPX4 pathway plays a vital role in regulating ferroptosis in tumor cells. By increasing the activity of system Xc^- and the synthesis of GSH, cells can enhance their antioxidant capacity and protect themselves from the harms of lipid peroxidation and ferroptosis. However, when the functions of system Xc^- or GPX4 are compromised, cells become unable to effectively counter lipid peroxidation and ferroptosis, ultimately leading to cell death.

Other pathways mediating ferroptosis

Exosomes are vesicular substances secreted by various cells, ranging from approximately 40 to 100 nm in size[37]. They can transfer a variety of bioactive molecules, including proteins, mRNA, and lncRNA, making them a novel communicator in cell signaling. Studies have shown that lncRNA within exosomes can regulate the transport and storage of iron ions by interacting with ferritin. Ferritin is a protein capable of binding and stabilizing iron ions, allowing it to transport excess iron ions extracellularly, thereby reducing the accumulation of free iron within cells and preventing iron-induced oxidative stress and ferroptosis[38]. In addition, exosomes can influence the occurrence of ferroptosis by regulating the accumulation of ROS in cells. Exosomes secreted by tumor-associated fibroblasts have been found to inhibit ferroptosis in gastric cancer cells, one mechanism being the reduction of ROS accumulation, which protects cells from lipid peroxidation and other forms of damage. Consequently, lncRNA derived from exosomes presents a potential therapeutic strategy to modulate iron metabolism and counteract ferroptosis, thereby influencing disease progression. Further research into the mechanisms by which exosome-derived lncRNA regulate ferroptosis will contribute to the development of new treatment strategies and offer fresh perspectives for the therapy of related diseases.

In summary, ferroptosis-related lncRNA mediates the occurrence of ferroptosis in tumor cells through multiple pathways, including iron ion pathways, lipid peroxidation pathways, and the system Xc^--GSH-GPX4 pathway. These pathways interact to coordinate the cellular responses to oxidative stress and lipid peroxidation, ultimately affecting the induction of ferroptosis.

The Role of Ferroptosis and related lncRNAs in tumor progress

Hepatocellular carcinoma

Hepatocellular carcinoma (HCC) is the sixth most common cancer globally and the third leading cause of cancer-related deaths[39]. However, only a small number of HCC patients are diagnosed at an early stage, thus missing the optimal timing for surgical intervention[40]. Research has demonstrated that ferroptosis induction as a promising strategy, where multiple lncRNAs exhibit differential regulatory mechanisms through

Table.1 The role of ferroptosis and related lncRNAs in tumor

LncRNA Name	Cancer Type	Regulation	Specific Molecular Mechanism	Associated Drugs/Small Molecules
KRAL	HCC	Antioxidant Pathway Regulation	Acts as a ceRNA to sponge miR-141, upregulate Keap1, and inhibit the Nrf2-dependent antioxidant pathway	5-Fluorouracil (5-FU)
GABPB1-AS1	HCC	Antioxidant Pathway Regulation	Directly downregulates PRDX5, bypassing miRNA regulation, inducing ROS-mediated lipid peroxidation	-
PVT1	HCC	System Xc^--GPX4 Regulation	Sponges miR-214-3p to relieve GPX4 suppression, leading to sorafenib resistance	Ketamine (inhibits PVT1 activity)
LINC01134	HCC	System Xc^--GPX4 Regulation	Suppresses GPX4 expression via miRNA sponging	Oxaliplatin
NEAT1	HCC	System Xc^--GPX4 Regulation	Acts as a ceRNA to sponge miR-362-3P, upregulates MIOX, and enhances NADPH/GSH production	Erastin, RSL3
	NSCLC	p53-Independent Pathways	Silencing reduces ACSL4, SLC7A11, and GPX4 expression, increasing Erastin sensitivity	Erastin
P53RRA	NSCLC	p53 -Dependent Regulatory	Binds G3BP1 to enhance p53 nuclear retention, inhibiting SLC7A11 transcription	-
MEG3	NSCLC	p53 -Dependent Regulatory Axis	Upregulates p53 expression to suppress tumor proliferation	Paclitaxel (PTX)
LINC00336	NSCLC	p53 -Dependent Regulatory Axis	Interacts with miR6852 via the p53-LSH-ELAVL1 axis, activating the CBS pathway	-
FERO	GC	Lipid Metabolism Regulation	Chemotherapy-induced upregulation stabilizes SCD1 mRNA via hnRNPA1, promoting MUFA synthesis to inhibit lipid peroxidation	Cisplatin, Paclitaxel (induce FERO expression)
ARHGEF26-AS1	EC	Lipid Metabolism Regulation	Sponges miR-372-3p to activate ADAM23, inhibiting GPX4, SLC3A2, and SLC7A11	-
CBSLR	GC	Ubiquitination Regulation	Recruits YTHDF2 under hypoxia to inhibit CBS mRNA transcription, reducing CBS expression and inducing ACSL4 ubiquitination	-
BDNF-AS	GC	Ubiquitination Regulation	Activates VDAC3 ubiquitination via the BDNF-AS/WDR5/FBXW7 axis	Erastin (targets VDAC3)
OIP5-AS1	BCa	System Xc^--GPX4 Regulation	1. Acts as ceRNA to sponge miR-128-3p, upregulating SLC7A11 (anti-ferroptosis)	

2. Binds cadmium to downregulate SLC7A11 (pro-ferroptosis)	Cadmium (pro-ferroptosis)			
UCA1	BCa	System Xc⁻-GPX4 Regulation	Sponges miR-16 to upregulate GLS2, driving glutamine metabolism and enhancing GSH synthesis/GPX4 activity	-
RP11-89	BCa	Iron Metabolism Regulation	Sponge miR-129-5p, upregulates PROM2, promoting exosomal iron efflux and reducing intracellular LIP	-

Figure.1 The main mechanisms involved in ferroptosis-related lncRNAs

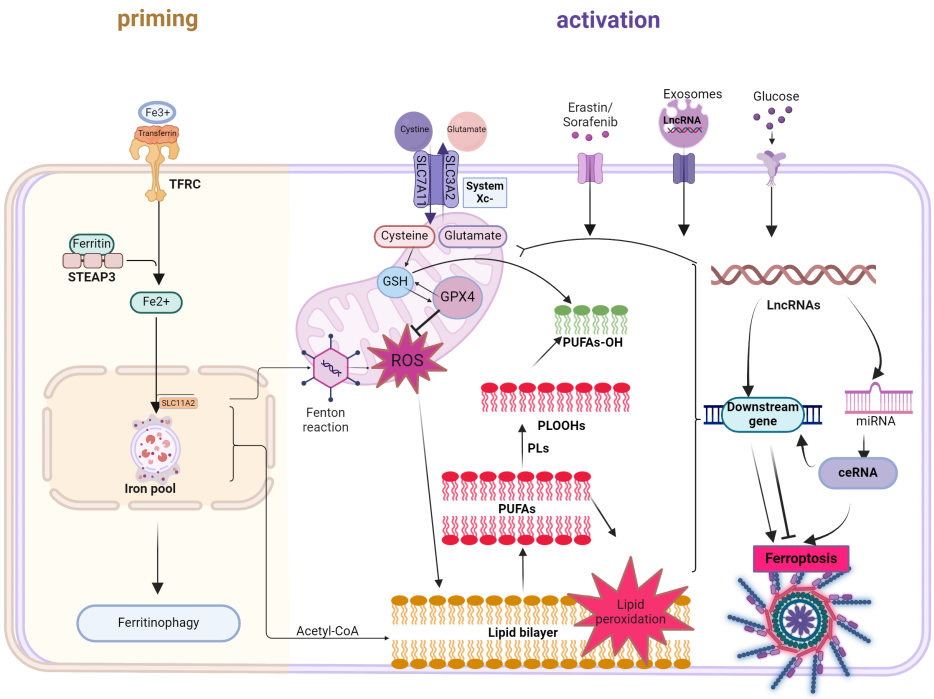

distinct molecular pathways[21],[41]. The current research reveals three predominant levels by which lncRNAs modulate ferroptosis in HCC:

Antioxidant Pathway Regulation

LncRNA and miRNA can regulate the occurrence of ferroptosis in HCC through the competing endogenous RNA (ceRNA) mechanism[42, 43]. For instance, the lncRNA KRAL enhances the expression of Keap1 when bound to miR-141, leading to the inactivation of the Nrf2-dependent antioxidant pathway[44]. Nrf2 is an important antioxidant factor during oxidative stress responses and is regulated by Keap1 (Kelch ECH associating protein 1)[45]. Sun et al. found that knocking out Nrf2-related genes induces ferroptosis in cells, inhibiting the proliferation of HCC cells[46]. In the cytoplasm, Nrf2 regulates the expression and generation of intracellular antioxidant proteins[47]and ROS[48] by binding to antioxidant response elements (ARE). Additionally, ferroptosis-related lncRNA can directly regulate the expression of ROS in tumor cells, thereby mediating lipid peroxidation. For example, lncRNA GABPB1-AS1 directly downregulates PRDX5 to induce ROS accumulation, bypassing miRNA-mediated regulation. This mechanism delivers rapid oxidative damage but lacks tissue specificity, risking systemic oxidative stress[49].

System Xc⁻-GPX4 Regulation

For instance, when lncRNA PVT1 specifically binds to miR-214-3p, it reduces miR-214-3p inhibitory effect on GPX4, leading to an increase in GPX4 expression and promoting ferroptosis in liver cancer cells. Conversely, inhibiting miR-214-3p expression or overexpressing GPX4 can reverse ferroptosis[50]. Moreover, Kang et al. [51] found that lncRNA LINC01134 can promote ferroptosis by affecting GPX4 expression . The nuclear-enriched abundant transcript 1 (NEAT1) interacts with miR-

362-3P through the ceRNA mechanism. promoting the expression of MIOX. Then, MIOX increases the production of NADPH and GSH. accelerating the occurrence of ferroptosis in HCC[52].

Reprogramming of Drug Sensitivity

These ferroptosis-related lncRNAs may interact with chemotherapeutic agents or ferroptosis inducers, offering novel strategies to overcome treatment resistance in HCC. KRAL synergizes with 5-fluorouracil (5-FU) by activating the Nrf2-mediated antioxidant pathway. PVT1 can suppress the induction of ferroptosis in HCC by ketamine, resulting in drug resistance. LINC01134 specifically enhancing the sensitivity of liver cancer patients to oxaliplatin treatment. NEAT1 significantly increasing the efficacy of small-molecule drugs like Erastin and RSL3 in inducing ferroptosis. Cross-talk between lncRNAs (e.g., NEAT1 and LINC01134 co-targeting GPX4) may produce synergistic or antagonistic effects, necessitating systems biology approaches to construct regulatory network models.

These studies indicate that lncRNA holds great promise as a target for inducing ferroptosis in the therapeutic treatment of HCC. Collectively, ferroptosis-related lncRNAs redefine HCC treatment paradigms by targeting redox homeostasis and drug-response pathways, offering novel strategies to counteract therapeutic resistance.The current research is mainly based on in vitro cell models and in vivo animal models, which may not fully reflect the complex tumor microenvironment and heterogeneity in human patients. Future research should focus on validating the findings in larger clinical cohorts to better understand the translational potential of ferroptosis-related lncRNAs in HCC.

Lung cancer

Lung cancer is the second most common cancer worldwide and is also one of the leading causes of cancer-related deaths[39]. Current treatment options for Non-small cell lung cancer (NSCLC) include chemotherapy, radiotherapy, surgical treatment, and biological therapy[53]. Over the past two decades, most patients with advanced NSCLC develop resistance to treatment, leading to further disease progression[54]. Therefore, there is an urgent need to study personalized treatment regimens for lung cancer, particularly for NSCLC, and to develop rational and effective combination therapies[43, 55]. Crucially, lncRNAs are emerging as key regulators of ferroptosis in NSCLC, primarily through their interaction with the p53 pathway and downstream metabolic networks. Below, we synthesize current findings by categorizing ferroptosis-related lncRNAs based on their functional mechanisms and clinical implications.

p53-Dependent Regulatory Axis

P53 gene, known as the "guardian of the genome", regulates cell survival and division under various stress conditions. Furthermore, p53 can induce ferroptosis in lung cancer by inhibiting SLC7A11[56]. Studies have found that lncRNA P53RRA promotes ferroptosis in lung cancer by binding to G3BP1 and enhancing p53 nuclear retention[57]. Additionally, the related genes were act in a negative regulatory manner with respect to p53[58]. For example, MEG3 can promote the expression of p53, thereby inhibiting NSCLC proliferation[59]. The combined use of lncRNA MEG3 and paclitaxel (PTX) significantly enhances the ability of PTX to kill tumor cells[60]. Additionnally, p53 may enhance the expression of lymphoid-specific helicase (LSH), which promotes ELAV-like RNA binding protein 1 (ELAVL1) expression and facilitates the interaction between LINC00336 and miR6852, ultimately activating cystathionine β-synthase (CBS), a marker of downstream ferroptosis-related pathways[61].

p53-Independent Pathways

Certain lncRNAs bypass p53 to directly regulate ferroptosis effectors. Recently, Wu[62]conducted a more in-depth study on the mechanisms of ferroptosis-related lncRNA in NSCLC. They discovered that silencing lncRNA NEAT1, in conjunction with Erastin treatment, significantly reduced the expression of acyl-CoA synthetase long chain family member 4 (ACSL4), SLC7A11, and GPX4, thereby increasing tumor cell sensitivity to ferroptosis.

In summary, research on ferroptosis-related lncRNAs reveals that the p53 gene participates in regulating ferroptosis in lung cancer cells through multiple pathways. p53 mediates the occurrence of ferroptosis through the system Xc^- -GSH-GPX4 pathway, inhibiting the transcription of the SLC7A11 gene in the nucleus to reduce cystine uptake and thereby limiting intracellular glutathione production, ultimately leading to ferroptosis in NSCLC. However, the clinical sample sizes in these studies are often small, which restricts the statistical power and the ability to draw definitive conclusions. Larger, well-powered clinical trials are needed to validate these findings and to better understand the clinical relevance of lncRNA-mediated ferroptosis in NSCLC.

Gastric and Esophageal Cancers

Gastric cancer (GC) and esophageal cancer (EC) are major contributors to digestive system malignancies, characterized by high heterogeneity and limited therapeutic options[39]. Recent studies increasingly indicate that ferroptosis and lncRNAs play crucial roles in the regulation of gastric and esophageal cancers. Thus, it is essential to develop new therapeutic strategies based on ferroptosis-related lncRNAs for these malignancies.

Lipid Metabolism Regulation

Exosomes are pivotal in the initiation and progression of gastric cancer[63]. Zhang et al. [64]discovered that the chemotherapy-induced ferroptosis-related exosomal lncRNA FERO regulates ferroptosis in gastric cancer stem cells. Chemotherapy (cisplatin/paclitaxel) upregulates FERO via USP7, which recruits hnRNPA1 to stabilize SCD1 mRNA. SCD1 catalyzes MUFA synthesis, reducing lipid peroxidation and suppressing ferroptosis in GC stem cells[65]. In esophageal cancer research, Ren et al.[66] developed a system using ferroptosis and iron metabolism-related lncRNAs to predict survival in esophageal squamous cell carcinoma, emphasizing their relationship with the tumor development. In addition, lncRNA ARHGEF26-AS1 has been found to activate the expression of receptor ADAM23 by adsorbing miR-372-3p[67]. When both lncRNA ARHGEF26-AS1 and ADAM23 are underexpressed, the prognosis for esophageal cancer patients is generally poor. ADAM23 inhibits the protein levels of GPX4, SLC3A2, and SLC7A11, thereby promoting ferroptosis in

esophageal cancer cells. Both in vivo and in vitro experiments demonstrate that overexpression of lncRNA ARHGEF26-AS1 and ADAM23 significantly suppresses tumor cell growth and metastasis.

Ubiquitination Regulation

Ubiquitination is involved in the regulation of ferroptosis in gastric cancer cells through epigenetic mechanisms[28]. Hypoxia-induced lncRNA CBSLR recruits YTHDF2 to the m6A-modified coding sequence of CBS mRNA, thereby inhibiting the transcription of CBS mRNA. The reduced expression level of CBS leads to a decrease in ACSL4 protein methylation, which in turn induces polyubiquitination and degradation of the corresponding protein, thus triggering ferroptosis GC[68, 69]. Moreover, lncRNA BDNF-AS activates the ubiquitination of downstream VDAC3 via the BDNF-AS/WDR5/FBXW7 axis, influencing ferroptosis in GC[70]. VDAC3, a key gene for ion transport across mitochondria, is typically overexpressed in malignant tumors and serves as a target site for Erastin[71]. Clinically, enhancing the efficacy of anticancer drugs while promoting cellular ferroptosis may be achieved by upregulating VDAC3 expression through the BDNF-AS axis.

Research on ferroptosis-related lncRNAs provides insights into the mechanisms mediating ferroptosis from multiple perspectives, including exosomesand ubiquitination. This addresses the current limitations in ferroptosis treatment carriers[72]. Tumor-derived ferroptosis exosomal lncRNAs can communicate signals related to drug resistance and angiogenesis to neighboring cells, thereby promoting the proliferation of gastric cancer cells. Therefore, targeted therapy against lncRNA FERO in gastric cancer exosomes presents a promising exosome-based treatment strategy. Such studies hold promise for advancing clinical diagnosis and prognosis in digestive system tumors, potentially leading to more effective targeted therapies for these cancers.

Prostate and Bladder Cancers

Prostate cancer (PCa) and bladder cancer (BCa), the most prevalent malignancies in the urinary system, collectively account for significant global cancer burden[73]. Both cancers share critical clinical challenges including insufficient diagnostic biomarkers and therapeutic targets, highlighting the importance of investigating ferroptosis-related lncRNAs as potential therapeutic avenues[74-76]. This section integrates the roles played by lncRNA within the following two frameworks, emphasizing their clinical significance.

System Xc^- -GPX4 Regulation

Emerging evidence reveals lncRNAs modulate System Xc^--GPX4 pathway through distinct mechanisms in urinary cancers. For instant, lncRNA OIP5-AS1 exhibits dual regulatory roles. First, OIP5-AS1 acts as a ceRNA by sequestering miR-128-3p, thereby upregulating SLC7A11 expression and suppressing ferroptosis. On the contrary, it can directly binds cadmium to downregulate SLC7A11, promoting cadmium-induced ferroptosis[77]. In addition, lncRNA UCA1 upregulates mitochondrial glutaminase 2 (GLS2) by sponging miR-16, driving glutamine metabolic reprogramming[78]. GLS2-mediated glutamine-to-glutamate conversion fuels system xc^--dependent cystine uptake and GSH synthesis, thereby suppressing lipid ROS toxicity[79]. Enhanced GSH sustains GPX4 activity to antagonize ferroptosis, while concurrently mitigating oxidative damage to promote bladder cancer survival[80].

Iron Metabolism Regulation

LncRNA RP11-89 orchestrates ferroptosis resistance by rewiring iron homeostasis through exosome-mediated iron effluxin in bladder cancer[81]. RP11-89 functions as a ceRNA to sequester miR-129-5p, derepressing PROM2 expression. PROM2 encodes prominin2, a key driver of multivesicular body (MVB) biogenesis. Prominin2 facilitates the packaging of ferritin-bound iron into MVBs, which are subsequently secreted as exosomes, effectively depleting intracellular LIP and suppressing Fenton reaction-driven lipid peroxidation[82].

In conclusion, it is evident that lncRNAs primarily modulate System Xc^--GPX4 and iron metabolism within the urinary system, thereby mediating the onset of ferroptosis. Future targeted use of MVB and other novel carriers has the potential to considerably enhance the delivery of drugs or lncRNAs to target cells, thereby improving therapeutic outcomes. These carriers can surmount limitations associated with conventional drug delivery methods, such as poor drug solubility and stability. Targeting these pathways more specifically could augment the efficiency of ferroptosis in clinical applications.

Conclusion and Future Perspectives

Ferroptosis is a novel form of regulated cell death that is distinct from other forms such as autophagy and pyroptosis. Ferroptosis not only contributes to tumor cell death but is also linked to aging[83, 84] and immunity[85, 86], providing new ideas and strategies for cancer immunotherapy and treatment. The relationship between ferroptosis and cancer therapy has a double-edged sword effect; however, our understanding of the relationship between lncRNA and ferroptosis remains limited. At present, the development of more precise animal models, such as patient-derived xenografts (PDX), will provide a better platform for studying ferroptosis and lncRNA responsiveness. Furthermore, integrating omics-based profiling, liquid biopsies, and machine learning models will be essential for overcoming challenges in ferroptosis research. Additionally, when combined with appropriate clinical chemotherapy agents, ferroptosis-related lncRNA can have a greater impact on cancer therapy, but the mechanisms involved and their clinical safety require further investigation.

Currently, some targeted drugs for caner, such as sorafenib, are widely used in the treatment of advanced HCC patients[87]. However, their effectiveness remains limited, while they can extend the overall survival of patients to some degree, many HCC patients have shown poor responses to sorafenib treatment and are prone to developing drug resistance[88, 89]. On one hand, the use of sorafenib can result in significant side effects, burdening patients. On the other hand, its targeting mechanism for HCC is relatively singular, primarily functioning through the inhibition of tumor angiogenesis and targeting the Raf/MEK/ERK pathway, leading to limitations in targeted therapy. The related ferroptosis lncRNAs mainly induces ferroptosis in HCC by regulating GPX4, increasing lipid peroxidation and influencing the expression of other

downstream ferroptosis-related iron metabolism genes. Moreover, they can significantly enhance tumor cells sensitivity to related small molecules, such as Erastin and commonly used clinical liver cancer drugs like sorafenib. Erastin specifically induces ferroptosis by inhibiting the system Xc^- -GSH-GPX4 pathway, increasing the feasibility of tumor-targeted therapies through combination with anticancer drugs. Although lncRNAs show promise in inducing ferroptosis, their clinical use has limitations: Firstly, the instability of lncRNAs can lead to low delivery efficiency, which is a major obstacle to their clinical use. Developing effective delivery systems (such as nanoparticles or inclusion bodies) is crucial for enhancing the stability and bioavailability of lncRNAs. Secondly, determining the optimal doses of lncRNA - based therapies and ferroptosis inducers is essential for maximizing therapeutic effects while minimizing side effects. This requires careful preclinical and clinical studies to establish dose - response relationships and identify the most effective combinations. Lastly, patients with different types of tumors may exhibit significant individual differences in their responses to combination therapies. Factors such as genetic background, tumor microenvironment, and previous treatment history may affect the effectiveness of different lncRNAs in mediating ferroptosis in different tumors. In conclusion, although the combination of lncRNA - mediated ferroptosis induction and traditional cancer therapies shows great potential, further research and development are needed to address clinical challenges and optimize treatment strategies. Future research should focus on improving the stability and delivery efficiency of lncRNAs, determining the optimal drug doses, understanding individual differences in treatment responses, and developing effective strategies to deal with potential adverse reactions.

Current research on lncRNAs mediating tumor ferroptosis remains limited, with their functional roles and mechanistic underpinnings incompletely characterized. In this review, we systematically analyze ferroptosis-associated lncRNAs across six malignancies spanning four biological systems, including hepatocellular carcinoma in the digestive system, and prostate/bladder cancers in the genitourinary system. We found that the mechanisms involved in ferroptosis vary across different tumors, but the core pathways are consistently centered around iron metabolism, lipid peroxidation, and the system Xc^- - GPX4 pathway. Research on lncRNA - mediated ferroptosis in other types of tumors is also on the rise. In the future, the relationship between the two will be further supplemented, providing more help for clinical cancer treatment.

Acknowledgements

Figures in the article were drawnusing Biorender https://www.biorender.com/.

Author Contributions

Wenpeng Pang was in charge of the proofreading and design of the manuscript. Qiulian Mo and Yunshan Qiu took responsibility for the writing of the manuscript. Yuni Liang, Qiaoying Wei, and Xuefei Fan were responsible for the collection and organization of literature on different tumors. All authors read and approved the final manuscript.

Competing Interests

The authors declare that they have no existing or potential commercial or financial relationships that could create a conflict of interest at the time of conducting this study.

Data Availability

All data needed to evaluate the conclusions in the paper are present in the paper or the Supplementary Materials. Additional data related to this paper may be requested from the authors.

References

[1] DIXON SJ, LEMBERG KM, LAMPRECHT MR, SKOUTA R, ZAITSEV EM, GLEASON CE, et al. (2012).Ferroptosis: an iron-dependent form of nonapoptotic cell death. Cell, 149(5): 1060-1072. https://doi.org/10.1016/j.cell.2012.03.042

[2] ELMORE S. (2007).Apoptosis: a review of programmed cell death. Toxicol Pathol, 35(4): 495-516. https://doi.org/10.1080/01926230701320337

[3] DU T, GAO J, LI P, WANG Y, QI Q, LIU X, et al. (2021). Pyroptosis, metabolism, and tumor immune microenvironment. Clin Transl Med, 11(8): e492. https://doi.org/10.1002/ctm2.492

[4] CAO JY, DIXON SJ. (2016).Mechanisms of ferroptosis. Cell Mol Life Sci, 73(11-12): 2195-2209. https://doi.org/10.1007/s00018-016-2194-1

[5] MOU Y, WANG J, WU J, HE D, ZHANG C, DUAN C, et al. (2019).Ferroptosis, a new form of cell death: opportunities and challenges in cancer. J Hematol Oncol, 12(1): 34. https://doi.org/10.1186/s13045-019-0720-y

[6] XIE Y, HOU W, SONG X, YU Y, HUANG J, SUN X, et al. (2016). Ferroptosis: process and function. Cell Death Differ, 23(3): 369-379. https://doi.org/10.1038/cdd.2015.158

[7] CESANA M, CACCHIARELLI D, LEGNINI I, SANTINI T, STHANDIER O, CHINAPPI M, et al. (2011).A long noncoding RNA controls muscle differentiation by functioning as a competing endogenous RNA. Cell, 147(2): 358-369. https://doi.org/10.1016/j.cell.2011.09.028

[8] STATELLO L, GUO CJ, CHEN LL, HUARTE M. (2021).Gene regulation by long non-coding RNAs and its biological functions. Nat Rev Mol Cell Biol, 22(2): 96-118. https://doi.org/10.1038/s41580-020-00315-9

[9] HUANG J, WANG J, HE H, HUANG Z, WU S, CHEN C, et al. (2021).Close interactions between lncRNAs, lipid metabolism and ferroptosis in cancer. Int J Biol Sci, 17(15): 4493-4513. https://doi.org/10.7150/ijbs.66181

[10] LIN W, ZHOU Q, WANG CQ, ZHU L, BI C, ZHANG S, et al. (2020).LncRNAs regulate metabolism in cancer. Int J Biol Sci, 16(7): 1194-1206. https://doi.org/10.7150/ijbs.40769

[11] LI J, MENG H, BAI Y, WANG K. (2016).Regulation of lncRNA and its role in cancer metastasis. Oncol Res,

23(5): 205-217. https://doi.org/10.3727/096504016x14549667334007
[12] XU W, ZHOU G, WANG H, LIU Y, CHEN B, CHEN W, et al. (2020).Circulating lncRNA SNHG11 as a novel biomarker for early diagnosis and prognosis of colorectal cancer. Int J Cancer, 146(10): 2901-2912. https://doi.org/10.1002/ijc.32747
[13] JIANG X, STOCKWELL BR, CONRAD M. (2021).Ferroptosis: mechanisms, biology and role in disease. Nat Rev Mol Cell Biol, 22(4): 266-282. https://doi.org/10.1038/s41580-020-00324-8
[14] VASAN N, BASELGA J, HYMAN DM. (2019).A view on drug resistance in cancer. Nature, 575(7782): 299-309. https://doi.org/10.1038/s41586-019-1730-1
[15] AVERETT C, BHARDWAJ A, ARORA S, SRIVASTAVA SK, KHAN MA, AHMAD A, et al. (2016).Honokiol suppresses pancreatic tumor growth, metastasis and desmoplasia by interfering with tumor-stromal cross-talk. Carcinogenesis, 37(11): 1052-1061. https://doi.org/10.1093/carcin/bgw096
[16] TANG D, KROEMER G. (2020).Ferroptosis. Curr Biol, 30(21): R1292-r1297. https://doi.org/10.1016/j.cub.2020.09.068
[17] GRAHAM RM, CHUA AC, HERBISON CE, OLYNYK JK, TRINDER D. (2007).Liver iron transport. World J Gastroenterol, 13(35): 4725-4736. https://doi.org/10.3748/wjg.v13.i35.4725
[18] HE YJ, LIU XY, XING L, WAN X, CHANG X, JIANG HL. (2020). Fenton reaction-independent ferroptosis therapy via glutathione and iron redox couple sequentially triggered lipid peroxide generator. Biomaterials, 241: 119911. https://doi.org/10.1016/j.biomaterials.2020.119911
[19] CHENG Z, LI Y. (2007).What is responsible for the initiating chemistry of iron-mediated lipid peroxidation: an update. Chem Rev, 107(3): 748-766. https://doi.org/10.1021/cr040077w
[20] BAO X, LUO X, BAI X, LV Y, WENG X, ZHANG S, et al. (2023).Cigarette tar mediates macrophage ferroptosis in atherosclerosis through the hepcidin/FPN/SLC7A11 signaling pathway. Free Radic Biol Med, 201: 76-88. https://doi.org/10.1016/j.freeradbiomed.2023.03.006
[21] WILBON AS, SHEN J, RUCHALA P, ZHOU M, PAN Y. (2023).Structural basis of ferroportin inhibition by minihepcidin PR73. PLoS Biol, 21(1): e3001936. https://doi.org/10.1371/journal.pbio.3001936
[22] CARDONA CJ, MONTGOMERY MR. (2023).Iron regulatory proteins: players or pawns in ferroptosis and cancer? Front Mol Biosci, 10: 1229710. https://doi.org/10.3389/fmolb.2023.1229710
[23] VON KRUSENSTIERN AN, ROBSON RN, QIAN N, QIU B, HU F, REZNIK E, et al. (2023).Identification of essential sites of lipid peroxidation in ferroptosis. Nat Chem Biol, 19(6): 719-730. https://doi.org/10.1038/s41589-022-01249-3
[24] LIANG D, MINIKES AM, JIANG X. (2022).Ferroptosis at the intersection of lipid metabolism and cellular signaling. Mol Cell, 82(12): 2215-2227. https://doi.org/10.1016/j.molcel.2022.03.022
[25] YUAN ZH, LIU T, WANG H, XUE LX, WANG JJ. (2021).Fatty Acids Metabolism: The Bridge Between Ferroptosis and Ionizing Radiation. Front Cell Dev Biol, 9: 675617. https://doi.org/10.3389/fcell.2021.675617
[26] YANG WS, STOCKWELL BR. (2016).Ferroptosis: Death by Lipid Peroxidation. Trends Cell Biol, 26(3): 165-176. https://doi.org/10.1016/j.tcb.2015.10.014
[27] DIXON SJ, STOCKWELL BR. (2014).The role of iron and reactive oxygen species in cell death. Nat Chem Biol, 10(1): 9-17. https://doi.org/10.1038/nchembio.1416
[28] CHEN X, LI J, KANG R, KLIONSKY DJ, TANG D. (2021). Ferroptosis: machinery and regulation. Autophagy, 17(9): 2054-2081. https://doi.org/10.1080/15548627.2020.1810918
[29] DE BAAT A, MEIER DT, FONTANA A, BöNI-SCHNETZLER M, DONATH MY. (2023).Cystine/Glutamate antiporter system xc- deficiency impairs macrophage glutathione metabolism and cytokine production. PLoS One, 18(10): e0291950. https://doi.org/10.1371/journal.pone.0291950
[30] ZHAO Y, LI Y, ZHANG R, WANG F, WANG T, JIAO Y. (2020). The role of erastin in ferroptosis and its prospects in cancer therapy. Onco Targets Ther, 13: 5429-5441. https://doi.org/10.2147/ott.S254995
[31] YAN Y, TENG H, HANG Q, KONDIPARTHI L, LEI G, HORBATH A, et al. (2023).SLC7A11 expression level dictates differential responses to oxidative stress in cancer cells. Nat Commun, 14(1): 3673. https://doi.org/10.1038/s41467-023-39401-9
[32] KOPPULA P, ZHUANG L, GAN B. (2021).Cystine transporter SLC7A11/xCT in cancer: ferroptosis, nutrient dependency, and cancer therapy. Protein Cell, 12(8): 599-620. https://doi.org/10.1007/s13238-020-00789-5
[33] XU T, DING W, JI X, AO X, LIU Y, YU W, et al. (2019). Molecular mechanisms of ferroptosis and its role in cancer therapy. J Cell Mol Med, 23(8): 4900-4912. https://doi.org/10.1111/jcmm.14511
[34] LATUNDE-DADA GO. (2017).Ferroptosis: Role of lipid peroxidation, iron and ferritinophagy. Biochim Biophys Acta Gen Subj, 1861(8): 1893-1900. https://doi.org/10.1016/j.bbagen.2017.05.019
[35] URSINI F, MAIORINO M. (2020).Lipid peroxidation and ferroptosis: The role of GSH and GPx4. Free Radic Biol Med, 152: 175-185. https://doi.org/10.1016/j.freeradbiomed.2020.02.027
[36] SEILER A, SCHNEIDER M, FöRSTER H, ROTH S, WIRTH EK, CULMSEE C, et al. (2008).Glutathione peroxidase 4 senses and translates oxidative stress into 12/15-lipoxygenase dependent- and AIF-mediated cell death. Cell Metab, 8(3): 237-248. https://doi.org/10.1016/j.cmet.2008.07.005
[37] THéRY C, ZITVOGEL L, AMIGORENA S. (2002).Exosomes: composition, biogenesis and function. Nat Rev Immunol, 2(8): 569-579. https://doi.org/10.1038/nri855
[38] BROWN CW, MERCURIO AM. (2020).Ferroptosis resistance mediated by exosomal release of iron. Mol Cell Oncol, 7(3): 1730144. https://doi.org/10.1080/23723556.2020.1730144
[39] SUNG H, FERLAY J, SIEGEL RL, LAVERSANNE M, SOERJOMATARAM I, JEMAL A, et al. (2021).Global Cancer Statistics 2020: GLOBOCAN Estimates of Incidence and Mortality Worldwide for 36 Cancers in 185 Countries. CA Cancer J Clin, 71(3): 209-249. https://doi.org/10.3322/caac.21660
[40] NIE J, LIN B, ZHOU M, WU L, ZHENG T. (2018).Role of ferroptosis in hepatocellular carcinoma. J Cancer Res Clin Oncol, 144(12): 2329-2337. https://doi.org/10.1007/s00432-018-2740-3

[41] CAPELLETTI MM, MANCEAU H, PUY H, PEOC'H K. (2020). Ferroptosis in liver diseases: an overview. Int J Mol Sci, 21(14): 4908. https://doi.org/10.3390/ijms21144908
[42] QIN Y, ZHANG D, ZHANG H, HOU L, WANG Z, YANG L, et al. (2022).Construction of a ferroptosis-related five-lncRNA signature for predicting prognosis and immune response in thyroid carcinoma. Cancer Cell Int, 22(1): 296. https://doi.org/10.1186/s12935-022-02674-z
[43] FEI X, HU C, WANG X, LU C, CHEN H, SUN B, et al. (2021). Construction of a Ferroptosis-Related Long Non-coding RNA Prognostic Signature and Competing Endogenous RNA Network in Lung Adenocarcinoma. Front Cell Dev Biol, 9: 751490. https://doi.org/10.3389/fcell.2021.751490
[44] WU L, PAN C, WEI X, SHI Y, ZHENG J, LIN X, et al. (2018). lncRNA KRAL reverses 5-fluorouracil resistance in hepatocellular carcinoma cells by acting as a ceRNA against miR-141. Cell Commun Signal, 16(1): 47. https://doi.org/10.1186/s12964-018-0260-z
[45] NGUYEN T, NIOI P, PICKETT CB. (2009).The Nrf2-antioxidant response element signaling pathway and its activation by oxidative stress. J Biol Chem, 284(20): 13291-13295. https://doi.org/10.1074/jbc.R900010200
[46] SUN X, OU Z, CHEN R, NIU X, CHEN D, KANG R, et al. (2016). Activation of the p62-Keap1-NRF2 pathway protects against ferroptosis in hepatocellular carcinoma cells. Hepatology, 63(1): 173-184. https://doi.org/10.1002/hep.28251
[47] KANSANEN E, KUOSMANEN SM, LEINONEN H, LEVONEN AL. (2013).The Keap1-Nrf2 pathway: mechanisms of activation and dysregulation in cancer. Redox Biol, 1(1): 45-49. https://doi.org/10.1016/j.redox.2012.10.001
[48] DENICOLA GM, KARRETH FA, HUMPTON TJ, GOPINATHAN A, WEI C, FRESE K, et al. (2011).Oncogene-induced Nrf2 transcription promotes ROS detoxification and tumorigenesis. Nature, 475(7354): 106-109. https://doi.org/10.1038/nature10189
[49] QI W, LI Z, XIA L, DAI J, ZHANG Q, WU C, et al. (2019). LncRNA GABPB1-AS1 and GABPB1 regulate oxidative stress during erastin-induced ferroptosis in HepG2 hepatocellular carcinoma cells. Sci Rep, 9(1): 16185. https://doi.org/10.1038/s41598-019-52837-8
[50] HE GN, BAO NR, WANG S, XI M, ZHANG TH, CHEN FS. (2021).Ketamine Induces ferroptosis of liver cancer cells by targeting lncRNA PVT1/miR-214-3p/GPX4. Drug Des Devel Ther, 15: 3965-3978. https://doi.org/10.2147/dddt.S332847
[51] KANG X, HUO Y, JIA S, HE F, LI H, ZHOU Q, et al. (2022). Silenced LINC01134 enhances oxaliplatin sensitivity by facilitating ferroptosis through GPX4 in hepatocarcinoma. Front Oncol, 12: 939605. https://doi.org/10.3389/fonc.2022.939605
[52] ZHANG Y, LUO M, CUI X, O'CONNELL D, YANG Y. (2022). Long noncoding RNA NEAT1 promotes ferroptosis by modulating the miR-362-3p/MIOX axis as a ceRNA. Cell Death Differ, 29(9): 1850-1863. https://doi.org/10.1038/s41418-022-00970-9
[53] ALDUAIS Y, ZHANG H, FAN F, CHEN J, CHEN B. (2023).Non-small cell lung cancer (NSCLC): A review of risk factors, diagnosis, and treatment. Medicine (Baltimore), 102(8): e32899. https://doi.org/10.1097/md.0000000000032899
[54] RAMALINGAM SS, VANSTEENKISTE J, PLANCHARD D, CHO BC, GRAY JE, OHE Y, et al. (2020).Overall survival with osimertinib in untreated, EGFR-mutated advanced NSCLC. N Engl J Med, 382(1): 41-50. https://doi.org/10.1056/NEJMoa1913662
[55] WANG M, HERBST RS, BOSHOFF C. (2021).Toward personalized treatment approaches for non-small-cell lung cancer. Nat Med, 27(8): 1345-1356. https://doi.org/10.1038/s41591-021-01450-2
[56] KANG R, KROEMER G, TANG D. (2019).The tumor suppressor protein p53 and the ferroptosis network. Free Radic Biol Med, 133: 162-168. https://doi.org/10.1016/j.freeradbiomed.2018.05.074
[57] MAO C, WANG X, LIU Y, WANG M, YAN B, JIANG Y, et al. (2018).A G3BP1-interacting lncRNA promotes ferroptosis and apoptosis in cancer via nuclear sequestration of p53. Cancer Res, 78(13): 3484-3496. https://doi.org/10.1158/0008-5472.Can-17-3454
[58] ZHANG EB, YIN DD, SUN M, KONG R, LIU XH, YOU LH, et al. (2014).P53-regulated long non-coding RNA TUG1 affects cell proliferation in human non-small cell lung cancer, partly through epigenetically regulating HOXB7 expression. Cell Death Dis, 5(5): e1243. https://doi.org/10.1038/cddis.2014.201
[59] LU KH, LI W, LIU XH, SUN M, ZHANG ML, WU WQ, et al. (2013).Long non-coding RNA MEG3 inhibits NSCLC cells proliferation and induces apoptosis by affecting p53 expression. BMC Cancer, 13: 461. https://doi.org/10.1186/1471-2407-13-461
[60] XU J, SU C, ZHAO F, TAO J, HU D, SHI A, et al. (2018). Paclitaxel promotes lung cancer cell apoptosis via MEG3-P53 pathway activation. Biochem Biophys Res Commun, 504(1): 123-128. https://doi.org/10.1016/j.bbrc.2018.08.142
[61] HAYANO M, YANG WS, CORN CK, PAGANO NC, STOCKWELL BR. (2016).Loss of cysteinyl-tRNA synthetase (CARS) induces the transsulfuration pathway and inhibits ferroptosis induced by cystine deprivation. Cell Death Differ, 23(2): 270-278. https://doi.org/10.1038/cdd.2015.93
[62] WU H, LIU A. (2021).Long non-coding RNA NEAT1 regulates ferroptosis sensitivity in non-small-cell lung cancer. J Int Med Res, 49(3): 300060521996183. https://doi.org/10.1177/0300060521996183
[63] FU M, GU J, JIANG P, QIAN H, XU W, ZHANG X. (2019). Exosomes in gastric cancer: roles, mechanisms, and applications. Mol Cancer, 18(1): 41. https://doi.org/10.1186/s12943-019-1001-7
[64] ZHANG H, WANG M, HE Y, DENG T, LIU R, WANG W, et al. (2021).Chemotoxicity-induced exosomal lncFERO regulates ferroptosis and stemness in gastric cancer stem cells. Cell Death Dis, 12(12): 1116. https://doi.org/10.1038/s41419-021-04406-z
[65] PéREZ-HERAS AM, MAYNERIS-PERXACHS J, COFáN M, SERRA-MIR M, CASTELLOTE AI, LóPEZ-SABATER C, et al. (2018).Long-chain n-3 PUFA supplied by the usual diet decrease plasma stearoyl-CoA desaturase index in non-hypertriglyceridemic older adults at high vascular risk. Clin Nutr, 37(1): 157-162. https://doi.org/10.1016/j.clnu.2016.11.009
[66] NIU R, ZHAO F, DONG Z, LI Z, LI S. (2022).A stratification system of ferroptosis and iron-metabolism related

LncRNAs guides the prediction of the survival of patients with esophageal squamous cell carcinoma. Front Oncol, 12: 1010074. https://doi.org/10.3389/fonc.2022.1010074
[67] CHEN C, ZHAO J, LIU JN, SUN C. (2021).Mechanism and role of the neuropeptide LGI1 receptor ADAM23 in regulating biomarkers of ferroptosis and progression of esophageal cancer. Dis Markers, 2021: 9227897. https://doi.org/10.1155/2021/9227897
[68] YANG H, HU Y, WENG M, LIU X, WAN P, HU Y, et al. (2022). Hypoxia inducible lncRNA-CBSLR modulates ferroptosis through m6A-YTHDF2-dependent modulation of CBS in gastric cancer. J Adv Res, 37: 91-106. https://doi.org/10.1016/j.jare.2021.10.001
[69] YAO X, YANG P, JIN Z, JIANG Q, GUO R, XIE R, et al. (2019). Multifunctional nanoplatform for photoacoustic imaging-guided combined therapy enhanced by CO induced ferroptosis. Biomaterials, 197: 268-283. https://doi.org/10.1016/j.biomaterials.2019.01.026
[70] HUANG G, XIANG Z, WU H, HE Q, DOU R, LIN Z, et al. (2022). The lncRNA BDNF-AS/WDR5/FBXW7 axis mediates ferroptosis in gastric cancer peritoneal metastasis by regulating VDAC3 ubiquitination. Int J Biol Sci, 18(4): 1415-1433. https://doi.org/10.7150/ijbs.69454
[71] MALDONADO EN, SHELDON KL, DEHART DN, PATNAIK J, MANEVICH Y, TOWNSEND DM, et al. (2013).Voltage-dependent anion channels modulate mitochondrial metabolism in cancer cells: regulation by free tubulin and erastin. J Biol Chem, 288(17): 11920-11929. https://doi.org/10.1074/jbc.M112.433847
[72] PANG JY, LI PL, AFERIN B, YAN Y, WANG JM. (2021). New strategies for cancer treatment based on ferroptosis. Modern Oncology, 29(06): 1058-1061.
[73] BRAY F, LAVERSANNE M, SUNG H, FERLAY J, SIEGEL RL, SOERJOMATARAM I, et al. (2024).Global cancer statistics 2022: GLOBOCAN estimates of incidence and mortality worldwide for 36 cancers in 185 countries. CA Cancer J Clin, 74(3): 229-263. https://doi.org/10.3322/caac.21834
[74] CASADEI C, DIZMAN N, SCHEPISI G, CURSANO MC, BASSO U, SANTINI D, et al. (2019).Targeted therapies for advanced bladder cancer: new strategies with FGFR inhibitors. Ther Adv Med Oncol, 11: 1758835919890285. https://doi.org/10.1177/1758835919890285
[75] HERNANDO POLO S, MORENO MUñOZ D, ROSERO RODRíGUEZ AC, SILVA RUIZ J, ROSERO RODRíGUEZ DI, COUñAGO F. (2021).Changing the History of Prostate Cancer with New Targeted Therapies. Biomedicines, 9(4):392. https://doi.org/10.3390/biomedicines9040392
[76] POSADAS EM, LIMVORASAK S, FIGLIN RA. (2017). Targeted therapies for renal cell carcinoma. Nat Rev Nephrol, 13(8): 496-511. https://doi.org/10.1038/nrneph.2017.82
[77] ZHANG Y, GUO S, WANG S, LI X, HOU D, LI H, et al. (2021). LncRNA OIP5-AS1 inhibits ferroptosis in prostate cancer with long-term cadmium exposure through miR-128-3p/SLC7A11 signaling. Ecotoxicol Environ Saf, 220: 112376. https://doi.org/10.1016/j.ecoenv.2021.112376
[78] LI HJ, LI X, PANG H, PAN JJ, XIE XJ, CHEN W. (2015).Long non-coding RNA UCA1 promotes glutamine metabolism by targeting miR-16 in human bladder cancer. Jpn J Clin Oncol, 45(11): 1055-1063. https://doi.org/10.1093/jjco/hyv132
[79] BUCZKOWSKA J, SZELIGA M. (2023).Two Faces of Glutaminase GLS2 in Carcinogenesis. Cancers (Basel), 15(23). https://doi.org/10.3390/cancers15235566
[80] JIAO K, CHENG J, WANG Q, HAO M. (2024).LncRNA UCA1 enhances NRF2 expression through the m(6)A pathway to mitigate oxidative stress and ferroptosis in aging cardiomyocytes. J Bioenerg Biomembr, 56(6): 607-617. https://doi.org/10.1007/s10863-024-10045-8
[81] LUO W, WANG J, XU W, MA C, WAN F, HUANG Y, et al. (2021).LncRNA RP11-89 facilitates tumorigenesis and ferroptosis resistance through PROM2-activated iron export by sponging miR-129-5p in bladder cancer. Cell Death Dis, 12(11): 1043. https://doi.org/10.1038/s41419-021-04296-1
[82] BROWN CW, AMANTE JJ, CHHOY P, ELAIMY AL, LIU H, ZHU LJ, et al. (2019).Prominin2 Drives Ferroptosis Resistance by Stimulating Iron Export. Dev Cell, 51(5): 575-586.e574. https://doi.org/10.1016/j.devcel.2019.10.007
[83] CORADDUZZA D, CONGIARGIU A, CHEN Z, ZINELLU A, CARRU C, MEDICI S. (2023).Ferroptosis and Senescence: A Systematic Review. Int J Mol Sci, 24(4). https://doi.org/10.3390/ijms24043658
[84] MAZHAR M, DIN AU, ALI H, YANG G, REN W, WANG L, et al. (2021).Implication of ferroptosis in aging. Cell Death Discov, 7(1): 149. https://doi.org/10.1038/s41420-021-00553-6
[85] GONG D, CHEN M, WANG Y, SHI J, HOU Y. (2022).Role of ferroptosis on tumor progression and immunotherapy. Cell Death Discov, 8(1): 427. https://doi.org/10.1038/s41420-022-01218-8
[86] LU Y, XIE X, LUO L. (2024).Ferroptosis crosstalk in anti-tumor immunotherapy: molecular mechanisms, tumor microenvironment, application prospects. Apoptosis, 29(11-12): 1914-1943. https://doi.org/10.1007/s10495-024-01997-8
[87] LI Q, CHEN K, ZHANG T, JIANG D, CHEN L, JIANG J, et al. (2023).Understanding sorafenib-induced ferroptosis and resistance mechanisms: Implications for cancer therapy. Eur J Pharmacol, 955: 175913. https://doi.org/10.1016/j.ejphar.2023.175913
[88] PEARSON H, MARSHALL LV, CARCELLER F. (2020). Sorafenib in pediatric hepatocellular carcinoma from a clinician perspective. Pediatr Hematol Oncol, 37(5): 412-423. https://doi.org/10.1080/08880018.2020.1740844
[89] LADD AD, DUARTE S, SAHIN I, ZARRINPAR A. (2024). Mechanisms of drug resistance in HCC. Hepatology, 79(4): 926-940. https://doi.org/10.1097/hep.0000000000000237

Review Article

Life Conflux

Effects and Mechanisms of Parental Electromagnetic Radiation Exposure on Offspring Health: A Narrative Review

Authors

Xiwen Yang, Jiaming Guo, Hongli Yan

Correspondence

smmuguojiaming@126.com (J. Guo), hongliyan@smmu.edu.cn (H. Yan)

Graphical Abstract

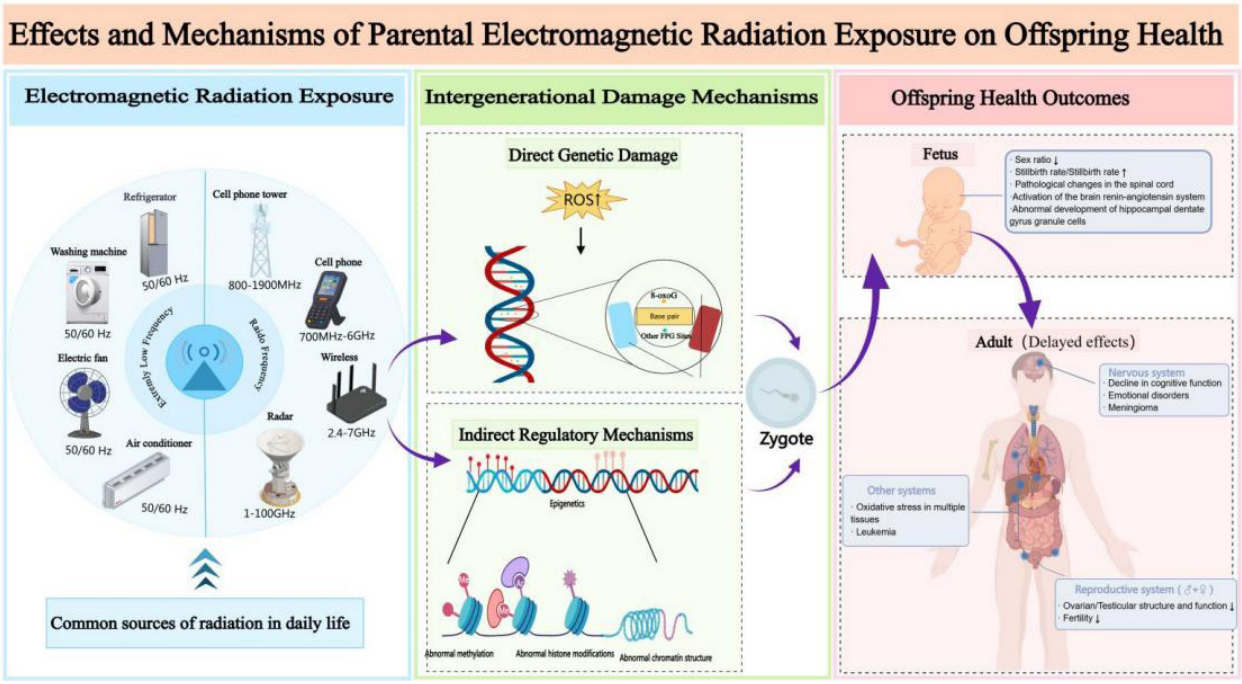

https://doi.org/10.71321/24d64c27

Review Article

Life Conflux

Effects and Mechanisms of Parental Electromagnetic Radiation Exposure on Offspring Health: A Narrative Review

Xiwen Yang [1,2], Jiaming Guo [3*], Hongli Yan [2*]

Received: 2025-01-22 | Accepted: 2025-02-17 | Published online: 2025-03-30

Abstract

The advancement of technology has heightened concerns regarding the potential health effects of electromagnetic radiation (EMR) exposure on future generations. This review aims to synthesize current research on the health impacts of parental EMR exposure on offspring, focusing on underlying biological mechanisms and providing scientific evidence to support preventive health recommendations. Studies suggest parental EMR exposure may detrimentally impact offspring's neurological and reproductive systems. Numerous animal experiments and epidemiological studies indicate associations between EMR exposure and adverse outcomes, such as fetal dysplasia, cognitive impairment, and reproductive damage. This review further examines possible mechanisms, such as oxidative stress, apoptosis, and DNA damage. Investigating the health effects of EMR on offspring is crucial for developing preventive measures and intervention strategies to reduce congenital disabilities and enhance reproductive health. Given the methodological inconsistencies and variable results in existing studies, future research should focus on refining experimental designs to assess the long-term impacts of different EMR frequencies and intensities on developing individuals, thereby clarifying their public health implications. This review seeks to consolidate findings on the effects of parental EMR exposure on offspring health, elucidate underlying mechanisms, and provide evidence-based recommendations to support public health interventions for future generations.
Keywords: Electromagnetic radiation; Offspring; Nerve; Reproductive system

Introduction

With technological advancements, the application of electromagnetic radiation in high-tech fields such as 5G networks and satellite communication is continuously expanding. This phenomenon has raised concerns about EMF (Electromagnetic Fields) exposure among the public.

Electromagnetic radiation is produced by the interaction of varying electric and magnetic fields, transmitting energy through space in waveform. Common examples include radio waves and microwaves, both of which are integral to daily life and technological applications. Electromagnetic radiation is broadly classified into radio frequency (RF) radiation (3 MHz to 300 GHz) and extremely low frequency (ELF) radiation (3 to 300 Hz), based on the frequency of the waves. The power density of electromagnetic radiation represents the amount of energy at a specific location, typically measured as power per unit area. This metric[1], expressed in watts per square meter (W/m^2), is used to quantify the strength or intensity of electromagnetic radiation. The unit of Specific Absorption Rate (SAR)[2] is watts per kilogram (W/kg), representing the electromagnetic radiation power absorbed by biological tissue per unit mass. SAR is commonly used to assess whether devices comply with international safety standards, with an average limit of 2.0 W/kg.

To assess the potential health impacts of long-term exposure to electromagnetic radiation in various populations, the World Health Organization (WHO) convened 300 experts[3], who identified six priority areas of concern: cancer, heat-related effects, adverse reproductive outcomes, electromagnetic hypersensitivity, cognitive impairment, and oxidative stress. Adverse reproductive outcomes are considered one of the most critical factors influencing human development. During the embryonic development phase, embryos are highly susceptible to environmental influences. Electromagnetic waves can affect the developing embryo, potentially impacting fetal health. Studies have shown[4] that parental environmental exposure is one of the primary factors leading to congenital diseases in children. This review focuses on the health impacts of maternal and paternal electromagnetic radiation (EMR) exposure on offspring, with particular emphasis on underlying biological mechanisms and intergenerational effects. While maternal EMR exposure has been extensively investigated in fetal development research, paternal exposure remains significantly understudied. This asymmetry in scientific

1 School of Health Science and Engineering, University of Shanghai for Science and Technology, Shanghai 200093, China

2 Reproductive Medicine Center, Changhai Hospital, Naval Medical University, Shanghai 200433, China.

3 Department of Radiation Medicine, Faculty of Naval Medicine, Naval Medical University, Shanghai 200433, China

* Corresponding Author.

attention underscores a critical research gap: the lack of systematic comparisons between maternal and paternal EMR exposure in terms of biological mechanisms, critical sensitive windows, and long-term health outcomes. The present review aims to synthesize findings from epidemiological studies and animal experiments to compare the similarities and differences between maternal and paternal EMR exposure in mechanisms of action, critical exposure windows, and health consequences. Through systematic synthesis and comprehensive analysis, this study seeks to provide a scientific foundation for a holistic understanding of the potential risks posed by parental EMR exposure to offspring health, while offering insights to guide future research directions and inform public health intervention strategies.

Methods

Search strategy

We developed this systematic review according to the Preferred Reporting Items for Systematic Reviews and Meta-Analyses (PRISMA) recommendations. The search was performed using three different databases: PubMed, Google Scholar and Web of Science. To identify the publications eligible for inclusion we used the keywords “Electromagnetic radiation”; “Offspring”; “Nerve”; “Reproductive system” in the following search query: ((“electromagnetic radiation” AND “offspring” AND “parents”) AND “health”).Moreover, to limit the results, we applied the following research filters: articles published from 1 January 1990 to 1 August 2024, exclusion of animal studies and inclusion of publications in English only. As shown in Figure 1, an initial screening identified 70 candidate articles. After eliminating duplications, the initial screening of the studies was performed using information available in both the titles and the abstracts and 63 potentially relevant articles were retrieved in full text and assessed for eligibility according to the following inclusion criteria:

–Inclusion of both human and anima as study subject, with inclusion of offspring;

–Assessment of EMF exposure in parents ;

–Inclusion of offspring health risks(For example, reproductive system damage, neurological damage, etc.)

The publications were included in the analysis only if they met all the eligibility criteria. Through the reading of the references of the included studies, after a full assessment of the potentially relevant studies, 45 articles met the eligibility criteria and were
included in the systematic review.

Data extraction

During the analysis of the methodology and the results from the different studies, the authors noticed how these had been expressed either in a non-homogeneous or in a non-standardized manner. Therefore, the 45 articles in this systematic review were: 10 epidemiological studies, 35 animal experimentation. Relevant data were extracted, including exposure time, source of exposure, frequency,average power density, SAR, intergenerationally inherited phenotype ,mechanism.

Figure 1. PRISMA flow diagram.

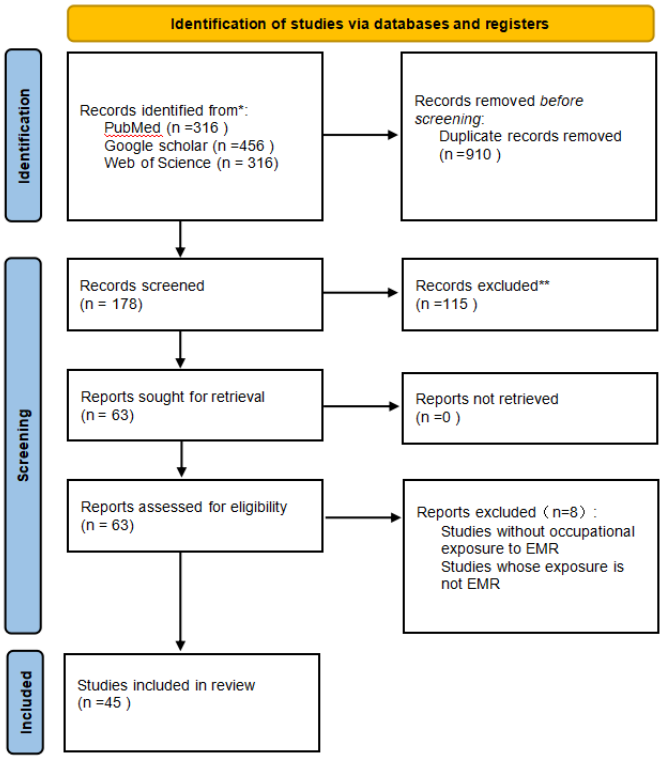

Methodological limitations

Given the substantial heterogeneity in animal study designs (e.g., species, exposure models, frequencies, and endpoints), we did not apply a single standardized risk of bias tool across all included studies. Instead, we evaluated study quality narratively, emphasizing reproducibility, exposure characterization, and biological plausibility of outcomes. Studies lacking basic methodological information (e.g., exposure parameters or offspring outcome data) were excluded to maintain baseline quality control.

Results and Discussion

Neurobehavioral development in offspring

Parental prenatal exposure to environmental EMF influences early embryonic neurological development, resulting in potential adverse effects on fetal growth and maturation. The brain, being one of the most sensitive organs to EMF exposure, may experience various types of neurological damage [5], including neurological lesions, brain tumor formation, and cognitive and mood abnormalities. These adverse effects of electromagnetic radiation on the embryonic nervous system may potentially persist into postnatal life and adulthood. Some of these changes and the regulatory mechanisms involved are summarized in Table 1.

1) Abnormalities in nervous system development

Abnormal neurological development refers to deviations in the structural and functional formation of brain tissue during the embryonic stage. The development of the nervous system is a complex and highly coordinated process. Considering this complexity, numerous studies have focused on the

potential effects of electromagnetic radiation exposure during critical developmental windows. Studies have investigated the effects of different durations of exposure to 900 MHz radiofrequency radiation during gestation, ranging from one hour to six hours per day. Ayşe İkinci Keleş et al. [6, 7] found that exposure for one hour per day adversely impacted the morphological integrity of the spine and vertebrae in the offspring. Ersan Odaci et al.[8] found that the development of granule cells within the dentate gyrus of the hippocampus in rats was significantly affected by 900 MHz exposure. Aysu Kilic et al. [9] found that exposing both male and female rats to 900 MHz throughout the entire gestation period activated the brain renin-angiotensin system in the offspring, potentially leading to neuroinflammation and increased oxidative stress. Additionally, Haghani et al. [10] exposed pregnant rats to 900 MHz electromagnetic radiation for 6 hours per day, resulting in significant alterations in the electrophysiological properties of Purkinje neurons in the offspring. Several studies have explored the potential link between electromagnetic field (EMF) exposure and neurological disorders. The mixed results from these studies highlight the complexity of the relationship between EMF exposure and nervous system development. While some studies indicate a potential risk, such as the association with meningiomas and central nervous system disorders, other studies fail to find significant evidence, suggesting that further research with more refined methodologies is needed to clarify these findings.

2) Neurological lesions

Electromagnetic fields (EMFs) can cause neurodegenerative syndromes and, in severe cases, may lead to diseases such as Parkinson's disease and Alzheimer's disease [11]. An epidemiological study conducted in Norway used data from 1967 to 1995. The study investigated the exposure of parents of 1.2 million newborns to electromagnetic fields. It found an association between potential central nervous system disorders and parental exposure to a 50 Hz magnetic field. [12]. A case-control study conducted in southwest France between May 1999 and April 2001 found that occupational or residential exposure to extremely low-frequency (ELF) EMFs may be associated with an increased risk of meningiomas[13]. However, a study by A.J. De Roos et al. [14] found no statistically significant association between the incidence of neuroblastoma in 538 children diagnosed in the USA or Canada between 1992 and 1994 and parental exposure to very low-frequency EMFs. A potential reason for these differing results could be the varying timing of exposure during critical periods of neurodevelopment. For example, prenatal exposure to electromagnetic fields may have a greater impact on fetal brain development, potentially leading to meningiomas or central nervous system disorders. In contrast, the relationship between electromagnetic fields and childhood neuroblastoma appears less clear, suggesting that certain types of EMF exposure may have a more limited effect on the development of specific childhood cancers.

3) Neurocognitive disorder

Cognitive impairment refers to a pathological condition characterized by abnormalities in the higher cognitive functions of the brain, such as learning, memory, thinking, and judgment, ultimately leading to cognitive decline. Indicators of cognitive impairment include reduced learning ability, diminished spatial memory, and inattention. For instance, a study by Moazamehosadat et al. [15] found that daily exposure of pregnant rats to 900 MHz radiofrequency radiation from mobile phones impaired cognitive performance in their female offspring. Yanchun Zhang et al. [16] exposed rats to high-frequency microwaves at 9.417 GHz, which are commonly used in certain industrial and communication devices, throughout gestation, resulting in gender-dependent learning and memory deficits, with males exhibiting more pronounced impairments compared to females.

An epidemiological study [17] utilizing data from 83,884 mother-child pairs across five countries provided a large-scale assessment of the potential effects of maternal mobile phone use during pregnancy, suggesting an association with an increased risk of behavioral problems in offspring, particularly hyperactivity/inattention problems. However, another experiment [18]exposed pregnant rats to 7.5 KHz electromagnetic radiation and did not observe significant impairments in cognitive function in the offspring. These discrepancies in findings may be attributed to differences in exposure parameters (e.g., frequency, power density), exposure duration, and species-specific responses, highlighting the complexity of assessing the effects of electromagnetic fields on neurodevelopment.

One possible explanation for the varying results could be differences in exposure parameters, such as frequency, power density, and duration, which may significantly influence the extent and nature of cognitive impairment. For example, high-frequency EMF exposure (e.g., 9.417 GHz) may have a more pronounced effect on brain development than low-frequency exposure (7.5 kHz), as higher frequencies penetrate tissues more effectively and may induce stronger biological effects. Furthermore, species-specific responses could contribute to some of the discrepancies observed, as different animal models may exhibit varying reactions to EMF exposure due to inherent differences in brain structure and metabolism. Gender differences in susceptibility might also be a factor; as demonstrated by Zhang et al. [16], males exhibited more severe cognitive deficits than females, suggesting that hormonal or developmental differences could influence the response to EMFs.

4) Emotional disturbance

Regarding emotional disturbances, Burcu Acikgoz et al. [19] found that exposing pregnant rats to EMF was associated with increased anxiety-like behaviors in the offspring. Similarly, Yanchun Zhang et al. [16] demonstrated that exposure to 9.417 GHz during pregnancy was associated with heightened anxiety and reduced depressive-like behaviors in the offspring. Although these findings indicate possible links between EMF exposure and mood disturbances, relatively few studies have comprehensively explored mood disorders in offspring. Exposure to electromagnetic fields during pregnancy may interfere with maternal and fetal hormonal regulation, particularly hormones such as cortisol, oxytocin, and estrogen, which are involved in stress response and emotional processing. This disruption could contribute to emotional and behavioral problems in the offspring.

Table 1. The impact of parental electromagnetic radiation exposure on neurobehavioral development in offspring

Exposed Object	Exposure Time/source of exposure	Frequency	Average Power Density	SAR	Intergenerationally Inherited Phenotype	Main Mechanism	Ref
pregnant rat	Exposure period: GD13.5-delivery Duration of exposure: 1h/day	900MHz	/	/	Pathological changes in the spinal cord	epigenetic	[6]
pregnant rat	Exposure period: GD23-PND 40 Duration of exposure: 1h/day	900MHz	/	/	activation of the brain renin-angiotensin system	oxidative stress	[9]
pregnant rat	Exposure period: 13 to 21 days before delivery Duration of exposure: 1h/day	900MHz	/	/	Pathologic changes in the vertebrae	/	[7]
pregnant rat	Exposure period: the entire pregnancy Duration of exposure: 1h/day	900MHz	1±0.4 W/cm2	2 W/kg	abnormal development of hippocampal dentate gyrus granule cells	Impaired cytokines	[8]
pregnant rat	Exposure period: the entire pregnancy Duration of exposure: 6h/day	900MHz	/	0.5-0.9 W/kg	the electrophysiological properties of Purkinje neurons are altered	/	[10]
pregnant rat	Exposure period: the entire pregnancy	900MHz	/	0.3-0.9 W/kg	decline in cognitive function	/	[15]
pregnant rat	Exposure period: GD3.5-GD18 Duration of exposure: 12h/day	9.417GHz	1.93 W/cm2	2 W/kg	there are sex differences in emotional disorders and cognitive function	/	[16]
pregnant rat	Exposure period: the entire pregnancy Duration of exposure: 24h/day	7.5 kHz MF (12 or 120 μT)	/	/	no effect	/	[18]
human parents	Exposure period: occupational exposure	50 Hz	/	/	cause central nervous system diseases in offspring	/	[12]
human parents	Exposure period: occupational exposure & residential exposure	ELF	/	/	cause meningioma in offspring	/	[13]
pregnant human mother	Exposure period: the entire pregnancy	radiofrequency radiation from mobile phones	/	/	may cause behavioral disorders, particularly ADHD/inattention	/	[17]
human parents	Exposure period: occupational exposure	extremely low-frequency magnetic fields (>0.4 μT)	/	/	There is no evidence that parental electromagnetic spectrum exposure causes neuroblastoma in offspring	/	[14]

Reproductive system damage in offspring.

Due to the unique structure and function of the reproductive system, it is particularly vulnerable to environmental factors, including electromagnetic fields (EMF); therefore, parental exposure to EMF may negatively impact reproductive health and fertility by interfering with hormonal balance and gamete production [20]. Moreover, EMF exposure may affect not only the reproductive health of individuals but also the health of their offspring through genetic and epigenetic alterations. Table 2 summarizes some of these changes and the possible regulatory mechanisms involved.

1) Male reproductive system damage

Nevin Ersoy et al. [21] found that prenatal and postnatal exposure to 50-Hz, 3-mT EMF resulted in increased apoptosis and structural alterations in the testes of the offspring. Similarly, Alper Özorak et al. [22] exposed 32 pregnant mice to three frequencies—2.45 GHz, 900 MHz, and 1,800 MHz—and found that their offspring showed increased oxidative stress in testicular tissue and exhibited signs of precocious puberty, as indicated by accelerated sexual maturation. In contrast, Song Yan et al. [23] exposed male mice to 2.0 GHz RF EMR and did not observe any significant damage to the testicular structure or changes in sperm quality in the offspring. However, exposure of pregnant rats to 2.45 GHz RF EMR was reported [24] to have deleterious effects on postnatal testicular development, including impaired germ cell differentiation and disrupted spermatogenic process, which in turn impaired the spermatogenic cycle and male reproductive function. The studies reviewed demonstrate a range of effects of electromagnetic field (EMF) exposure on male reproductive health, particularly with respect to testicular function and spermatogenesis in offspring. While some studies report significant damage, others find no observable harm, suggesting that the outcomes may be influenced by several factors, including variations in experimental design, species-specific responses, and differences in the timing and duration of exposure.

2) Female Reproductive System Injury

B. M. Ryan et al.[25] exposed F0 generation rats to electromagnetic fields (EMF) at 60 Hz for 17 weeks and found that parameters related to fertility, including litter size, gestational latency, and sex ratio, were not impaired in the F0, F1, and F2 generations. Acikgoz Burcu et al. [26] exposed rats to 50 Hz, 3 mT EMF both prenatally and postnatally, which was associated with impaired ovarian structure and function in female offspring, potentially through increased iNOS levels. According to report[27], simultaneous whole-body exposure of pregnant rats to eight different communication signal EMFs, with frequencies ranging from 800 MHz to 5.2 GHz, did not result in any adverse effects on pregnancy or developmental outcomes in the F1 and F2 generations. Satoru Takahashi et al. [28] found that whole-body exposure to 2.14 GHz RF-EMR for 20 hours per day during gestation and lactation did not result in adverse effects on fertility, embryotoxicity, or teratogenicity in the F1 and F2 generations.A critical factor influencing the observed variability in outcomes is the timing of exposure. Studies that exposed rats to EMFs during specific developmental windows, such as gestation and early postnatal stages, may have led to more pronounced effects, particularly on the female reproductive system, as evidenced by Acikgoz Burcu et al. [26]. During these sensitive periods, hormonal and cellular processes essential for organ development, including those of the ovaries, may be more susceptible to disruption, which could explain the ovarian dysfunction observed in female offspring.

3) Damage to the human reproductive system

In recent years, environmental factors are increasingly recognized as having a significant detrimental impact on the reproductive health of human offspring. It has been reported [29] that occupational exposure to electromagnetic fields (EMFs) from sources such as high-frequency antennas, communication equipment, substations, and radiolocation stations can alter the sex ratio of offspring, characterized by a decreased proportion of male infants and an increased proportion of female infants. N. Mageroy et al. [30] analyzed data from a cross-sectional study of 2,265 current employees of the Norwegian Navy. They found an increased risk of congenital anomalies and stillbirths among crew members serving on the KNM Kvikk following the installation of a 750 W high-frequency transmitter. Valborg Baste and colleagues conducted a cohort study [31] using data from the Norwegian Medical Birth Registry (singleton births, n = 37,920). The study found that acute paternal exposure to electromagnetic radiation was associated with an increased risk of perinatal death and pregnancies complicated by preeclampsia. Similarly, Valborg Baste [32] found that paternal exposure to mobile phone radiation during the six months prior to conception was associated with an increased risk of perinatal mortality, potentially due to alterations in sperm DNA integrity. A study [33] examined 53 workers who were occupationally exposed to electrical fields at a 400 kV substation for more than five years. The findings indicated that the workers had a relatively lower number of offspring compared to general population data, with a decreased proportion of male offspring. The evidence suggests that electromagnetic field (EMF) exposure may have significant implications for reproductive health, particularly concerning male fertility and paternal effects on pregnancy outcomes. Notably, alterations in sex ratios and an increased incidence of perinatal complications associated with paternal EMF exposure raise concerns about the broader environmental impact on human reproduction. Given the growing prevalence of EMF exposure in contemporary society, it is imperative to investigate the underlying mechanisms that mediate these associations and to develop preventive strategies aimed at mitigating potential risks to future generations.

Damage to other system functions in offspring

The effects of electromagnetic fields (EMFs) on human health are not limited to the reproductive and nervous systems but may also extend to other vital organs, including the liver, heart, and kidneys (Table 3). For example, exposing pregnant rats to 900 MHz EMF for one hour per day resulted in oxidative stress and histopathological alterations in the liver of the offspring postnatally [34]. In addition to its effects on the liver, prolonged prenatal exposure of rats to high-frequency EMFs (900, 1800, and 2100 MHz) was associated with significant alterations in myocardial tissue structure and function [35]. A study [36] also investigated the effects of mobile phone (900-1800 MHz) induced electromagnetic radiation on the redox state of the

Table 2. The impact of parental electromagnetic radiation exposure on the reproductive system of offspring

Exposed Object	Exposure Time/source of exposure	Frequency	Average Power Density	SAR	Intergenerationally Inherited Phenotype	Mechanism	Ref
pregnant rat	Exposure period: the entire pregnancy - PND 24/48 Duration of exposure: 4h/day 5day/week	50 Hz (3-mT)	/	/	Testicular structural changes and germ cell apoptosis.	epigenetic	[21]
pregnant rat &offspring	Exposure period: GD7-postpartum Duration of exposure: 20h/day	2.14GHz	/	Female rat: 0.066-0.093 W/kg offspring: 0.068-0.146 W/kg	No effect	/	[28]
pregnant rat & offspring	Exposure period: the entire pregnancy - PND 42 Duration of exposure: 1h/day 5day/week	2.45 GHz, 900 MHz, 1800 MHz (single radiation exposure)	0.12 W/m²	0.18±0.07 W/kg	Precocious puberty and testicular oxidative damage	/	[22]
male mice	Exposure period: 14week Duration of exposure: 3h/day	2.0 GHz	2.5 W/m2	0.125-0.5 W/kg	Body weight trajectory and glucose metabolism are altered in F1 male mice	/	[23]
pregnant rat & offspring	Exposure period: the entire pregnancy - PND 63 Duration of exposure: 4h/day	50 Hz (3 mT)	/	/	Ovarian structure and function are impaired	iNOS is activated	[26]
pregnant rat & offspring	Exposure period: DG7 - PND 42 Duration of exposure: 20h/day	800MHz 2GHz 2.4GHz 2.5GHz 5.2GHz (mixed radiation)	/	0.08- 0.4W/kg	Pregnancy and fertility are not impaired	/	[27]
pregnant rat	Exposure period: the entire pregnancy Duration of exposure: 2h/day	2.45GHz	/	1.73 W/kg	Male reproductive system is impaired	/	[24]
human parents	Exposure period: occupational exposure	high-frequency electro-magnetic fields	/	/	Congenital birth defects and stillbirth	/	[30]

human parents	Exposure period: occupational exposure	High-frequency antennas and communi-cation devices, substations, physical therapists, radio navigation stations, etc.	/	/	The proportion of male offspring is reduced	/	[29]
human father	Exposure period: occupational exposure 1.Acute exposure - within three months before pregnancy 2.chronic exposure - more than three months before pregnancy	2.1-4MHz 9.4GHz 9.1GHz	/	/	Increased perinatal mortality rate	/	[31]
human father	Exposure period: the six months before pregnancy	radio-frequency radiation from mobile phones	/	/	Increased perinatal mortality rate	/	[32]

heart, liver, kidney, cerebellum, and hippocampus in rats and their offspring, and they found that exposure to mobile phones during pregnancy induced oxidative stress in various tissues of the offspring, including the liver, kidneys, and heart.

Zozan Guleken et al. [37] investigated the long-term effects of extremely low-frequency magnetic fields (ELF-MF, 50 Hz), further highlighting the broad impacts of EMF exposure on biological systems. They showed that long-term EMF exposure is an environmental factor affecting serum parameters and may impair the oxidative-antioxidant balance of the organism. Short-term exposure to Wi-Fi-induced EMR before and after birth in rats may lead to an imbalance in tooth elemental composition, specifically affecting calcium and phosphorus levels, due to oxidative stress [38]. Alper Özorak et al. [39] exposed pregnant rats to three different frequencies (2.45 GHz, 900 MHz, and 1,800 MHz) and found that EMR led to nephrogenic oxidation in the growing offspring. Similarly, Joseph M. Lary et al. [40] reported that exposure of pregnant rats to a 27.12-MHz radiofrequency field caused fetal malformations, such as microphthalmia and brain enlargement, due to a radiation-induced increase in rectal temperature of 5°C, which may have contributed to these malformations.

Laboratories [46] have also used rabbits as research subjects, briefly exposing them to 1800 MHz radiation without finding significant pathological changes in the tissues and organs of the offspring. Furthermore, Mark S. Pearce et al. [41] analyzed data from the Northern Regional Registry of Malignant Diseases in the Young (NRYPMDR), comprising 4,723 cases, and found that occupational exposure to EMFs significantly increased the risk of developing leukemia, particularly acute lymphoblastic leukemia (ALL), in the male offspring. Similarly, Reid [42] found a moderate increase in the risk of acute lymphoblastic leukemia (ALL) in children whose mothers were occupationally exposed to extremely low-frequency (ELF) electromagnetic fields. These findings highlight the wide-ranging potential health risks associated with electromagnetic field (EMF) exposure, including organ damage, developmental malformations, and an elevated risk of cancer. However, the variability in results across different studies necessitates further investigation to elucidate the underlying mechanisms, identify factors that influence susceptibility. A more comprehensive understanding of these issues is essential for accurately assessing the public health implications of EMFs in our increasingly interconnected and technology-driven society.

Table 3: The impact of parental electromagnetic radiation exposure on other tissues and organs in offspring

Exposed Object	Exposure Time/source of exposure	Frequency	Average Power Density	SAR	Intergene-rationally Inherited Phenotype	Mechanism	Ref
Pregnant rat	Exposure period: DG13-DG21 Duration of exposure: 1h/day	900MHz	0.54 W/m2	0.027 W/kg	Oxidative stress and pathological changes occur in the liver	/	[34]
Pregnant rat	Exposure period: 20day Duration of exposure: 6h/day, 12h/day, 24h/day	1800,2100, 2450 MHz (single radiation exposure)	/	0.087 W/kg, 0.12 W/kg, 0.17 W/kg	Myocardial tissue is damaged	/	[35]
Pregnant mice	Exposure period: 20day Duration of exposure: 2h/day	900-1800MHz	/	/	Oxidative stress in various tissues and organs.	/	[36]
pregnant rat	Exposure period: 42day (From pregnancy to lactation) Duration of exposure: 24h/day	50 Hz (500μT)	/	/	Affects serum parameters and increases lipid peroxidation and oxidative stress	/	[37]
pregnant rat	Exposure period: 42day (From pregnancy to lactation) Duration of exposure: 2h/day	2.45GHz	/	0.009 ±0.002 W/kg	Imbalance in the oxidative stress status of the teeth	/	[38]
pregnant rat	Exposure period: the entire pregnancy - PND 42						
Duration of exposure: 1h/day 5day/week	900 MHz, 1800 MHz, 2.45 GHz (single radiation exposure)	0.12 W/m²	0.18 ±0.07 W/kg	Oxidative damage to the kidneys	/	[22]	
pregnant rat	Exposure period: DG9 Duration of exposure: 2h, 15min	27.12 MHz	/	10.8 ± 0.3 W/kg	Offspring malformations	/	[40]

pregnant rabbit	Exposure period: 7day Duration of exposure: 15min/day	1800MHz	0.519 W/m^2	/	No effect	/	(46]
human father	Exposure period:occupational exposure	power devices high-frequency communication devices radiological imaging equipment	/	/	Increased risk of leukemia in male offspring	/	[41]
human mother	Exposure period: occupational exposure	ELE	/	/	Increased risk of acute lymphoblastic leukemia in offspring	/	(42]

Conclusion

In summary, most recent animal studies and clinical evidence indicate that parental exposure to electromagnetic radiation, even at low doses, can adversely affect offspring health, impacting various organs and tissues, including the liver, brain, and reproductive system. Furthermore, long-term exposure to high-frequency radiation poses a greater hazard to offspring due to prenatal exposure compared to short-term exposure. However, a limited number of studies provide conflicting evidence, suggesting that under certain conditions, EMR exposure may not always lead to adverse health outcomes. These conflicting findings underscore the need for further well-controlled studies to clarify the conditions under which electromagnetic radiation might be harmful or benign to offspring health.

Existing studies on the health impacts of parental exposure to electromagnetic radiation (EMR) on offspring exhibit significant discrepancies, with contradictory findings attributable to the complex interplay of multidimensional factors. Firstly, inconsistencies in experimental design parameters represent a core cause. Variations in the selection of EMR frequency (e.g., 900 MHz vs. 7.5 kHz), intensity (differences in specific absorption rate (SAR) ranges), and exposure duration (1 to 24 hours/day) across studies could result in an undefined threshold for biological effects. High-frequency radiation, due to its stronger penetration ability, is more likely to induce oxidative stress or epigenetic alterations, whereas low-frequency or short-term exposure may obscure effects through biological adaptive mechanisms. Secondly, heterogeneity in study subjects and experimental models limits the comparability of outcomes. Physiological response differences between rodents and humans, strain-specific sensitivities in experimental animals (e.g., heightened hippocampal neuron vulnerability in rats compared to rabbits), and sex-specific responses (e.g., males being more prone to cognitive deficits) may all contribute to divergent conclusions. Thirdly, methodological limitations exacerbate uncertainty in results. Epidemiological studies relying on retrospective exposure assessments are prone to recall bias and susceptible to confounding factors (e.g., occupational chemical exposure), whereas animal experiments, despite controlled variables, fail to accurately replicate real-world multifrequency composite exposures and are limited by low statistical power in small-sample studies. Furthermore, diversity in biological endpoints and detection techniques (e.g., selection of oxidative stress markers, depth of epigenetic analyses) further complicates data interpretation.

The health effects of parental radiation exposure on offspring are complex, and only a small portion of the literature has explored the mechanisms of intergenerational inheritance, such as oxidative stress, iNOS activation, and epigenetic changes. However, these studies have primarily explored superficial mechanisms through animal experiments. Epigenetics, by contrast, provides a promising avenue for investigating deeper underlying mechanisms. Epigenetics is considered a form of non-genetic mechanism that regulates gene expression without altering the DNA sequence. A review [43] highlighted that environmental factors can induce behavioral changes in mammals, and these behavioral changes may be inherited by the next generation, thereby influencing the behavior of multiple generations. The external environment influences key carriers of epigenetic information, such as DNA methylation, histone modifications, and non-coding RNAs, which alters gene expression patterns and thus affects an individual's health [44]. These trait changes can not only persist throughout an individual's life but can sometimes be inherited across generations. With advancements in technology, the emergence of new techniques has provided powerful tools for studying the complex mechanisms of epigenetics, such as high-throughput sequencing technologies (e.g., Whole-Genome Bisulfite Sequencing and ChIP-seq), single-cell epigenetic technologies (e.g., scRNA-seq), and single-cell Hi-C technology [45]. These technologies help reveal how genes are regulated in different environments, developmental stages, and disease states

The current research literature on the effects of parental exposure to electromagnetic radiation (EMR) on offspring

health is limited and faces several significant challenges. Firstly, the potential effects of EMR on offspring health may take years or even decades to manifest, making it difficult to conduct intergenerational genetic delayed-effect studies. Many contemporary studies do not include sufficiently long observation periods. Secondly, there is no consensus among researchers regarding standardized exposure conditions and outcome assessment methods, leading to inconsistencies in study conclusions. Additionally, more accurate simulations of exposure timing are needed in existing experiments. The health effects of EMR exposure on offspring may vary significantly depending on the timing, and real-life parental exposure often involves extended periods, including simultaneous postnatal exposure for both the offspring and the mother. This complexity makes accurate assessment and simulation of exposure conditions challenging. Moreover, species differences between humans and animal models, such as rats and rabbits, necessitate caution when extrapolating findings from animal experiments to clinical settings. Finally, mechanistic studies on intergenerational inheritance remain relatively unexplored, highlighting the need for further research using more sophisticated scientific methods to elucidate these mechanisms.

While existing research predominantly focuses on the direct impacts of maternal EMR exposure on embryonic development, paternal exposure has garnered increasing attention in recent years. This review reveals significant differences between maternal and paternal EMR exposure in mechanisms, sensitive windows, and health outcomes, as outlined below:

Divergent Mechanisms of Action

Maternal EMR exposure during pregnancy directly affects embryos through placental transmission, inducing oxidative stress, DNA damage, and epigenetic alterations [6,9,21,26]. For instance, gestational exposure of rats to 900 MHz EMR activates the renin-angiotensin system in offspring brains, leading to neuroinflammation [9]. In contrast, paternal EMR exposure primarily exerts its effects through compromised sperm DNA integrity or epigenetic modifications. Occupational paternal exposure to high-frequency EMR (e.g., 2.1–4 MHz) correlates with elevated perinatal mortality in offspring, likely mediated by sperm DNA fragmentation or mitochondrial dysfunction [31–32].

Sensitivity of Exposure Windows

The embryonic period—particularly organogenesis—represents the critical window for maternal exposure. Studies indicate that maternal exposure to 9.417 GHz microwaves during early gestation (GD3.5–GD18) induces sex-dependent cognitive dysfunction in offspring [16], whereas late-gestation exposure may provoke emotional disturbances [19]. Paternal sensitivity is concentrated during male gametogenesis (spermatogenesis). For example, frequent paternal mobile phone use within six months pre-conception is associated with increased perinatal mortality [32], suggesting cumulative genetic damage during spermatogenesis.

Heterogeneity in Health Outcomes

Maternal EMR exposure is predominantly linked to offspring neurological abnormalities (e.g., cognitive deficits, anxiety-like behaviors) and structural malformations (e.g., spinal dysplasia) [6,16]. Epidemiological studies also suggest maternal mobile phone use during pregnancy may elevate offspring hyperactivity risk [17]. Paternal exposure, however, more profoundly impacts reproductive health and sex ratios. Occupational paternal exposure to high-frequency EMR (e.g., radar stations, communication devices) significantly reduces male offspring proportions [29]. Additionally, paternal exposure is associated with elevated leukemia risk in offspring [41–42], potentially via germline mutations.

Systematic comparisons of paternal and maternal EMR exposure mechanisms and health effects are imperative to delineate pathway- and window-specific hazards, thereby informing targeted public health interventions.

Although existing evidence remains inconclusive, it suggests that adopting precautionary measures could mitigate potential risks. During critical windows of reproductive development (e.g., preconception, pregnancy, and early postnatal stages), exposure to high-frequency electromagnetic radiation (EMR) sources, such as 5G and mobile communication devices, should be minimized due to its established association with oxidative stress and epigenetic dysregulation in offspring. Occupational groups with high EMR exposure (e.g., telecommunications and healthcare workers) should prioritize protective strategies, including maintaining a safe distance from radiation sources and utilizing protective equipment. Regulatory frameworks should mandate standardized EMR dosimetry labeling on consumer electronic devices and adjust specific absorption rate (SAR) limits based on developmental stage sensitivity. Furthermore, public health communications should provide evidence-based guidance while avoiding the exaggeration of potential risks. However, these recommendations remain provisional—longitudinal studies investigating intergenerational epigenetic mechanisms are urgently required to address persistent uncertainties.

Overall, the evidence on the effects of EMR exposure on the health of offspring is still limited, and the underlying mechanisms remain poorly understood. As digital healthcare systems advance, it will become easier to conduct large-scale, longitudinal tracking of individual radiation exposure in the population, thereby enabling more precise investigations into the delayed effects of intergenerational inheritance. In addition, recent technological advancements enable the detection and quantification of DNA methylation, histone modifications, and RNA expression. These new approaches can also help uncover mechanisms of intergenerational inheritance from an epigenetic perspective or other relevant angles, and further identify reliable biomarkers of EMR exposure for future clinical diagnostics and treatments. This facilitates early intervention to prevent genetic diseases and birth defects, ultimately promoting healthy reproduction and childbearing.

Acknowledgements

Not applicable.

Funding Information

This study is sponsored by Natural Science Foundation of

Shanghai (24ZR1480000) and Shanghai Eastern Talent Plan (QNWS2024027).

Ethics Approval and Consent to Participate

Ethical issues (Including plagiarism, informed consent, misconduct, data fabrication and/or falsification, double publication and/or submission, redundancy, etc.) have been completely observed by the authors.

Competing Interests

The authors declare that they have no existing or potential commercial or financial relationships that could create a conflict of interest at the time of conducting this study.

Data Availability

All data needed to evaluate the conclusions in the paper are present in the paper or the Supplementary Materials. Additional data related to this paper may be requested from the authors.

References

[1] Muhibbullah M, Haleem AMA, Ikuma Y. (2017). Frequency dependent power and energy flux density equations of the electromagnetic wave. Results in Physics.7,435-9.http://https://doi.org/10.1016/j.rinp.2017.01.006

[2] Gautam R, Singh KV, Nirala J, Murmu NN, Meena R, Rajamani P. (2019). Oxidative stress-mediated alterations on sperm parameters in male Wistar rats exposed to 3G mobile phone radiation. Andrologia.51(3),e13201.http://https://doi.org/10.1111/and.13201

[3] Verbeek J, Oftedal G, Feychting M, van Rongen E, Rosaria Scarfì M, Mann S, et al. (2021). Prioritizing health outcomes when assessing the effects of exposure to radiofrequency electromagnetic fields: A survey among experts. Environment International.146,106300.http://https://doi.org/10.1016/j.envint.2020.106300

[4] Mahaldashtian M, Khalili MA, Anbari F, Seify M, Belli M. (2022). Challenges on the effect of cell phone radiation on mammalian embryos and fetuses: a review of the literature. Zygote.30(2),176-82.http://10.1017/S0967199421000691

[5] Lagorio S, Blettner M, Baaken D, Feychting M, Karipidis K, Loney T, et al. (2021). The effect of exposure to radiofrequency fields on cancer risk in the general and working population: A protocol for a systematic review of human observational studies. Environment International.157,106828.http://https://doi.org/10.1016/j.envint.2021.106828

[6] Keleş Aİ. (2020). Morphological changes in the vertebrae and central canal of rat pups born after exposure to the electromagnetic field of pregnant rats. Acta Histochemica.122(8),151652.http://https://doi.org/10.1016/j.acthis.2020.151652

[7] Keleş Aİ, Süt BB. (2021). Histopathological and epigenetic alterations in the spinal cord due to prenatal electromagnetic field exposure: An H3K27me3-related mechanism. Toxicology and Industrial Health.37(4),189-97.http://10.1177/0748233721996947

[8] Odaci E, Bas O, Kaplan S. (2008). Effects of prenatal exposure to a 900 MHz electromagnetic field on the dentate gyrus of rats: a stereological and histopathological study. Brain Research.1238,224-9.http://https://doi.org/10.1016/j.brainres.2008.08.013

[9] Kilic A, Ustunova S, Bulut H, Meral I. (2023). Pre and postnatal exposure to 900 MHz electromagnetic fields induce inflammation and oxidative stress, and alter renin-angiotensin system components differently in male and female offsprings. Life Sciences.321,121627.http://https://doi.org/10.1016/j.lfs.2023.121627

[10] Haghani M, Shabani M, Moazzami K. (2013). Maternal mobile phone exposure adversely affects the electrophysiological properties of Purkinje neurons in rat offspring. Neuroscience.250,588-98.http://https://doi.org/10.1016/j.neuroscience.2013.07.049

[11] Feychting M, Ahlbom A, Kheifets L. (2005). EMF and health. Annu Rev Public Health.26,165-89.http://10.1146/annurev.publhealth.26.021304.144445

[12] Blaasaas KG, Tynes T, Irgens A, Lie RT. (2002). Risk of birth defects by parental occupational exposure to 50 Hz electromagnetic fields: a population based study. Occup Environ Med.59(2),92-7.http://10.1136/oem.59.2.92

[13] Baldi I, Coureau G, Jaffré A, Gruber A, Ducamp S, Provost D, et al. (2011). Occupational and residential exposure to electromagnetic fields and risk of brain tumors in adults: a case-control study in Gironde, France. Int J Cancer.129(6),1477-84.http://10.1002/ijc.25765

[14] De Roos AJ, Teschke K, Savitz DA, Poole C, Grufferman S, Pollock BH, Olshan AF. (2001). Parental occupational exposures to electromagnetic fields and radiation and the incidence of neuroblastoma in offspring. Epidemiology.12(5),508-17.http://10.1097/00001648-200109000-00008

[15] Razavinasab M, Moazzami K, Shabani M. (2016). Maternal mobile phone exposure alters intrinsic electrophysiological properties of CA1 pyramidal neurons in rat offspring. Toxicol Ind Health.32(6),968-79.http://10.1177/0748233714525497

[16] Zhang Y, Li Z, Gao Y, Zhang C. (2015). Effects of fetal microwave radiation exposure on offspring behavior in mice. J Radiat Res.56(2),261-8.http://10.1093/jrr/rru097

[17] Birks L, Guxens M, Papadopoulou E, Alexander J, Ballester F, Estarlich M, et al. (2017). Maternal cell phone use during pregnancy and child behavioral problems in five birth cohorts. Environ Int.104,122-31.http://10.1016/j.envint.2017.03.024

[18] Kumari K, Koivisto H, Capstick M, Naarala J, Viluksela M, Tanila H, Juutilainen J. (2018). Behavioural phenotypes in mice after prenatal and early postnatal exposure to intermediate frequency magnetic fields. Environ Res.162,27-34.http://10.1016/j.envres.2017.12.013

[19] Acikgoz B, Ersoy N, Aksu I, Kiray A, Bagriyanik HA, Kiray M. (2022). Gender differences in effects of prenatal and postnatal exposure to electromagnetic field and prenatal zinc on behaviour and synaptic proteins in

rats. J Chem Neuroanat.122,102092.http://10.1016/j.jchemneu.2022.102092
[20] Agarwal A, Singh A, Hamada A, Kesari K. (2011). Cell phones and male infertility: a review of recent innovations in technology and consequences. Int Braz J Urol.37(4),432-54.http://10.1590/s1677-55382011000400002
[21] Ersoy N, Acikgoz B, Aksu I, Kiray A, Bagriyanik HA, Kiray M. (2022). The Effects of Prenatal and Postnatal Exposure to 50-Hz and 3 mT Electromagnetic Field on Rat Testicular Development. Medicina (Kaunas).59(1).http://10.3390/medicina59010071
[22] Özorak A, Nazıroğlu M, Çelik Ö, Yüksel M, Özçelik D, Özkaya MO, et al. (2013). Wi-Fi (2.45 GHz)- and mobile phone (900 and 1800 MHz)-induced risks on oxidative stress and elements in kidney and testis of rats during pregnancy and the development of offspring. Biol Trace Elem Res.156(1-3),221-9.http://10.1007/s12011-013-9836-z
[23] Yan S, Ju Y, Dong J, Lei H, Wang J, Xu Q, et al. (2022). Paternal Radiofrequency Electromagnetic Radiation Exposure Causes Sex-Specific Differences in Body Weight Trajectory and Glucose Metabolism in Offspring Mice. Front Public Health.10,872198.http://10.3389/fpubh.2022.872198
[24] Andrašková S, Holovská K, Ševčíková Z, Andrejčáková Z, Tóth Š, Martončíková M, et al. (2022). The potential adverse effect of 2.45 GHz microwave radiation on the testes of prenatally exposed peripubertal male rats. Histol Histopathol.37(3),287-99.http://10.14670/hh-18-402
[25] Ryan BM, Symanski RR, Pomeranz LE, Johnson TR, Gauger JR, McCormick DL. (1999). Multigeneration reproductive toxicity assessment of 60-Hz magnetic fields using a continuous breeding protocol in rats. Teratology.59(3),156-62.http://10.1002/(sici)1096-9926(199903)59:3<156::Aid-tera7>3.0.Co;2-b
[26] Burcu A, Nevin E, Ilkay A, Amac K, Alper BH, Muge K. (2020). The effects of prenatal and postnatal exposure to electromagnetic field on rat ovarian tissue. Toxicology and Industrial Health.36(12),1010-8.http://10.1177/0748233720973136
[27] Shirai T, Wang J, Kawabe M, Wake K, Watanabe S-i, Takahashi S, Fujiwara O. (2017). No adverse effects detected for simultaneous whole-body exposure to multiple-frequency radiofrequency electromagnetic fields for rats in the intrauterine and pre- and post-weaning periods. Journal of Radiation Research.58(1),48-58.http://10.1093/jrr/rrw085
[28] Takahashi S, Imai N, Nabae K, Wake K, Kawai H, Wang J, et al. (2009). Lack of Adverse Effects of Whole-Body Exposure to a Mobile Telecommunication Electromagnetic Field on the Rat Fetus. Radiation Research.173(3),362-72.http://10.1667/rr1615.1
[29] Baste V, Riise T, Moen BE. (2008). Radiofrequency electromagnetic fields; male infertility and sex ratio of offspring. European Journal of Epidemiology.23(5),369-77.http://10.1007/s10654-008-9236-4
[30] Mageroy N, Mollerlokken OJ, Riise T, Koefoed V, Moen BE. (2006). A higher risk of congenital anomalies in the offspring of personnel who served aboard a Norwegian missile torpedo boat. Occupational and Environmental Medicine.63(2),92.http://10.1136/oem.2005.021113
[31] Baste V, Moen BE, Oftedal G, Strand LÅ, Bjørge L, Mild KH. (2012). Pregnancy Outcomes After Paternal Radiofrequency Field Exposure Aboard Fast Patrol Boats. Journal of Occupational and Environmental Medicine.54(4),431-8.http://10.1097/JOM.0b013e3182445003
[32] Baste V, Oftedal G, Møllerløkken OJ, Hansson Mild K, Moen BE. (2015). Prospective Study of Pregnancy Outcomes After Parental Cell Phone Exposure: The Norwegian Mother and Child Cohort Study. Epidemiology.26(4),613-21.http://10.1097/ede.0000000000000293
[33] Knave B, Gamberale F, BergstrÖM S, Birke E, Iregren A, Kolmodin-Hedman B, Wennberg A. (1979). Long-term exposure to electric fields: A cross-sectional epidemiologic investigation of occupationally exposed workers in high-voltage substations. Scandinavian Journal of Work, Environment & Health.5(2),115-25
[34] Topal Z, Hanci H, Mercantepe T, Erol HS, Keleş ON, Kaya H, et al. (2015). The effects of prenatal long-duration exposure to 900-MHz electromagnetic field on the 21-day-old newborn male rat liver. Turk J Med Sci.45(2),291-7.http://10.3906/sag-1404-168
[35] Bozok S, Karaagac E, Sener D, Akakin D, Tumkaya L. (2022). The effects of long-term prenatal exposure to 900, 1800, and 2100 MHz electromagnetic field radiation on myocardial tissue of rats. Toxicology and Industrial Health.39(1),1-9.http://10.1177/07482337221139586
[36] Bahreyni Toossi MH, Reza SH, Maryam MMF, Mahmoud H, Mahdiyeh H, Razieh M, et al. (2018). Exposure to mobile phone (900–1800 MHz) during pregnancy: tissue oxidative stress after childbirth. The Journal of Maternal-Fetal & Neonatal Medicine.31(10),1298-303.http://10.1080/14767058.2017.1315657
[37] Guleken Z, Sarıbal D, Uyulan C, Keles A, Depciuch J. (2021). Investigating Bio-interface Effects of Chronic ELF-MF Exposure before and after Neonatal Life on Rat Offspring Using Spectroscopy and Biochemical Assays. Biointerface Research in Applied Chemistry.12(1),795 - 808.https://doi.org/10.33263/BRIAC121.795808
[38] Çiftçi ZZ, Kırzıoğlu Z, Nazıroğlu M, Özmen Ö. (2015). Effects of Prenatal and Postnatal Exposure of Wi-Fi on Development of Teeth and Changes in Teeth Element Concentration in Rats. Biological Trace Element Research.163(1),193-201.http://10.1007/s12011-014-0175-5
[39] Özorak A, Nazıroğlu M, Çelik Ö, Yüksel M, Özçelik D, Özkaya MO, et al. (2013). Wi-Fi (2.45 GHz)- and Mobile Phone (900 and 1800 MHz)-Induced Risks on Oxidative Stress and Elements in Kidney and Testis of Rats During Pregnancy and the Development of Offspring. Biological Trace Element Research.156(1),221-9.http://10.1007/s12011-013-9836-z
[40] Lary JM, Conover DL, Johnson PH, Burg JR. (1983). Teratogenicity of 27.12-MHz radiation in rats is related to duration of hyperthermic exposure. Bioelectromagnetics.4(3),249-55.https://doi.org/10.1002/bem.2250040305
[41] GÜLER ÖZTÜRK G, Tomruk A, Ozgur E, Seyhan N. (2010). The effect of radiofrequency radiation on DNA and lipid damage in non-pregnant and pregnant rabbits and their newborns. General physiology and biophysics.29(1).https://10.4149/gpb_2010_01_59

[42] Pearce MS, Hammal DM, Dorak MT, McNally RJQ, Parker L. (2007). Paternal occupational exposure to electromagnetic fields as a risk factor for cancer in children and young adults: A case-control study from the North of England. Pediatric Blood & Cancer.49(3),280-6.https://doi.org/10.1002/pbc.21021
[43] Reid A, Glass DC, Bailey HD, Milne E, de Klerk NH, Downie P, et al. (2011). Risk of childhood acute lymphoblastic leukaemia following parental occupational exposure to extremely low frequency electromagnetic fields. British Journal of Cancer.105(9),1409-13.http://10.1038/bjc.2011.365
[44] Bohacek J, Mansuy IM. (2015). Molecular insights into transgenerational non-genetic inheritance of acquired behaviours. Nature Reviews Genetics.16(11),641-52.http://10.1038/nrg3964
[45] Cavalli G, Heard E. (2019). Advances in epigenetics link genetics to the environment and disease. Nature.571(7766),489-99.http://10.1038/s41586-019-1411-0
[46] Nagano T, Lubling Y, Stevens TJ, Schoenfelder S, Yaffe E, Dean W, et al. (2013). Single-cell Hi-C reveals cell-to-cell variability in chromosome structure. Nature.502(7469),59-64.http://10.1038/nature12593

Research Article

Life Conflux

Unraveling the Role of Anoikis in Non-Alcoholic Fatty Liver Disease Progression and Immune Cell Infiltration

Authors

Yuming Wang, Xinqiang Li, Jijun Shan, Ruidong Ding, Jinzhen Cai

Correspondence

caijinzhen@qdu.edu.cn (J. Cai)

Graphical Abstract

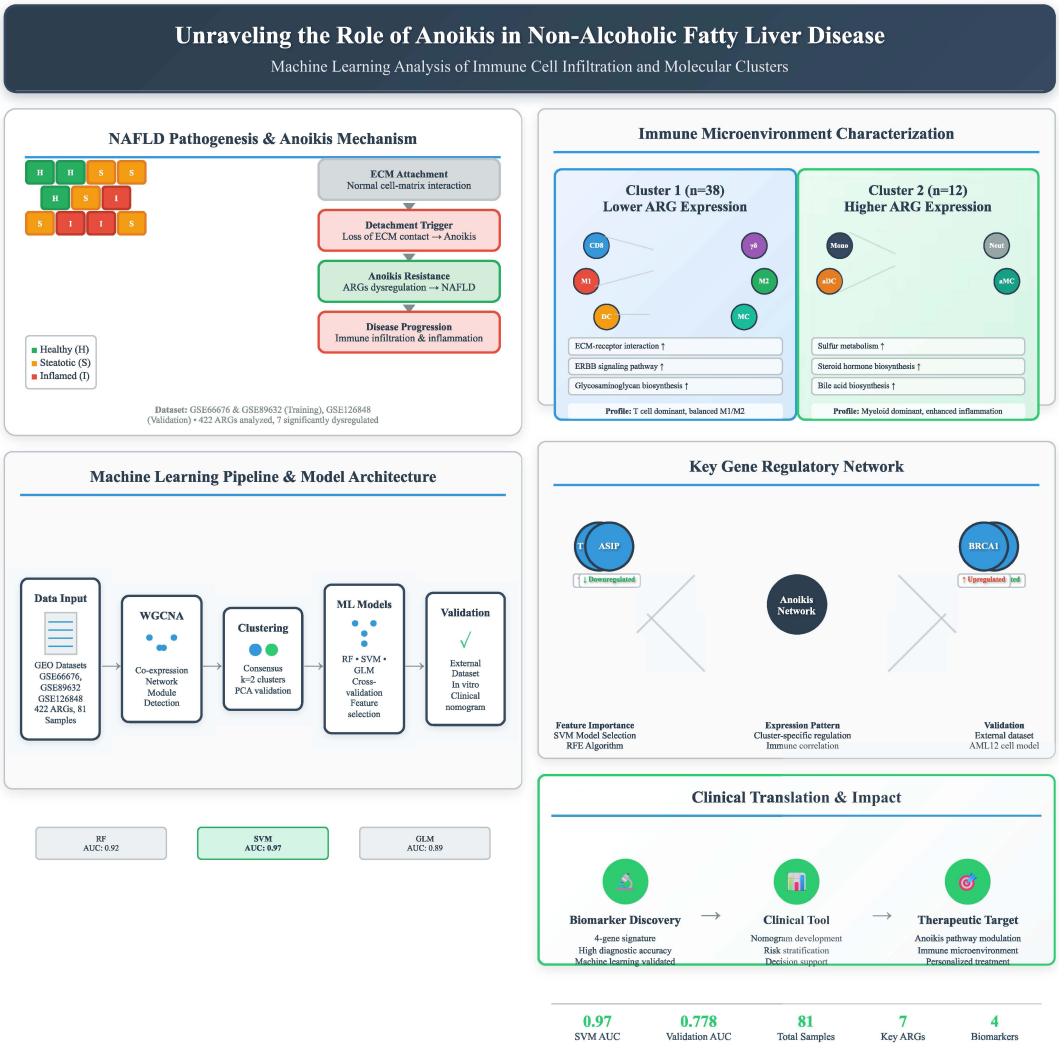

https://doi.org/10.71321/p63ws623

Research Article Life Conflux

Unraveling the Role of Anoikis in Non-Alcoholic Fatty Liver Disease Progression and Immune Cell Infiltration

Yuming Wang [1,2], Xinqiang Li [1,2], Jijun Shan [3], Ruidong Ding [1,2], Jinzhen Cai [1,2*]

Received: 2025-01-16 | Accepted: 2025-03-23 | Published online: 2025-03-30

Abstract

Background: Non-alcoholic fatty liver disease (NAFLD) is a prevalent chronic liver disease with complex molecular mechanisms. Anoikis, a distinct form of programmed cell death, has been implicated in disease progression, but its specific role in NAFLD remains unclear. This study aims to identify anoikis-related molecular clusters, explore their immune characteristics, and construct a predictive model for NAFLD prognosis.
Methods: Gene expression profiles of NAFLD samples were obtained from the Gene Expression Omnibus (GEO) database. Weighted gene co-expression network analysis (WGCNA) was applied to identify cluster-specific differentially expressed genes. Immune infiltration analysis was conducted to evaluate the association between anoikis-related clusters and immune cell composition. Machine learning was used to screen feature genes, and a predictive model was developed. The model's performance was assessed using nomograms, calibration curves, and decision curve analysis (DCA).
Results: Two distinct anoikis-related molecular clusters were identified, each exhibiting unique immune microenvironment characteristics. Cluster 1 showed higher levels of CD8 T cells, γ-delta T cells, and macrophages (M1 and M2), while Cluster 2 had increased monocytes, activated dendritic cells, and neutrophils, reflecting inflammatory heterogeneity. Four key genes (TMEM169, THBS1, ASIP, and BRCA1) were identified through machine learning and incorporated into a predictive model. The model's accuracy in predicting NAFLD prognosis was confirmed through nomograms, calibration curves, and DCA.
Conclusion: This study established an anoikis-related prognostic model for NAFLD and identified key genes involved in disease progression. The findings provide novel insights into the interplay between anoikis, immune responses, and NAFLD, offering potential biomarkers and therapeutic targets for personalized treatment.
Keywords: NAFLD, Anoikis, Apoptosis, Machine learning

Introduction

Non-alcoholic fatty liver disease (NAFLD), characterized by inflammation, has rapidly emerged as the leading cause of chronic liver disease globally[1]. Because of the rising incidence of metabolic syndrome, obesity, and diabetes worldwide, NAFLD now affected approximately one-quarter of the global population[2]. Regional variations exist, with the highest prevalence observed in the Middle East (32%) and South America (30%), followed by North America and Europe (24%), Asia (27%), and the lowest in Africa (13%) [3]. NAFLD is defined as a spectrum of diseases where more than 5% of hepatocytes exhibit steatosis alongside metabolic risk factors, notably obesity. NAFLD represents the hepatic manifestation of metabolic syndrome and is classified histologically into nonalcoholic fatty liver (NAFL) and nonalcoholic steatohepatitis (NASH)[4]. Despite extensive research, the pathogenesis of NAFLD remains poorly understood, underscoring the urgent need for reliable biomarkers for its diagnosis.

Apoptosis, a fundamental organismal defense mechanism, curtails abnormal cell proliferation by preventing the reattachment of detached cells[5]. Emerging studies highlighted the significant role of apoptosis in NAFLD [6–8]. Anoikis, a specific form of apoptosis triggered by cell detachment from the extracellular matrix (ECM), is critical for tissue homeostasis and development, originally identified in endothelial and epithelial cells.

The regulatory mechanisms underlying anoikis in NAFLD remain elusive, warranting further investigation. In this context, we conducted a comprehensive analysis utilizing publicly available databases and bioinformatics tools to identify anoikis-related genes (ARGs) implicated in NAFLD onset and progression. Subsequent analyses focused on the regulatory networks of ARGs and their associations with the immune microenvironment. This research aims to elucidate the function of ARGs in NAFLD and identify novel therapeutic targets.

1Organ Transplantation Center, Affiliated Hospital of Qingdao University, Qingdao, China
2Institute of Organ Donation and Transplantation, Medical College of Qingdao University, Qingdao, China
3Department of Hepatic Surgery, Fudan University Shanghai Cancer Center, Shanghai Medical College, Fudan University, Shanghai, 200032, People's Republic of China.
* Corresponding Author.

Methods and Materials

Data collection and processing

The datasets GSE66766, GSE89632, and GSE126848 were obtained from the Gene Expression Omnibus (GEO) database (http://www.ncbi.nlm.nih.gov/geo/). GSE66676 was generated using the GPL66244 platform and comprised 67 samples, including 34 normal liver tissue controls and 33 NAFLD tissue samples. The GSE89632 dataset, based on the GPL14951 platform, contained 63 samples, of which 24 were normal liver controls and 39 were NAFLD tissue samples. All samples were included in the current analysis, with quality control ensuring the removal of samples with >10% missing values or low-quality metrics, such as inadequate signal intensity or inconsistent replicates. Additionally, GSE126848, utilizing the GPL14877 platform, included 57 samples, consisting of 26 normal liver controls and 31 NAFLD tissue samples, and was employed as the validation set in this study. Batch effects in the integrated datasets (GSE66676 and GSE89632) were adjusted using the "SVA" package, employing parameters that accounted for known covariates, such as platform differences. Missing values in the datasets were imputed using k-nearest neighbor (KNN) imputation. A power analysis was performed to confirm the adequacy of sample sizes, ensuring statistical reliability for downstream analyses.

Evaluating the immune cell infiltration

CIBERSORT was employed using the LM22 signature matrix to estimate the immune cell subtype composition for each sample based on gene expression profiles. The p-value for each sample was calculated using Monte Carlo sampling to assess the statistical significance of the deconvolution results. Differences in immune cell abundance between groups were evaluated using the Wilcoxon rank-sum test. In this study, a p-value < 0.05 was considered statistically significant.

Correlation analysis of ARGs and immune cell infiltration

To further validate the association between ARG expression and immune cell characteristics related to NAFLD, the correlation between ARG expression levels and the relative proportions of immune cells was analyzed. Spearman's correlation coefficient and the corresponding p-value were calculated to assess the strength and significance of the associations, with a p-value < 0.05 considered statistically significant. The results were visualized using the 'corrplot' R package (version 0.92).

Unsupervised clustering of NAFLD patients

Anoikis-related genes (ARGs) were retrieved from the GeneCard database (https://www.genecards.org/), resulting in a consistent set of 422 genes across all cohorts (Supplementary Table 1). To investigate the molecular heterogeneity of non-alcoholic fatty liver disease (NAFLD), an unsupervised clustering analysis was performed based on the expression profiles of seven cuproptosis-associated genes with significantly altered expression. This analysis, conducted using the k-means algorithm across 1000 iterations, classified 50 NAFLD samples into distinct clusters. The maximum number of subtypes was set at k = 9, and the optimal number of subtypes was determined using a combination of the cumulative distribution function (CDF) curve, consensus matrix, and consensus cluster score (>0.9). Principal Component Analysis (PCA) further demonstrated distinct anoikis-related patterns across the subtypes, with the results visualized using the 'ggplot2' package.

Gene set variation analysis (GSVA) analysis

The enrichment analysis of different ARG clusters was conducted using the GSVA R package (version 2.11). For further GSVA analysis, the 'c2.cp.kegg. v7.4.symbols' and 'c5. go.bp.v7.5.1.symbols' files were obtained from the MSigDB database. Differentially enriched pathways and biological functions between ARG clusters were identified by comparing GSVA scores, using the 'LIMMA' R package (version 3.52.1) to assess statistical significance.

Weighted gene co-expression network analysis (WGCNA)

Based on gene clustering, weighted gene co-expression network analysis (WGCNA) was applied to identify highly correlated gene modules in NAFLD samples across gene subgroups [9]. Concurrently, WGCNA was performed on the combined dataset of normal and NAFLD samples to identify shared gene modules. By intersecting the results from disease-specific WGCNA and anoikis-related gene WGCNA, we identified NAFLD gene modules significantly associated with anoikis. The "good Samples Genes" function was employed to filter out low-quality genes and samples. An appropriate soft-thresholding power (β) was selected to compute the adjacency matrix, ensuring scale-free topology. Co-expression modules were then identified through hierarchical clustering and the dynamic tree cut algorithm, with a minimum module size set at 100 genes. Module eigengenes were subsequently calculated to represent the expression profiles of each module, and the eigengene network was visualized to illustrate the relationships between modules.

Construction of multiple machine learning prediction models

Using two distinct ARG clusters, machine learning models were constructed with the 'caret' R package (version 6.0.91), including the random forest (RF), support vector machine (SVM), and generalized linear model (GLM). RF leverages multiple independent decision trees for classification or regression tasks [10], while SVM creates a hyperplane with maximum margin to separate positive from negative instances in the feature space [11]. The GLM, an extension of linear regression, estimates relationships between normally distributed correlated features and categorical or continuous independent variables [12]. Feature selection was performed using recursive feature elimination (RFE) with 10-fold cross-validation to identify the most informative features, minimizing overfitting. Cross-validation was implemented using stratified 5-fold validation to ensure balanced representation of clusters across splits. Model parameter optimization was conducted using a grid search approach combined with cross-validation to select the best hyperparameters. Model comparison was based on performance metrics, including accuracy, precision, recall, F1-score, and area under the receiver operating characteristic (AUC-ROC) curve, providing a comprehensive evaluation.

The 50 NAFLD samples were randomly split into a training set (70%, n = 35) and a validation set (30%, n = 15). Model

parameters were automatically optimized, and all models were evaluated through 5-fold cross-validation. The 'Dalex' package (version 2.4.0) was employed to interpret the models, providing insights into residual distribution and feature importance. The area under the receiver operating characteristic (ROC) curve was visualized using the 'proc' R package(version1.18.0). The optimal model was selected based on performance metrics, and the top five predictive genes associated with NAFLD were identified as key variables.

Analysis of the diagnostic value of biomarkers

The receiver operating characteristic (ROC) curve was generated using the 'pROC' R package, and the area under the ROC curve (AUC) was calculated to assess model performance. The discriminatory ability of the key predictor genes in distinguishing NAFLD from non-NAFLD was externally validated using the GSE126848 dataset.

Construction and validation of nomogram models

Eigengenes were combined to construct nomograms using the 'rms' R package. The accuracy of the nomogram was then evaluated through a calibration curve, comparing predicted versus observed outcomes. Additionally, decision curve analysis was performed to assess the clinical utility of the nomogram, determining its net benefit across different threshold probabilities.

Cell culture

AML12 cells were maintained in a 5% CO2 incubator at 37°C, supplemented with 10% fetal bovine serum (FBS, Gibco, USA) and 1% penicillin-streptomycin (Gibco). To model non-alcoholic fatty liver disease (NAFLD) in vitro, hepatocytes were exposed to a medium containing 0.25 mM palmitic acid (PA, Sigma-Aldrich) and 0.5 mM oleic acid (OA, MedChemExpress) for the indicated durations. A fatty acid-free bovine serum albumin control was used to assess baseline conditions.

Oil red O staining

Oil Red O staining was performed to evaluate lipid droplet formation in AML12 cells, following a previously established protocol [13]. In brief, cells were washed twice with PBS, fixed in 4% paraformaldehyde for 30 minutes, and then stained with a 0.5% Oil Red O solution prepared in 60% isopropanol for 30 minutes. After staining, cells were rinsed with PBS before imaging. Lipid droplets were visualized and images were captured using an inverted microscope (ZEISS Corporation) at 100× magnification.

Statistical analysis

All data are expressed as the mean ± standard deviation (SD). Statistical comparisons between groups were conducted using an unpaired two-tailed Student's t-test. A p-value of less than 0.05 was considered statistically significant. All statistical analyses were performed using GraphPad Prism 8 (GraphPad Software, San Diego, USA) and R software (version 4.2.2; https://www.r-project.org/).

Results

Identifying AR-DEGs in Patients with NAFLD

The microarray datasets GSE63067 and GSE89632 were obtained from the Gene Expression Omnibus (GEO) database to elucidate the biological functions of anoikis regulators in the development and progression of non-alcoholic fatty liver disease (NAFLD). We assessed the expression profiles of 422 anoikis-associated genes between NAFLD and non-NAFLD controls using a merged dataset that was successfully cleared of batch effects(S-Figure1A-D). This dataset included 50 NAFLD tissues and 31 normal liver tissues. Seven significant differential expression genes were identified as key anoikis regulators: SIK1, PTGS2, MYC, THBS1, IL6, EPHA2, and TNFRSF12A (Figure 1A-B). Notably, these genes exhibited elevated expression in NAFLD patients compared to non-NAFLD controls. Correlation analysis of the differentially expressed anoikis genes revealed a strong synergistic interaction between THBS1 and TNFRSF12A (Figure 1C-D). Further investigation into these correlations highlighted the complex interplay among these genes. Immune infiltration analysis, utilizing the CiberSort algorithm, visualized differences in the proportions of 22 infiltrating immune cell types between NAFLD and non-NAFLD subjects (Figure 1E). The results indicated higher levels of M1 macrophages, M2 macrophages, and resting mast cells in NAFLD tissues, suggesting that immune system alterations are implicated in NAFLD pathogenesis. Additionally, correlation analysis revealed associations between anoikis-related genes and various immune cell types, including resting dendritic cells, activated dendritic cells, resting mast cells, activated mast cells, and γ-delta T cells (Figure 1F). These findings underscore the significant role of anoikis-related genes in modulating immune infiltration and highlight their potential impact on the development and progression of NAFLD.

Identification of anoikis clusters in NAFLD

Additionally, 50 NAFLD samples were categorized based on the expression profiles of seven differentially expressed anoikis-related genes (ARGs) using a consensus clustering algorithm. This analysis aimed to identify the expression patterns of genes associated with anoikis in NAFLD. The optimal number of clusters was determined to be two (k=2), where the clustering was most stable (Figure 2A), and the cumulative distribution function (CDF) curve displayed minimal fluctuation within the consensus index range of 0.3 to 0.4 (Figure 2B). When k ranged from 2 to 9, the difference between the areas under the CDF curves (for k and k-1) indicated the optimal clustering at k = 2 (Figure 2C). Furthermore, the concordance scores for each subtype were greater than 0.9 when k=2 (Figure 2D).

Consequently, the 50 NAFLD patients were divided into two distinct groups: Group 1 (n = 38) and Group 2 (n = 12). Principal Component Analysis (PCA) further corroborated the significant differences between the two clusters (Figure 2E). These findings highlight distinct expression patterns of anoikis-related genes in NAFLD, suggesting varied underlying mechanisms and potential therapeutic targets within these patient subgroups.

Figure 1. Expression of ARGs in NAFLD. (**A**) Boxplots illustrating the differential expression of seven ARGs between NAFLD patients and non-NAFLD controls, with significance levels denoted as p < 0.05, *p < 0.01, **p < 0.001, and ns indicating no significance. (**B**) Heatmap showing the expression patterns of the seven ARGs (**C**) Correlation analysis of nine differentially expressed CRGs. (**D**) Gene interaction network of the seven differentially expressed ARGs. (**E**) Comparative analysis of the relative abundance of 22 infiltrating immune cell types between NAFLD and non-NAFLD controls. (**F**) Boxplots representing differences in immune cell infiltration between NAFLD and non-NAFLD cohorts, with significance levels as p < 0.05, *p < 0.01, **p < 0.001, and ns indicating no significance. (**G**) Correlation analysis between the expression of seven differentially expressed ARGs and infiltrating immune cells.

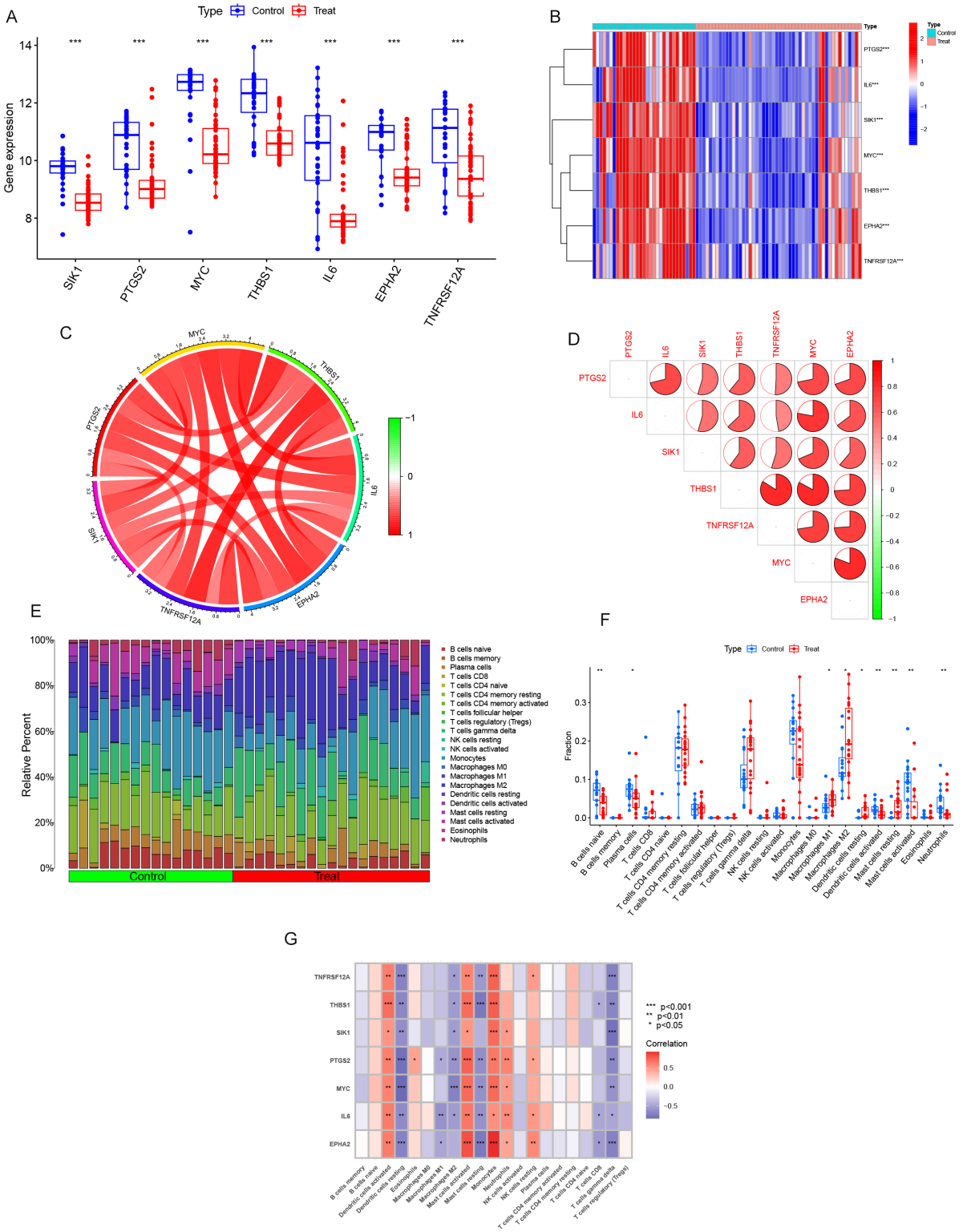

https://doi.org/10.71321/p63ws623

Differential expression of genes regulated by anoikis and immune infiltration signatures of associated anoikis clusters

To further elucidate the molecular characteristics of the identified subgroups, we comprehensively assessed the expression differences of seven critical anoikis-related genes (ARGs) between Cluster 1 and Cluster 2. Notably, Cluster 2 exhibited significantly higher expression levels of these seven CRGs (Figure 3A, B). To provide a detailed immune infiltration analysis, we utilized the CIBERSORT algorithm with LM22 signatures to quantify 22 immune cell types from bulk RNA-seq data. The analysis revealed distinct immune microenvironment profiles between the clusters (Figure 3C, D). Cluster 1 displayed significantly higher proportions of CD8 T cells ($p = 0.003$), γ-delta T cells ($p = 0.002$), M1 macrophages ($p = 0.005$), M2 macrophages ($p = 0.004$), resting dendritic cells ($p = 0.01$), and resting mast cells ($p = 0.008$). In contrast, Cluster 2 was characterized by elevated proportions of monocytes ($p = 0.002$), activated dendritic cells ($p = 0.001$), activated mast cells ($p = 0.007$), and neutrophils ($p = 0.003$). Furthermore, the immune cell ratio between pro-inflammatory (e.g., M1 macrophages) and anti-inflammatory (e.g., M2 macrophages) populations was higher in Cluster 1, suggesting a more inflammatory phenotype. These findings underscore the divergent immune landscapes between the anoikis-related clusters. Differential immune cell infiltration, particularly the balance between pro- and anti-inflammatory populations, may play a pivotal role in the pathogenesis and progression of NAFLD across these subgroups.

Construction of gene weighted co-expression module and gene screening

The Weighted Gene Co-Expression Network Analysis (WGCNA) algorithm was employed to construct co-expression networks and modules in normal controls and individuals with NAFLD, aiming to identify key gene modules associated with NAFLD. Co-expressed gene modules were identified with the soft power value set to 9 and the scale-free R2 set to 0.9 (Figure 4A). The dynamic tree cut algorithm yielded four distinct co-expressed gene modules, each represented by different colors, and a topological overlap matrix (TOM) heat map was generated (Figure 4B–E). Subsequent analysis of the module-clinical signature co-expression, correlating control and NAFLD groups, revealed that the blue module was most closely associated with NAFLD, comprising 566 genes (Figure 4F). This module demonstrated a strong positive correlation with module-associated genes. Further, the WGCNA algorithm was used to analyze key gene modules closely related to anoikis genes. Soft threshold parameters $\beta = 9$ and $R2 = 0.9$ were selected as the most suitable for constructing scale-

Figure 2. Identification of anoikis-related molecular patterns in NAFLD. (**A**) Consensus clustering matrix for k = 2, displaying the sample groupings. (**B–E**) Representative cumulative distribution function (CDF) curves for k values ranging from 2 to 9. (**C**) Relative changes in CDF delta area curves at different k values. (**D**) Consensus scores for each subtype across the range of k values (k = 2 to 9). (**E**) Principal component analysis (PCA) plot revealing the classification of NAFLD patients into two distinct molecular subtypes.

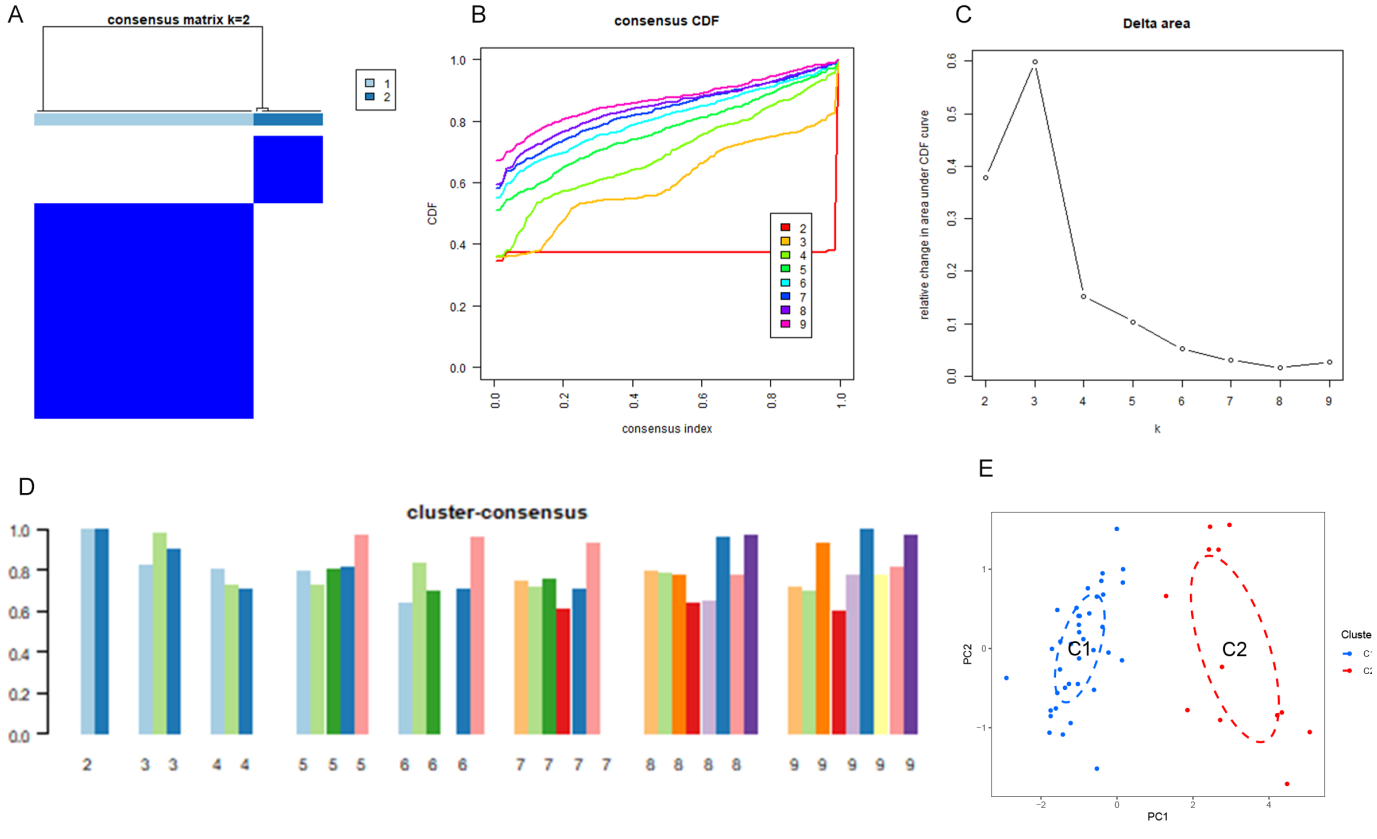

free networks (S-Figure 3A). Six significant modules were identified, and heatmaps depicting the TOMs of all module-associated genes were generated (S-Figure 3B–E). Analysis of the module-clinical feature relationships between Cluster 1 and Cluster 2 revealed a high correlation between the yellow module (221 genes) and NAFLD clusters (S-Figure 3F). Additionally, correlation analysis indicated that the brown module genes were significantly associated with selected modules

These findings highlight the importance of the blue and yellow modules in NAFLD and their potential involvement in the disease's molecular mechanisms, providing valuable insights for future research into NAFLD pathogenesis and therapeutic targets.

Identification of cluster-specific DEGs and functional annotation

A total of 161 cluster-specific differentially expressed genes (DEGs) were identified by intersecting module-associated genes of anoikis with those from NAFLD and non-NAFLD individuals (S-Figure 4A). To elucidate the functional differences between the clusters, Gene Set Variation Analysis (GSVA) was performed on these cluster-specific DEGs. GSVA scores were calculated using a Kolmogorov-Smirnov-like rank-based method to determine pathway enrichment levels across clusters. The analysis revealed that Cluster 2 exhibited upregulation in pathways related to sulfur metabolism, steroid hormone biosynthesis, and bile acid biosynthesis, while Cluster 1 showed increased expression in glycosaminoglycan biosynthesis, chondroitin sulfate metabolism, ECM-receptor interactions, and the ERBB signaling pathway (S-Figure 4C). Furthermore, Biological Process analysis was performed using the over-representation analysis (ORA) method, applying a hypergeometric test with a significance threshold of adjusted p-value < 0.05 (S-Figure 4B). These findings underscore distinct functional pathways associated with each cluster, providing insights into the molecular mechanisms underlying NAFLD and its potential therapeutic targets.

Machine learning model construction and evaluation

A total of 161 module-related genes, intersected from individuals with and without NAFLD based on anoikis-associated gene subsets, were analyzed to identify cluster-specific genes with high diagnostic potential. Three established machine learning models—Random Forest (RF), Support Vector Machine (SVM), and Generalized Linear Model

Figure 3. Differential analysis of feature gene expression and immune characteristics between anoikis clusters. (**A**) Boxplots displaying the expression levels of nine feature genes across the two anoikis subtypes, with significance levels indicated (p < 0.05, **p < 0.001, ns, not significant). (**B**) Heatmap illustrating the differential expression of these nine feature genes between the anoikis subtypes. (**C**) Relative abundances of 22 infiltrating immune cell types across the two anoikis clusters. (**D**) Boxplots showing the differences in immune cell infiltration between the anoikis subtypes (p < 0.05, ns, not significant).

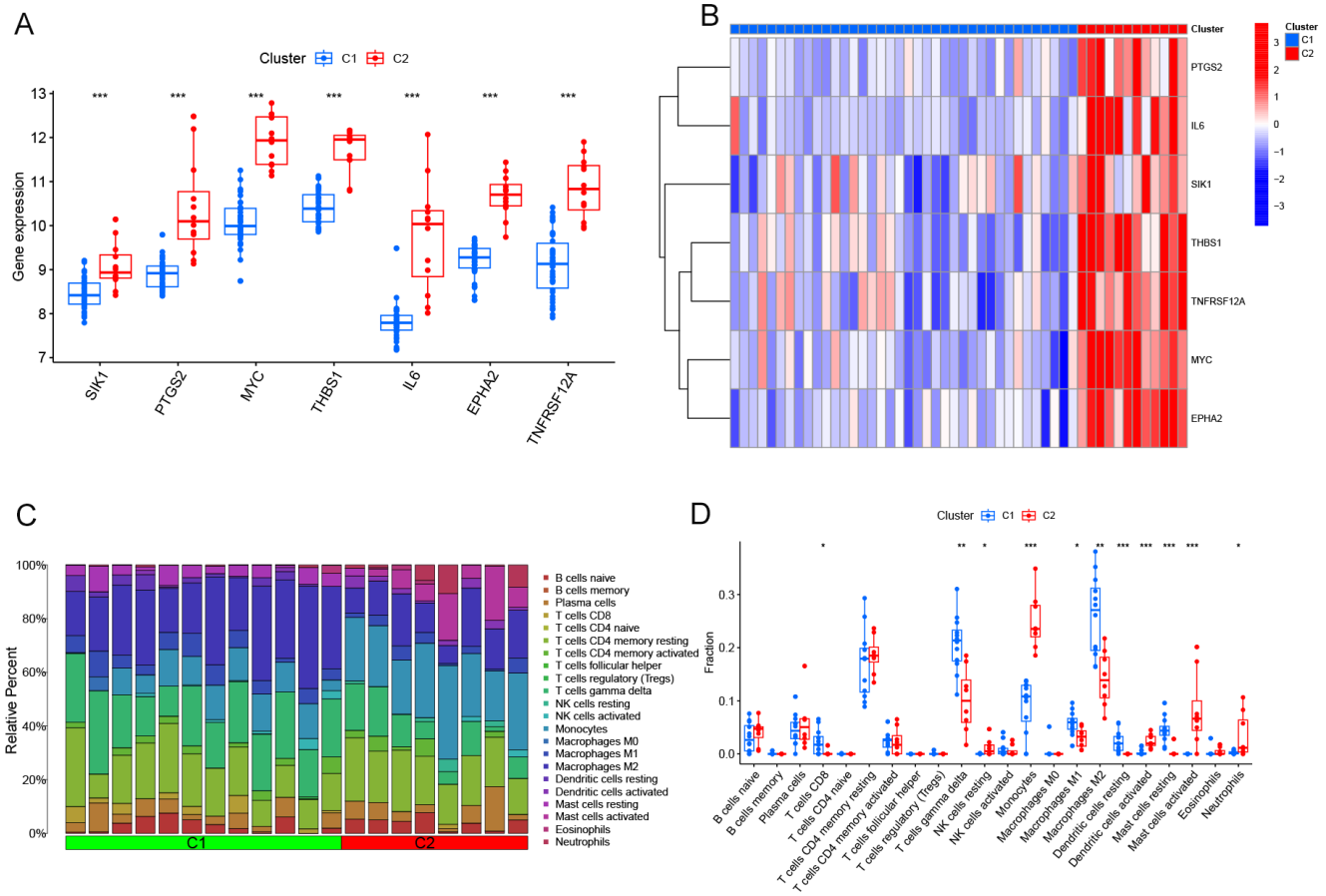

(GLM)—were developed to evaluate these genes. Model performance was interpreted using the R package 'Dalex,' and residual distributions for each model in the test set were plotted. The GLM and RF models exhibited relatively low residuals (Figure 5A-B). The top 10 significant feature variables for each model were ranked based on root mean square error (RMSE) (Figure 5D).

The discriminative performance of the models was assessed through receiver operating characteristic (ROC) curve analysis with fivefold cross-validation. The SVM model demonstrated the highest area under the ROC curve (AUC=0.97, Figure 5C), indicating superior performance in distinguishing between clusters. Consequently, the four most significant variables (TMEM169, THBS1, ASIP, BRCA1) from the SVM model were selected for further analysis.

Validation in dataset GSE126848, which includes 31 NAFLD patients and 26 normal controls, confirmed the expression differences of these signature genes. Specifically, THBS1 and ASIP were downregulated in NAFLD, while TMEM169 and BRCA1 were upregulated (S-Figure 5A, B). ROC analysis in this validation set demonstrated effective diagnostic performance for NAFLD (AUC = 0.778, S-Figure 5C). A nomogram was constructed to predict NAFLD progression, incorporating point values for each characteristic variable. The nomogram's standard curve validated its capacity to accurately assess NAFLD progression (S-Figure 2A, B). Decision curve analysis further indicated that the nomogram offers clinical benefit for NAFLD patients. Collectively, these findings suggest that this subset of anoikis-associated genes can effectively differentiate NAFLD from non-NAFLD cases.

In vitro experiments further verified the results

In vitro studies were conducted using AML12 cells. AML12 cells were treated with oleate (OA) and palmitate (PA) to induce fat accumulation, mimicking hepatic steatosis. Following free fatty acid (FFA) induction, cells exhibited increased fat accumulation (Figure 6A–B). Expression of TMEM169 and BRCA1 was elevated, while ASIP and THBS1 expression decreased (Figure 6C).

Discussion

NAFLD is the most prevalent chronic liver disease, with its incidence steadily increasing over the past two decades due to lifestyle and dietary changes. While apoptosis and pyroptosis

Figure 4. Co-expression network of differentially expressed genes in NAFLD. (A) Determination of the optimal soft-thresholding power for network construction. (B) Dendrogram of clustered genes, with distinct co-expression modules represented by different colors. (C) Clustering of module eigengenes. (D) Heatmap showing the correlations among the five identified modules. (E) Correlation analysis between module eigengenes and clinical status, with rows indicating modules and columns representing clinical traits. (F) Scatter plot depicting the relationship between module membership in the blue module and gene significance for NAFLD.

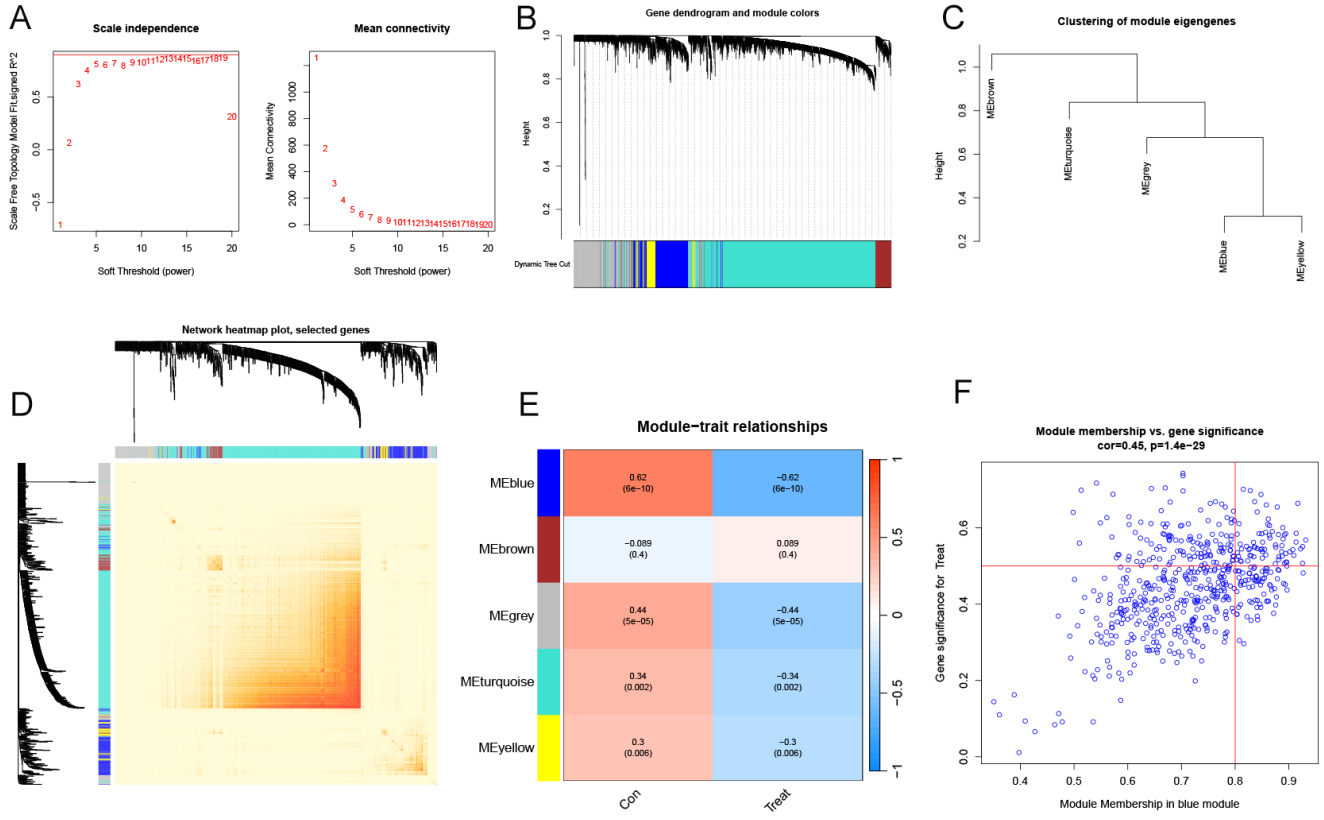

Figure 5. Construction and evaluation of RF, SVM, and GLM machine learning models. (**A**) Boxplots displaying the residuals for each machine learning model, with the red dot indicating the root mean square error (RMSE). (**B**) Cumulative residual distribution across the models. (**C**) ROC analysis of the three machine learning models, assessed via 5-fold cross-validation in the testing cohort. (**D**) Key features identified in the RF, SVM, and GLM models.

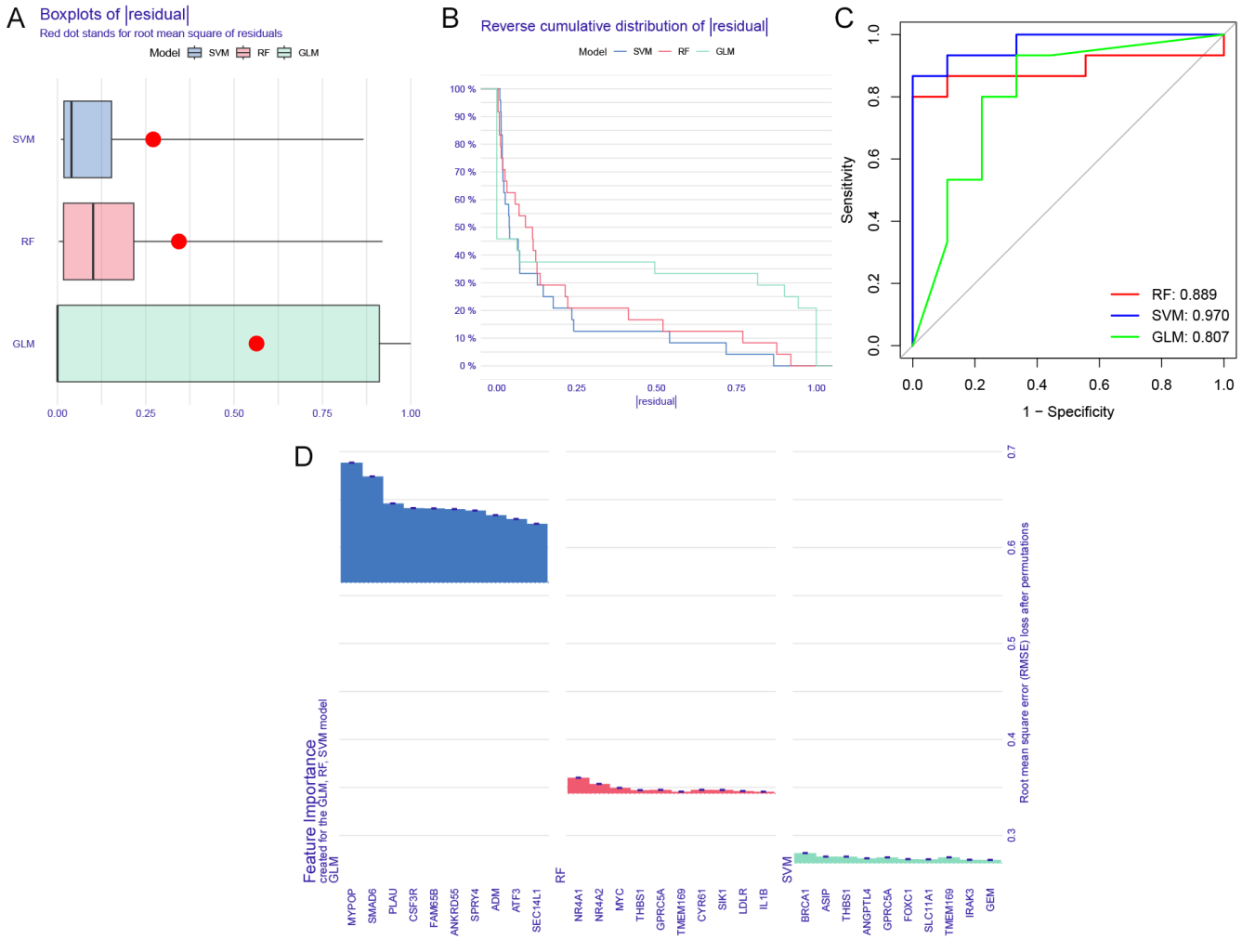

Figure 6. Verification of model gene mRNA expression levels in AML12 cells. β-Actin served as the control. (**A-B**) Oil Red O staining of the cells, with magnification at ×100. (**C**) Relative mRNA levels of TMEM169, THBS1, ASIP, and BRCA1, normalized to β-Actin. Data are presented as mean ± s.d. $p < 0.05$; *$p < 0.01$; **$p < 0.001$.

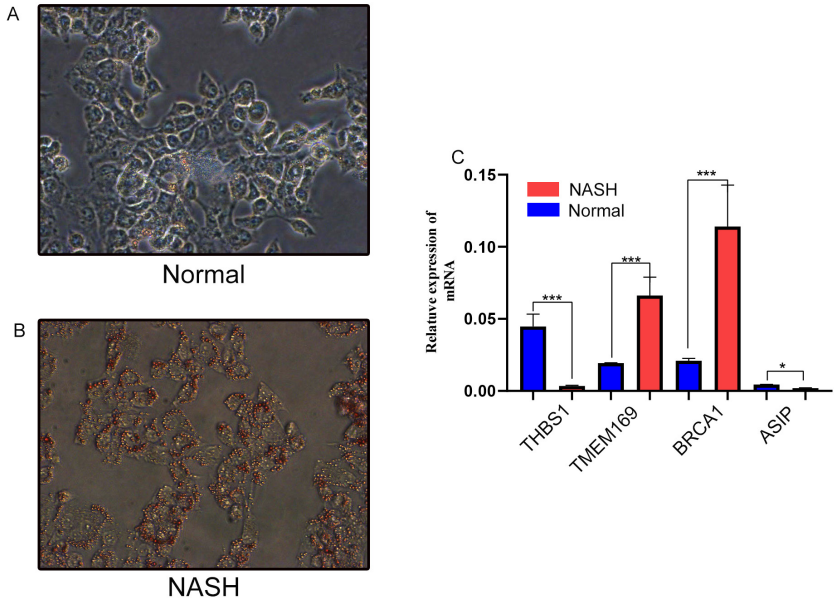

have been studied extensively, the role of anoikis in NAFLD remains unclear. Our findings highlight seven anoikis-related genes (SIK1, MYC, IL6, TNFRSF12A, PTGS2, THBS1, EPHA2) as critical regulators of NAFLD pathogenesis. These genes were significantly upregulated in NAFLD patients compared to healthy controls, with THBS1 and TNFRSF12A showing a strong synergistic correlation. This aligns with prior research emphasizing the pivotal roles of macrophages in NAFLD progression [15,16]. The polarization of macrophages into pro-inflammatory (M1) and anti-inflammatory (M2) phenotypes plays a dual role in promoting inflammation and facilitating tissue repair, respectively. Additionally, our study demonstrated that Cluster 2, characterized by high expression of ARGs, exhibited enhanced immune activation, as evidenced by elevated monocyte and neutrophil levels. Pathway enrichment revealed that Cluster 2 was predominantly associated with sulfur metabolism, steroid hormone biosynthesis, and bile acid biosynthesis, consistent with previous studies linking these pathways to immune activation and inflammation in NAFLD [19,20]. By integrating immune infiltration data with ARG expression, we provide a comprehensive understanding of how anoikis impacts NAFLD progression.

The machine learning-based SVM model achieved the highest predictive accuracy (AUC = 0.970), identifying TMEM169, THBS1, ASIP, and BRCA1 as key diagnostic markers. This model was validated using external datasets, ensuring its generalizability. THBS1, a critical mediator of hepatocyte homeostasis, and BRCA1, associated with multiple cancer types including hepatocellular carcinoma, were notably overexpressed in HCC, corroborating our findings. However, the practical implementation of this model poses challenges, including the need for large-scale validation in diverse populations and integration with clinical workflows. Additionally, population heterogeneity, such as ethnic and regional differences in NAFLD prevalence, may influence the generalizability of our findings. The inclusion of a nomogram further enhances clinical applicability, offering a user-friendly tool for NAFLD risk assessment. Despite these advancements, limitations such as a relatively small sample size and the lack of longitudinal clinical data warrant further investigation. Future studies should explore the dynamic interplay between ARGs and the immune microenvironment in larger cohorts.

Conclusion

This study establishes the critical role of anoikis in the progression and immune cell infiltration of non-alcoholic fatty liver disease (NAFLD). By identifying and validating two distinct anoikis-related molecular clusters and four key genes (TMEM169, THBS1, ASIP, and BRCA1), the research supports a predictive model with high accuracy.

Acknowledgements

Not applicable.

Author Contributions

Jinzhen Cai, Yuming Wang contributed to the research design. Jinzhen Cai, Yuming Wang, Xinqiang Li, Jijun Shan and Ruidong Ding contributed to the data management and statistical analyses. Jinzhen Cai, Yuming Wang wrote the manuscript. All authors reviewed the manuscript.

Funding Information

This work was supported by the National Natural Science Foundation of China (No. 82370666) and the Science Foundation of Shandong Province (No. ZR2022MH292).

Conflict of Interest

The authors declare no conflict of interest.

Data Availability

All data needed to evaluate the conclusions in the paper are present in the paper or the Supplementary Materials. Additional data related to this paper may be requested from the authors.

Reference:

[1] Guo X, Yin X, Liu Z, & Wang J. (2022). Non-Alcoholic Fatty Liver Disease (NAFLD) Pathogenesis and Natural Products for Prevention and Treatment. Int J Mol Sci, 23(24). https://doi.org/10.3390/ijms232415489

[2] Younossi Z, Anstee QM, Marietti M, Hardy T, Henry L, Eslam M, et al. (2018). Global burden of NAFLD and NASH: trends, predictions, risk factors and prevention. Nat Rev Gastroenterol Hepatol, 15(1), 11-20. https://doi.org/10.1038/nrgastro.2017.109

[3] Younossi ZM, Koenig AB, Abdelatif D, Fazel Y, Henry L, & Wymer M. (2016). Global epidemiology of nonalcoholic fatty liver disease-Meta-analytic assessment of prevalence, incidence, and outcomes. Hepatology, 64(1), 73-84. https://doi.org/10.1002/hep.28431

[4] Byrne CD, & Targher G. (2015). NAFLD: a multisystem disease. J Hepatol, 62(1 Suppl), S47-64. https://doi.org/10.1016/j.jhep.2014.12.012

[5] Li Y, Pan Q, Cheng M, & Wu Z. (2023). Identification and validation of anoikis-associated gene SNCG as a prognostic biomarker in gastric cancer. Aging (Albany NY), 15(7), 2541-2553. https://doi.org/10.18632/aging.204626

[6] Ni K, & Meng L. (2024). Mechanism of PANoptosis in metabolic dysfunction-associated steatotic liver disease. Clin Res Hepatol Gastroenterol, 48(7), 102381. https://doi.org/10.1016/j.clinre.2024.102381

[7] Sun HJ, Jiao B, Wang Y, Zhang YH, Chen G, Wang ZX, et al. (2024). Necroptosis contributes to non-alcoholic fatty liver disease pathoetiology with promising diagnostic

and therapeutic functions. World J Gastroenterol, 30(14), 1968-1981. https://doi.org/10.3748/wjg.v30.i14.1968
[8] Li R, Xue W, Wei H, Fan Q, Li X, Qiu Y, et al. (2023). Research Progress of Pyroptosis in Fatty Liver Disease. Int J Mol Sci, 24(17). https://doi.org/10.3390/ijms241713065
[9] Langfelder P, & Horvath S. (2008). WGCNA: an R package for weighted correlation network analysis. BMC Bioinformatics, 9, 559. https://doi.org/10.1186/1471-2105-9-559
[10] Rigatti SJ. (2017). Random Forest. J Insur Med, 47(1), 31-39. https://doi.org/10.17849/insm-47-01-31-39.1
[11] Tan M, Pu J, & Zheng B. (2014). Optimization of breast mass classification using sequential forward floating selection (SFFS) and a support vector machine (SVM) model. Int J Comput Assist Radiol Surg, 9(6), 1005-1020. https://doi.org/10.1007/s11548-014-0992-1
[12] Weng G, Clark K, Akbarian A, Noudoost B, & Nategh N. (2024). Time-varying generalized linear models: characterizing and decoding neuronal dynamics in higher visual areas. Front Comput Neurosci, 18, 1273053. https://doi.org/10.3389/fncom.2024.1273053
[13] Chu MJ, Hickey AJ, Tagaloa S, Zhang L, Dare AJ, MacDonald JR, et al. (2014). Ob/ob mouse livers show decreased oxidative phosphorylation efficiencies and anaerobic capacities after cold ischemia. PLoS One, 9(6), e100609. https://doi.org/10.1371/journal.pone.0100609
[14] Roychowdhury S, McCullough RL, Sanz-Garcia C, Saikia P, Alkhouri N, Matloob A, et al. (2016). Receptor interacting protein 3 protects mice from high-fat diet-induced liver injury. Hepatology, 64(5), 1518-1533. https://doi.org/10.1002/hep.28676
[15] Kazankov K, Jørgensen SMD, Thomsen KL, Møller HJ, Vilstrup H, George J, et al. (2019). The role of macrophages in nonalcoholic fatty liver disease and nonalcoholic steatohepatitis. Nat Rev Gastroenterol Hepatol, 16(3), 145-159. https://doi.org/10.1038/s41575-018-0082-x
[16] Wang Y, Smith W, Hao D, He B, & Kong L. (2019). M1 and M2 macrophage polarization and potentially therapeutic naturally occurring compounds. Int Immunopharmacol, 70, 459-466. https://doi.org/10.1016/j.intimp.2019.02.050
[17] Gong H, He Q, Zhu L, Feng Z, Sun M, Jiang J, et al. (2024). Associations between systemic inflammation indicators and nonalcoholic fatty liver disease: evidence from a prospective study. Front Immunol, 15, 1389967. https://doi.org/10.3389/fimmu.2024.1389967
[18] Wang YF, Zhang WL, Li ZX, Liu Y, Tan J, Yin HZ, et al. (2024). METTL14 downregulation drives S100A4(+) monocyte-derived macrophages via MyD88/NF-κB pathway to promote MAFLD progression. Signal Transduct Target Ther, 9(1), 91. https://doi.org/10.1038/s41392-024-01797-1
[19] Liu Z, Huang H, Ruan J, Wang Z, & Xu C. (2024). The sulfur microbial diet and risk of nonalcoholic fatty liver disease: a prospective gene-diet study from the UK Biobank. Am J Clin Nutr, 119(2), 417-424. https://doi.org/10.1016/j.ajcnut.2023.11.012
[20] Bin DH, Liu F, Peng KP, Zhan M, Tan Y, Liu Q, et al. (2024). The relationship between follicle-stimulating hormone and metabolic dysfunction-associated fatty liver disease in men. Nutr Diabetes, 14(1), 52. https://doi.org/10.1038/s41387-024-00314-1
[21] Deo RC. (2015). Machine Learning in Medicine. Circulation, 132(20), 1920-1930. https://doi.org/10.1161/circulationaha.115.001593
[22] Bai J, Xia M, Xue Y, Ma F, Cui A, Sun Y, et al. (2020). Thrombospondin 1 improves hepatic steatosis in diet-induced insulin-resistant mice and is associated with hepatic fat content in humans. EBioMedicine, 57, 102849. https://doi.org/10.1016/j.ebiom.2020.102849
[23] Mei J, Wang R, Xia D, Yang X, Zhou W, Wang H, et al. (2020). BRCA1 Is a Novel Prognostic Indicator and Associates with Immune Cell Infiltration in Hepatocellular Carcinoma. DNA Cell Biol, 39(10), 1838-1849. https://doi.org/10.1089/dna.2020.5644